SEISMIC FRAGILITY ANALYSIS OF RC FRAME BUILDINGS WITH STRUCTURAL WALLS

by

Nabajit Sarkar

DEPARTMENT OF CIVIL ENGINEERING
INDIAN INSTITUTE OF TECHNOLOGY GUWAHATI
GUWAHATI-781039, INDIA

July 2024

SEISMIC FRAGILITY ANALYSIS OF RC FRAME BUILDINGS WITH STRUCTURAL WALLS

A Thesis Submitted
in Partial Fulfillment of the Requirements
for the Degree of

DOCTOR OF PHILOSOPHY

by

Nabajit Sarkar

DEPARTMENT OF CIVIL ENGINEERING
INDIAN INSTITUTE OF TECHNOLOGY GUWAHATI
GUWAHATI-781039, INDIA

July 2024

CERTIFICATE

It is certified that the work contained in this thesis titled "*Seismic Fragility Analysis of RC Frame Buildings with Structural Walls"* by **Mr. Nabajit Sarkar** bearing roll no. 186104021, has been carried out under my supervision and submitted to Indian Institute of Technology Guwahati for the award of the degree of **Doctor of Philosophy**. This work has not been submitted elsewhere for a degree to the best of my knowledge and belief.

Date:
Place: IIT Guwahati

Dr. Kaustubh Dasgupta
Associate Professor
Department of Civil Engineering
Indian Institute of Technology Guwahati
Guwahati-781039, Assam, India

ABSTRACT

Recent years have seen rapid urbanization and substantial economic growth, resulting in a concentration of population in smaller urban areas. This population growth has led to a notable increase in the construction of highrise buildings. Especially in regions prone to earthquakes, the multistoried Reinforced Concrete (RC) frame buildings are provided with RC structural walls, commonly known as shear walls, to enhance the lateral strength and lateral stiffness of the buildings. Thus, a detailed understanding of the seismic behaviour of these structural walls is imperative when evaluating the seismic performance of those highrise buildings.

In the context of seismic performance evaluation for any structure, one of the major aspects is the assessment of its seismic vulnerability. These assessments aim to measure the likelihood of different degrees of damage occurring at various levels of earthquake shaking, quantified by the intensity level of seismic hazard. The coherent connection between the seismic hazard and its consequences on the vulnerable structural elements, is established by employing fragility relationships that associate distinct seismic intensity levels with the relevant seismic response parameters.

The present study aims to carry out a comprehensive seismic fragility evaluation of an RC frame building with structural walls using finite element modelling of the structural elements and then subjecting the numerical model to nonlinear dynamic analyses using earthquake ground motion records. As the first step in fragility estimation, the appropriate Engineering Demand Parameter (EDP) is chosen for the RC wall-frame structure as past research does not prescribe the same. Earlier studies have primarily focussed on the choice of optimal Intensity Measures (IMs) as compared to the efficient selection of the appropriate EDP for reliable fragility analysis. Along with the selection of EDP, the input ground motion records are also selected for further analyses.

As the primary contributors to response variability are the stochastic nature of ground motions (aleatory) and the uncertainties related to structural capacity (epistemic), the sensitivity of seismic response parameters for the RC wall-frame structure is studied, taking into consideration the possible uncertainties in material properties and structural modelling. The effect of propagation of various sources of uncertainty in the fragility assessment is also studied through the seismic response.

Next, analyses on the isolated slender RC wall are carried out to prescribe predictive equations for estimating lateral drift levels to achieve the different damage state thresholds. Using the Genetic Programming algorithm, the expressions are obtained based on a substantial dataset comprising numerically analysed specimens of RC walls. The applicability of the equations is enhanced by comparing with the experimental results of the past studies. As the predictive equations are based on the structural parameters of the wall, the estimated lateral drift values hold good for the wide range of performance levels of an RC wall.

Finally, the present study concludes by integrating findings related to key fragility parameter selection, uncertainty analysis, and damage state definitions to estimate fragility for the considered building typology. It distinctly highlights the impact of both epistemic uncertainty and the commonly addressed aleatory uncertainty on fragility relationships. A focused effort is made to develop and assess fragility relationships, considering both scalar and vector-valued IMs, for both a specific RC wall-frame structure and the entire RC wall-frame building. Finally, a simplified procedure is presented for deriving reliable fragility estimates with a reduced number of ground motion records while maintaining comparability with estimates using the complete record set.

Overall, the present study on seismic fragility assessment provides comprehensive insights into the seismic performance of RC wall-frame buildings across different levels of seismic demand. The study contributes to addressing several key questions within the fragility assessment framework, particularly for RC wall-frame building typologies, encompassing the incorporation of appropriate uncertainty sources in seismic response analysis, the decision between analysing a structural system using a representative frame or the entire building structure, the utilization of either single or multiple IMs for reliable fragility estimates, and the reduction of computational complexity without compromising efficiency in fragility assessments. In a wider perspective, the study suggests that the numerical framework employed here can be a valuable tool for deriving fragility estimates for various structural components and systems exposed to different types of hazards in future research.

ACKNOWLEDGMENT

Firstly, I would like to record my profound gratitude to Dr. Kaustubh Dasgupta for his invaluable guidance and unwavering support throughout my post-graduate journey. As my M.Tech degree advisor and later as my research mentor, he continuously supported and motivated me, shaping this thesis into its present form. From the inception to the completion of this thesis, his unwavering guidance and encouragement have been instrumental. Words are insufficient to convey my heartfelt appreciation for his exceptional advising, patience, and consistent support that enabled my involvement and performance in this research. I will forever cherish his role as a guiding light throughout my career at IIT Guwahati since 2016.

I express sincere gratitude to my doctoral committee members, Prof. Anjan Dutta, Prof. Hemant B. Kaushik, and Dr. Sachin S. Gautam, for their comprehensive review of my research work, as well as for the guidance, encouragement, and appreciation they provided. Prof. Anjan Dutta deserves special mention as he imparted the fundamental principles of the core subject through insightful lectures on structural dynamics. A special thanks goes to Prof. Hemant B. Kaushik for his valuable suggestions and insights during the review process, significantly enhancing the quality of this study. I sincerely acknowledge the time and patience of Dr. Sachin S. Gautam dedicated to this research work.

I would like to take this opportunity to express my appreciation to my seniors at IIT Guwahati, Dr. Nishant Sharma, Dr. Benazir Fatima Ahmed, and Soumi Rajbanshi, for their consistent encouragement, kind words, and unwavering support. Special recognition is due to my friends and colleagues at IIT Guwahati—Begum Emte Ajom, Nilanjan Samantha, and Jayawant S. Ghadge—for the enjoyable moments, laughter, and fruitful discussions that significantly enriched this journey; without them, life during this period would not have been the same.

I extend my heartful gratitude to my colleagues and seniors at NIT Manipur, whose support and motivation were instrumental in completing this thesis. I am also thankful to my special friends from Manipur who have consistently been there for me, providing encouragement and pushing me to reach this stage in my life.

Finally, the most significant figures in my life—my parents, little sister, and grandmother—are the ones to whom I am forever indebted for their unconditional love and care. They have consistently been my rock-solid support system, even during the darkest times.

TABLE OF CONTENTS

LIST OF FIGURES

LIST OF TABLES

LISTS OF SYMBOLS AND ABBREVIATIONS

SYMBOLS

Symbol	Description
a	: Intercept in log-space for the power-law relationship of seismic demand-response
a/v	: Ratio of peak ground acceleration to peak ground velocity
a_1, a_2	: Material constant in steel rebar
a_3, a_4	: Parameters determined experimentally in steel rebar
A_g	: RC structural wall cross-sectional area
$A95$	: Level of acceleration which contains up to 95% of Arias intensity
α_1	: Modal mass coefficient corresponding to fundamental mode
b	: Slope in log-space for the power-law relationship of seismic demand-response
$\bar{b}$	: Ratio between the strain hardening slope and modulus of elasticity
C	: Structural capacity limit
c_v	: Coefficient of variation
$c_{v_{S_a(T)}}^{NGMR}$	: Coefficient of variation of $S_a(T)$ values for $NGMR$ fragility surfaces, associated with EP of 16%, 50% and 84%
$c_{v_{S_a(T)}}^{NGMR+1}$	: Coefficient of variation of $S_a(T)$ values for $NGMR+1$ fragility surfaces, associated with EP of 16%, 50% and 84%
$\left(c_{v_{NGMR}}^{NGMR+1}\right)_{@S_a(T_i)}$	: Absolute value of ratio of the difference between $c_{v_{S_a(T_i)}}^{NGMR+1}$ and $c_{v_{S_a(T_i)}}^{NGMR}$ corresponding to different $S_a(T_i)$ values
$c_{v_{NGMR}}^{NGMR+1}$	: Average of $\left(c_{v_{NGMR}}^{NGMR+1}\right)_{@S_a(T_1)}$ and $\left(c_{v_{NGMR}}^{NGMR+1}\right)_{@S_a(T_2)}$
D	: Seismic demand
DS	: Damage state
d_y	: Yield displacement
d_u	: Ultimate displacement
DI_{HRC}	: HRC-damage index
ε_c	: Concrete strain
ε_{psc0}	: Concrete strain corresponding to the maximum compressive strength
ε_{pscU}	: Concrete strain corresponding to the ultimate crushing strength

ε_{sy} : Yield strain of steel rebar

ε_u : Ultimate strain of steel rebar

ε_s : Strain in steel rebar

ε_r : Strain corresponding to the point of reversal in the stress-strain relationship of steel rebar

ε_0 : Strain corresponding to the intersection of the elastic and yield asymptotic branches in the stress-strain relationship of steel rebar

E_c : Initial tangent modulus of concrete

EDP_i : Response value obtained from IDA

$\overline{EDP}$: Mean value of response parameter

$\overline{EDP}_i$: Calculated response values on the regression line

E_0 : Initial slope for concrete compressive stress-strain curve

E_{ts} : Concrete tensile elastic modulus

E_h : Strain hardening slope of steel rebar

E_s : Modulus of elasticity of steel rebar

f_c : Concrete stress

$f_c{}'$: Concrete compressive cylinder strength

f_{ck} : Characteristic concrete compressive cube strength

f_{pc} : Concrete compressive strength in 28 days

f_{pcu} : Concrete ultimate strength

f_t : Concrete tensile strength

f_y : Yield strength of longitudinal reinforcement bars

f_{yh} : Yield strength of transverse reinforcement bars

FS_{Tol} : Fragility surface tolerance value

GMR_{Tol} : Ground motion record tolerance value

H_w : Height of RC structural wall

IM^{DSi} : IM corresponding to a specific damage state threshold

K : Kent-Park concrete coefficient

L_{be} : Boundary element length in a RC structural wall

L_{be}/L_w : Ratio of boundary element length to wall length

L_w : Length of RC structural wall

M	: Magnitude of the earthquake
m_b	: Building mass
PF_1	: Participation factors corresponding to fundamental mode
$P/A_g f_{ck}$	: Axial load ratio
P	: Axial force acting at the top of RC structural wall specimen
R	: Sample correlation coefficient
R^2	: Coefficient of determination
R_m^2	: Confirmation index
$\bar{R}$	: Distance between the seismic source and the site
R'	: Cyclic curvature parameter
R_0	: Value of R' during initial loading
S_a	: Spectral acceleration
$S_{a,geo}(T)$	: Geometric average of spectral acceleration from the period range of 0.1 second to 2.5 seconds
$S_{a,geo}(T_1,2\times T_1)$	: Geometric average of $S_a(T_1)$ and $S_a(2\times T_1)$
S_a^{GMR}	: Spectral acceleration of an individual ground motion record spectrum
S_a^{TRS}	: Spectral acceleration of target response spectrum
$\left(S_{a_{NGMR}}^{NGMR+1}\right)_{@S_a(T_i)}$	: Absolute value of ratio of the difference between $\{S_{a(T_i)}^{NGMR+1}\}_{@50\%\,EP}$ and $\{S_{a(T_i)}^{NGMR}\}_{@50\%\,EP}$ corresponding to different $S_a(T_i)$ values
$S_{a_{NGMR}}^{NGMR+1}$	: Average of $\left(S_{a_{NGMR}}^{NGMR+1}\right)_{@S_a(T_1)}$ and $(Sa_{NGMR}^{NGMR+1})_{@S_a(T_2)}$
S_d	: Spectral displacement
S_i	: First-order Sobol sensitivity index
S_s	: Sample sizes
$S75$	: Slope of Husid plot between 5% and 75% of total Arias intensity
$S95$	: Slope of Husid plot between 5% and 95% of total Arias intensity
T	: Time period
t_i	: Trial number for deriving EFS
V	: Base shear
x_l	: Lower bound of the confidence interval for the mean of a log-normal distribution
x_u	: Upper bound of the confidence interval for the mean of a log-normal distribution

x_i : Confidence interval relative width

y_i : Simulated output for i^{th} sample

$\bar{y}$: Average of simulated outputs

y_i^* : Predicted output for i^{th} sample

$\overline{y^*}$: Average of predicted outputs

λ : Ratio between E_0 and the slope at ε_{psU}

σ : Standard deviation of the natural logarithm of response values

σ_{EDP} : Standard deviation of residual response parameter values from the regression line

σ_0 : Stress corresponding to the intersection of the elastic and yield asymptotic branches in the stress-strain relationship of steel rebar

σ_r : Stress corresponding to the point of reversal in the stress-strain relationship of steel rebar

σ_s : Stress in steel rebar

σ_{sy} : Yield stress in steel rebar

σ_u : Ultimate stress in steel rebar

σ_1^*, σ_2^* : Logarithmic standard deviation of vector valued IM

η_1^*, η_2^* : Logarithmic mean of vector valued IM

ξ : Viscous damping ratio

ζ : Magnitude of plastic strain from preceding excursion

δ_{DS} : Difference in exceedance probability of individual damage states

$\emptyset_{1,roof}$: Roof level amplitude of the fundamental mode

μ_d : Median value of EDP

β_{EDP} : Response parameter dispersion measure

β_A : Dispersion measure due to aleatory uncertainty

β_E : Dispersion measure due to epistemic uncertainty

β_M : Dispersion measure due to modelling uncertainty

β_{AE} : Dispersion measure due to both aleatory and epistemic uncertainties

$\beta_{AE,t}$: Dispersion measure due to aleatory, epistemic and modelling uncertainties

ρ : Population correlation coefficient

ρ^* : Correlation coefficient of vector valued IM

ρ_{be} : Boundary element longitudinal reinforcement ratio

ρ_{web}	: Web longitudinal reinforcement ratio
ρ_s	: Volumetric ratio of transverse reinforcement and concrete core
θ_{ds}	: Lateral Drift level at damage state threshold
Δ	: Absolute difference between dispersion measure for a specific S_s and those obtained when S_s = 50
Δ_{ISD}, $\Delta_{Sa(T1)}$	: Scatter measure value of IDA points
$\Delta_{DSi,sim}$	: Simulated lateral drift level for i^{th} sample at a specific damage state
$\Delta_{DSi,pred}$	: Predicted lateral drift level for i^{th} sample at a specific damage state
Δ_{IM}	: Average difference between $S_a(T_1)$ and $S_a(T_2)$ values
Δ_{FF}	: Average difference between fragility estimates for single IM and two IMs
Δ_{exp}	: Lateral drift limits reported in existing experimental studies
Δ_{pred}	: Lateral drift limits predicted using proposed expressions
Δ_{roof}	: Lateral displacement

ABBREVIATIONS

Notation	Description
ADRS	: Acceleration-Displacement Response Spectra
AI	: Arias Intensity
AIFS	: All-Inclusive Fragility Surfaces
ALR	: Axial Load Ratio
AR	: Aspect Ratio
CP	: Collapse Prevention
CSM	: Capacity Spectrum Method
EDP	: Engineering Demand Parameter
EFS	: Efficient Fragility Surfaces
EP	: Exceedance Probability
ExIDA	: Extended Incremental Dynamic Analysis
FEM	: First Element Method
FOSM	: First-Order Second Moment
GP	: Genetic Programming
HRC	: Homogenised Reinforced Concrete
IDA	: Incremental Dynamic Analysis

IM	: Intensity Measure
IO	: Immediate Occupancy
ISD	: Inter-Storey Drift
LHS	: Latin Hypercube Sampling
LS	: Life Safety
MDOF	: Multi Degree of Freedom
MAE	: Mean Absolute Error
MFA	: Maximum Floor Acceleration
ML	: Machine Learning
MSC	: Maximum Story Curvature
MCC	: Maximum Concrete Compressive Strain
MCS	: Monte-Carlo Simulation
NDA	: Nonlinear Dynamic Analysis
NSA	: Nonlinear Static Analysis
PBEE	: Performance-Based Earthquake Engineering
PGA	: Peak Ground Acceleration
RC	: Reinforced Concrete
RD	: Roof Displacement
RMSE	: Root Mean Square Error
SD	: Significant Duration
SDOF	: Single Degree of Freedom
SRSS	: Square Root of the Sum of the Squares
TDA	: Tornado Diagram Analysis
XGBoost	: Extreme Gradient Boosting

CHAPTER 1

INTRODUCTION

1.1 Overview

Over the past few decades, earthquakes have emerged as one of the most catastrophic natural occurrences, causing significant loss of human lives and valuable properties. On an annual basis, approximately 20 major earthquakes, with magnitudes surpassing 7, are recorded worldwide, leading to immense devastation, particularly in terms of human casualties. Moreover, the swift economic expansion and contemporary urbanization have resulted in a considerable concentration of the population within relatively smaller urban areas. Consequently, there has been a notable rise in the construction of tall and slender buildings to address the needs of accommodating the continuously growing populace. Depending on the structural characteristics, those tall buildings can be extremely vulnerable to the severe earthquake shaking. Thus, it is imperative to consider seismic risk assessment with a focus on the primary source of damage, namely, the insufficient seismic resilience of the constructed surroundings.

One of the common categories of multistoried buildings seen in urban areas is the Reinforced Concrete (RC) frame building. In earthquake-prone regions, RC structural walls are provided in these buildings to enhance the seismic resistance through increased lateral strength and lateral stiffness. This also leads to reduction of lateral sway of the building and overall improvement in the lateral stability during severe earthquake shaking. The same is also highlighted through the famous statement: *"We cannot afford to build multi-storeyed reinforced concrete buildings meant to resist severe earthquakes without shear walls."* - Mark Fintel, a noted consulting engineer in USA.

Based on the tectonic settings, over 50% of the landmass in India is prone to moderate to severe earthquake shaking (Sitaram et al., 2015). The seismic vulnerability of the country's current building infrastructure has been starkly revealed on various occasions by historical earthquakes (Figure 1.1). This unequivocally underscores the vulnerability of the entire spectrum of buildings across the nation to earthquakes. This vulnerability encompasses not just non-engineered rural dwellings but also engineered multi-story structures in urban regions, all of which remain inadequately shielded against seismic events. While it is

established that high magnitude earthquakes occur relatively infrequently as compared to the low magnitude earthquakes, there exists a tendency among the general population and local regulatory entities to overlook the importance of earthquake-resistant design while constructing buildings, primarily based on the financial considerations. Furthermore, a majority of conventional RC structures in the Indian subcontinent have been built primarily to withstand gravity loads, devoid of any regard for seismic resilience. Despite stringent seismic design regulations, stakeholders often overlook them due to economic constraints and a shortage of skilled labour. As a result, it becomes imperative to analyse the structures' susceptibilities under varying earthquake levels, with the primary objective of evaluating potential losses of life and property damage caused by earthquakes.

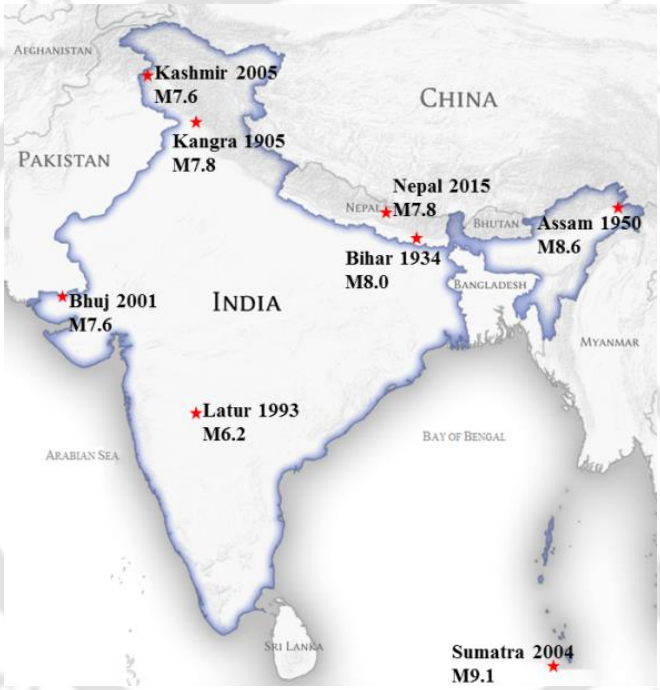

Figure 1.1 Map showing a few of the major earthquakes recorded in India

Within the realm of seismic risk assessment, it is a customary practice to conduct seismic vulnerability analyses. These analyses serve the purpose of quantifying the probability that systems facing potential risks will experience varying levels of damage across a spectrum of intensities of seismic hazard. This is achieved through the development of fragility relationships, aiming to link a specific seismic intensity level with an appropriate seismic response parameter.

The evaluation of seismic vulnerability for structures typically involves a two-step methodology. Initially, fragility assessment is performed, establishing a relationship between

the actual damage incurred and a quantifiable measure of seismic intensity. Subsequently, in the following stage, fragility functions are translated into vulnerability functions using suitable damage-to-loss relationships. It is within this framework that the fragility estimates are gaining increasing significance as an irreplaceable instrument for seismic risk evaluation, forging a linkage between the seismic hazard inherent to a zone and the consequences of potential earthquakes on the built environment. In essence, fragility functions depict continuous relationships that outline the probabilities related to a system(s), pertaining to the attainment or exceedance of predetermined levels of damage across various levels of earthquake intensities.

1.2 Major Concerns and Need of the Study

The concept of structural fragility to seismic forces is inherently tied to uncertainty, which arises from various sources of both aleatory (random) and epistemic (knowledge-based) factors (Ellingwood and Kinali, 2009; Der Kiureghian and Ditlevsen, 2009). The lack of a clear consensus on how to accurately incorporate aleatory and epistemic uncertainties into seismic fragility predictions, particularly in relation to buildings with RC structural walls, often impedes the establishment of reliable and coherent risk assessment protocols. Moreover, the dispersion measurement values that represent different uncertainties, specified in the seismic design standards and guidelines, lack categorization for distinct building archetypes and intermediate structural performance levels. Consequently, there is a major requirement to meticulously delineate and propagate the various sources of uncertainty throughout the analysis process in order to ensure reliable estimates of seismic damage for buildings with RC structural walls.

For the efficient execution of Performance-Based Earthquake Engineering (PBEE), the establishment of well-defined, measurable thresholds for distinct levels of damage states is essential, with a particular emphasis on the critical structural components inherent to a building system. While seismic damage to other elements can carry implications for structural safety and economics, the significance of structural walls as the central component of the lateral load-resisting system in wall-frame structures necessitates a thorough assessment and effective estimation of the probabilities associated with attaining various damage states in these essential structural elements. The existing definitions of damage states for RC structural walls rely on empirical limits and do not offer predictions for damage thresholds derived from the fundamental design attributes of the wall.

Ensuring a reliable assessment of the vulnerability of RC structures requires the accurate representation of seismic loading in dynamic response analyses. As earthquake shaking is random in nature, representation of the unpredictable seismic loading becomes a challenge. For fragility estimates, the prevalent approach has been to predominantly rely on a single parameter to relate the level of seismic intensity (loading) and the projected structural damage in terms of fragility relations. Nonetheless, relying solely on a solitary ground-motion parameter disregards the variability inherent in estimated damage, potentially resulting in significant consequences for the accurate seismic fragility assessment of structures.

Assessing analytical fragility relations for the vulnerability evaluation of RC structures demands substantial computational time, particularly in conducting essential dynamic analyses. While striving for a more precise depiction of seismic hazard in PBEE, development of fragility relations using vector-valued Intensity Measures (IMs) can enhance accuracy but requires significantly increased computational efforts as compared to single IM-based fragility functions. Efficiently choosing a set of ground motion records that aptly represent a seismic scenario is a fundamental step in estimating optimal fragility functions. Existing earthquake record selection criteria are often based on factors like magnitude, site-to-source distance, and duration, with limited attention to the building's structural attributes. Incorporating an additional criterion into the selection process, one that ensures the chosen input records best mirror the seismic response of the studied structures, would be a valuable addition. The present study aims to incorporate the mentioned aspects in seismic fragility assessment of RC frame building with structural walls.

1.3 Objectives of the Present Study

The present study aims to conduct a comprehensive seismic fragility assessment of RC wall-frame buildings. The salient objectives of the present study are:

(a) To study the characterization and propagation of both aleatory and epistemic uncertainties through nonlinear response analyses for fragility formulation of RC wall-frame building.

(b) To prescribe closed-form expressions for predicting lateral drift levels at various damage state thresholds, contingent upon primary wall characteristics.

(c) To offer seismic fragility estimates for RC wall-frame building using both scalar intensity measures and vector-valued intensity measures.

(d) To optimize the computational effort by deriving accurate fragility functions for a reduced set of ground motion records, while maintaining comparability with estimates from the complete set of ground motion records.

1.4 Organisation of the Dissertation

The dissertation comprises eight chapters, including the current one, which serves as an introduction to the research topic and emphasizes the importance of conducting the present study. Chapter 2 offers an updated summary of research on assessing the seismic vulnerability of RC structural systems. It reviews different assessment methods, discusses their pros and cons, and emphasizes the need for a careful examination of various factors, such as fragility parameters and uncertainty modelling. The chapter also underscores the importance of defining damage states in earthquake performance assessments. It includes a comprehensive review of relevant studies, particularly those focused on RC wall-frame buildings, identifying areas where past research has been lacking. In conclusion, the chapter outlines the research scope based on these identified gaps.

Chapter 3 offers a concise overview of the modelling approaches used in the present study. This includes a validation study aimed at confirming the accuracy of the modelling methodology and finite element framework utilized, with a comparison to existing experimental data from the literature. Additionally, the chapter delves into the selection of the appropriate parameters for deriving fragility functions, specifically focusing on input ground motions and EDP required for formulating these probabilistic functions.

Chapters 4 and 5 are aimed at appropriate characterization and propagation of the different sources of uncertainty pertaining to fragility analysis of structural systems. Chapter 4 specifically examines the impact of uncertain structural parameters on different response parameters of the considered RC wall-frame structure through a sensitivity analysis. This analysis employs a regression-based machine learning approach and Sobol sensitivity indices to assess the relative importance of these uncertainties. Chapter 5 establishes a comprehensive framework by applying extended Incremental Dynamic Analysis (IDA) to the considered RC wall-frame building, integrating both ground motion randomness (aleatory) and uncertainty in structural capacity (epistemic) into seismic response analysis. The chapter illustrates the quantification of dispersion measures for various considered uncertainties, which is determined through statistical analyses of the summarized IDA curves.

In an effort to establish reliable fragility estimates for various performance levels of the studied building typology, Chapter 6 introduces the development of precise expressions for predicting lateral drift at different damage states. Using Genetic Programming algorithm and drawing from an extensive dataset of several numerically analysed RC structural wall specimens, the chapter incorporates various wall structural parameters in the estimation of these expressions. The chapter further includes an evaluation of the performance of the developed expressions by comparing them with few of the existing damage state thresholds when predicting a subset of the available experimental results for RC wall components.

Chapter 7 signifies the concluding part of the present work, where the previous chapters' findings are integrated to achieve the overall objective: assessing the fragility relationships for the considered RC wall-frame building. Within this chapter, fragility relationships are developed and evaluated for both a specific RC wall-frame structure and the entire RC wall-frame building. This chapter aims to assess and analyse how different sources of uncertainty collectively impact seismic fragility. Additionally, it investigates and compares the characteristics of the established fragility relationships when considering scalar IMs with vector-valued IMs. In conclusion, the chapter presents a simplified procedure for deriving fragility estimates with fewer ground motion records, ensuring their compatibility with estimates obtained from the complete record set.

Finally, Chapter 8 provides an overview of the key findings of the research, discusses significant conclusions drawn from the study, and briefly addresses the study's limitations and outlines potential scope for future research.

CHAPTER 2

REVIEW OF LITERATURE

2.1 Overview

Fragility functions play a pivotal role in evaluating the seismic integrity of structural systems and offer a multifaceted means to perform vulnerability assessment for systems at potential risk to seismic hazard. Fragility assessments involve the evaluation of the seismic performance of structures that exemplify the prevailing building typology at a specific site. These evaluations result in fragility functions, which depict the likelihood of a specific degree of damage as a consequence of various earthquake scenarios. Vulnerability of a building stock under the impact of a particular seismic event is a direct reflection of the structural seismic response; utilizing an appropriate seismic loss prediction model, the resulting fragility relationships can be used for deriving the economic impacts on the society from the seismic hazard.

In order to evaluate the seismic fragility estimates for structures, it is essential to have a comprehensive understanding of the assessment methodologies. The objective of this chapter is to present a concise overview of past studies pertaining to seismic fragility assessment of RC building structures. In this context, various methodologies previously advocated in the literature for conducting seismic fragility assessments have been examined and are presented here. The advantages and disadvantages associated with the commonly employed procedures for fragility assessment are underscored. Seismic fragility estimates, being probabilistic in nature, demands a keen introspection of the various aspects associated with the formulation of these relationships, like the choice of different fragility parameters, uncertainty modelling etc. The fragility relationships that emerge from vulnerability studies depict the probability of exceeding various levels of damage states under a given seismic intensity level. This highlights the crucial necessity of reviewing and comprehending the structural damage state definitions utilized in the contemporary studies on seismic performance assessment. Lastly, a thorough review of pertinent seismic fragility studies, specifically those performed for RC wall-frame buildings has been undertaken. Based on the review of the past studies, areas that have not been addressed in detail in prior fragility studies of RC building structures have been identified. Finally, based on the identified gap areas of research, the scope of work for the current study is outlined.

2.2 Seismic Fragility Assessment Procedures

Various methodologies worldwide, notably in Japan and the United States, have significantly advanced the development of fragility relationships. However, a cautious approach is essential when adopting default fragility functions to characterize the seismic vulnerability of a structural system or the factors influencing the corresponding fragility relationships. A prime example is the widely-used HAZUS recommendations (FEMA, 2003) for fragility estimation, initially devised for US buildings but broadly applied globally, leading to disparities when structures adhere to diverse seismic design codes. Such complexities are particularly prominent when investigating extensive building inventories with constrained data acquisition capabilities. Discrepancies in construction methods, even within identical code standards, indicate substantial influence over fragility and vulnerability functions. Consequently, it is advisable to derive fragility estimates utilising structural performance evaluation results obtained from nonlinear analyses of the reference structure(s) (D'Ayala and Meslem, 2013). Originally introduced for evaluating vulnerability of nuclear power plant structures, seismic fragility analysis entails constructing fragility curves that quantify the probability of exceeding certain structural performance levels with increasing seismic intensity (Kennedy et al., 1980). These curves outline the exceedance probability of various structural performance thresholds (Figure 2.1). Seismic damage metrics, known as damage-states, characterize these thresholds, and each curve denotes the likelihood of exceeding a specific damage state with the increase of seismic intensity level.

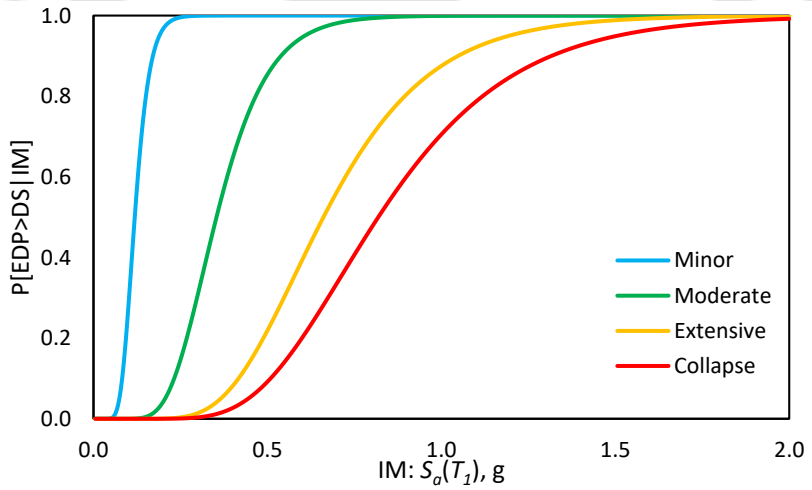

Figure 2.1 Schematic fragility curves for different seismic performance levels.

Fragility refers to the degree to which built environment might be harmed or disturbed by the effects of a specific hazard. This vulnerability of structure(s) is influenced by factors like

their characteristics, construction, and closeness to seismically active regions. It is imperative that seismic fragility is significantly conditioned on the capacity of the structural system to resist seismic forces. It signifies how likely a structure is to be damaged due to a specific intensity level of seismic loading. The primary objectives of evaluating structural fragility to seismic events are as follows:

- Estimating the susceptibility of structures and infrastructure to seismic hazards.
- Determining structural deficiencies and prospective regions of damage in the built environment.
- Diminishing the consequences of seismic events on structures and communities.
- Classifying structures based on their susceptibility to allocate resources more efficiently.
- Evolving measures to amplify the seismic resistance of structures.
- Contributing information to facilitate the development or enhancement of seismic building codes and regulations.
- Facilitating post-major earthquake emergency management.

Evaluating the seismic fragility of different building types through advanced methodologies holds significant importance in mitigating seismic risks within urban regions. To enhance seismic risk management for infrastructure networks, there's a clear need for a futuristic and comprehensive methodological tool. This tool would facilitate streamlined and impactful mitigation strategies. Given this context, numerous organizations in earthquake-prone regions have developed standards and recommendations to guide the assessment of the anticipated response, strength, and safety of existing structures.

Drawing from previous literature, procedures for seismic fragility assessment can be mainly classified as (a) expert elicitation or judgemental methods, (b) empirical methods, (c) analytical methods and (d) hybrid methods.

2.2.1 Expert Elicitation or Judgemental Methods

The most ancient and straightforward technique among the aforementioned approaches is the expert elicitation method or judgemental method. In this technique, civil engineers possessing expertise in the realm of seismic engineering estimate the damage probability of a structural system under varying levels of seismic intensities. The development of a structured method for enhancement of the expert based approach of developing fragility functions involved the contributions of various authors. Cooke and Goossens (2000), for example, introduced standard convention, exhaustive methodologies, and recommendations for the approach of

eliciting expert opinions, along with strategies for incorporating such information into uncertainty assessment. The expert opinion approach relies entirely on the judgments of designated experts who evaluate the average loss or the likelihood of damage to the structural systems exposed to seismic hazards. This method proves particularly valuable in scenarios with limited actual damage information from previous seismic events or in situations where appropriate numerical models are unavailable. In their study, Clemen and Winkler (1999) stated that expert elicitation data is aggregated using two basic criteria: mathematical and behavioural. Broadly speaking, mathematical techniques for eliciting expert judgments are generally considered to be more dependable, replicable, and impartial in consolidating expert opinions as compared to behavioral methods (Jaiswal et al., 2012; Rossetto et al., 2014).

In mathematical approaches for expert judgment elicitation, experts independently present their personal probability assessments for uncertain quantities, without mutual interaction. These estimates are subsequently integrated mathematically, frequently employing procedures that involve either weighting each individual's assessments (as demonstrated by Cooke in 1991) or employing Bayesian metrics (as shown by Morris in 1997). Jaiswal et al. (2012) utilized Cooke's classical approach (Cooke, 1991), based on mathematical approach of expert elicitation method, to formulate fragility relationships associated with collapse damage state for RC and unreinforced masonry structures, correlated with Peak Ground Acceleration (PGA).

Conversely, behavioural approaches strive to foster a form of collective agreement among experts, often prompting them to engage in mutual interaction and exchange their evaluations. A widely recognized behavioural approach is the Delphi methodology, which originated in the early 1950s through the work of Dalkey (1969). This method involves experts anonymously evaluating estimates provided by eight other experts in the panel. Each expert subsequently has an opportunity to reassess their original evaluation in light of the reviews from their peers. The procedure continues iteratively until a specific degree of concurrence or consensus is achieved among the expert evaluations. Subsequently, this approach integrated a self-rating system, enabling experts to assess their own estimates.

Billah and Alam (2014) emphasized the findings of ATC-13 (1985), a document that compiles damage matrices and risk assessments for prevalent infrastructures in California based on the input of 42 expert opinions. Guided by their input, a Damage Probability Matrix (DPM) emerged, with the seismic hazard characterized by the modified Mercalli intensity

measure. Expert elicitation exclusively drives this methodology, hinging on questionnaires, expert assessments, and the quantity of consulted experts. However, these evaluations may encompass variabilities and slightly compromise accuracy, thereby influencing robustness of the outcome.

The steps involved in fragility assessment of structural systems based on expert elicitation methodology are presented in Figure 2.2. The diagram illustrates that following the establishment of a well-suited panel consisting of experts in earthquake engineering, a pertinent set of questionnaires or survey forms is devised.

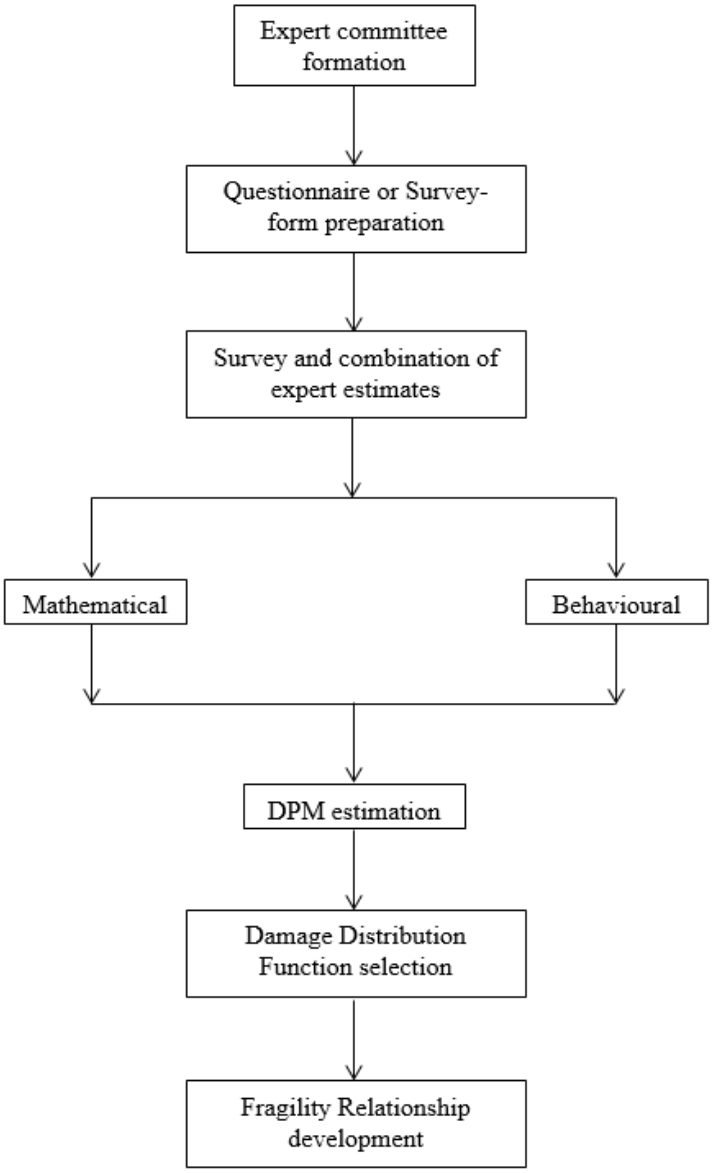

Figure 2.2 Procedure to evaluate fragility function based on expert elicitation.

Drawing on their expertise and insights gained from prior seismic events, the experts provide the estimates. Utilizing the feedback from the expert council, a damage matrix encompassing

IM and corresponding damage scenarios can be formulated. This can be achieved by employing either the mathematical or behavioural approach to combine the data. By utilizing the DPM in conjunction with an appropriate distribution function, fragility relationships can be derived.

2.2.2 Empirical Methods

The fragility functions developed by the empirical methods are formulated using observed damage data subsequent to seismic event occurrences. Numerous researchers have constructed empirical fragility functions through comprehensive surveys of structural systems exposed to seismic forces. Basoz and Kiremidjian (1997) conducted pioneering research in the realm of empirical fragility functions. Derived from field damage observations following the 1994 Northridge earthquake, fragility relationships were established through the employment of logistic regression techniques. Similarly, Yamazaki et al. (1999) formulated fragility curves utilizing reconnaissance data from the 1995 Kobe earthquake. In the context of the same Kobe earthquake, Shinozuka et al. (2000) and Der Kiureghian (2002) assessed fragility function parameters using the Maximum Likelihood Method and Bayesian technique, respectively. Recently, Gaudio et al. (2023) developed empirical seismic fragility curves for different RC building structures in Italy, utilizing post-earthquake damage data acquired from the Irpina (1980) and L'Aquila (2009) earthquakes.

During the early years, the empirical methodology for developing fragility functions was established and calibrated based on macroseismic intensities. This approach emerged due to the prevailing practice of defining hazard maps predominantly in relation to these distinct damage scales, as elaborated by Calvi et al. (2006). Empirical methods stood as the primary and feasible approach for several years in formulating extensive seismic risk assessments of the vulnerable structural systems. The empirical fragility estimates rely on the data source from which the on-field reconnaissance data were collected. Typically, this data is acquired from either a single seismic event or multiple occurrences.

Deriving fragility curves from actual on-field damage data offers the advantage of incorporating the impact of practical scenarios like soil-structure interaction, site effects, and the diverse seismic responses of specific structural systems, including their failure modes. Nonetheless, a significant limitation lies in the fact that the resultant curves are inherently tied to a specific geographic region represented by distinct soil conditions, seismic attributes (such as magnitude, focal depth, hypocentral distance), and structural characteristics.

Additionally, only a limited number of regions worldwide have managed to contribute to post-seismic event damage and loss-to-damage ratio data from a substantial quantity of structural systems, reaching a scale that permits the establishment of dependable empirical fragility functions.

The steps involved in formulation of empirical fragility relationships are presented in Figure 2.3. Empirical methodologies typically yield results in two distinct forms: seismic response-damage interrelation, *i.e.*, in terms of DPMs and fragility curves. In the initial form, the expected likelihood of reaching a specific damage level when subjected to a certain seismic intensity level is depicted discretely, while in the later form, the likelihood of exceeding a particular damage state threshold is represented as a continuous function of the seismic intensity level.

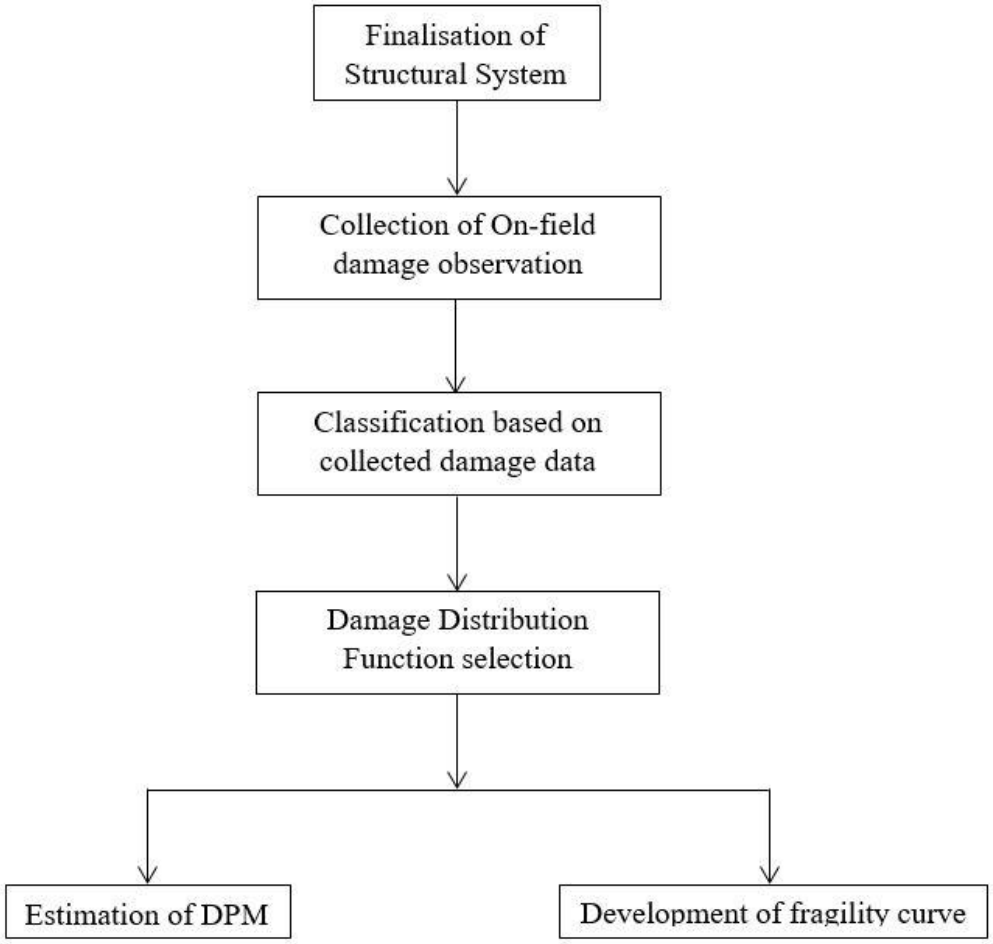

Figure 2.3 Procedure to evaluate fragility function based on empirical methodology.

2.2.3 Analytical Methods

Analytical methods are often used to develop fragility functions due to their superior ability to represent seismic vulnerability from a structural engineering perspective. These approaches establish an explicit connection between structural system attributes, seismic response parameters, and the resulting structural damage (Rossetto et al., 2013). In the past decade, these analytical fragility models have garnered growing interest in the academic discourse, which is attributed to their capacity to address the shortcomings of subjective expert-elicitation based fragility estimates and empirical fragility functions restricted insufficiency of data (Gidaris et al., 2017). As computational capabilities and modelling approaches continue to progress, enabling the incorporation of diverse structural response characteristics such as shear-flexure-axial interaction, soil-structure interaction, concrete confinement action, and buckling of steel rebars, improved analytical methodologies for deriving fragility relations have been proposed (Rossetto and Elnashai, 2003). Also, as highlighted by Calvi et al. (2006), the technological enhancement in evaluation of seismic hazard like the use of spectral ordinates in seismic hazard maps instead of traditional measures (macro-seismic intensity or PGA), contribute to the ever-increasing popularity of analytical procedures in seismic risk analyses.

Fragility relationships can be derived utilizing a wide range of analytical procedures, such as elastic spectral analysis, nonlinear static analysis (Shinozuka et al., 2000) or nonlinear response history analysis (Ji et al., 2009) and Incremental Dynamic Analysis (IDA) (Nazari and Saatcioglu, 2017, Manfredi et al., 2023). Section 2.3 outlines and deliberates on the predominant procedures related to the utilization of analytical techniques in establishing fragility functions. Relying on numerical models to evaluate the seismic response of structures, analytical procedures provide the advantage of directly, transparently, and comprehensively considering various structural element attributes, alongside clearly addressing uncertainties inherent to assessment processes. However, it's important to note that these analytical methods inherently demand a greater volume of exhaustive input details and are computationally more intensive, in comparison to empirical procedures (Del Gaudio et al., 2015).

Figure 2.4 shows the procedural steps of seismic fragility assessment for structural systems using analytical methodologies. These methodologies involve initially developing an accurate numerical model that well represents the considered structural system. A decision must be

made regarding the trade-off between the reliability and complexity of the model and its cost-effectiveness. The developed numerical models need to be analysed using appropriate performance assessment techniques to establish a correlation between structural damage levels and various seismic intensity levels. The resulting structural response obtained from numerical analyses is then integrated with seismic demand to derive fragility relationships through suitable probabilistic seismic demand models.

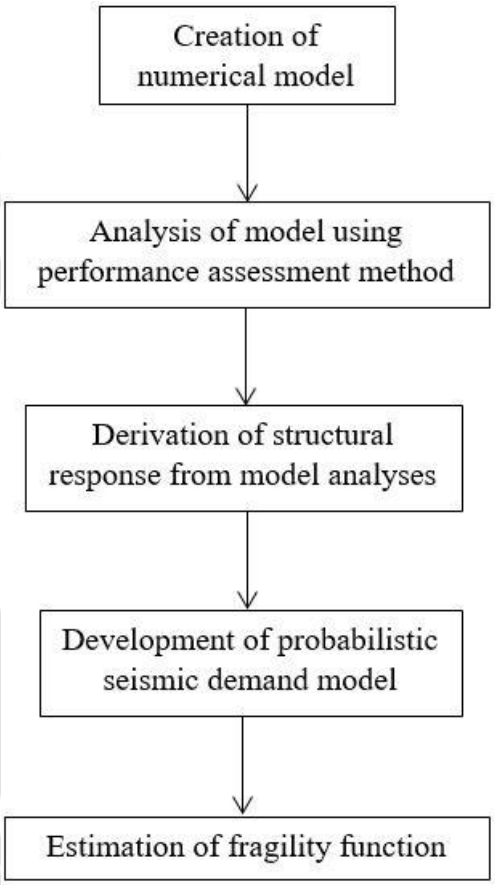

Figure 2.4 Procedure to evaluate fragility function based on analytical methodology.

2.2.4 Hybrid Methods

Beyond the primary three methodologies discussed earlier for formulating fragility functions for structural systems, there exists a fourth category of procedure known as hybrid method. This approach integrates various data sources, including analytical, empirical, or expert elicitation-based information. Various techniques for estimating fragility relationships come with their own set of strengths and limitations. To address the limitations inherent in other approaches, such as insufficient post-earthquake damage statistics, subjectivity in expert-elicitation based data, and uncertainties and modelling shortcomings linked to analytical methods, the concept of hybrid fragility curves have been introduced in the past literature.

The hybrid procedure aims to minimize the computational complexity of analytical modelling based fragility estimation while mitigating the subjective bias inherent in the expert elicitation based method (Kappos et al., 2006).

Hybrid DPM and fragility functions typically combine damage data from actual seismic events (empirical data), which closely resemble the geographical region and building typology under examination, with structural seismic response data obtained from analyses of numerical models representing the reference structural system (analytical data) (Calvi et al., 2006). Among the initial hybrid approaches, Kappos et al. (1998) introduced a methodology where the structural damage statistics utilized to evaluate fragility relationships was obtained through a fusion of numerical analyses and post-seismic event reconnaissance inspections. Kappos et al. (1998) have performed vulnerability assessment of the prevalent RC building inventories in Greece through hybrid approach, incorporating the results from nonlinear dynamic and static analyses of the scenarios for which no empirical data were available, highlighting the potential of such methodologies. Penelis et al. (1989) utilized the hybrid technique to evaluate fragility functions, merging IDA results with the damage data observed after the Thessaloniki earthquake of 1978. Tian et al. (2023) also developed seismic fragility estimates for RC structural wall systems using a hybrid approach that integrates results from experiments and numerical simulations.

While hybrid methodologies provide an alternative for estimating suitable fragility functions, they do come with a few limitations, including the need for extrapolating seismic damage statistics and establishing the relationship between seismic hazard and seismic response of the structures (Kappos, 1997). Also, this approach includes considerable aleatory and epistemic uncertainties, leading to substantial variance within the probabilistic model. Despite garnering significant research attention, the application of this method for developing fragility functions remains relatively constrained in the context of buildings.

The advantages and disadvantages of different methodologies for developing fragility estimates are presented in Table 2.1.

Table 2.1 Strength and limitations of different approaches for estimating fragility functions

Method	Advantages	Disadvantages
Expert elicitation based	Useful in absence of sufficient actual damage observation. Elementary procedure.	Highly subjective. Entirely conditioned on competency of the experts.

	All elements considered.	Lacks accuracy and frequently skewed.
Empirical	Exhibit the real seismic fragility. Portray an accurate depiction.	Site and building-specific. Insufficient information. Variability in damage assessment.
Analytical	Enhanced accuracy. Reduced skewness. Various uncertainty sources considered.	Computationally expensive. Time-intensive. Conditioned on performance assessment techniques used.
Hybrid	Combines empirical and analytical approach. Can consider post-seismic event damage observation statistics. Computationally efficient.	Necessity for diverse data inputs. Significant variability in the demand model.

2.3 Seismic Performance Assessment Procedures

This section offers an extensive examination of prominent seismic performance assessment techniques; whose outcomes serve as the foundation for estimating analytical fragility functions. The objective is to enhance comprehension of these methodologies by signifying and discussing their key facets, thereby elucidating the benefits and limitations of various approaches to facilitate informed decision-making processes. The rising popularity of employing analytical methodologies to develop fragility functions can be attributed to their capability to accurately depict the relationship between structural response and seismic demand. However, there exists a consensus within the academic circle regarding the necessity of striking a suitable equilibrium between the advantages offered by analytical procedures and the greater allocation of resources needed for executing the structural performance analyses for generating analytical fragility relationships. A range of performance assessment techniques, spanning from basic static analysis to advanced nonlinear time history analysis, have been utilized in the past to simulate structural responses under seismic loading and create analytical fragility functions. The subsequent sections present a concise outline of the various existing performance assessment methods employed to derive analytical fragility functions.

2.3.1 Nonlinear Static Analysis

Nonlinear Static Analysis (NSA), commonly referred to as pushover analysis, has gained extensive recognition as a pivotal analytical method for evaluating how seismic forces impact both new and pre-existing structural systems when exposed to diverse load scenarios. In stark contrast to linear analysis, which presumes a straightforward correlation between forces and displacements, NSA takes into account the nonlinear characteristics exhibited by materials and the geometrical complexities that can arise as loads intensify. True to its name, this approach primarily constitutes a static analysis, wherein static loads are incrementally applied until the structure reaches its collapse state. The term "nonlinear" arises from the utilization of nonlinear numerical models to represent the structural system. NSA provides valuable insights into possible failure modes, patterns of deformation, and the structural capacity to resist loads. As a result, it becomes an invaluable instrument for appraising structural soundness, formulating retrofit tactics, and strengthening overall safety amidst intricate loading circumstances. Among commonly used NSA procedures for assessing structural seismic responses, methods like the Capacity Spectrum, Displacement Coefficient, and N2 are often employed.

- **Capacity-Spectrum Method**

The comprehensive approach of the Capacity Spectrum Method (CSM) involves conducting a nonlinear pushover analysis to derive the pushover curve, depicting the relationship between base shear (V) and lateral displacement (Δ_{roof}). Subsequently, this pushover curve, also referred to as the capacity curve, is transformed into a capacity-spectrum curve. This curve, characterized by bilinear or multilinear acceleration-displacement relationships, effectively represents the response of the structures under the influence of both gravity and lateral forces. The performance point is established through the overlay of the capacity spectrum curve with the seismic demand curve, obtained from the response spectra. The intersection of these two curves signifies the seismic performance point (Freeman, 2004). With the performance point determined for different ground motion intensity, the corresponding fragility functions can be derived subsequently.

The process of transforming the demand curve and capacity curve into Acceleration-Displacement Response Spectra (ADRS) format, a crucial step in CSM, is schematically depicted in Figure 2.5. Using established protocols rooted in the fundamentals of structural dynamics, the response spectrum curve for a specific earthquake record can be estimated.

Converting a response spectrum from the conventional representation of spectral acceleration (S_a) plotted against time period (T) to the ADRS format requires the calculation of the corresponding spectral displacement (S_d) value for each data point along the curve. This transformation is achieved through the utilization of Eq 2.1. To generate the capacity spectrum from the capacity curve, a step-by-step transformation to fundamental mode spectral coordinates is required. Each point (V, Δ_{roof}) on the capacity curve is then transformed into the corresponding point (S_a, S_d) on the capacity spectrum as,

$$S_d = \frac{T^2}{4\pi^2} S_a \tag{2.1}$$

$$S_a = \frac{V}{W \times \alpha_1} ; S_d = \frac{\Delta_{roof}}{PF_1 \times \emptyset_{1,roof}} \tag{2.2}$$

where, α_1 and PF_1 are the modal mass coefficient and participation factors corresponding to the fundamental mode of the structure, respectively. $\emptyset_{1,roof}$ is the roof level amplitude of the fundamental mode.

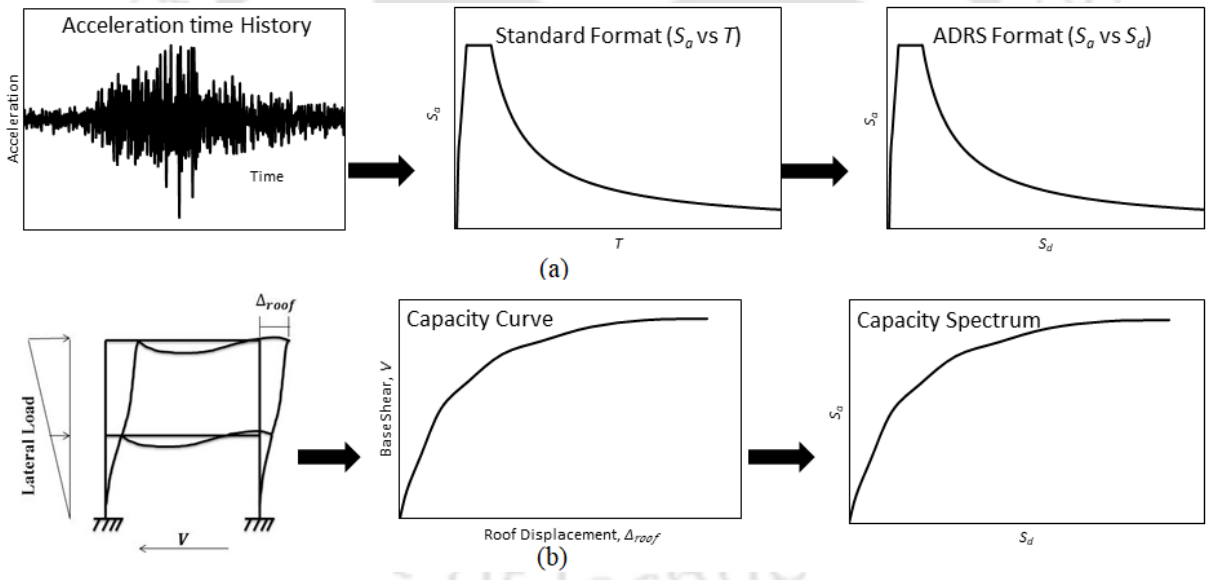

Figure 2.5 Graphical representation of steps for deriving (a) Response Spectrum and (b) Capacity Spectrum in ADRS format.

Initially introduced by Freeman et al. (1975), the Capacity Spectrum Method (CSM) was employed as a rapid assessment technique to perform the seismic vulnerability assessment of structural elements at Puget Sound Naval Shipyard, Washington. Following its inception, this method has been incorporated into seismic design standards and regulations across the globe. For instance, ATC-40 (1996) suggested three options for employing the CSM, denoted as techniques A, B, and C. Techniques B and C presented challenges in terms of implementation

and programming due to the overgeneralizations inherent in technique B and the substantial graphical constituents in technique C. Technique A offers a rather simplified analytical approach that can be readily implemented into software frameworks. This procedure necessitates an iterative approach to achieve convergence on the performance point, ensuring that the demand spectrum intersects with the capacity spectrum within an acceptable tolerance level. However, there were criticisms of the proposed technique A by Fajfar (1999) and Chopra and Goel (2000), who argued that it tends to underestimate structural deformation. As a result, modifications were introduced to technique A in FEMA-440 (2005), particularly in the estimation of equivalent viscous damping, which represents hysteretic damping. Furthermore, the Modified Acceleration-Displacement Response Spectrum was developed as an enhancement to accurately depict seismic demand by scaling down the elastic response spectrum, which is influenced by changes in structural ductility and damping. Figure 2.6 illustrates a schematic representation of the performance point where the capacity spectrum and the demand spectrum intersect.

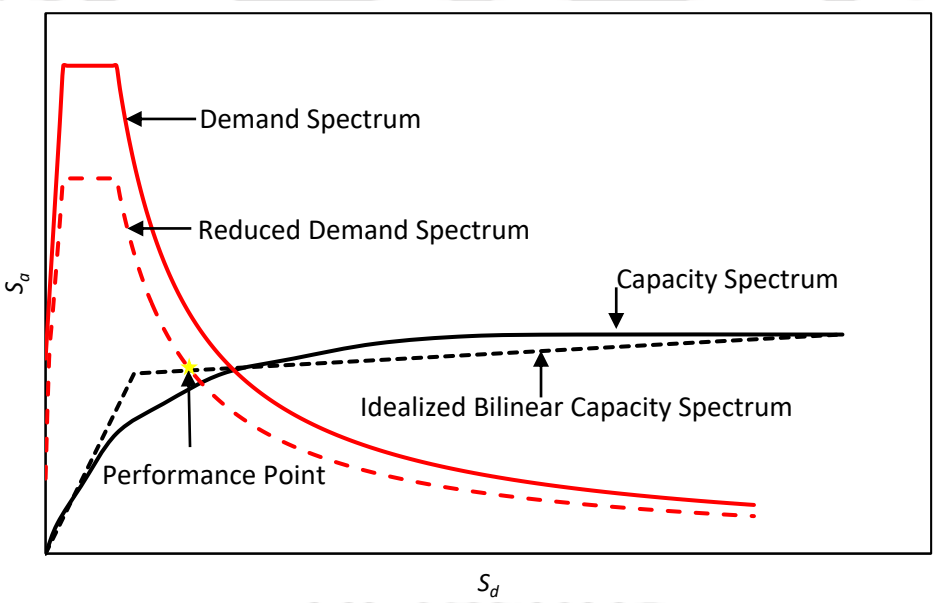

Figure 2.6 Performance point as per CSM (ATC-40, 1996).

The primary benefit of CSM lies in its reliability as a simplified static approach for emulating the dynamic seismic behaviour of structural systems. Additionally, since this analysis is conducted until failure, it facilitates the assessment of both collapse load and ductility capacity. The generation of a capacity curve through pushover analysis cannot directly incorporate the exact input ground motion leading to collapse, as the dynamic attributes are not considered in the analysis. Furthermore, the inclusion of higher mode effects once a

localized mechanism is initiated and concerns regarding cumulative damage have been highlighted as notable limitations of pushover analysis.

2.3.2 Nonlinear Dynamic Analysis

Nonlinear Dynamic Analysis (NDA) stands as a more thorough and meticulous approach that records the time-dependent response of structures to dynamic loads. It explicitly accommodates the fluctuating forces and displacements over time, providing a more precise portrayal of how a structure behaves under seismic forces. NDA incorporates the dynamic interactions among different structural elements and material nonlinearities, rendering it suitable for simulating real-world scenarios.

The advancement in computer processing power has considerably enhanced the precision of analysis results through the utilization of more advanced and reliable methods. Consequently, analyses have transitioned from linear static to linear dynamic, nonlinear static, and nonlinear dynamic approaches (Vamvatsikos and Cornell, 2002). In contrast to linear analyses that presume linear behaviour confined within elastic boundaries, NDA factors in material and geometric nonlinearities, rendering it an indispensable instrument for evaluating structures subject to substantial deformations, yielding, and other nonlinear phenomena. NDA functions within the time domain and encompasses the numerical resolution of equations of motion for a structure exposed to dynamic forces. In this process, ground motion records serve as input excitations, replicating the time-dependent response of structural models and depicting their behaviour in real seismic scenarios. This leads to a chronological record of structural responses, unveiling the progressive development of stresses, strains, and deformations throughout the seismic occurrence.

NDA stands as an advanced and potent technique, marked by its capability to grasp complex temporal interactions, accommodate material and geometric nonlinearities, and furnish a comprehensive record of response over time. Nevertheless, its implementation demands significant computational resources, expertise, and precise input data, rendering it better suited for specialized applications rather than routine evaluations.

Over time, various approaches have been employed for the evaluation of structural performance through NDA, utilizing both real and artificially generated ground motions scaled to different intensity levels. Among these methodologies, incremental dynamic analysis, multiple stripe analysis, cloud analysis, and others have gained prominence.

However, to maintain conciseness, the present discussion will focus in-depth on incremental dynamic analysis in the subsequent section.

- **Incremental Dynamic Analysis**

Incremental Dynamic Analysis (IDA), a nonlinear dynamic analysis technique developed by Vamvatsikos and Cornell (2002), has gained prominence in recent years for assessing structural behaviour across varying seismic load intensities. This method entails subjecting a numerical model of a structure to a series of earthquake records, each adjusted to different intensity levels, resulting in response parameter curves as a function of seismic intensity levels. Utilizing nonlinear analysis yields a solitary performance point that can verify structural design and evaluate performance under particular loading conditions. In contrast, pushover analysis offers a "continuous" perspective of structural seismic response, encompassing elasticity, yielding, and ultimate collapse with incremental lateral loading. IDA employs a similar approach to the pushover analysis, scaling seismic loads until failure of the structural model. The chosen intensity levels should ensure the transition of the structure's behaviour from linear elasticity to ultimate collapse. In this manner, IDA offers dual benefits. It provides a comprehensive insight into the spectrum of structural responses across varying seismic intensity levels, enabling assessment of seismic performance under different levels of ground motions, from mild to severe. Additionally, it aids in estimating the dynamic capacity of the overall structural system.

Following this approach, nonlinear time history analysis is conducted while gradually amplifying the seismic intensity until the analysis encounters either global dynamic instability or numerical instability. The primary result of IDA analyses is the IDA curve (Figure 2.7), showcasing the correlation between the maximum inter-storey drift at any building level or other Engineering Demand Parameter (EDP) and the spectral acceleration, $S_a(T)$, or other Intensity Measure (IM), derived from the scaled earthquake record.

The reliability of IDA results is influenced by three key factors: adept choices of effective EDPs and IMs, a robust nonlinear structural model, and the judicious choice of earthquake records. Selecting the right combination of EDP and IM is crucial in IDA, as the resulting IDA curve for the structural system is significantly influenced by the chosen EDP-IM pairing. It is essential to establish that the chosen numerical model aligns with the intended analysis type and maintains an adequate level of complexity. In this regard, it becomes necessary to establish hysteresis curves for both structural and potentially non-structural components,

utilize median values for parameters linked to structural attributes, encompass various potential modes of component damage and failure, and incorporate static gravity actions (D'Ayala et al., 2014). The precision of IDA outcomes and the level of intricacy involved are notably influenced by the quantity and selection of earthquake records. A Single-Record IDA investigation involves performing dynamic analyses on a specific structural model, with the earthquake time-history scaled by a certain factor, leading to a solitary IDA curve (Figure 2.7). It is commonly referred to as IDA or dynamic pushover analysis, involving a sequence of NDA conducted using scaled versions of an input motion. The scaling of IM levels aims to encompass the entire spectrum, spanning from elastic behaviour to nonlinear responses and eventually to the structural collapse. As the structural response, and consequently the IDA curve, is notably influenced by the attributes of earthquake records, relying solely on single-record IDA might not always capture the full spectrum of structural behaviour. To address this limitation, multi-record IDA involves employing multiple earthquake records with varying intensities. This approach provides a comprehensive insight into the structure's performance across a diverse range of ground motions, generating a collection of multi-record IDA curves (Figure 2.8). A multi-record IDA constitutes a compilation of single-record IDA outcomes, utilizing consistent IMs and identical EDP.

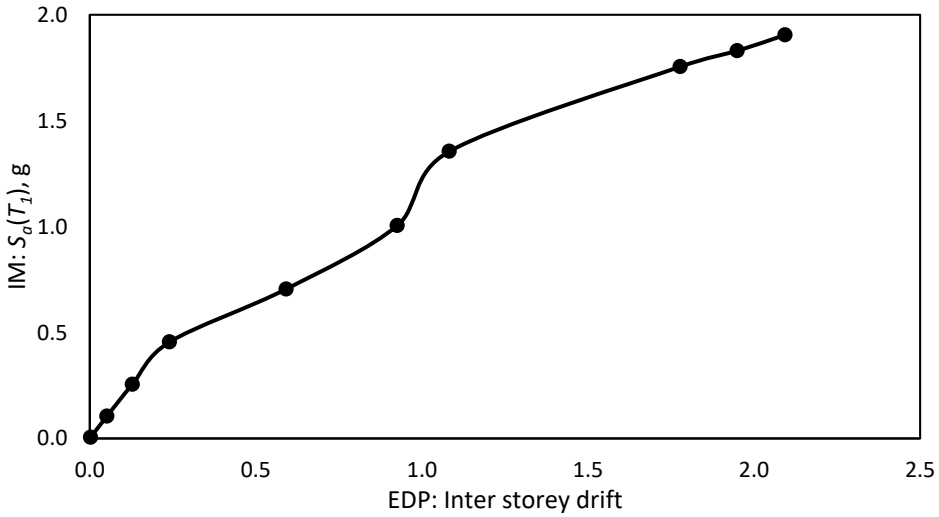

Figure 2.7 Schematic representation of single-record IDA curve.

Careful selection of suitable scaling levels for the earthquake records in IDA is vital to derive reliable estimations of the EDP distribution associated with a specific IM. This assumes that the statistical correlation remains largely unaffected by earthquake magnitude and the distance between the seismic source and the site ($\bar{R}$), as highlighted by Vamvatsikos and Cornell (2004). The 'Hunt and Fill' algorithm, introduced by Vamvatsikos and Cornell

(2002), serves as a crucial tool for determining the optimal number of IM levels and consequently optimizing the analysis count. The Hunt and Fill algorithm builds upon the basic stepping algorithm proposed by Yun et al. (2002). This enhanced approach accelerates the convergence towards the flat portion of an IDA curve by employing larger step sizes within a defined tolerance range, which is referred to as the 'hunting' phase of the algorithm. In practice, IDA curves often exhibit flattening as they approach the collapse point, necessitating finer IM discretization in this region.

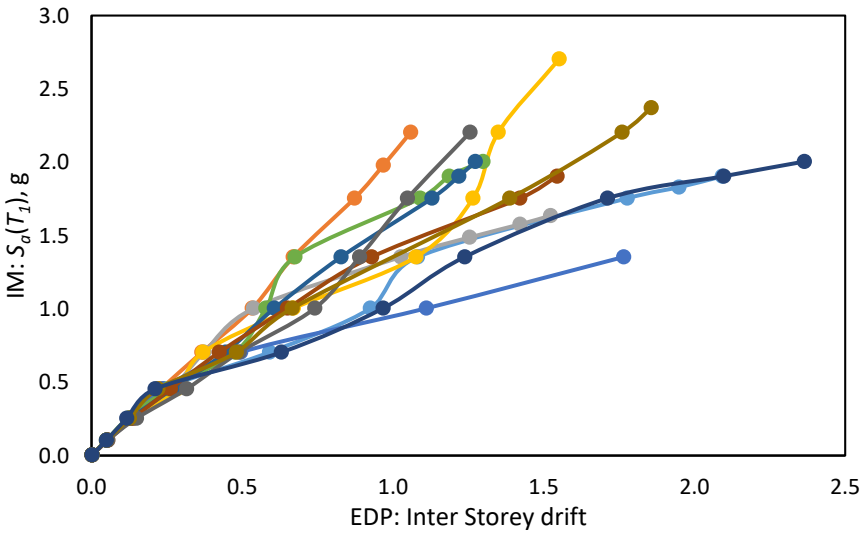

Figure 2.8 Schematic representation of multi-record IDA curve.

Due to its precision in capturing structural behaviour and responses under seismic forces, coupled with the progress in computational capacities, the IDA method has gained widespread usage in generating fragility and vulnerability curves for a wide array of engineering structural systems. Historically, various researchers (including Mwafy et al., 2015; Esteghamati et al., 2017; Ellingwood et al., 2007; Zareian et al., 2010; Dolsek, 2009) have employed IDA to evaluate the structural response of diverse RC structures under varying degrees of ground motion intensity. Some of these studies have extended the findings from IDA to conduct fragility or vulnerability analyses for the reference structural systems.

2.4 Ingredients of Analytical Fragility Formulation

The evaluation of seismic fragility for structures is a crucial procedure that examines a structure's susceptibility to seismic occurrences. This assessment encompasses a methodical strategy for comprehending how varying intensities of ground shaking correlate with potential damage or structural failure. The analytical method for determining fragility

functions involves developing complex mathematical models that represent a structure's response across varying degrees of ground shaking. Researchers and professionals utilize these structural models in conjunction with probabilistic ground motion data and advanced computational methods to formulate fragility functions. The seismic fragility for a structure can be described as a probabilistic function denoting the likelihood of an earthquake-induced demand (D) for the structure, determined through numerical analysis, attaining or exceeding a designated structural capacity limit (C) at a specific ground excitation level, indicating a breach of a targeted damage state (DS). A fragility function is thus characterized by one or more scalar IMs that encapsulate seismic intensity properties. Notably, the focus often centres on the case of a singular IM for constructing fragility curves, in contrast to multi-dimensional surfaces, such as those involving two IMs. Formally, fragility is defined as the conditional probability function of attainment or exceedance of a specific damage state at particular intensity value of the ground excitation. It is essentially a function of the intensity measure, and can be expressed as

$$P(fragility) = P[DS|IM] = P[D \geq C|IM] \tag{2.3}$$

The significance of fragility in nearly all seismic-related investigations stems from the presence of uncertainty (Gidaris et al., 2017). This uncertainty pertains to both the structural capacity of the system and the correlated seismic demand. Ground motion IMs, structural response parameters represented by EDPs, Damage States (DS) definitions, and the accompanying uncertainties collectively constitute the foundational components of the analytical fragility framework for structural systems. Figure 2.9 outlines the procedures involved in deriving analytical fragility functions for the considered building structure. The following sections present a concise discussion of the important features related to the fragility framework.

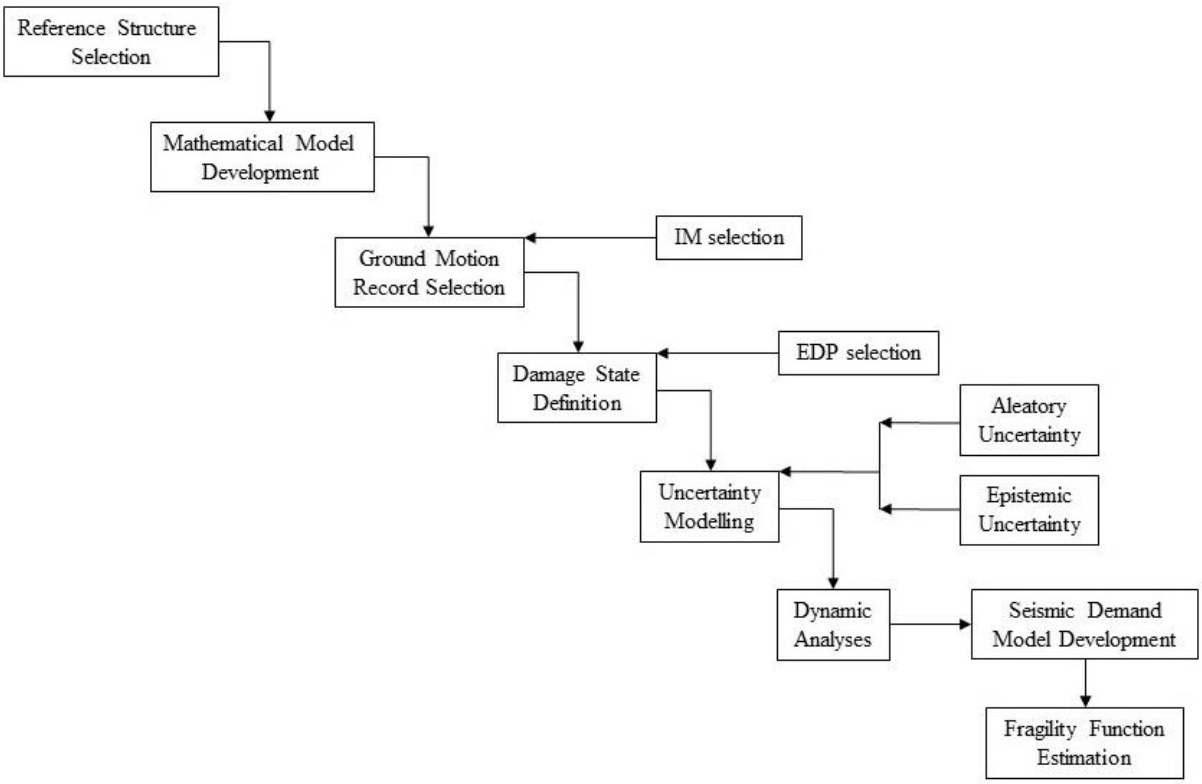

Figure 2.9 Flowchart depicting analytical seismic fragility assessment framework.

2.4.1 Intensity Measures

Intensity Measures (IMs) play a pivotal role in seismic risk assessment for the built environment, where seismic hazard and structural fragility intertwine as functions of earthquake IMs (Deierlein et al., 2003). An IM serves as a metric reflecting the extent of earthquake severity at a specific location and function as an interface variable that efficiently distinguishes between seismology and engineering. Seismologists estimate IM statistical properties through probabilistic seismic hazard analysis, while structural engineers streamline their assessments by focusing on IM levels, rather than multiple seismological parameters. Leveraging insights from seismology, structural engineers are commonly tasked with estimating the distribution of structural response, damage, or loss that a particular structure may incur when exposed to specified IM values, expanding upon the foundational information and understanding required to correlate seismic events and IMs. Thus, IMs facilitate communication and information exchange between seismologists and engineers, streamlining understanding despite potential oversimplification (Kazantzi and Vamvatsikos, 2015).

Establishing a robust correlation between the measure of seismic damage and structural capacity is essential for enhancing the precision of seismic performance assessment and

effectively diminishes the variability in predicting structural response. Identifying an ideal IM that efficiently represents the key ground motion attributes, holds significant importance for reliable seismic response assessment. Numerous IMs for ground shaking representation have been adopted in the literature, as effective indicators of structural damage severity. These IMs can be broadly classified into three different categories. The first category encompasses conventional IMs that depict the seismological parameters—examples include effective duration, peak amplitudes of an earthquake, Arias intensity, etc. Notably, earthquake magnitude and distance from the fault are excluded from this category as they cannot be directly derived from the accelerogram (Mackie and Stojadinovic, 2005). The second category comprises IMs that are based on spectral ordinates derived from SDOF systems subjected to the specific ground motion record, such as S_a, pseudo-spectral velocity, and different response spectrum IMs, among others. The third category employs an arbitrary filter on the actual ground motion record to generate more effective demand models, as detailed in Mackie and Stojadinovic (2005).

The variability within earthquake records can be expressed through either a scalar or a vector parameter known as the IM. In this context, the careful selection of an appropriate IM is of paramount importance to ensure the accuracy of probabilistic seismic evaluations for a structural system. In an ideal scenario, the selected IMs should encompass distinct qualities, including convenience, efficiency, and sufficiency (Luco and Cornell, 2007; Ebrahimian and Jalayer, 2020). Convenience pertains to the ease of acquiring suitable IMs, necessitating their alignment with available attenuation relationships. This primarily confines the use of IMs within the domain of peak amplitudes of earthquake excitation and (pseudo) spectral acceleration values, which currently receive significant seismological attention. Efficiency refers to establishing a robust mathematical correlation between seismic response and IM. This entails using IMs for which structural response, gauged through EDPs, exhibits minimal variability between different ground motion records at a certain IM level. This condition facilitates evaluating conditional EDP distributions with a limited number of time-history analyses, without inducing significant estimation discrepancies (Benjamin and Cornell, 1970). Sufficiency underscores the independence of the structural response to IM for specific magnitude and source-to-site distance. It mandates that the IM captures the influence of essential seismological parameters, eliminating bias from factors like varying magnitudes, distances, or fault rupture mechanisms. A sufficient IM ensures that structural response probabilistically hinges solely on the IM, and not on the other seismological parameters

facilitating accurate predictions of seismic fragility estimates. While efficiency might result in finer-tuned fragility relationships, marked by reduced variability, sufficiency ensures heightened accuracy in fragility estimation—thus, the presence of one doesn't inherently indicate the presence of the other.

Over the past decade, there has been significant research focus on the choice of a suitable IM to characterize the uncertainty in ground motion records. The predominantly utilized IMs in studies evaluating the seismic performance of structural systems are: spectral acceleration values $S_a(T_N)$ at different effective periods of the structure (e.g. Ji et al., 2009; Vamvatsikos and Cornell, 2002); peak ground acceleration (e.g. Ji et al., 2009); peak ground velocity (e.g. Kim et al., 2021); peak ground displacement (e.g. Pejovic and Jankovic, 2016; Wang et al., 2013); functions of S_a and spectral shape at specific periods (e.g. Kim et al., 2021; Cordova et al., 2000; Vamvatsikos and Cornell, 2002); spectral averaging IMs (e.g. Alwaeli et al., 2020; Kazantzi and Vamvatsikos, 2015); energy-based, integral-based, and spectral-velocity-based IMs (e.g. Kim et al., 2021; Wang et al., 2013).

Nonetheless, as emphasized by Gehl et al. (2012), the conventional approach to constructing fragility curves overlooks the uncertainty stemming from relying on a single IM, incapable of encompassing the complete spectrum of ground motion attributes. Consequently, recent endeavours have emerged to consider the impact of multiple IMs on structural damage, as seen in studies by Baker and Cornell (2005), Kafali and Grigoriu (2007), Seyedi et al. (2010), and Koutsourelakis (2010).

2.4.2 Engineering Demand Parameters

Beyond evaluating the seismic performance of structural systems, a crucial subsequent step in generating analytical fragility estimates involves linking structural performance with seismic damage. Within this context, various seismic damage measures, also denoted as Engineering Demand Parameters (EDPs), are documented in literature. These EDPs establish correlations between seismic responses and the potential for anticipated damage. Essentially, EDPs encompass seismic response quantities utilized for anticipating the damage incurred by both structural and non-structural components due to seismic excitations. These seismic damage measures hold equivalent significance to IMs in performing seismic fragility assessments, as the shape of resulting fragility functions heavily relies on the chosen EDP.

In the realm of seismic performance and vulnerability assessment, past research and contemporary design guidelines have employed various EDPs for accuracy and reliability. These EDPs, employed to characterize structural responses, can be categorized into two primary groups: direct and processed EDPs, as outlined by Whittaker et al. (2004). Direct EDPs are those directly calculated through analysis or simulation of the mathematical model of a specific structural system. These measurements encompass structural responses or behaviours during earthquakes, like peak inter-storey drift or maximum roof displacement. On the other hand, processed EDPs are derived from direct EDP values and incorporate data on the local or global capacities of the structural system. These processed EDPs undergo specific calculations or modifications to capture specific facets of structural response or behaviour, such as ductility ratios or the damage index recommended by Park and Ang (1985).

Timchenko (2002) categorized the array of EDPs into three main groups according to the structural parameters necessary for their computation: dynamic parameters of the structure, displacement parameters, and displacement coupled with cumulative damage. Several researchers have utilized the dynamic parameters of structures, such as natural frequencies, mode shapes, and damping, as damage measures (e.g., Zembaty et al., 2006). Nevertheless, EDPs rooted in the dynamic characteristics of structure lack information regarding localized and storey-level seismic damage. Frequently employed EDPs for fragility assessments of structural systems are founded on displacement parameters, like maximum floor acceleration and peak storey curvature, due to their ease of analytical derivation (e.g., Jiang et al., 2015; Stocchi and Richard, 2019). Additionally, displacement parameters (such as drift and ductility) are generally recognized as superior for simulating structural response within the inelastic range (Priestley, 1997). Lastly, certain EDPs, considering cyclic effects of seismic loads and encompassing energy dissipation and maximum displacement, have been recommended to account for the dynamic nature of seismic actions, exemplified by the damage index measure (e.g., Park and Ang, 1985; Sengupta et al., 2016).

Numerous modern seismic performance assessment methods, such as ATC-58 (2009), have provided insights into the establishment and quantification of EDPs for comprehensive structural response evaluations. Presently, among the several options available, the Inter-Storey Drift ratio (ISD) has gained prominence and is commonly employed in seismic fragility studies. Several design guidelines, including FEMA-356 (2000), utilize ISD as an EDP for accurate damage estimation. In other research efforts, such as that by Nazari and

Saatcioglu (2017), ISD has been endorsed for creating seismic vulnerability assessment tools, specifically fragility curves, tailored to representative classes of RC wall buildings in Canada. Similarly, Pejovic and Jankovic (2016) have recommended ISD as an EDP for investigating the seismic vulnerability of RC tall buildings in the Southern Euro-Mediterranean region. Gulec et al. (2010) have developed fragility functions that incorporate ISD as an EDP for RC walls with low aspect ratios, aiming to assist in the vulnerability assessment of wall-frame structures. Furthermore, Teweldebrhan et al. (2023) utilised maximum and residual ISD to derive seismic fragility functions for cross-laminated timber coupled wall structural systems located in Vancouver, Canada.

In the past, several other EDPs have also been used by researchers to assess the seismic response of structural systems. Xu et al. (2018) employed ISD along with component-based and material-based damage indices as EDPs to evaluate seismic vulnerability functions for a Steel Reinforced Concrete frame structure and concluded that the component-based damage index was more reliable. Stocchi and Richard (2019) quantified the sensitivity of six EDPs: Peak ISD, Eigen frequency drop off, Ductility, Hysteretic energy over total input energy, Zero period acceleration, and Amplification ratio with respect to the building typology (frame with or without RC structural walls). The amplification ratio was found to be the least sensitive, while zero period acceleration was the most sensitive EDP. Xiong et al. (2019) advocated the use of storey curvature as EDP to quantify the storey level seismic damage of the structural wall components and concluded that the proposed use of storey curvature as an EDP is a better alternative to traditional EDPs for quantifying the flexural damage of regular slender structural walls. Jiang et al. (2015) used the plastic rotation at the member ends and the peak ISD as EDPs to investigate the seismic vulnerability of RC wall-frame structures designed according to the Chinese design code.

2.4.3 Seismic Performance Levels

To comprehensively understand the structural response to seismic forces, the establishment of thresholds for Damage States (DS) is crucial. These thresholds categorize the continuous spectrum of damage into discrete states, each with specific implications for the structure, its components, and occupants. Each DS is linked to a target exceedance probability, creating performance levels that hold significance as they represent real-world consequences such as structural and non-structural harm, casualties, downtime of infrastructure, repair expenses, and more, thereby bridging the engineering aspects of EDPs with the broader group of

stakeholders utilizing the outcomes of the vulnerability assessment of the built environment. The definition of each DS involves setting limits for EDPs, which, when surpassed, lead to a higher damage state. Thus, the precise formulation of comprehensive damage states and the subsequent determination of performance levels are pivotal components of seismic fragility investigations.

Broadly, structural damage refers to alterations in a structure that impact its functionality. Damage is typically categorized into two primary types: visible damage, known as apparent damage, includes observable issues like cracks, spalling, or component separation. In contrast, mechanical damage denotes shifts in the mechanical characteristics of the structural system, such as alterations in fundamental time period, stiffness, or residual ductility.

Seismic damage is most effectively delineated by breaking it down into its distinct elements: structural and non-structural. The damage to the structural elements, encompassing both the systems that resist gravitational forces and lateral loads, can carry significant risks. On the other hand, damage to non-structural elements in structure(s), which includes architectural features like partition walls and ceilings, together with mechanical and electrical systems, predominantly leads to financial and societal losses, and typically results in casualties of relatively mild to moderate intensity. Typically, the criteria for defining damage state thresholds predominantly rely on structural damage, although non-structural damage can be equally crucial and more responsive to factors like drift or acceleration. This bias is a consequence of the challenges posed by the traditional assessment procedures in evaluating non-structural damage, which in turn leads to the commonly overlooked contribution of non-structural damage in shaping the definitions of damage states.

In existing literature, a variety of damage states or performance levels have been proposed for different types of building structures. The establishment of damage states for individual buildings or building inventories is typically based on two distinct criteria: qualitative and quantitative. Most building codes and seismic design standards, such as ASCE/SEI-41 (2006) and FEMA P-750 (2009), often embrace the qualitative approach in setting damage state thresholds. This involves describing damage state thresholds in non-numeric terms, providing a qualitative assessment of a structure's condition by considering visible signs such as cracks, deformations, and other indications of both structural and non-structural damage. Although lacking the precision of quantitative measurements, these qualitative definitions furnish a pragmatic and accessible means to convey the gravity of damage. On the other hand, defining

limit states based on quantitative criteria necessitates mathematical expressions of localized damage indicators grounded in predetermined building performance levels. This method entails a more precise and measurable strategy to evaluate seismic-induced structural damage. In contrast to qualitative definitions that rely on descriptive terms, quantitative definitions employ specific engineering parameters and measurements, such as displacement, acceleration, curvature, and other quantifiable factors that reflect how the structure responds to ground shaking. While quantitative definitions yield valuable insights into the technical dimensions of seismic damage, they do involve higher computational costs due to the need for more extensive data collection and analysis.

Given the diversity of research objectives, distinct performance levels can be defined for structures based on the desired outcomes of a study. Commonly employed damage state levels, observed in existing literature, encompass Slight damage, Moderate damage, Extensive damage, and Collapse damage (Kircher et al., 1997; Dumova-Jovanoska, 2004; Lagomarsino et al., 2006; Barbat et al., 2007). Similarly, Immediate Occupancy (IO), Life Safety (LS), and Collapse Prevention (CP) have been used as performance benchmarks (ASCE/SEI 41-06, 2006; Kinali and Ellingwood, 2007; FEMA, 2009; Mwafy, 2012). Additional classifications include No damage, Negligible damage, Light Reparable damage, Moderate Reparable damage, Irreparable damage, Severe damage, and Collapse State damage (Rossetto and Elnashai, 2003; Ghobarah, 2004). These selections reflect the range of approaches taken in characterizing performance levels in seismic vulnerability research.

Every predetermined damage state assigned to a structural system requires a conceptual definition, whether directly articulated or indirectly implied, in connection with a particular damage event or pattern. As a result, various methodologies have been recommended within seismic design standards and earlier research endeavours to address this requirement. In FEMA-273 (1997), a range of performance levels linked to damage states was outlined, utilizing qualitative descriptions of damage indicators pertaining to both structural and non-structural components in conventional building structures (as presented in Table 2.2). The performance levels defined in European Macroseismic Scale (EMS 98) (Grünthal in 1998) is derived from the MSK 64 scale by Medvedev and Sponheuer from 1969. Unlike the MSK 64 scale primarily used by seismologists, EMS 98 is specifically developed to facilitate collaboration between engineers and seismologists. It serves as the foundation for assessing seismic intensity in European nations and has been adopted in several non-European

countries as well. The table detailing the damage descriptions for various damage states of RC buildings according to EMS 98 can be found in Table 2.3.

Table 2.2 FEMA 273 (1997) definition of performance levels associated with different damage states

	Building Performance Levels			
	Operational (O) Level	Immediate Occupancy (IO) Level	Life Safety (LS) Level	Collapse Prevention (CP) Level
Overall Damage	Very Light	Light	Moderate	Severe
Structural Elements	Structure substantially retains original strength and stiffness	Structure substantially retains original strength and stiffness	Some residual strength and stiffness left in all stories	Little residual stiffness and strength
	Minor cracking of facades, partitions, and ceilings as well as structural elements	Minor cracking of facades, partitions, and ceilings as well as structural elements	Gravity-load-bearing elements function. No out-of-plane failure of walls or tipping of parapets. Damage to partitions	Load-bearing columns and walls function. Infills and unbraced parapets failed or at incipient failure
	No permanent drift	No permanent drift	Some permanent drift	Large permanent drifts
	All systems important to normal operation are functional	Elevators can be restarted Fire protection operable	-	Some exits blocked
	-	-	Building may be beyond economical repair	Building is near collapse
Non-Structural elements	Negligible damage occurs. Power and other utilities are available, possibly from standby sources	Equipment and contents are generally secure, but may not operate due to mechanical failure or lack of utilities	Falling hazards mitigated but many architectural, mechanical, and electrical systems are damaged	Extensive damage

Table 2.3 Classification of damage to RC buildings as per EMS-98. (Grünthal, 1998)

Damage Level	Damage Description
Grade 1: Negligible to slight damage (no structural damage, slight non-structural damage)	Fine cracks in plaster over frame members or in walls at the base. Fine cracks in partitions and infills.

Grade 2: Moderate damage (slight structural damage, moderate non-structural damage)	Cracks in columns and beams of frames and in structural walls. Cracks in partition and infill walls; fall of brittle cladding and plaster. Falling mortar from the joints of wall panels.
Grade 3: Substantial to heavy damage (moderate structural damage, heavy non-structural damage)	Cracks in columns and beam column joints of frames at the base and at joints of coupled walls. Spalling of concrete cover, buckling of reinforced rods. Large cracks in partition and infill walls, failure of individual infill panels.
Grade 4: Very heavy damage (heavy structural damage, very heavy non-structural damage)	Large cracks in structural elements with compression failure of concrete and fracture of rebars; bond failure of beam reinforced bars; tilting of columns. Collapse of a few columns or of a single upper floor.
Grade 5: Destruction (very heavy structural damage)	Collapse of ground floor or parts (e. g. wings) of buildings.

By utilizing inter-storey drift (ISD) as an EDP, a broad range of numerical thresholds have been incorporated in existing literature to delineate damage state levels linked to varying performance levels across a variety of RC structural systems. The seismic design standard ASCE/SEI 41-06 (2007) proposed drift values aligned with three performance levels for RC structural wall systems, namely 0.5% for IO (minor cracking), 1% for LS (extensive concrete crushing), and 2% for CP (buckling of reinforcement). In the SEAOC blue book (1999), suggested ISD values for RC structural walls were presented as follows: 0.4% for SP1 (indicating negligible damage), 0.9% for SP2 (indicative of minor to moderate reparable damage), 1.4% for SP3 (suggesting moderate to major irreparable damage), and 2.1% for SP4 (representing a collapse performance level).

In the research conducted by Vamvatsikos and Cornell (2004) focusing on steel moment-resisting framed structures, the features of the Incremental Dynamic Analysis (IDA) curves were employed to establish the conceptual definitions for CP and collapse damage state levels. CP was correlated with the point on the curve which indicated an 80% decrease in slope, while the collapse damage state was associated with reaching the flat region, indicating a state of global dynamic instability. Ji et al. (2009) performed an extensive study on a 54-storey RC wall-frame building, undertaking nonlinear static and nonlinear dynamic analyses to establish the conceptual definitions for the three chosen damage states (Serviceability, Damage Control, and Collapse Prevention), presented in Table 2.4.

Table 2.4 Damage state definitions (Ji et al., 2009)

Performance Level	Damage State	Damage Description
Damage State 1 (DS1)	Serviceability	Initiation of minor cracks in main resisting members
Damage State 2 (DS2)	Damage Control	Initial yielding of longitudinal reinforcement or the development of the first plastic hinge, whichever occurs first
Damage State 3 (DS3)	Collapse Prevention	Attainment of the ultimate capacity in the primary load-bearing elements and the initiation of the descending segment on the capacity curve

Lagomarsino et al. (2006) and Barbat et al. (2007) are among the researchers who have introduced damage states divided into four distinct levels, utilizing spectral displacement as the criterion. In this methodology, damage states are directly defined using two key capacity points: yield displacement (d_y) and ultimate displacement (d_u), as outlined in Table 2.5 and Table 2.6.

Table 2.5 Damage threshold values (Lagomarsino et al., 2006)

Damage State	Threshold spectral Displacement	Structural (SD) and non-structural (N-SD) damage
Slight	$0.7d_y$	No SD slight N-SD
Moderate	$1.5d_y$	Slight SD moderate N-SD
Extensive	$0.5(d_y + d_u)$	Moderate SD heavy N-SD
Complete	d_u	Heavy SD very heavy N-SD Very heavy SD

Table 2.6 Damage state threshold values (Barbat et al., 2007)

Damage State	Threshold Spectral Displacement
Slight	$0.7d_y$
Moderate	d_y
Extensive	$d_y + 0.25(d_u - d_y)$
Complete	d_u

Alternatively, a limit state can be defined based on structural behaviour or repair potential. In terms of structural behaviour, three performance levels can be considered: elastic, inelastic,

and collapse. Alternatively, focusing on repair feasibility, Ghobarah (2004) introduced five limit states: no damage, reparable damage, irreparable damage, extreme, and collapse, all linked to inter-storey drift (ISD), as presented in Table 2.7.

Performance levels for damage states are often quantified using deformation criteria, including indicators like concrete cracking, initial steel yielding, and extensive concrete cracks, which are particularly relevant for ductile systems. These descriptions not only gauge the extent of damage but also assess repair feasibility and associated costs. Rossetto and Elnashai (2003) introduced a novel damage scale, the Homogenised Reinforced Concrete (HRC) damage scale, which is divided into seven damage states: none, slight, light, moderate, extensive, partial collapse, and collapse. These states, detailed in Table 2.8, outline expected structural and non-structural damage for four primary types of RC structures. To further define these limit states, a damage index, the HRC-damage index (DI_{HRC}), is employed, offering a numerical reference scale aligned with the structural response parameter of peak ISD. The equations to calculate the HRC-damage index (DI_{HRC}) are presented in Eqs. (2.9–2.12).

Table 2.7 Damage states defined with ISD for RC wall systems (Ghobarah, 2004)

State of damage	Ductile Walls (%)	Squat Walls (%)
No damage	< 0.2	< 0.1
Reparable damage		
1. Light	0.4	0.2
2. Moderate	< 0.8	< 0.4
Irreparable damage(> Yield point)	> 0.8	> 0.4
Severe damage → Life sate → Partial Collapse	1.5	0.7
Collapse	>2.5	>0.8

$$DI_{HRC} = 34.89 \ln\left(ISD_{max}\,\%\right) + 39.39 \text{ , } \textit{for non-ductile MRF} \quad (2.91)$$

$$DI_{HRC} = 22.49 \ln\left(ISD_{max}\,\%\right) + 66.88 \text{ , } \textit{for infilled frames} \quad (2.20)$$

$$DI_{HRC} = 39.31 \ln\left(ISD_{max}\,\%\right) + 52.98 \text{ , } \textit{for shear wall systems} \quad (2.31)$$

$$DI_{HRC} = 27.89 \ln\left(ISD_{max}\,\%\right) + 56.36 \text{ , } \textit{for general structures} \quad (2.42)$$

Table 2.8 The HRC-Scale: Typical damage expected in ductile, non-ductile and infilled RC moment resisting frames and in RC wall structures (Rossetto and Elnashai, 2003)

DI_{HRC}	DAMAGE STATE	DUCTILE MRF	NON-DUCTILE	INFILLED MRF	SHEAR WALL

		MRF			
0	None	No damage	No damage	No damage	No damage
10	Slight	Fine cracks in plaster partitions/infills	Fine cracks in plaster partitions/infills	Fine cracks in plaster partitions/infills	Fine cracks in plaster partitions/infills
20		Start of structural damage	Start of structural damage	Start of structural damage	Start of structural damage
30	Light	Hairline cracking in beams and columns near joints (<1mm)	Hairline cracking in beams and columns near joints (<1mm)	Cracking initiates from corners of openings	Hairline cracking on shear wall surfaces & coupling beams
40				Diagonal cracking of walls. Limited crushing of bricks at b/c connections	Onset of concrete spalling at a few locations
50		Cracking in most beams & columns	Flexural & shear cracking in most beams & columns	Increased brick crushing at b/c connections	Most shear walls exhibit cracks
60	Moderate	Some yielding in a limited number	Some yielding in a limited number	Start of structural damage	Some walls reach yield capacity
70		Larger flexural cracks & start of concrete spalling	Shear cracking & spalling is limited	Some diagonal shear cracking in members especially for exterior frames	Increased diagonal cracking & spalling at wall corners
80		Ultimate capacity reached in some elements – large flexural cracking, concrete spalling & re-bar buckling	Loss of bond at lap-splices, bar pull-out, broken ties	Extensive cracking of infills, falling bricks, out-of-plane bulging	Most shear walls have exceeded yield, some reach ultimate capacity, boundary element distress seen.
	Extensive	Short column failure	Main re-bar may buckle or elements fail in	Partial failure of many infills, heavier damage	Re-bar buckling, extensive

90			shear	in frame members, some fail in shear	cracking & through-wall cracks. Shear failure of some frame members
100	Partial Collapse	Collapse of a few columns, a building wing or single upper floor	Shear failure of many columns or impending soft-storey failure	Beams &/or columns fail in shear causing partial collapse. Near total infill failure	Coupling beams shattered and some shear walls fail
	Collapse	Complete or impending building collapse	Complete or soft-storey failure at ground floor	Complete or impending building collapse	Complete or impending building collapse

2.4.4 Uncertainties in the Seismic Fragility Framework

Seismic fragility assessment plays a critical role in understanding the vulnerability of buildings and infrastructure to earthquakes. However, this process is inherently complex and riddled with various uncertainties that can significantly impact the reliability and efficiency of the results. These uncertainties arise from a multitude of sources and factors, ranging from the inherent variability of ground motion records to the intricacies of structural behaviour and modelling assumptions. In essence, fragility inherently encapsulates a fundamental layer of uncertainty, which is shaped by a multitude of sources encompassing both aleatory and epistemic uncertainties (Ellingwood and Kinali, 2009; Der Kiureghian and Ditlevsen, 2009). In the domains of seismic performance analysis and vulnerability assessment challenges, these sources of uncertainty are distinguished as aleatory uncertainty, which emerges from the innate natural variations observed in the results of recurring experiments, and epistemic uncertainty, which arises due to the constraints and imperfections in available knowledge, manifesting as modelling and statistical uncertainties.

Aleatory uncertainty stems from the inherent randomness within a system or process and cannot be eliminated but can only be managed. In the context of seismic fragility formulation, the principal source of aleatory uncertainty is the variability from one record to another in the demand-response relationship, originating from the natural randomness of ground motions (e.g. Porter et al., 2002; Lee and Mosalam, 2005). If a sufficient number of input records are employed in the analysis procedure, aleatory uncertainty can be integrated to generate

dependable analytical fragility estimates with a reasonable degree of confidence. Despite being unavoidable in stochastic processes like fragility estimation, seismic design regulations have attempted to provide standardized or approximate values for the added dispersions corresponding to aleatory uncertainty.

Epistemic uncertainty arises from a dearth of knowledge, ignorance, or coarse modelling, and it is generally reducible through the acquisition of more information and enhanced understanding. Enhancing comprehension of variables, often achieved through collecting and analysing more data and refining predictive models, tends to diminish epistemic uncertainties. Modelling uncertainty emerges because every model, whether conceptual or mathematical, inherently simplifies reality. This stems from limited knowledge about the geometric and mechanical attributes of the structure and inherent limitations of the model in correlating and conducting structural analyses (e.g. Liel et al., 2009; Kazantzi et al., 2013; Karaton et al., 2020; Wang and Jia, 2022).

In the development of analytical fragility functions, the typical methodologies encompass a series of steps aimed at assessing uncertainty. These steps involve identifying sources of uncertainty related to both capacity and demand, quantifying these uncertainties, and incorporating them into the derivation of fragility estimates. Uncertainty concerning capacity is influenced by various parameters tied not only to the structural characteristics of the building—such as mechanical properties, structural features, geometry, and dimensions—but also to the numerical model employed for computing the structural capacity. This structural model's accuracy depends on factors like the level of detailing, the completeness of the mathematical model, and the performance evaluation technique. Concurrently, the uncertainty in demand originates from how well the seismic demand is depicted, achieved using either actual earthquake records or design spectra from seismic guidelines. These representations must account for the diversity observed between different records, encompassing the varying aspects of the seismic source mechanism, attenuation, and the influences of site effects on the seismic event. Metwally et al. (2022) performed variance-based sensitivity analysis for RC masonry wall structures considering model uncertainty and uncertainties in material and geometric properties.

In the recent past, researchers have endeavoured to conduct sensitivity analyses on seismic response parameters across diverse structural systems, addressing a broad spectrum of uncertainties in seismic fragility assessment. Lee and Mosalam (2005) quantified the

variability in seismic response for a RC wall-frame building due to the uncertainty in input motions and structural properties. Choudhury and Kaushik (2018) evaluated the influence of the uncertainty in material and geometrical properties on the seismic demand of RC frames with and without infill walls. Liel et al. (2009) observed structural modelling uncertainties to be of prime importance while determining the seismic capacity for RC moment resisting frame buildings. Porter et al. (2002) studied the influence of the uncertainty in key input parameters (namely, seismic load intensity measure, material properties, component fragility and system repair cost) on the repair cost sensitivity of a RC building.

In the literature, several techniques have been employed to perform sensitivity analysis for the uncertainty in input parameters. These include tornado diagram analysis (TDA) (Porter et al., 2002; Seo and Linzell, 2013), the first-order second moment (FOSM) method (Lee and Mosalam, 2005; Baker and Cornell, 2008; Jia et al., 2023), and the Monte-Carlo simulation (MCS) method (Stocchi and Richard, 2019; Kim et al., 2011). TDA is primarily used to illustrate the variation in the structural response when each input parameter is fixed at both a higher and a lower value, with all other parameters fixed at their mean values. However, in TDA, the combined effect of the input variables on the output response is not reflected as the parameters are varied individually. In the FOSM method, the mean and standard deviation of the structural response are established based on the first and second moments of the input variable parameters. But the reliability of the FOSM method is sceptical whenever a nonlinear relationship exists between the input variables and the model output (Gokkaya et al., 2016). Even though MCS provides reliable stochastic evaluation of the structural response, it is typically computationally expensive. More recently, the advancement of Machine Learning (ML) techniques has led to its recurrent application in the field of structural engineering. Mangalathu and Jeon (2018) used 539 experimental results to develop ML models for predicting shear strength of RC beam-column joints. Huang and Burton (2019) used ML techniques to evaluate the collapse capacity of RC frames with infills. Meanwhile, Hwang et al. (2021) predicted the seismic capacity of RC building frames using ML based methodology, while considering the modelling related uncertainty. Zhang et al. (2023) conducted uncertainty and sensitivity analyses to explore the influence of various uncertain parameters on the fire resistance potential of RC slabs. Furthermore, Mostafaei et al. (2022) utilized artificial neural network techniques to examine the seismic stability reliability, and sensitivity analysis of dam abutments, incorporating various geometric and structural properties as random variables.

Also, numerous studies have underscored the importance of quantifying and integrating multi-parameter uncertainties into the seismic performance assessment of structural systems. For example, Choudhury and Kaushik (2019) delved into the impact of various sources of uncertainty when estimating fragility functions for RC building frames with masonry infill walls. Sousa et al. (2016) explored how randomness in structural capacity and variability in seismic demand influence seismic fragility estimates for RC building frame structures. Ellingwood and Kinali (2007) demonstrated how strong-motion variability and random structural parameters propagate through a structural vulnerability assessment of steel building frames, particularly in low-to-moderate seismicity regions of Central and Eastern United States. Similarly, Kazantzi et al. (2013) examined the effects of uncertainties related to structural modeling on the seismic response variability of a four-story steel moment-resisting frame building. Additionally, Karaton et al. (2020) conducted a study on the impact of modeling uncertainties in nonlinear seismic analysis of RC wall-frames, with a specific focus on damping ratio variability and structural damping categories. Based on a thorough uncertainty quantification and sensitivity analysis of an RC structural component, Hariri-Ardebili et al. (2024) emphasized the importance of modelling uncertainty compared to material uncertainty in influencing the variability of drift response. Furthermore, Mohamed et al. (2023) assessed the impact of various sources of uncertainty on the seismic fragility relationships of masonry-infilled RC frame systems.

Previous researchers have proposed stochastic approaches to incorporate various sources of uncertainty into the seismic performance assessment of structural systems. Notably, methods such as the FOSM technique (Haselton, 2006) and MCS (Gokkaya et al., 2016) have been commonly employed for uncertainty analysis in seismic design and response assessment. Baker and Cornell (2008) recommended the use of numerical integrations alongside FOSM approximations to investigate the impact of uncertain variables on seismic response parameters. However, the accuracy of the FOSM procedure may be questionable for positively nonlinear functions (Liel et al., 2009). Liel et al. (2009) introduced a framework that combines response surface analysis with Monte Carlo methods to assess the influence of modeling uncertainties on calculated collapse fragilities. While Monte Carlo methods are considered reliable for stochastic evaluation of structural responses, they are computationally expensive (Lee and Mosalam, 2005), necessitating a practical balance between computational demands and reliability. Dolsek (2009) quantified the effects of both aleatory and epistemic

uncertainties on structural seismic responses by utilizing an extended adaptation of IDA (Vamvatsikos and Cornell, 2002).

2.5 Seismic Performance of RC Wall-Frame Buildings

Previous research on the seismic performance of RC wall-frame buildings has been instrumental in advancing the comprehension of the behaviour, susceptibilities, and resilience of these structures during earthquake shaking. These studies have significantly influenced seismic design regulations, construction methodologies, and retrofitting strategies aimed at enhancing the comprehensive seismic resilience of RC wall-frame buildings.

Extensive research efforts have been directed towards exploring the seismic behaviour of RC wall-frame buildings using both experimental tests and numerical simulations. Experimental investigations frequently entail subjecting scaled or full-scale structural wall specimens to simulated earthquakes, facilitating an evaluation of their performance across diverse loading scenarios. These experiments yield valuable insights into aspects like structural wall deformations, modes of failure, load dispersion, and the efficacy of various reinforcement approaches. Researchers have conducted experimental and numerical assessments on specimens extracted from RC wall-frame buildings that sustained damage during significant seismic occurrences globally, such as the 2003 Bingöl earthquake and the 2010 Chile earthquake. Through the utilization of nonlinear static and nonlinear dynamic analyses, these studies have delved into the effects of diverse material and geometrical wall attributes. Researchers, including Thomsen and Wallace (2003), Dazio et al. (2009), and others, have carried out these assessments to glean insights into the behaviour of damaged RC wall-frame buildings and to comprehend the impact of varying characteristics on their response.

Advanced computational tools have augmented experimental investigations through numerical simulations, offering researchers the capacity to delve into a broader spectrum of scenarios and variables. These simulations facilitate the examination of complex structural behaviours, including nonlinear material response, interactions between structural walls and other structural components, and the influence of various design parameters on seismic performance. By employing techniques such as finite element analysis, researchers can attain a more profound understanding of the dynamic response exhibited by RC wall-frame buildings and their susceptibilities across varying levels of earthquake intensity.

The implementation of reliable Performance Based Earthquake Engineering (PBEE) often necessitates the assessment of fragility and vulnerability relationships for the prime force-resisting system of a structure. In this context, a considerable number of researchers have undertaken seismic fragility assessments for RC structural wall elements, which frequently serve as vital lateral force-resisting components in regions characterized by heightened seismic activity. To illustrate, Nazari and Saatcioglu (2017) utilized fiber-discretized sections to model structural walls, employing Incremental Dynamic Analysis (IDA) to produce fragility curves for four RC wall-frame buildings in Vancouver, corresponding to three distinct performance levels. Dabaghi et al. (2019) employed IDA to derive seismic collapse fragility curves for eleven diverse RC wall-frame buildings, investigating the influence of wall design parameters on fragility, including storey count, wall length, boundary element length, and transverse reinforcement spacing in boundary elements. Pejovic and Jankovic (2016) conducted a seismic fragility assessment for 20-, 30-, and 40-storey RC wall-frame buildings subjected to seismic excitation typical of the Southern Euro-Mediterranean zone. Alwaeli et al. (2020) undertook a comprehensive analytical fragility assessment of RC wall-frame buildings, varying the number of stories and considering diverse seismic scenarios. The study yielded two sets of fragility curves: one set was derived from 40 actual ground motion records, while the other was created using a reduced number of input motions, ensuring consistent reliability levels. Echeverria et al. (2022) formulated seismic fragility relationships for medium-rise RC wall structural systems, focusing on fishbone-type buildings characterized by high wall densities, thin unconfined walls subjected to high axial loads, and notable vertical irregularities.

Jiang et al. (2015) scrutinized the reliability of the prevailing Chinese seismic design standard by conducting an analytical seismic fragility assessment for 45 10-storey RC wall-frame buildings designed in compliance with the Chinese code, resulting in the derivation of fragility curves corresponding to four different damage state levels: fully operational, operational, reparable, and collapse prevention. In his study, Mwafy (2012) assessed the fragility predictions for 6 benchmark RC wall-frame buildings, exhibiting heights ranging from 10 to 60 stories, in alignment with the seismic design principles and building methods predominant in the UAE region. These fragility functions were established through an extensive array of nonlinear static and dynamic collapse analyses, drawing from 20 earthquake records that align with the most recent comprehension of the seismo-tectonic attributes of the UAE. Sadraddin et al. (2016) examined how structural wall configuration

influenced the fragility assessment of a 12-storey RC high-rise structure, revealing that the inclusion of structural walls enhanced the structural performance across all investigated damage states. Wen et al. (2002) assessed the effects of site conditions and epicentral distance on fragility estimates for a 21-storey RC wall-frame building constructed in Hong Kong during the 1960s. Pozo et al. (2023) compared the estimated seismic fragility relationships of various slender RC wall building systems using different numerical modelling approaches. Verdugo et al. (2017) formulated analytical fragility curves for a 20-storey Chilean RC wall-frame building, accounting for seismic variability by utilizing a collection of 28 earthquake records.

Certain prior investigations have been dedicated to examining the probabilistic seismic fragility correlations for RC dual core wall structural systems, assessing their response under various earthquake scenarios. In their study, Ji et al. (2009) conducted a seismic fragility evaluation for a pre-existing 54-storey RC building featuring a dual core wall system. This assessment was built upon the outcomes of inelastic nonlinear dynamic analyses carried out on a simplified lumped-parameter model of the reference structure. The fragility predictions were meticulously derived, accounting for both aleatory and epistemic uncertainties. Additionally, they incorporated new threshold values for damage states, established through detailed nonlinear static analyses. Deger et al. (2014) examined a pair of 42-storey RC buildings situated in Los Angeles, California, with the aim of assessing and contrasting the cost-effectiveness and seismic performance between a dual core-wall structural system and a coupled core wall system. Deger and Wallace (2016) further examined the seismic performance and cost efficiency of the same 42-storey building, considering design standards from the International Building Code (IBC 2006) and the Los Angeles Tall Building Structural Design Council (LATBSDC 2008). Esteghamati et al. (2018) investigated the impact of the ASCE 7-10 (2010) design drift limits on the seismic performance of 20-, 25-, and 30-storey RC dual system high-rise buildings. This investigation encompassed fragility relationships, seismic demand hazard, and adjusted collapse margin ratios, drawing upon IDA results derived from finite element models of the considered structures.

Probabilistic analysis, which includes fragility assessment, has found widespread use in quantifying the probability of different damage states in low-rise shear-critical RC structural wall systems subjected to different levels of seismic intensity. Low aspect ratio RC walls, distinguished by a height-to-length ratio of less than 2, serve as a structural system used in buildings and infrastructure to enhance earthquake resistance. Gulec et al. (2010) derived

fragility relationships for low-rise RC walls, facilitating subsequent evaluations of the performance of buildings and other structures that integrate these specific structural elements. These relationships were established through a meticulous review and statistical analysis of data sourced from tests conducted on a variety of wall configurations, including rectangular, barbell, and flanged designs. Subsequently, Rivera and Whittaker (2019) refined the previously developed fragility estimates for low aspect ratio RC walls, as presented by Gulec et al. (2010). This update involved considering damage data at zero lateral loading, signifying the post-earthquake condition or the initial phase of repair, in contrast to the prior approach that relied on damage data collected during peak lateral loading.

Previous research on evaluating the seismic performance of RC wall-frame buildings has played an essential role in advancing seismic engineering. For instance, Mwafy et al. (2015) examined the interplay between seismic performance and the economic aspects of RC wall-frame buildings. Their study focused on 5 60-storey buildings commonly found in the UAE, each featuring different concrete strengths, ranging from 45 MPa to 110 MPa. The study involved a comprehensive estimation of the seismic performance of these structures, employing thorough IDAs and fragility estimates as key assessment tools. Zareian and Krawinkler (2010) conducted a probabilistic collapse capacity estimation for moment-resisting frames and RC wall structural elements, examining the impact of fundamental structural parameter variation and seismic IM selection. Fox et al. (2015) explored the effectiveness of various seismic assessment methods, including Direct Displacement-Based Assessment, nonlinear static analysis, and nonlinear dynamic analysis, in accurately forecasting deformation demands, particularly focusing on roof displacement, inter-storey drift ratio, and wall curvatures. Gogus and Wallace (2015) assessed the seismic performance of a total of 40 RC wall structures, comprising 20 special and 20 ordinary walls, which exhibited diverse heights, seismic design classifications, and axial load levels. These walls were modelled using fiber discretized cross-sections, and the evaluation encompassed both static pushover and IDA methods to determine the collapse margin ratio for each individual structure. Xu et al. (2023) assessed the seismic performance of RC frame-wall dual structural systems, comparing systems where structural walls primarily bear lateral loads with those where walls support both lateral and vertical loads.

2.6 Literature Gaps and Rationale of the Study

Given the insights obtained from the available literature, it becomes evident that in the modern world, where major seismic events are occurring with heightened frequency, the accurate evaluation of seismic fragility in key structural systems within the built environment holds immense significance. This evaluation not only aids in comprehensively understanding structural vulnerability but also guides mitigation strategies and enhances community resilience against seismic occurrences. A multitude of approaches, spanning from empirical techniques to nonlinear static and dynamic analyses, have emerged for the seismic evaluation of various structural systems. Extensive efforts have been devoted to refining the effectiveness of these structural performance evaluation methodologies, with a primary aim being the reduction of computational resources and time necessary for conducting in-depth seismic evaluations. The quest for suitable engineering demand parameters and seismic intensity measures to accurately characterize seismic demands on structures has been a focal point of several research efforts. Reliable probabilistic seismic assessment of structures necessitates the appropriate characterization and propagation of different uncertainties through the analyses, along with their impact on the sensitivity of the structural seismic performance. Selecting a damage scale for evaluating buildings plays a pivotal role in establishing fragility functions, and various groups of researchers have proposed diverse and intriguing approaches to delineate limit states for seismic damage in structures, along with corresponding thresholds for different structural systems. Integrating all the key components, seismic fragility assessment of different structural systems for wide range of performance levels have been performed by researchers.

Although the literature review identifies the gamut of studies conducted, extensive studies on seismic fragility evaluation of RC wall-frame buildings, remains limited. Apart from that aspect, the following points highlight the research gaps in the present context:

- While previous research has concentrated on selecting a suitable seismic intensity measure to establish fragility relationships for RC wall-frame buildings, the literature is notably lacking in discussions regarding the selection of an effective EDP for accurately characterizing fragility estimates for this particular structural typology.
- Conventionally, the probabilistic assessment of fragility estimates often revolves around factoring in the uncertainty linked to seismic demand (aleatory). Yet, achieving a comprehensive fragility relationship requires a deliberate inclusion of the uncertainty

associated with structural capacity (epistemic). The comprehensive characterization and propagation of both aleatory and epistemic sources of uncertainty in fragility analyses, especially concerning RC wall-frame buildings, has rarely been documented in existing literature.

- Establishing clearly defined and quantifiable thresholds corresponding to various levels of damage states is imperative to attain reliable structural seismic fragility functions. The current definitions of damage states for RC structural walls hinge on empirical criteria, lacking predictions for damage thresholds considering different wall structural parameters.
- Essentially, considering multiple seismic IMs enriches the fragility assessment process by capturing a broader range of ground motion effects, reducing uncertainty associated with relying solely on one IM, and enabling a more accurate understanding of seismic vulnerability. In the context of evaluating fragility estimates for RC structural wall systems, the conventional practice has predominantly centered on a solitary parameter to link seismic intensity levels with the expected structural damage within fragility relationships.
- None of the existing studies have currently endeavoured to reduce computational costs and time for estimating seismic fragility relationships using multiple seismic IMs, particularly for the RC wall-frame structure typology, through truncated set of ground motion records while maintaining comparable damage probabilities to those obtained from complete record set.

2.7 Scope of the Present Study

Drawing from the identified gaps in existing literature, the objectives of the present study, as previously outlined in Chapter 1, can be succinctly framed as the "Comprehensive seismic fragility evaluation of RC wall-frame buildings." To fulfil this objective, the following scope of work is delineated:

- To establish reliable fragility relationships for the considered RC wall-frame structure, appropriate selection of few key components pertaining to structural response-seismic demand characterization are performed, namely EDPs and input ground motion records.
- The inherent randomness in structural capacity and the record-to-record variability into seismic response analysis are integrated by employing augmented incremental dynamic analyses. This approach is expected to realistically capture and disseminate various

sources of uncertainty during the fragility assessment of the considered RC wall-frame structure.

- Closed-form expressions for prediction of lateral drift levels across different damage states of an isolated slender RC structural wall, are developed using Genetic Programming. A substantial dataset of numerically assessed specimens of RC structural walls is utilized, with a focus on numerous essential wall structural parameters as independent variables for estimation.
- Fragility functions are developed for an RC wall-frame building and a representative exterior wall-frame extracted from the benchmark building, and then compared to identify the level of seismic vulnerability. The fragility relationships are obtained for the specific building typology, considering both scalar IMs and vector-valued IMs.
- A simplified methodology is developed to obtain efficient fragility estimates for the considered RC wall-frame building utilizing fewer ground motion records, while ensuring comparability with estimates from the complete record set.

CHAPTER 3

NUMERICAL MODELLING AND FRAGILITY PARAMETER SELECTION

3.1 Overview and Motivation

In order to achieve the objectives of the present study, Finite Element Method (FEM) is used to carry out the numerical simulations. In this chapter, the different modelling approaches employed in the current study as well as the material properties for simulating nonlinear response are discussed. The considered structure is simulated and assessed within the OpenSEES (McKenna et al., 2000) software framework, and the modelling methodology is validated by comparing the results with existing experimental findings found in the literature. Furthermore, to establish the reliability of the derived fragility functions for the RC wall-frame structure, this chapter explores the input ground motions and Engineering Demand Parameters (EDPs) needed to formulate these probabilistic functions. Two different set of ground motions are considered for performing the Incremental Dynamic Analysis (IDA), namely one set selected considering the strong-motion parameters and the other set selected with respect to geophysical parameters. Results of nonlinear dynamic analyses are quantitatively compared, and it is observed that the both sets of records can estimate seismic response with the same reliability when conditioned on the appropriate choice of EDP. The efficiency of the EDP in the seismic response prediction is evaluated based on statistical analyses of the IDA results.

3.2 Details of the Structural System

For evaluating the seismic fragility of RC wall-frame buildings, an 8-storey RC wall-frame building conforming to the latest Indian seismic design principles (BIS, 2000; and BIS, 2016a) and situated in Seismic Zone V as per IS 1893 Part I (BIS, 2016b), is adopted as the structural system in the present study. The plan dimensions of the building, structural element arrangement and design are typical and widely seen within the regions with high seismicity in the Indian subcontinent. The building is assumed to be free from the effects of soil-structure interaction and also infill walls; elevator cores and staircases are also not considered for the numerical model. The architectural floor plan and the typical reinforcement layout for the

beam, column, and structural wall are depicted in Figures 3.1 and 3.2, respectively. A structural wall is placed solely within the central bay in each direction, without any additional ones in the other bays. The building is designed as per the Indian design codes (BIS, 2000; and BIS, 2016a), based on the results of linear static analysis of the building model using the computer software SAP2000 (CSI, 2015).

The building has plan dimensions of 15m × 9m and a height of 25.5m, with a floor-to-floor height of 3m. The columns are designed with dimensions of 400mm × 400mm, while the beams have dimensions of 230mm × 400mm. The slab thickness is 150mm, and the RC structural walls are 200mm thick. The analysis and design of the building are carried out using M30 grade concrete and Fe500 grade steel reinforcement bars.

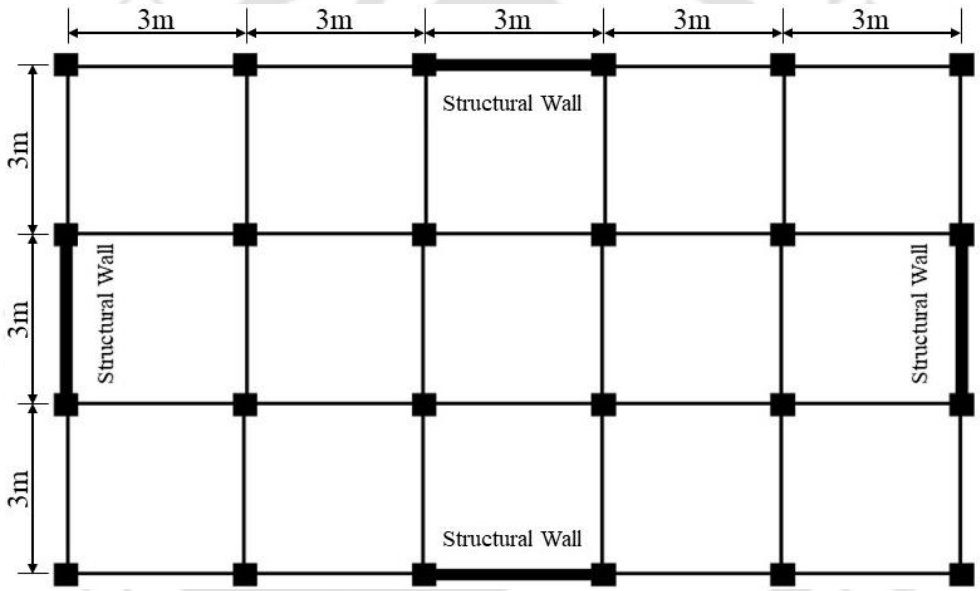

Figure 3.1 Typical floor plan of the RC wall-frame building considered in the present study.

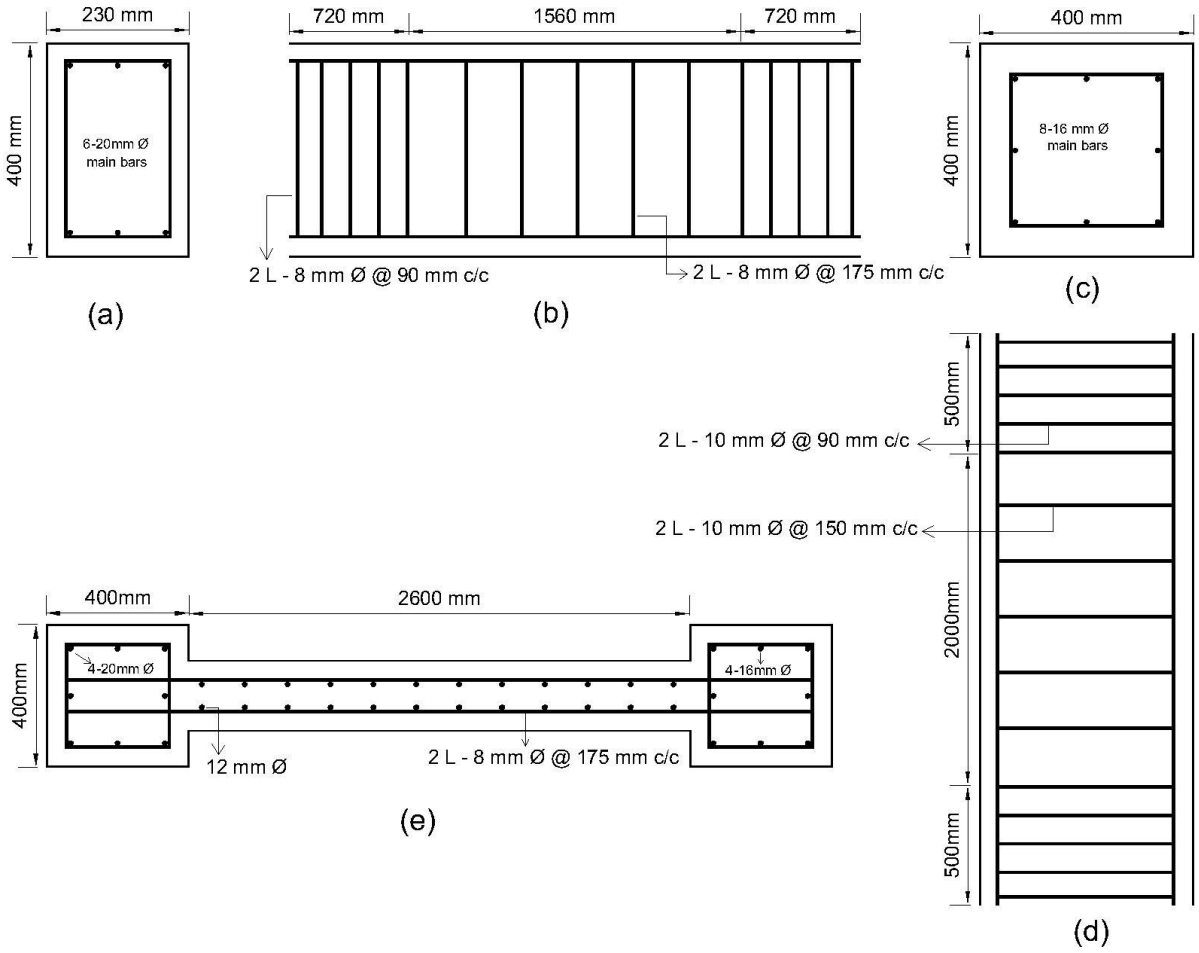

Figure 3.2 Reinforcement details in (a) beam cross-section, (b) beam longitudinal section, (c) column cross-section, (d) column longitudinal section and (e) RC wall cross-section.

3.3 Material Models

In an RC structure, the structural elements are anticipated to experience significant nonlinear deformations during strong seismic events. Therefore, conducting a precise and reliable seismic fragility assessment requires assigning suitable material properties to the different constituent elements (such as concrete and steel reinforcement bars) to accurately replicate the expected inelastic seismic response. The selected material models must be capable of accurately characterising both the monotonic response and hysteretic relationships exhibited during cyclic behaviour. From the array of constitutive models available in the OpenSEES material archive, the choice of material models should aim for a balance between accurately representing nonlinear structural behaviour and computational efficiency. Opting for a highly computationally intensive model may lead to significant challenges when analysing large

structural models. The subsequent sections outline the material models applied in the present study to simulate the nonlinear performance of RC components.

3.3.1 Concrete Model

The concept of concrete confinement is fundamental to the performance of RC structures, signifying the ability of transverse reinforcement elements like stirrups or hoops to restrict the lateral expansion of concrete under axial loads or lateral forces, such as those generated by earthquakes. This confinement mechanism plays a pivotal role in improving the ductility and strength of RC elements, through prevention of early cracking and delaying the initiation of concrete crushing. Therefore, it is of utmost importance to adequately model both the confined core concrete and the unconfined cover concrete for realistic assessment of the structural performance of RC wall-frame structure.

In the current study, both confined and unconfined concrete are modelled using the *Concrete02* material model available in OpenSEES. This model accounts for linear tension softening, as depicted in the general stress-strain relationship (Figure 3.3) and can accurately represent cyclic strength degradation. In Figure 3.3, f_{pc} and f_{pcu} denote the concrete compressive strength in 28 days and concrete ultimate strength, respectively; ε_{psc0} and ε_{pscU} are the strain in concrete corresponding to the maximum compressive strength and the ultimate crushing strength, respectively; E_0 and λ indicate the initial slope for the compressive stress-strain curve and the ratio between E_0 and the slope at ε_{psU}, respectively. The assumed elastic modulus for the tensile behaviour of concrete is (Ko and Phung, 2014):

$$E_{ts} = \frac{f_t}{0.002} \tag{3.1}$$

where, f_t represents the concrete tensile strength and can be evaluated as $f_t = 0.7\sqrt{f_{pc}}$.

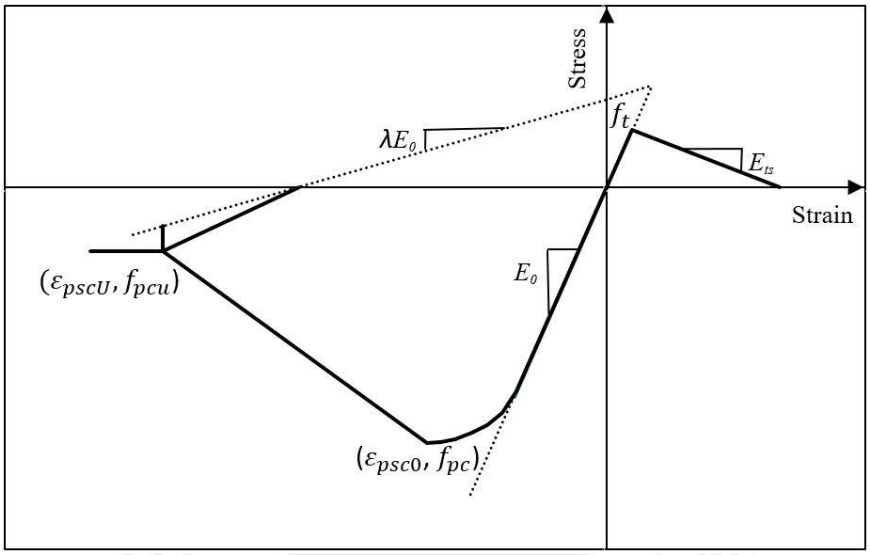

Figure 3.3 Stress-strain relationship for *Concrete02* material model (Mazzoni et al., 2009).

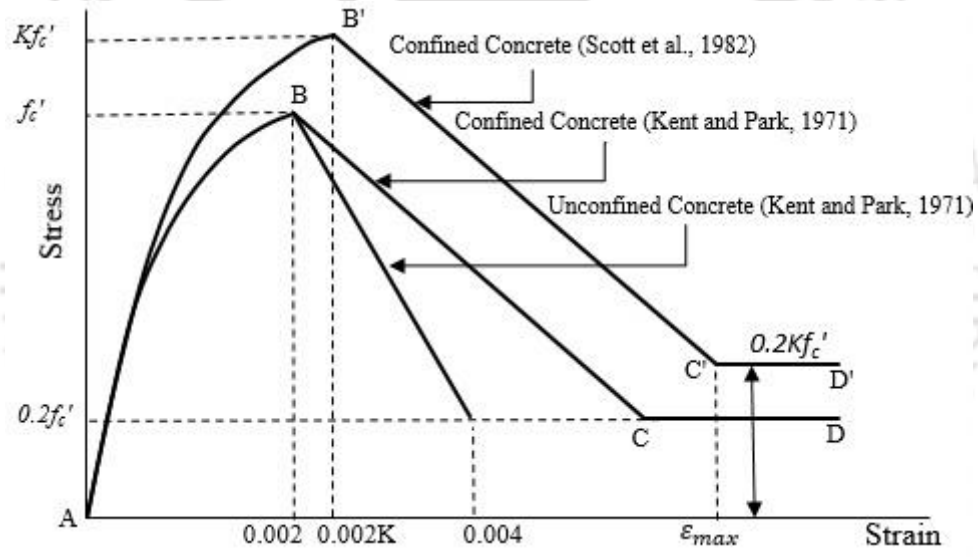

Figure 3.4 Concrete stress-strain relationships: Kent and Park (1971) and the modified Kent and Park (Scott et al., 1982) models.

It should be emphasized that the *Concrete02* material model is derived from the Kent-Park-Scott concrete model. The stress-strain characteristics of unconfined concrete is represented by the Kent-Park model (Kent and Park, 1971), while the confined concrete follows the modified Kent-Park model (Scott et al., 1982). Figure 3.4 illustrates the stress-strain relationships for both confined and unconfined concrete, as defined in the Kent-Park-Scott concrete model.

In the case of unconfined concrete, within the segment AB, which occurs before reaching the point of maximum stress, the stress-strain relationship can be described by Eq. 3.1. Here, f_c represents the concrete stress, ε_c signifies the concrete strain, and f_c' denotes the concrete

cylinder strength. Upon reaching the maximum stress, in the BC segment, the stress-strain relationship exhibits a linear decline until the failure stress is attained, which for unconfined concrete is consistently set at $0.2f_c'$.

$$f_c = f_c' \left[\frac{2\varepsilon_c}{0.002} - \left(\frac{\varepsilon_c}{0.002}\right)^2\right] \tag{3.1}$$

As previously mentioned, an effective layout of transverse reinforcement has the potential to significantly improve both the strength and ductility of RC members. The original Kent-Park concrete model (1971), as shown in Figure 3.4, accounts for the effect of confinement by enhancing the ductility of the concrete (segment BCD) but does not consider an increase in concrete strength due to confinement. To address this limitation, Scott et al. (1982) introduced the modified Kent-Park model, which accurately represents both the increase in strength and ductility of concrete due to confinement. Although both the original and the modified Kent-Park models exhibit a similar stress-strain relationship before reaching the maximum stress, the key difference between the models lies in the magnitude of the maximum stress and the corresponding strain value (segment AB'). The modified Kent-Park concrete model incorporates a factor 'K' to adjust the stress and strain values in accordance with the original Kent-Park model. The factor 'K' is determined using the following expression:

$$K = 1 + \frac{\rho_s f_{yh}}{f_c'} \tag{3.2}$$

where, ρ_s denotes the volumetric ratio of the transverse reinforcement and the concrete core bounded within the outside of stirrups, and f_{yh} represents the yield strength of the transverse reinforcement bars.

Much like the original model, the modified Kent-Park model characterizes the post-peak stress-strain relationship of confined concrete with a linear descending branch (segment B'C'). The maximum strength of confined concrete is constrained to 20% of the peak strength (Kf_c'). The ultimate strain of concrete confined by transverse reinforcement is evaluated as follows:

$$\varepsilon_{max} = 0.004 + 0.9\rho_s \frac{f_{yh}}{300} \tag{3.3}$$

3.3.2 Steel Rebar Model

As stated earlier, the chosen material model must possess the capacity to demonstrate both strength degradation and hysteretic behaviour. When it comes to reinforcing steel, strength degradation occurs primarily due to the buckling of the steel rebars at the locations where the cover concrete has cracked or got spalled off first, followed by crushing or shear failure of the core concrete. During severe earthquake shaking, inherent brittleness of concrete often leads to early cracking or spalling at relatively lower seismic intensity levels. This leads to the exposure of steel reinforcement bars, which, owing to their ductile nature, substantially govern the behaviour of RC sections at higher seismic intensity levels. Hence, it is of paramount importance to accurately characterize the stress-strain relationship of reinforcing steel when conducting numerical simulations for RC sections. In addition to the ability of the model to replicate the peak stress-strain relationship and hysteresis behaviour of steel rebars, it should also be equipped to incorporate various phenomena observed in steel rebars during cyclic loading. These include the Bauschinger effect, which entails a reduction in the yield stress of the reinforcement bar in compression due to prior tensile deformation. Additionally, the model must account for isotropic hardening, which denotes the strengthening of reinforcing steel when exposed to plastic deformation, regardless of direction of loading applied either tensile or compressive.

In the present study, the steel rebars are modelled using the Steel02 uniaxial material model available in the OpenSEES framework. This model is based on the constitutive stress-strain relationship originally proposed by Menegotto and Pinto (1973) and later refined by Filippou et al. (1983). Figure 3.5 illustrates a generic stress-strain relationship for the Menegotto-Pinto steel model, where the characteristics of the model are determined by specific factors, including stress and strain values at the yield and ultimate points $(\sigma_{sy}, \varepsilon_{sy})$ and $(\sigma_u, \varepsilon_u)$, respectively, the modulus of elasticity (E_s), and the ratio between the strain hardening slope and the initial slope, denoted as $\bar{b} = E_h/E_s$.

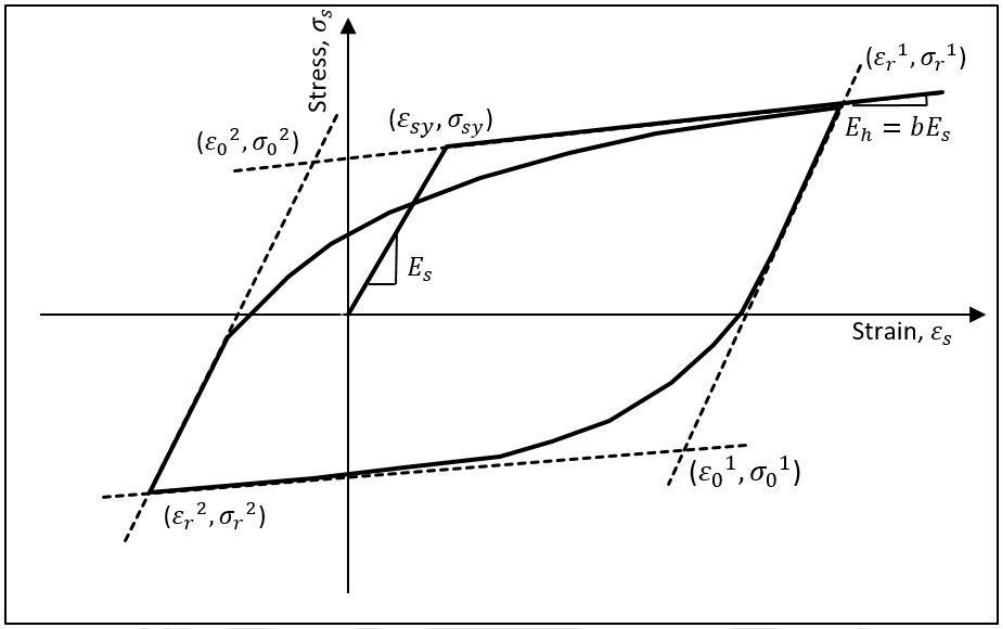

Figure 3.5 Stress-strain relationship used for reinforcing steel bars (Menegotto and Pinto, 1973).

The relationship exhibits a curved transition, shifting from a linear asymptote associated with the elastic segment characterized by a slope of E_s to another linear asymptote representing the strain hardening segment with a slope of E_h. Mathematically, the relationship is expressed as follows:

$$\sigma^* = \bar{b}\varepsilon^* + \frac{(1-\bar{b})\varepsilon^*}{\left(1+\varepsilon^{*R'}\right)^{\frac{1}{R'}}} \tag{3.4}$$

The degree of curvature in the transition curve connecting the two straight-line asymptotes is controlled by a cyclic curvature parameter R', allowing for the representation of the Bauschinger effect. The parameter R' is defined as a function of ζ using Eq. 3.5, where ζ represents the magnitude of plastic strain from the preceding excursion.

$$R' = R_0 - \frac{a_1\zeta}{a_2+\zeta} \tag{3.5}$$

where, R_0 is the value of R' during the initial loading and a_1 and a_2 are material coefficient values. The correlation between the normalized stress-strain pair $(\sigma^*, \varepsilon^*)$ in Eq. 3.4 and the uniaxial stress-strain pair $(\sigma_s, \varepsilon_s)$ is depicted as follows:

$$\sigma^* = \frac{\sigma_s-\sigma_r}{\sigma_0+\sigma_r} \tag{3.6}$$

$$\varepsilon^* = \frac{\varepsilon_s-\varepsilon_r}{\varepsilon_0+\varepsilon_r} \tag{3.7}$$

where, (σ_0,ε_0) represent the stress-strain pair at the point where the two linear asymptotes intersect, corresponding to a particular cycle under consideration; and (σ_r, ε_r) represent the point corresponding to the previous load reversal.

The Menegetto-Pinto steel model offers advantages in terms of numerical efficiency and its ability to provide accurate results that align closely with experimental findings from cyclic tests on reinforcing steel bars. However, one of its drawbacks is its inability to account for the influence of isotropic hardening. To address this limitation, Filippou et al. (1983) introduced modifications to the original Menegetto-Pinto steel model. These modifications incorporate the isotropic hardening effect by adjusting the yield stress after each strain reversal, based on the peak plastic strain observed in the preceding cycle. The modified yield stress ($\overline{\sigma_{sy}}$) is expressed as:

$$\overline{\sigma_{sy}} = \sigma_{sy} a_3 \left(\frac{\varepsilon_{max}}{\varepsilon_{sy}} - a_4 \right) \tag{3.8}$$

where, a_3 and a_4 factors calibrated based on experimental results, ε_{max} denotes the peak strain magnitude at the point of load reversal, ($\sigma_{sy}, \varepsilon_{sy}$) refer to the stress-strain values corresponding to the yield point.

3.4 Structural Modelling

Structures designed in compliance with modern seismic standards are expected to delve well into the nonlinear domain when subjected to strong earthquake motions. To analytically assess the seismic behaviour of these structures, it is imperative to create accurate numerical models that capture their complex response. This is achieved by discretizing the structural geometry into multiple elements and creating mathematical representations of various structural components. These mathematical models must account for both elastic and nonlinear behaviours. Balancing computational efficiency with accurate response characterization is crucial when idealizing the seismic behaviour of structural members, which is essential for obtaining realistic estimates of the structural response. In the present study, appropriate numerical modelling methodology is employed in the OpenSEES framework to carry out further analysis.

The nonlinear elements in the structure are modelled using the “nonlinearBeamColumn” element in the OpenSEES platform. This element relies on the flexibility formulation of beam-column components, which employs precise interpolation of internal forces (Spacone et

al., 1996). It takes into account the distribution of plastic deformation throughout the length of the member, and to achieve this, it incorporates five integration points within the length of the element. The cross-section of the member is modelled using a "FiberSection" approach, which involves dividing the cross-section into layers, comprising the concrete component and the steel rebars. When adopting the fiber technique in this modelling approach, each element is depicted as a single line coinciding with the centreline of the member. The response parameter (such as stress or force) within each fiber section along the axis of the element is determined based on the strain computed using the material constitutive models that characterize local behaviour. To simplify the mathematical modelling and analysis of complex structures, the inertial forces within the structural system are approximated by assuming that the mass of the entire structure is concentrated or "lumped" at specific locations on each floor level. This technique involves consolidating the mass of the structural components at the nodes where the frame members intersect on each floor, thereby representing the mass distribution within a multi-story building.

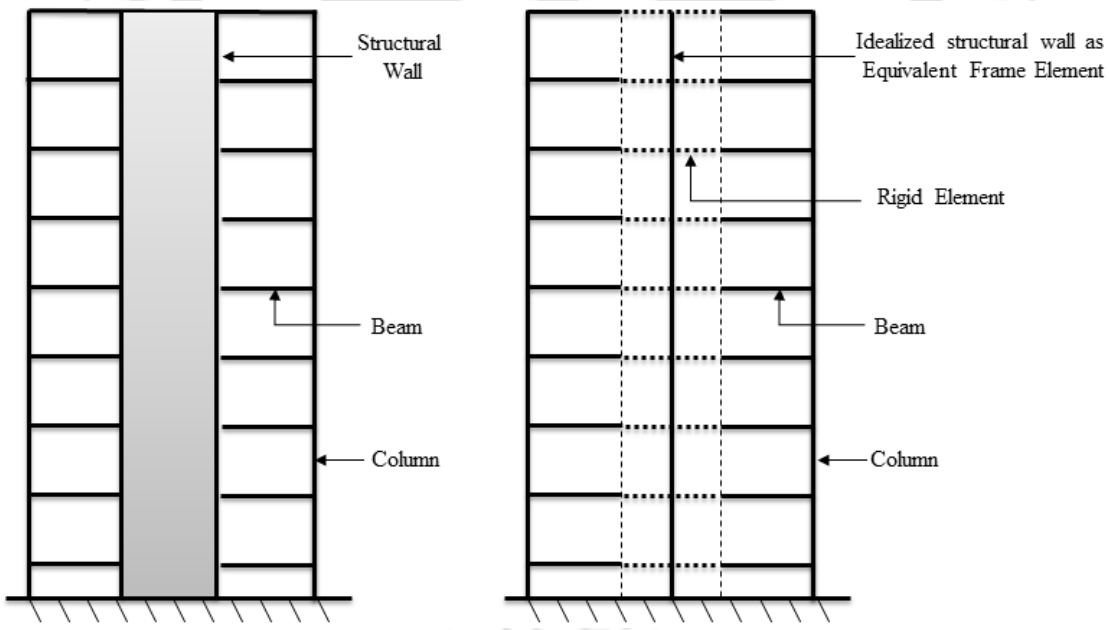

Figure 3.6 Idealization of structural wall member as an equivalent frame element.

The equivalent frame element model (Figure 3.6) is employed here to simulate structural walls due to its numerous advantages, including ease of implementation and computational efficiency (Beyer et al., 2008; Lowes et al., 2019). This approach involves idealizing the structural wall components using one-dimensional frame elements coinciding with the centerline of the wall section, with cross-sectional properties resembling those of the wall itself (Chaallal and Ghlamallah, 1996). To accurately capture the geometry and monolithic

behaviour of the wall-frame system, rigid elements are used to connect the nodes at the centerline of the wall section and those at the adjacent column ends.

A reliable analytical seismic assessment of a building structure requires comprehensive NDAs of the idealized numerical model. While OpenSEES is an effective framework for three-dimensional (3D) modelling and analysis, conducting numerous NDAs for a full 3D building structure model can be computationally intensive, especially when considering a broad spectrum of ground motion records. Therefore, in the present study to investigate the different key facets of seismic fragility formulation (such as uncertainty assessment, performance level identification); a two-dimensional (2D) modelling approach is adopted to idealize the numerical model of the considered structural system. The adopted 2D nonlinear model represents a cross-sectional slice of the 3D building system under consideration. This 2D numerical model idealizes an exterior frame in the transverse direction of the considered building, including three bays and a central structural wall element. The 2D idealized model employs two-noded frame elements, with each node having three degrees of freedom: two displacements and one in-plane rotation in perpendicular directions.

However, to substantiate the reliability of the fragility estimates derived for 2D RC wall-frame structure, a comparison is made with fragility estimates derived for the 3D building structural system in Section 7.6. For this purpose, the considered RC wall-frame building structure is numerically idealized as a 3D model and analysed to evaluate the fragility functions. The 3D numerical model of the building structure also utilizes two-noded frame elements but has six degrees of freedom at each node, encompassing three displacements and three in-plane rotations in perpendicular directions.

3.5 Validation of Modelling Methodology

In order to ensure the reliability and accuracy of response simulations in numerical studies, it is imperative to conduct a validation study before embarking on exhaustive analyses. To confirm the suitability of the modelling approach, a comparison between simulated and experimentally obtained results from the literature is presented. This comparison utilizes observed data from experimental tests conducted on cantilever structural wall specimens by Thomsen and Wallace (2004) and Liu (2004), with their details listed in Table 3.1. Figure 3.7 shows the cross-sectional view of the considered wall specimens, and the comparison of numerical and experimental results in terms of load-displacement curves is shown in Figure

3.8. It can be observed that the finite element modeling approach and the subsequent analysis methodology are able to capture the experimental global response successfully, and thus get validated for further use in the present study.

Table 3.1 Experimentally tested wall specimen details (Thomsen and Wallace, 2004; Liu 2004)

	Length (mm)	Height (mm)	Thickness (mm)	Concrete compressive strength (MPa)	Yield strength of steel bars (MPa)	Axial load ratio
RW2	1220	3660	102	42.8	414	0.10
W1	1200	4000	200	35	457.7	0.07

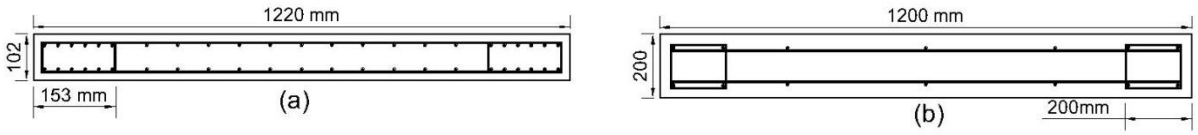

Figure 3.7 Reinforcement details of (a) RW2 (Thomsen and Wallace, 2004) and (b) W1 specimens (Liu 2004).

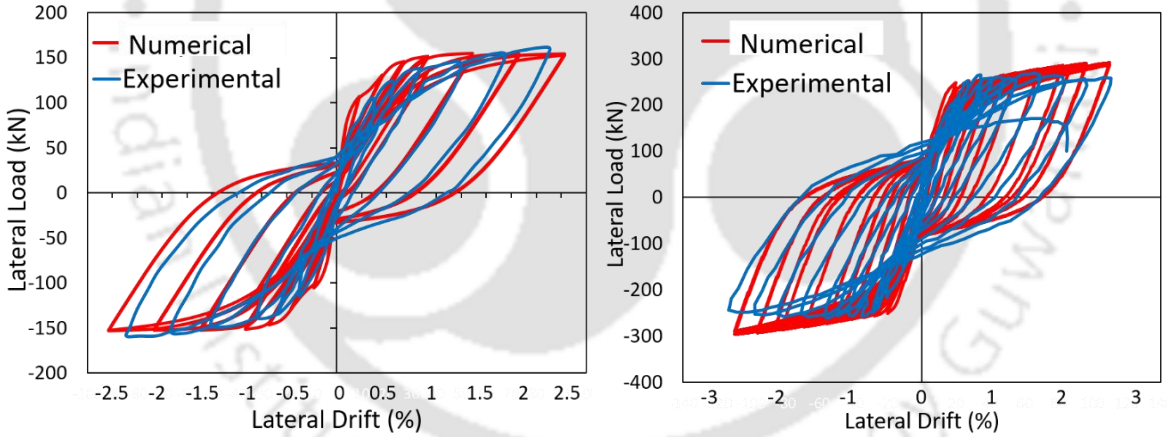

Figure 3.8 Force displacement response of (a) RW2 (Thomsen and Wallace, 2004) and (b) W1 specimens (Liu 2004).

3.6 Seismic Response Analysis

The present study assesses the seismic fragility functions of the examined structural system by utilizing the structural performance results obtained through extensive NDAs. Although NDAs can be time-consuming and computationally demanding, the resulting structural responses closely resemble the actual behaviour of the structure. Numerous techniques exist in the literature for accurately characterizing the relationship between EDPs and IMs to

perform NDA. To minimize uncertainties, this process requires conducting a significant number of analyses using various ground motion records at different seismic intensity levels. Multiple stripe analysis, as proposed by Jalayer and Cornell (2009), involves analyzing ground motion records scaled to specific intensity levels. Another method, known as cloud analysis, developed by Jalayer (2003), involves analysing ground motion records, whether scaled or unscaled, at various intensity levels to establish the EDP-IM relationship. However, the most commonly used and the one employed in the present study is Incremental Dynamic Analysis (IDA) introduced by Vamvatsikos and Cornell (2002). IDA entails analysing a set of ground motions scaled to different seismic intensity levels to evaluate recorded EDPs. Plotting these (EDP, IM) pairs results in continuous curves known as IDA curves. The scaling of intensity levels is adjusted to cover the entire range from elasticity to the final global collapse state. To achieve this, a hunt and fill algorithm, as outlined by Vamvatsikos and Cornell (2004), is utilized in the present study. The reliable and efficient estimation of structural seismic performance using IDAs relies on selecting an appropriate set of input ground motion records and the careful choice of EDPs and IMs, as discussed in the following subsections.

3.6.1 Ground Motion Records

In an effort to choose the most suitable set of ground motion records for the seismic response analysis of the considered building type, an evaluation is conducted to assess how input motions, assembled using different criteria, affect the structural response parameters. By statistically examining seismic response parameters relative to different sets of ground motion records, conclusions are drawn about the impact of various selection criteria for input motions. This process aids in identifying and confirming a specific set of records for further analysis of the seismic fragility of the considered building structure.

Two sets of ground motion records, each assembled using distinct criteria, are employed to investigate the influence of the different suites of input motions on the seismic response of the chosen building typology. These records are sourced from the Pacific Earthquake Engineering Research Center (PEER strong ground motion database, 2006). All the ground motion records used can be defined as ordinary, which are recorded on free-field instrumentation, belonging to C-D soil type of NEHRP and also excluding near field records (those with nearest distance to fault rupture smaller than 10 km) so as to negate pulse-type effects. The number of accelerograms to be used for the response analysis of structures under

seismic loads has been a subject of research for several studies. Hancock et al. (2007) and Cimellaro et al. (2011) suggest considering a minimum of 3 and 20 ground motion records, respectively, for evaluating the fragility functions of structures when using first mode spectral acceleration for scaling the records. Several international seismic design guidelines (ASCE/SEI 7–10, 2010; Eurocode 8: Part 1, 2003) recommend using at least 7 records to estimate seismic response of buildings with acceptable accuracy. In recent times, two guidelines, ATC-58 (2009) and ASCE 7-10 (2010), advocate using minimum of 11 records for accurate estimation of the demand-capacity relationship of building structures. Therefore, both sets of ground motion employed in performing the response analysis of the considered building frame consist of eleven records each.

- **Strong-Motion Parameter based Record Set (Set-I)**

The first set of 11 ground motion records is selected based on specific strong-motion parameters, namely Peak Ground Acceleration (PGA) and Peak Ground Velocity (PGV). These records are chosen from the 22 records documented in FEMA-P695 (2008). The 22 prescribed records involved earthquakes with magnitudes exceeding 6.5. The choice of 11 records among the 22 records of FEMA-P695 (2008) is made based on suitable values of the ratio of PGA and PGV (referred to as a/v ratio hereafter). Researchers in the past (e.g., Kwon and Elnashai, 2006) have highlighted the fact that the damaging potential of ground motion records is highly dependent on the frequency content of the records, which is indicated in the shape of acceleration response spectrum. In order to minimize the variability among the inelastic response of structures, ground motions with similar frequency content are preferred. The a/v ratio of records can serve as a criterion for categorizing ground motion in relation to the earthquake magnitude-distance range (M-$\bar{R}$) relationship, duration, and frequency content of ground motion (Tso et al., 1992). Kazaz (2010) suggested selecting ground motions with an a/v ratio smaller than $10s^{-1}$ to ensure that motions with erratic frequency content are not chosen for seismic response analysis. Thus, for this set of input records, 11 records are selected from the 22 specified in FEMA-P695 (2008), based on the criteria of an a/v ratio ($< 10s^{-1}$), and are presented in Table 3.2.

Table 3.2 Strong-Motion Parameter based Record Set (Set-I)

Sl. No.	Earthquake (year)	M	Station data source	Distance to Source (km)	PGA(g)
1	Northridge (1994)	6.7	Beverly Hills - Mulhol	17.2	0.49
2	Northridge (1994)	6.7	Canyon Country-WLC	12.4	0.40
3	Hector Mine (1999)	7.1	Hector	12.0	0.33
4	Imperial Valley (1979)	6.5	El Centro Array #11	12.5	0.38
5	Kobe, Japan (1995)	6.9	Shin-Osaka	28.5	0.22
6	Kocaeli, Turkey (1999)	7.5	Duzce	15.4	0.36
7	Kocaeli, Turkey (1999)	7.5	Arcelik	13.5	0.13
8	Landers (1992)	7.3	Yermo Fire Station	23.8	0.24
9	Landers (1992)	7.3	Coolwater	20.0	0.42
10	Manjil, Iran (1990)	7.4	Abbar	13.0	0.50
11	Superstition Hills (1987)	6.5	El Centro Imp. Co.	18.5	0.36

- **Geophysical Parameter based Record Set (Set-II)**

The second set of 11 ground motion records is chosen using a common approach, which involves considering magnitude-distance bins as a geophysical parameter representing various earthquake scenarios. Several dynamic analysis studies (Ji et al., 2009; Zareian and Krawinkler, 2010) have been conducted on structures in which ground motions were categorized using different M- $\bar{R}$ bins. The categorization of M- $\bar{R}$ bins used in these research studies was examined to establish the M- $\bar{R}$ bins for selecting the records, which are denoted as:

- Large Magnitude-Short Distance Bin, LMSR, (6.0< M <7.5, 12km< $\bar{R}$ <40km)
- Large Magnitude-Long Distance Bin, LMLR, (6.0< M <7.5, 40km<$\bar{R}$ <90km)
- Small Magnitude-Short Distance Bin, SMSR, (5.4< M <6.0, 12km< $\bar{R}$ <40km)

This set of ground motion records (Table 3.3) is compiled with consideration of significant variations in PGA levels, energy content, and total duration of the records. Among the various alternate measures of energy proposed over the years, the Arias Intensity is the most commonly used parameter. The strong motion duration of a record is defined by the time span between 5% and 95% of the Arias Intensity (Trifunac and Brady, 1975). As shown in

Table 3.3, the considered ground motions exhibit significant variation in terms of Arias Intensity (ranging from 0.05m/s to 2.15m/s) and strong motion duration (ranging from 8.9sec to 50.4sec). The damage potential of a particular ground motion can be effectively characterized by its Arias Intensity and strong motion duration (Choudhury and Kaushik, 2018).

Table 3.3 Geophysical parameter based record set (Set-II)

Sl. No.	Category	Earthquake (year)	*M*	Station data source	Distance to Source (km)	PGA(g)	Arias Intensity (m/s)	Strong motion duration (sec)
1	LMSR	Spitak Armenia (1988)	6.77	Gukasian	23.99	0.20	0.28	10.5
2		Northridge-01 (1994)	6.69	Castaic - Old Ridge Route	20.72	0.57	1.39	9.1
3		Kocaeli Turkey (1999)	7.51	Arcelik	13.50	0.13	0.43	11.1
4		Kocaeli Turkey (1999)	7.51	Duzce	15.37	0.22	2.15	11.8
5		Christchurch New Zealand (2011)	6.20	SWNC	25.45	0.19	0.47	8.9
6		Landers (1999)	7.30	Yermo Fire Station	23.80	0.17	0.46	18.9
7	LMLR	Northridge-01 (1994)	6.69	Carson - Water St	49.81	0.08	0.20	23.4
8		Kobe Japan (1995)	6.90	Chihaya	49.91	0.078	0.12	12.0
9		Kocaeli Turkey (1999)	7.51	Bursa Tofas	60.43	0.077	0.70	41.2
10		Christchurch New Zealand (2011)	6.20	AMBC	41.08	0.03	0.05	43.6
11	SMSR	Molise-01 Italy (2002)	5.70	Castiglione Messer Marino	34.29	0.0057	0.002	50.4

3.7 Engineering Demand Parameter and Intensity Measure

The formulation of fragility functions through seismic performance assessment methods, especially IDA, is significantly influenced by the estimated IDA curves. These IDA curves, in turn, depend heavily on the selection of two crucial variables: EDP and IM. Therefore, accurately establishing fragility relationships for building structures necessitates the careful choice of these fundamental variables, EDP and IM. The seismic performance level of structures is essentially represented through EDPs. EDPs serve the purpose of quantifying damage to both structural and non-structural components of buildings, thereby aiding in the evaluation of fragility estimates for these structures. Conversely, IM can be viewed as the bridge connecting geophysical parameters (such as magnitude and source-to-site distance) with the seismic response of structural systems. Typically, fragility functions for structures are constructed by analysing seismic structural performance across different IM levels, rather than considering a combination of various earthquake seismic characteristics.

Multiple EDPs are explored here, in order to determine the most efficient representation of structural seismic response, which will be used further in the study for fragility evaluation of the considered building structure. All EDPs considered have been frequently used in the past vulnerability studies. The discussed response parameters are elaborated upon as follows.

- Inter-Storey Drift ratio

The ISD, in simple terms, can be defined as the maximum ratio of the relative in-plane displacements between two successive floor levels and the corresponding storey height. It is one of the most straightforward EDPs, which can be evaluated by analysing either a linear or nonlinear model. It is a global damage measure well-equipped to efficiently represent both structural and non-structural deformations.

- Roof displacement

The maximum roof displacement is a global deformation measure that requires monitoring and can serve as an effective EDP. Roof displacement is a widely used EDP for assessing the seismic behaviour of structures. It quantifies the maximum horizontal displacement experienced by the uppermost level or storey of a building structure as a consequence of ground shaking. As seen in an ideal structure on application of lateral load, the top level component is expected to be undergoing the maximum deformation, thus roof displacement is investigated in the present study.

- Floor acceleration

In the present study, floor acceleration is used as a potential EDP, representing the horizontal component of acceleration of the associated storey. It can be employed for damage assessment to investigate the seismic damage of non-structural systems and equipment, configured in a way that renders them highly vulnerable to significant floor accelerations.

- Concrete Compressive Strain

The concrete compressive strain is a popular material-level EDP used to investigate the seismic damage of RC structural wall components. The material strain of different structural systems can be evaluated from either linear or nonlinear analysis of finite element models. The evaluated strain can serve as an efficient EDP in the vulnerability studies as it distinctly represents the corresponding material seismic damage.

- Storey Curvature

To assess seismic damage at the storey level in structural systems, storey curvature is utilized as an EDP, which is defined as the peak curvature within each storey level. In simpler terms, storey curvature can be estimated as the maximum ratio of the relative in-plane rotation between two successive floor levels and the corresponding storey height. Typically, when analysing the seismic response of structures, the top or bottom of the storey tends to exhibit the maximum curvature for each storey.

In vulnerability studies, careful consideration of the seismic IM is extremely important as it quantitatively represents the key ground motion characteristics, namely amplitude, frequency content, and strong motion duration. Establishing a strong correlation between the EDP and the IM enhances the precision of seismic performance evaluation and reduces the variability in predicting structural responses. Consequently, it is imperative to identify an optimal IM that effectively correlates with a suitable EDP. In order to create fragility functions that can accurately and effectively depict the diverse response states of a structure to varying earthquake records of increasing intensity, it is essential to establish an appropriate measure of ground motion intensity. A suitable seismic IM should effectively capture the ground motion characteristics that significantly influence the inelastic structural response under earthquake loading. Hence, an ideal IM should encompass details about both the earthquake motion itself and the structural characteristics, making it a more comprehensive indicator of structural performance.

Over the years, a range of IMs, spanning from simple to more complex ones, have been proposed. Some rely solely on ground motion parameters, such as Peak Ground Acceleration (PGA), while others consider both ground motion and structural characteristics, like spectral acceleration (S_a). PGA, a peak amplitude parameter of ground motion, has been widely adopted as a seismic IM in past vulnerability studies (Ji et al., 2009; Jiang et al., 2015; Pejovic and Jankovic, 2016). It exhibits a high correlation with seismic inertial forces in structures, particularly in the case of rigid structures. However, aside from amplitude, PGA cannot adequately capture other ground motion characteristics, such as frequency content and strong motion duration, which have a significant impact on the seismic behavior of structures. Notably, recent research has emphasized the limited correlation of PGA with the structural damage (Liao et al., 2001; Yakut and Yilmaz, 2008). Therefore, for a more realistic representation of earthquake intensity levels, spectral IMs are preferred over other options due to their simplicity, non-requirement of extensive analysis, and their ability to incorporate structural knowledge.

The elastic spectral acceleration at the fundamental period of a structure, denoted as $S_a(T_1)$, has emerged as an effective IM, especially for low- to mid-rise buildings, owing to its structure-specific nature. It has become a commonly employed parameter in assessing the earthquake damage potential. The majority of current seismic codes and standards, such as FEMA 356 (2000), Eurocode 8 (2003), and ASCE/SEI 41-06 (2008), utilize spectral acceleration to characterize the seismic hazard. $S_a(T_1)$ is frequently employed as the default scaling parameter for seismic response analyses and forms the basis for the design procedures outlined in these codes. Numerous studies, including those by Elenas and Meskouris (2001) and Shome et al. (1998), have demonstrated its efficiency in characterizing the seismic response of buildings when compared to non-structure-specific IMs like PGA. However, it is worth noting that recent research has highlighted limitations in its applicability, particularly for tall buildings (Vamvatsikos and Cornell, 2005), and structural systems exposed to near-field earthquake records (Luco and Cornell, 2007).

In the present study, the 8-story building constructed with RC structural walls, can be categorized as a mid-rise structure. Also, the study is particularly focused on far-field earthquake records. Considering the mid-rise design and architectural symmetry of the building, it is reasonable to infer that the fundamental period predominantly governs the dynamic response of the structure. Additionally, the decision to exclude near-fault earthquake

records provides a rationale for employing $S_a(T_1)$ as the seismic IM when estimating fragility in this specific context.

3.8 Selection of Ground Motion Records and EDP

This section presents the outcomes of response history analyses conducted on the considered RC wall-frame structure. Statistical analyses of the response history analysis results are conducted to select a specific set of input records, which are chosen from the two available sets, namely one assembled using strong-motion parameters and the other using geophysical parameters. This selected set of records is subsequently utilized for further analysis of the considered structure, with the goal of accurately establishing fragility relationships. The results obtained from IDAs of the examined RC wall-frame structure, conducted using the hunt and fill algorithm, are employed to pinpoint the most suitable EDP from the various EDPs explored. This selection process aims to precisely characterise the relationship between the chosen EDP and the IM, specifically $S_a(T_1)$, across varying levels of earthquake intensities.

3.8.1 Ground Motion Records

The entire process of selecting a specific set of input earthquake records involves the following key steps: conducting response history analyses for the RC wall-frame structure using each set of input records, examining and comparing the responses obtained from time-history analyses for each set (assessing whether any distinct characteristics are observed in the response parameters derived from sets assembled using different criteria), and finally concluding regarding the selection of a particular set of input records. The two sets of earthquake records assembled using specific criteria consist of ground motion records characterized by a wide range of earthquake characteristics (Figure 3.9). It presents the response spectrum corresponding to individual ground motion records, together with the median response spectrum for the records pertaining to the specific set. It is notable that there are significant differences observed in both the median response spectra and the individual record response spectra between the two sets of earthquake records.

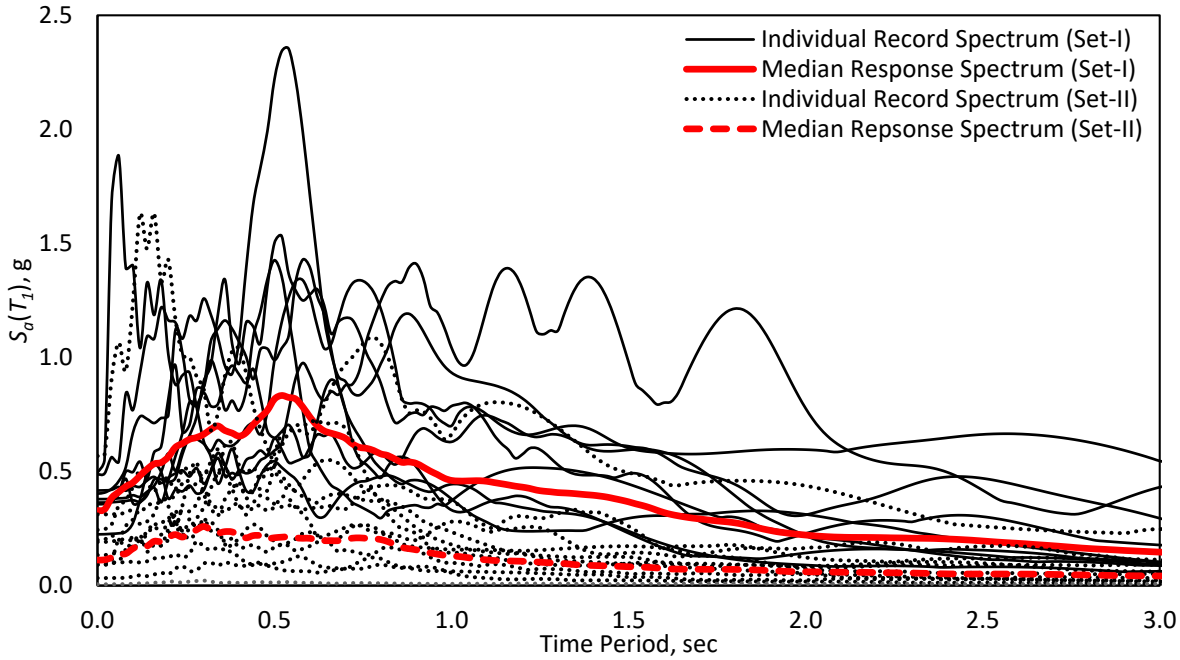

Figure 3.9 Plot of response spectra of original input records of dataset Set-I and Set-II.

To ensure a fair and unbiased comparison between the two record sets and prevent biases resulting from variations in magnitude, normalization to a common scale is imperative. This involves scaling the input records to eliminate disparities in magnitude levels and, consequently, assessing their relative influence on structural response parameters. The input records in Set-II, assembled using geophysical parameters, are scaled to align the resulting median response spectrum with similar IM values, specifically $S_a(T_1)$ ordinates, with those derived from the median response spectrum of Set-I, which was compiled using strong-motion parameters. From the eigenvalue analysis of the RC wall-frame structure, the fundamental natural period is obtained as 0.51sec. The $S_a(T_1)$ values for the median response spectra of the original datasets of Set-I and Set-II earthquake records are 0.82g and 0.21g, respectively. Therefore, the ground motion records in Set-II are adjusted to achieve a median response spectrum with a $S_a(T_1)$ value of 0.82g. Figure 3.10 displays the response spectrum of individual records alongside the median response spectrum for the original records of Set-I and the scaled records of Set-II. Notably, it is observed that the response spectrum obtained from the original records of Set-I and the scaled records of Set-II exhibit a relatively higher degree of similarity, especially at $S_a(T_1)$ ordinates, as compared to the similarity between two the original sets of records.

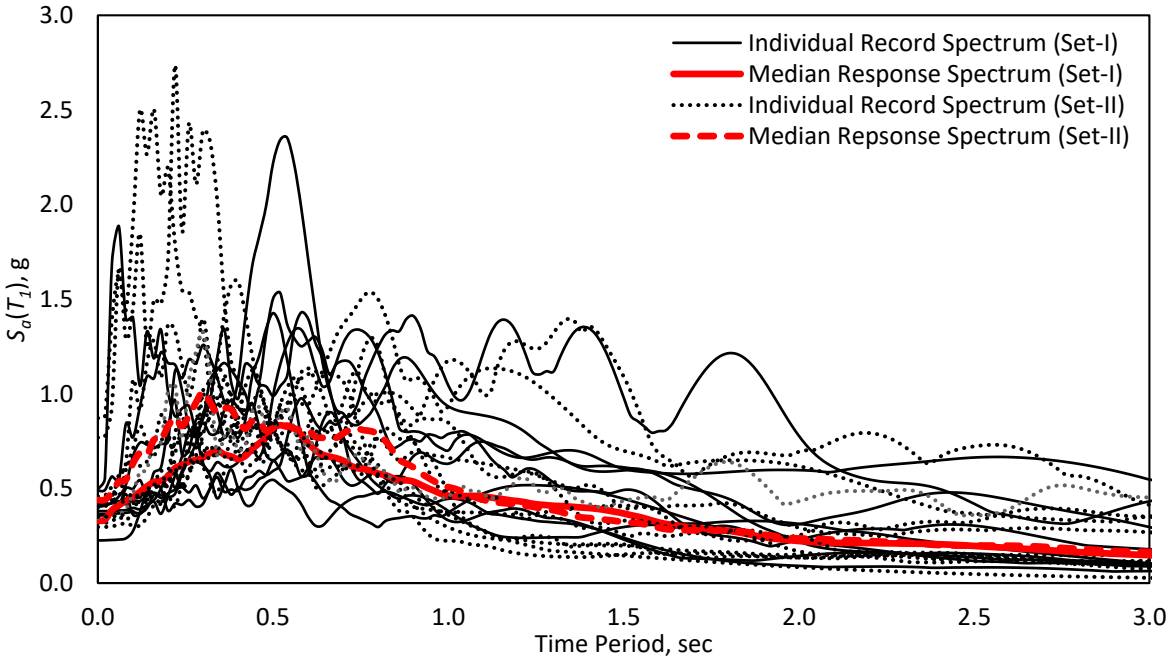

Figure 3.10 Plot of response spectra of original records of dataset Set-I and scaled records of dataset Set-II.

Subsequently, response history analyses are conducted for the considered RC wall-frame structure using the two sets of input records, which share a median response spectrum with consistent $S_a(T_1)$ values. Following this, various monitored response parameters from the response history analyses are evaluated to compare the impact of the two sets of input records. As outlined in the preceding section, five EDPs are investigated, namely (i) roof displacement (RD), (ii) maximum inter-story drift ratio (ISD), (iii) maximum floor acceleration (MFA), (iv) maximum storey curvature (MSC), and (v) maximum concrete compressive strain (MCC).

Table 3.4 displays the calculated EDP values derived from the response analyses of the considered structure, utilizing both the original records from Set-I and the scaled records from Set-II. Additionally, the table includes the median values of various EDPs for each record dataset and presents the ratio between the median EDP values for these two distinct record sets ($\frac{Median_{@SetI}}{Median_{@SetII}}$). If both sets of ground motions, characterized by identical median spectral acceleration at the fundamental natural period, yield relatively similar responses concerning the considered EDP, it would mitigate the impact of variability in ground motion selection on seismic response estimation. This alignment for the analysed RC wall-frame structure can be quantitatively verified by examining the ratio between the median values of the response parameters from the Set-I dataset records and those from the Set-II dataset

records, as shown in Table 3.4. Figure 3.11 also illustrates the ratios of the median values of various EDPs for the two record sets.

Table 3.4 Comparison of response parameters pertaining to two different sets of input record

Record No.	RD (m)		ISD (%)		MFA (m/s^2)		MSC (m^{-1})		MCC	
	Set-I	Set-II	Set-I	Set-II	Set-I	Set-II	Set-I	Set-II	Set-I	Set-II
1	0.27	0.16	1.16	0.70	14.70	8.24	0.0046	0.0022	0.0024	0.0014
2	0.10	0.12	0.44	0.53	11.30	11.70	0.0011	0.0017	0.0010	0.0013
3	0.08	0.10	0.37	0.47	10.26	10.52	0.0009	0.0011	0.0010	0.0011
4	0.08	0.13	0.36	0.57	13.59	18.98	0.0009	0.0019	0.0009	0.0014
5	0.12	0.07	0.54	0.39	8.74	22.81	0.0015	0.0006	0.0012	0.0007
6	0.10	0.17	0.46	0.74	8.91	10.13	0.0012	0.0027	0.0013	0.0017
7	0.02	0.13	0.08	0.60	3.15	12.51	0.0001	0.0020	0.0002	0.0014
8	0.06	0.09	0.30	0.44	6.70	17.51	0.0007	0.0014	0.0008	0.0013
9	0.15	0.11	0.67	0.51	11.49	8.69	0.0019	0.0015	0.0013	0.0012
10	0.09	0.09	0.44	0.42	20.21	12.82	0.0012	0.0012	0.0010	0.0011
11	0.08	0.10	0.40	0.46	9.02	19.64	0.0009	0.0013	0.0008	0.0012
Median	0.09	0.11	0.44	0.51	10.26	12.51	0.0011	0.0015	0.0010	0.0013
$\frac{Median_{@SetI}}{Median_{@SetII}}$	0.82		0.86		0.82		0.75		0.76	

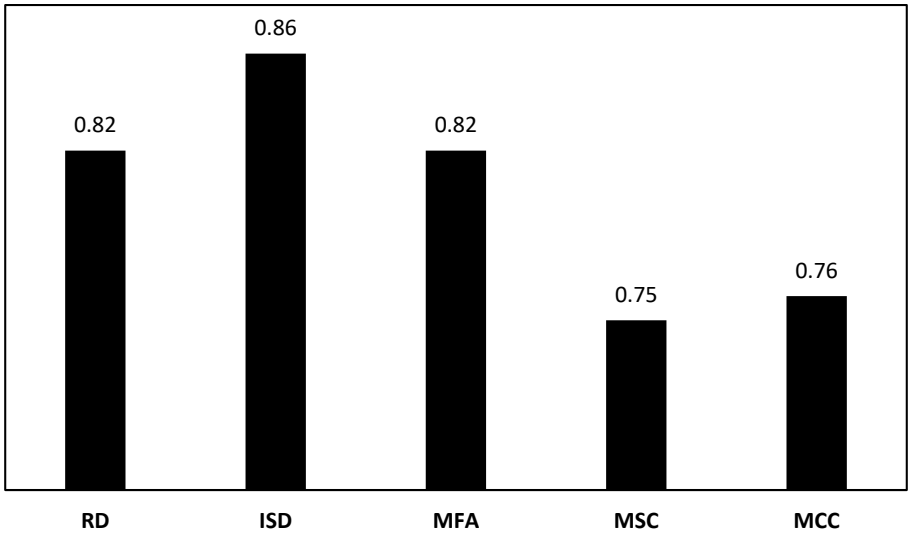

Figure 3.11 Ratio of the median result of different EDPs for the two set of records.

A higher ratio between the median responses of the two record sets signifies a greater degree of closeness or similarity in the expected response parameters when considering a specific set of earthquake records for analysis. The insights derived from Table 3.4 and Figure 3.11 suggest that the ratios of median values for the response parameter ISD show a relatively higher degree of similarity as compared to the other EDPs. This is evident as the ratio of

median values is relatively higher for ISD as compared to the other EDPs. Consequently, it can be concluded that choosing a ground motion based on either strong ground motion parameters or geophysical parameters would lead to comparable responses in terms of ISD. The results presented in the later parts of the study are derived by conducting IDA for the Set-II dataset records which are selected considering the geophysical parameters.

3.8.2 Selection of EDP

To identify the most effective EDP among the variables considered, IDAs of the RC wall-frame structure are conducted using the previously selected Set-II of ground motion records assembled based on geophysical parameters. Figure 3.12 displays the IDA curves for this set of ground motion records, with EDP on the horizontal axis and IM on the vertical axis. For brevity, only the IDA curves corresponding to the ISD response parameter are shown.

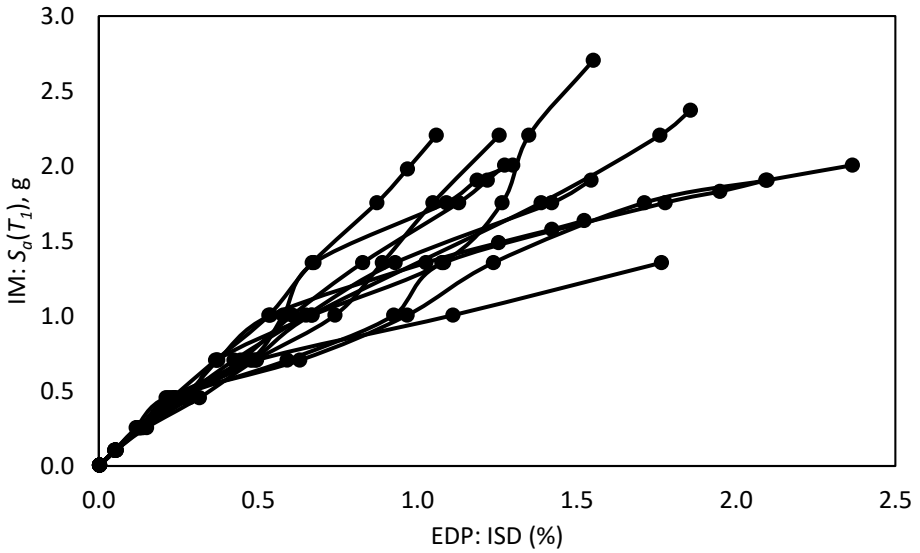

Figure 3.12 IDA curves for the RC wall-frame using Set-II input records.

The precise characterization of seismic responses in structural assessments through IDAs heavily relies on the relationship between EDP and IM. An ill-suited choice of EDP in relation to a specific IM can lead to significant discrepancies in IDA-derived results. This underscores the necessity of identifying the ideal EDP for evaluating the seismic performance of the RC wall-frame structure using $S_a(T_1)$ as the IM. Generally, the variable distribution of points seen in IDA curves is a consequence of input record variability. Reducing the dispersion of EDP values should improve the accuracy and efficiency of IDA results. To ensure more robust outcomes, the selection of the EDP is grounded in the statistical analysis of IDA results.

Firstly, to investigate the efficiency of the considered EDPs, regression analysis is performed on the seismic response values. Appropriate EDPs would be those which indicate low variation when input ground motion records are varied. In this analysis, the conventional power-law approximation (Cornell et al., 2002), commonly used to represent EDP|IM relationships, is employed as the regression line. The equation is obtained as

$$EDP = a\, IM^{\,b} \tag{3.9}$$

where b is the slope of the line in log-space and ln(a) is the intercept. The dispersion in the regression analysis is defined by the coefficient of variation (c_v) of the residual response parameter values from the regression line. Figure 3.13 shows the relationships between different EDPs and IM, derived from IDA and regression analyses, with dispersion values c_v indicated in all the figures. The dispersion value of the observed IDA points from the regression line is notably lower when considering response values in terms of ISD as compared to the other EDPs.

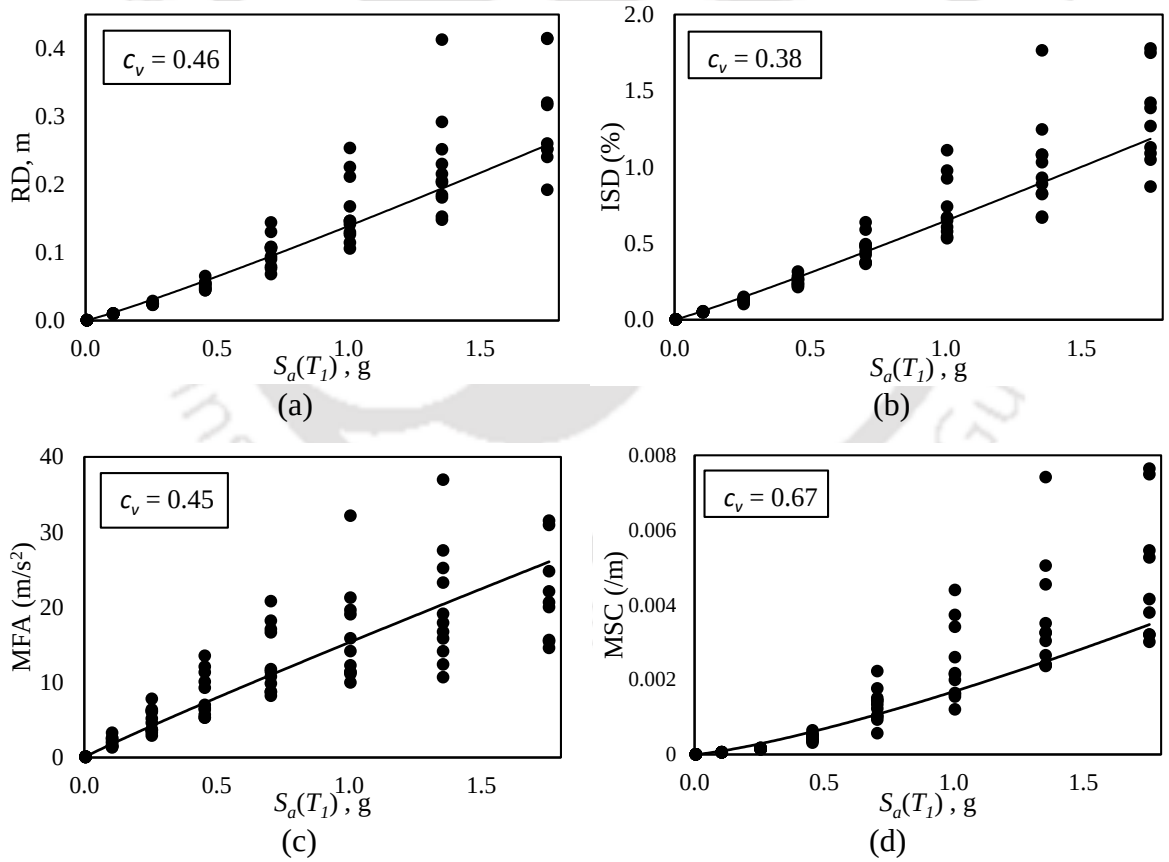

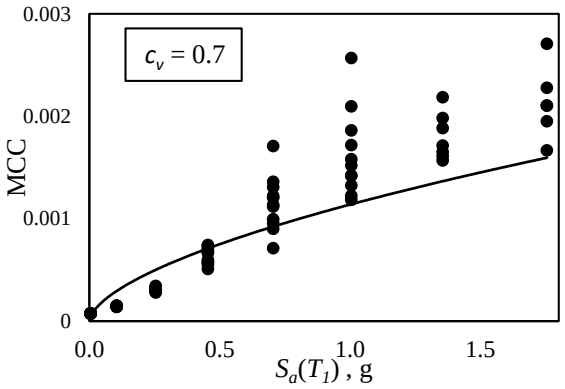

(e)

Figure 3.13 Relationship between IM as $S_a(T_1)$ and EDP as (a) RD, (b) ISD, (c) MFA, (d) MSC, and (e) MCC.

Also, across different seismic intensity levels, variations of the considered response parameters are shown in Figure 3.14, in terms of c_v of the natural logarithm of response values. It is observed that ISD yields the smallest dispersion (indicated by c_v) among the considered seismic response parameters. It can be observed that at certain intensity levels, the dispersion of the MSC response variables is almost twice as that of the ISD response variable. Thus, to achieve the same level of confidence in the estimates of the fragility studies using MSC as the response parameter as compared to those obtained using ISD as the EDP, it would necessitate twice the number of input earthquake records and subsequent computational effort as required in the latter case.

The deviation in the seismic response with different EDPs being considered is noted to be increasing along with the increase in the intensity levels of the ground motion. However, with MFA as the EDP, the deviation of the response value is observed to be within a constant range (0.25 to 0.35) irrespective of the seismic intensity levels. At lower intensity levels, all the considered EDPs, except for MFA, exhibit smaller dispersion values. As the intensity levels increase, the deviation in seismic response gradually increases for the other considered EDPs. Notably, there is a significant rise in the dispersion value of the MSC response parameter with increasing intensity levels. However, beyond a specific seismic intensity threshold, approximately 1.5g of $S_a(T_1)$, the dispersion in response values begins to decrease. This phenomenon can be attributed to structural model collapse occurring for several ground motion records during IDA (Figure 3.12). As a result, the number of IDA curves decreases beyond the 1.5g $S_a(T_1)$ threshold, leading to a noticeable reduction in the dispersion of seismic response values.

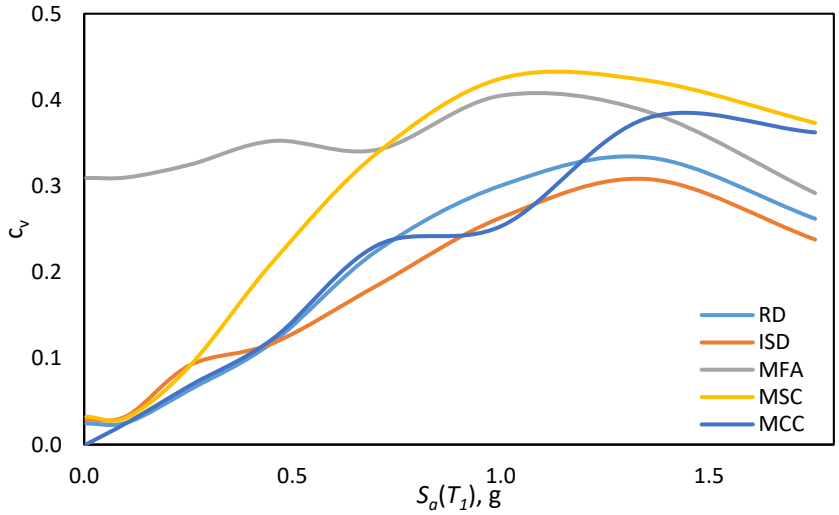

Figure 3.14 Variation in the coefficient of variation of the natural logarithm of response parameters at various intensity levels.

Finally, in order to determine which EDP aligns better with the chosen IM ($S_a(T_1)$), a quantitative assessment of their correlation is conducted using the coefficient of correlation defined as,

$$\rho = \frac{\sum_{i=1}^{n}(EDP_i - \overline{EDP})(S_{a,i} - \overline{S_a})}{\sqrt{\sum_{i=1}^{n}(EDP_i - \overline{EDP})^2 \sum_{i=1}^{n}(S_{a,i} - \overline{S_a})^2}} \tag{3.10}$$

where $\overline{EDP}$ and $\overline{S_a}$ are the mean values of seismic response and IM, respectively. Selecting the EDP that demonstrates a stronger correlation with the seismic IM is crucial for an effective structural fragility assessment of building systems. The correlation coefficients between various EDPs and the selected seismic IM, $S_a(T_1)$, as determined from the IDA results for the RC wall-frame structure, are shown in Table 3.5. It is evident that ISD exhibits a comparatively stronger correlation with $S_a(T_1)$ in comparison to the other alternatives.

Table 3.5 Correlation coefficient between different EDPs and IM

	EDP				
	RD	ISD	MFA	MSC	MCC
$S_a(T_1)$	0.996	0.998	0.979	0.988	0.996

Thus, considering the rationale presented earlier, it can be asserted that selecting ISD as the EDP provides a more accurate representation of the seismic response parameter as compared to other potential EDPs. Through regression analyses of the IDA results, it becomes evident that ISD exhibits the lowest deviation from the regression line when compared to the other considered EDPs. This observation implies that ISD is the least affected by variations in input

ground motion records, which is a crucial and essential quality for an effective EDP, capable of accurately representing structural damage across different seismic intensity levels while remaining unbiased and unaffected by the specific ground motion record used. The minimal dispersion, as indicated by the coefficient of variation (c_v) of the natural logarithm of ISD values across various seismic intensity levels, underscores the reliability and appropriateness of ISD as a suitable EDP for assessing the seismic performance of the considered building typology. This emphasizes the potential for significant resource and computational savings when deriving fragility relationships using ISD as the EDP, while maintaining the same level of confidence and efficiency as compared to the use of other considered EDPs. Utilizing ISD as the EDP also results in a relatively high correlation coefficient with the seismic IM of $S_a(T_1)$ when compared to the other considered EDPs. This demonstrates a robust interrelationship between the structural response parameter, represented by ISD, and the seismic IM in terms of $S_a(T_1)$. This strong correlation is a crucial aspect of the EDP-IM relationship, which is essential for formulating reliable fragility estimates.

3.9 Summary

This chapter provides a comprehensive discussion of the modelling approach and finite element framework used to develop a suitable structural model of the RC wall-frame building. An investigation is conducted to validate the numerical simulations by comparing them with experimentally obtained results from the literature, which indicate the successful capability of the adopted finite element modelling approach to accurately replicate the experimental global response. Also, this chapter makes a deliberate effort to examine the selection of a few key components in the fragility assessment of the structural system through nonlinear dynamic analysis, specifically EDPs and input ground motion records.

Firstly, two different suites of ground motion data are employed to investigate the influence of different selection criteria for input record datasets on the structural response of the RC wall-frame structure. These two sets of records are created based on strong ground motion parameters (PGA, PGV) and geophysical parameters (magnitude, source-to-site distance). It is observed that the median results of the response parameters for the two sets of records are virtually the same when one set of records is scaled to match the median spectral acceleration of the other set, especially when the response parameter is ISD. Thus, it can be inferred that selecting the ground motion, based on either the strong motion parameters or the geophysical parameters, would have a negligible effect on the seismic response of the considered RC

wall-frame building, provided the appropriate response parameter is chosen (in this case, ISD). The set of ground motion records, assembled using geophysical parameters, will be used to achieve the goal of fragility estimation for the RC wall-frame building structure in the present study.

The most efficient response parameter is identified based on regression analyses and statistical analyses of the results of IDAs conducted on the RC wall-frame structure. The efficiency of the considered response parameters is evaluated by the nature of their scatter in the EDP-IM space. The findings suggest that selecting ISD as the EDP offers a more precise representation of seismic response as compared to other potential EDPs. ISD demonstrates the least variability from the regression line in IDA results, indicating its resilience to input ground motion variations which is an important feature for an accurate and unbiased EDP. The low variation, as measured by the coefficient of variation (c_v) of ISD values across different seismic intensity levels, confirms that ISD is an efficient and suitable seismic response parameter for evaluating the performance of the studied building type. Additionally, employing ISD as the EDP results in a relatively high correlation coefficient with the seismic IM of $S_a(T_1)$ when compared to the other considered EDPs. This robust correlation between the structural response parameter and seismic demand is essential for an effective fragility assessment.

CHAPTER 4

RESPONSE PARAMETER SENSITIVITY TO UNCERTAIN INPUT VARIABLES

4.1 Overview and Motivation

Seismic fragility analysis serves as the framework for assessment and quantification of the vulnerability of structural systems within the built environment exposed to earthquake hazards. Ensuring the reliable execution of structural fragility assessments for future earthquake hazard scenarios is highly conditioned on the stochastic evaluation of the seismic performance of structures. Accurate estimation of the fragility functions demands exhaustive knowledge of the uncertainty in seismic loading, structural properties and modelling assumptions. Acknowledging the inherent uncertainty from all sources in structural seismic response analysis, proper understanding of these uncertainties is indispensable in order to enhance the confidence level of the resulting vulnerability relationships. Sensitivity analysis is frequently employed to interpret the interrelation between the input parameters and response of a numerical model and to examine the relative influence of the independent variables on the overall variability of the system output (Saltelli et al., 2000). Thus, it helps to identify the key input variables that significantly affect structural responses, necessitating further investigations to possibly mitigate their associated uncertainties.

There are only a few studies available in the literature that explore the impact of input variable uncertainties on the seismic response of RC wall-frame building stock, such as the work of Lee and Mosalam (2005), which, however, employed conventional methods of sensitivity analysis. Therefore, this chapter extends upon the latest advances in ML techniques, along with Sobol's indices, to investigate the sensitivity of material properties and uncertainties related to structural modelling on various response parameters of the RC wall-frame structure. In general, uncertainty in seismic loading is typically characterized by considering record-to-record variability or site-specific hazard curves (Yazdani et al., 2017), and hence the present study attempts to evaluate only the influence of uncertainty in structural parameters on the seismic response. To achieve this, 200 structural models are generated using the Latin Hypercube Sampling (LHS) technique (Iman and Conover, 1980), each with different realizations of the considered input random variables. The outputs from

the nonlinear response analyses of these structural models are then utilized to assess the relative significance of the input random variables on seismic response parameters through the adopted sensitivity analysis techniques. A comparative study is also presented to elucidate the seismic response variability resulting from uncertain structural variables and the record-to-record variability of input motions.

Reliable execution of vulnerability analysis of structural systems demands appropriate evaluation and quantification of the various sources of associated uncertainty. However, it is to be noted that the analytical framework for seismic fragility assessment can be computationally expensive if the relative significance of the different uncertain variables is not well apprehended. Thus, the findings of the present chapter can be utilized to identify the influential random variables to reduce the variability of the computational model output. Consequently, the insignificant random variables need to be excluded and even if some of them are considered as deterministic, nominal values need to be quantified as their estimates for computational simplification of the uncertainty analyses for efficient fragility assessment of the structural system.

4.2 Methods of Sensitivity Analysis

To ensure reliable sensitivity analysis results, it is necessary to explore the variation of input random variables and the representative model output response using various approaches. In this chapter, three different ML techniques have been used to conduct sensitivity analysis for the considered building typology, and the results have been validated using a more conventional method. ML is a major subfield of Artificial Intelligence, which emphasizes on making inference from available features and eventually establishes algorithms to predict reliable response variables (Siam et al., 2019). Among several techniques available in the literature to be used for ML, three different regression based ML algorithms are adopted for the present study, namely (a) decision tree, (b) random forest and (c) extreme gradient boosting (XGBoost). There are linear regression algorithms available for ML techniques, but due to their obvious shortcoming of not considering nonlinear relationships among the variables, the aforementioned ML algorithms are explored here.

A decision tree develops a regression model in the shape of a tree-like structure. It splits the database into smaller segments based on a group of binary rules while simultaneously developing a corresponding hierarchical decision tree. Each decision tree is a straightforward

model that starts with a root node, splits into decision nodes, and ends at leaf nodes. However, decision trees can sometimes be susceptible to overfitting (Hwang et al., 2021). The Random Forest stands as an improved ML algorithm that builds upon the principles of decision trees. It constitutes an ensemble-based methodology, where, in order to make more reliable predictions, multiple trees are induced, and the mean output of each independent tree is adopted as the eventual prediction (Breiman, 1996). XGBoost is a recently developed ML algorithm which integrates a decision tree model together with a gradient boosting algorithm for making predictions. It employs an iterative procedure, constructing a sequence of decision trees that form an ensemble, with each subsequent tree aimed at rectifying the errors made by its forerunner (Chen and Geustrin, 2016). Several researchers (Mangalathu and Jeon, 2018; Huang and Burton, 2019; Hwang et al., 2021) have utilized decision tree, random forest, and XGBoost algorithms, along with other machine learning techniques, for various applications in the field of structural engineering, such as predicting collapse capacity and shear strength for different structural systems.

The ML algorithms used in the present study are based on decision tree-based ensemble procedures. In decision tree models, the termination of leaf nodes is governed by an error-minimization pruning method known as the Gini impurity index. The relative significance of the input variables on the output response is evaluated based on the Gini index. Input parameters with lower Gini indices supposedly have a greater influence on the model outputs. In other words, the importance factor of input parameters, as evaluated from ML prediction models, denotes the frequency of use of the variables as root nodes in the decision trees.

Moreover, for the validation and comparison of sensitivity analysis results derived from ML techniques, the conventional and frequently adopted sensitivity analysis approach of Sobol indices (Sobol, 1993) is employed. Sobol sensitivity indices serve as indicators of the impact of each individual parameter or a group of parameters on the variance of the output response. The central concept of Sobol indices involves breaking down the total variance in the model output into portions attributed to individual factors and their interactions. These indices are categorized into first-order and multi-order indices. First-order indices gauge the contribution of individual factors to the output variance when they are analyzed independently. In contrast, multi-order indices consider the combined influence of multiple factors, encompassing their interactions with one another. The first-order Sobol sensitivity index is mathematically expressed as:

$$S_i = \frac{V[E[Y|X_i]]}{V[Y]} \tag{4.1}$$

where, $E[Y|X_i]$ represents the expected value of response parameter Y (e.g., ISD) conditioned on independent variable X_i (e.g., f_{ck}). In the recent past, Crozet et al. (2018) and Choudhury and Kaushik (2018) have performed sensitivity analyses of the seismic response of pounding structures and vertically irregular RC frames, respectively, using Sobol sensitivity indices.

4.3 Uncertain Input Parameters

In earthquake engineering, the overall variability of structural responses is mainly influenced by uncertainties in ground motion records and structural parameters. In the present study, the uncertainties related to structural properties, often referred to as epistemic uncertainty, are adopted as input parameters for evaluating the sensitivity analysis of the seismic response of the considered building structure. The set of uncertain input parameters related to structural capacity considered in the present study is determined based on a review and assessment of past studies (Lee and Mosalam, 2005; Yazdani et al., 2017), involving sensitivity analyses of the response parameters for RC structures with variation in uncertain structural parameters. Therefore, the uncertain input parameters considered for the sensitivity analysis of structural responses in the present study include variations in building mass (m_b), viscous damping ratio (ξ), and the strength and stiffness of materials.

The uncertainty in building mass is primarily caused by factors such as the materials used in construction, building geometry, and the characteristics of non-structural components. In this context, to model the probability distribution for uncertain building mass, the recommendation of Ellingwood et al. (1980) is followed which prescribes normal distribution of the uncertainty in building mass. The distribution is assumed to have a mean equal to the nominal mass and a coefficient of variation (c_v) of 10%. A brief review of the literature related to variability in viscous damping ratios is presented in the study by Porter et al. (2002). Their findings suggest that a reasonable estimate for the c_v of the uncertain viscous damping ratio for frame building structures lies in the range of 30% to 40%. Within this framework, the random variable associated with the uncertain viscous damping ratio is assumed to have a mean value of 5% and a c_v of 40%. The variability in material strength and stiffness of structures can be primarily attributed to the differences in certain design parameters and the actual as-built conditions, as well as a lack of accurate understanding of material behaviour. This uncertainty in structural strength and stiffness is often associated

with variations in material stress-strain behaviour. In the current study, uncertainty in structural strength is addressed by considering characteristic cube concrete compressive strength (f_{ck}) and the yield strength of reinforcement bars (f_y) as random variables. Additionally, the initial tangent modulus of concrete (E_c) and the modulus of elasticity (E_s) of reinforcement bars are treated as random variables to represent uncertainty in structural stiffness parameters. The statistical characteristics of these random variables are summarized in Table 4.1, and it is assumed that these variables follow a normal distribution (Yazdani et al., 2017).

Table 4.1 Statistical properties of the considered input parameters

Parameter		Mean	c_v	Reference
Mass (m_b)		Nominal mass	*10.0* %	Ellingwood et al., 1980
Viscous Damping (ξ)		*5%*	*40.0* %	Porter et al., 2002
Strength	f_{ck}	Nominal quantities	*17.5 %*	Mirza et al., 1979
	f_y		*10.0 %*	Mirza and MacGregor, 1979
Stiffness	E_c	Nominal quantities	*8.0 %*	Mirza et al., 1979
	E_s		*3.3 %*	Mirza and MacGregor, 1979

4.4 Ground Motion Records

As mentioned earlier, the impact of ground motion uncertainty on structural seismic response is commonly assessed through either record-to-record variability or a site-specific hazard curve. To assess the influence of record-to-record variability on structural seismic response, a set of 11 ground motion records is considered. Section 3.6.1 provides a detailed description of the selection criteria for these ground motion records. The 11 input records under consideration are listed in Table 3.3, chosen to encompass a wide range of earthquake scenarios based on magnitude-distance categorization (M-$\bar{R}$ bins).

However, it is essential to emphasize that the sensitivity analysis of response parameters for the considered building structure exclusively considers uncertainty in the structural capacity parameters, without addressing the uncertainty stemming from record-to-record variability. Instead, a comparative investigation is carried out to gauge the variability in response parameters due to uncertainty in structural properties with that resulting from uncertainty in ground motion records at different levels of seismic intensity.

In this context, performing sensitivity analysis on the seismic response parameters of the adopted RC wall-frame structure (detailed in Sections 3.3 and 3.4) with respect to variations in the considered structural parameters becomes computationally intensive and time-consuming when all the 11 ground motion records are used as input. Consequently, to ensure computational efficiency and to investigate the impact of uncertain structural parameters on response variability independently of the effects of record-to-record variability, sensitivity analysis for the RC wall-frame structure is conducted using a deterministic input ground motion.

Within the set of 11 considered ground motion records, the one that places the median seismic demand on the RC wall-frame structure is selected as the input ground motion record for the sensitivity analysis (Lee and Mosalam, 2005). To accomplish this, seismic response analyses are conducted for the adopted structure using all 11 unscaled ground motion records, with a focus on monitoring response variables concerning different EDPs. As outlined in Section 3.7, five EDPs are investigated for the sensitivity analysis of the response parameters, namely (a) roof displacement (RD), (b) maximum inter-story drift ratio (ISD), (c) maximum floor acceleration (MFA), (d) maximum story curvature (MSC), and (e) maximum concrete compressive strain (MCC). Based on the analysis results, the Northridge 1991 earthquake record (with a magnitude of 6.7, recorded at Carson – Water Station) is selected as the input record, as it represents the median ground motion record. The median ground motion record categorically signifies the record that produces the median seismic response among the set of 11 records. The response spectrum for each of the 11 ground motion records is shown in Figure 4.1(a), with specific distinction indicated for the response spectrum pertaining to the Northridge, 1991 record (Carson – Water Station). Figure 4.1(b) shows the seismic response for these records in terms of maximum inter-storey drift (ISD) as the EDP and spectral acceleration at the fundamental period ($S_a(T_1)$) as the seismic IM. For brevity, only ISD responses are presented, but similar graphs can be generated for other considered EDPs. It is also observed that among the 11 examined ground motion records, the Northridge 1991 record (Carson – Water Station) produces the median ISD value.

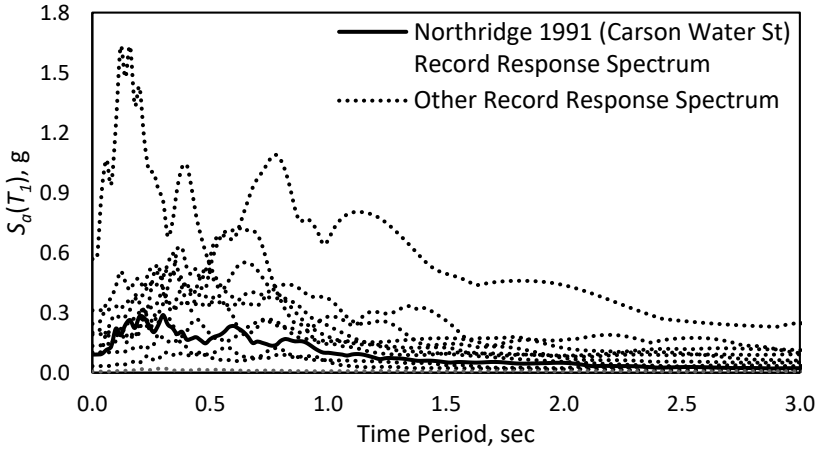

(a)

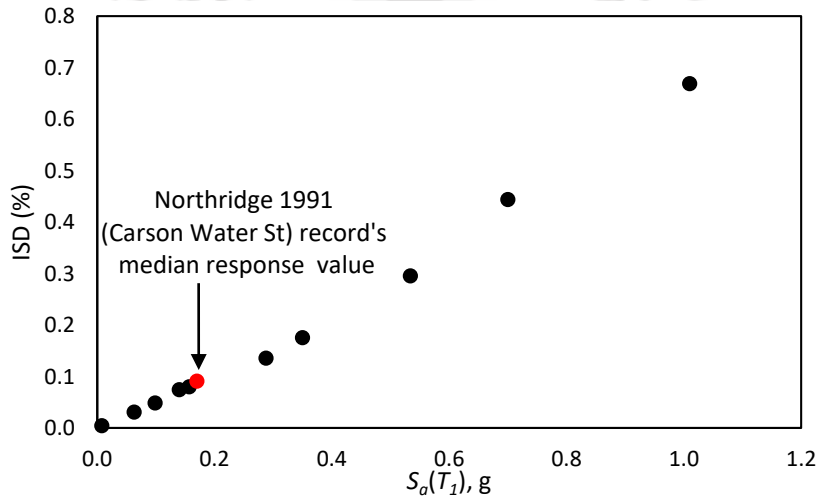

(b)

Figure 4.1 (a) Response spectrum; (b) Seismic response with ISD as EDP, for the set of 11 ground motion records.

4.5 Sensitivity Analysis of Response Parameters

In this section, the results of a comprehensive sensitivity analysis of response parameters for the RC wall-frame structure are presented. This analysis is based on a seismic response study involving numerical models of the RC wall-frame structure, developed to account for variations in key structural parameters. Specifically, 200 different models of the structure are created to investigate how changes in these structural parameters affect various response parameters. The Latin Hypercube Sampling (LHS) technique is employed to generate these unique structural models, strategically designed to support an extensive sensitivity analysis.

LHS serves as a robust statistical tool for systematically and efficiently exploring uncertainties in structural parameters and their subsequent impact on structural responses. Using LHS technique, Dolsek (2009) and Choudhury and Kaushik (2019) generated different

structural model samples for appropriate characterisation of associated uncertainties into the seismic response assessment. Within predefined ranges of structural parameters, LHS ensures a diverse and representative set of models. These 200 distinct structural models form the foundation for the exhaustive sensitivity analysis, allowing assessment of how variations in these parameters influence the behaviour and performance of the considered structural system.

As previously mentioned, state-of-the-art ML algorithms are used for sensitivity analysis in the present study. Subsequently, the outcomes of the ML-based sensitivity analysis are cross-verified with results obtained through the conventional sensitivity analysis with the variance-based approach using Sobol's indices.

The seismic response analysis of the 200 distinct structural models, all subjected to the Northridge 1991 earthquake (Carson Water St), serves as the foundation for the ML-based sensitivity analysis. Sobol's indices-based sensitivity analysis is executed using results from an additional set of 14,000 structural models, also developed through the LHS technique. The responses of these 14,000 models are predicted using the best-performing ML algorithm among the three considered options. The three ML algorithms are utilized to create prediction models for the responses of the initial 200 structural models. Subsequently, the best-performing ML algorithm is selected and applied to predict the responses of the remaining 14,000 structural models, which are then used in the Sobol's indices-based sensitivity analysis.

4.5.1 ML-based Sensitivity Analysis

The ML-based sensitivity analysis of response parameters relies on the dataset derived from the response analysis of 200 distinct structural models. Effective utilization of various ML algorithms necessitates the careful partitioning of this dataset into training and testing subsets, a critical step to assess and enhance the model's performance. The training subset plays a vital role in instructing the model about patterns and relationships within the data, allowing it to glean insights from the provided information. However, to truly evaluate the model's capacity to generalize and make accurate predictions on unseen or novel data, a separate testing subset becomes essential. This section of the data serves as a real-world benchmark, offering an opportunity to assess the model's performance on data it has not encountered during training.

In this context, the current dataset is categorized into two groups, namely (a) a training dataset and (b) a test dataset. To ensure the reliability of the results, a 7:3 ratio is employed for data segregation, with the training set comprising 70% of the total data, while the remaining 30% is designated for the test set (Hwang et al., 2021). This partitioning scheme ensures a robust evaluation of the ML-based sensitivity analysis.

The comprehensive relationship used in the ML algorithms to determine the EDP for different structural models of the RC wall-frame building can be denoted as:

$$EDP = f(RV_1, RV_2, RV_3, RV_4, RV_5, RV_6) \tag{4.2}$$

where, the model output EDP can be either of the considered seismic response parameters (*i.e.*, RD, ISD, MFA, MSC and MCC). The input parameters RV_1 through RV_6 represent the uncertain structural parameters of the considered building typology: $RV_1 = m_b$, $RV_2 = \xi$, $RV_3 = f_{ck}$, $RV_4 = f_y$, $RV_5 = E_c$ and $RV_6 = E_s$.

It is essential to ensure that input features are consistently scaled for efficient sensitivity analysis through ML algorithms. This practice prevents variables with larger ranges from dominating the learning process, leading to faster optimization algorithm convergence and improved model generalization. Normalized variables contribute to the generation of model coefficients or feature importance values that are more interpretable, aiding in gaining a deeper insight into the model's behaviour. In this context, the sensitivity analysis of the considered response parameters is conducted using model coefficients or feature importance values derived from the ML-based prediction models. To ensure consistency, all input random variables in the dataset utilised for the ML-based algorithms are normalized. Specifically, the input parameters are scaled with respect to the corresponding median values for the RC wall-frame structure.

The training dataset is used to develop predictive models for various ML algorithms, each aimed at predicting response variables. Subsequently, the testing dataset is employed to assess the models' performance on data not used in their development. The current investigation employs the Root Mean Square Error (RMSE) function as the objective function to evaluate the performance of various ML algorithm-based prediction models. The model efficiency is gauged by the RMSE value, based on the normalized input data, and this quantifies the disparity between the observed and the predicted response variables (Table 4.2).

Table 4.2 Performance comparison of different ML techniques for seismic response prediction

EDP	RMSE		
	Decision Tree	**Random Forest**	**XGBoost**
RD	0.26	0.17	0.13
ISD	0.24	0.16	0.13
MFA	0.65	0.51	0.50
MSC	0.31	0.21	0.19
MCC	0.21	0.15	0.12

The RMSE values for various models indicate that decision tree-based algorithms are the least reliable, while the XGBoost algorithm emerges as the most accurate predictor of response variables for a given set of unseen input parameters. This result aligns with the established observation with XGBoost being a highly developed and superior methodology as compared to decision tree and random forest techniques, consistently delivering the best predictive performance. Hwang et al. (2021) also supported the superiority of XGBoost based on their study, suggesting it as the preferred ML model among other linear and nonlinear algorithms for predicting the seismic response of RC building frames.

A notable observation drawn from the RMSE values, which gauge the efficiency of the considered ML algorithms, reveals that the selected EDPs can be categorised into two distinct groups. These groups consist of EDPs such as RD, ISD, and MCC, which yield favourable RMSE values, and EDPs such as MFA and MSC, which result in less favourable RMSE values. This categorization remains consistent regardless of the ML algorithm under consideration. The key differentiator between these two groups of EDPs lies in the variability of their observed values, *i.e.*, those in the first group, with lower RMSE values, have less variation, while those in the second group, with higher RMSE values, have greater variability.

The significant shift in ML model performance, particularly concerning MFA as an EDP, can be attributed to the fact that variations in floor acceleration with changes in the input parameters, tend to be more pronounced than for other EDPs like RD and ISD. On an average, the RMSE value of prediction models increases by nearly 50% when MSC is utilized as the EDP in contrast to MCC. It is important to note that MCC remains consistently observed at the ground storey level, while peak storey curvature varies along the height of the building. Consequently, with varying input parameters, the variation in compressive strain

values is relatively smaller as compared to storey curvature values, resulting in a significant performance difference among the ML algorithms when assessing MSC and MCC as response parameters.

The influence of uncertain structural parameters on seismic response variables is presented in Figure 4.2 for the different considered EDPs. Here, the sensitivity of EDP is represented in terms of relative importance factors of the input parameters when predicting the output response using different ML algorithms. The response parameters of the studied RC wall-frame structure are observed to be most sensitive to variations in the viscous damping ratio parameter. Additionally, the various ML algorithms used in this investigation unanimously identify the viscous damping ratio as the most sensitive parameter. This observation aligns with earlier studies by Yazdani et al. (2017), Dolsek (2009), and Lee and Mosalam (2005), which also highlighted viscous damping as a significant variable influencing the sensitivity of response parameters in RC structures. The prominence of viscous damping as the most sensitive parameter is justified by the fact that the variability considered for this parameter is the highest as compared to other uncertain structural properties. Furthermore, concrete compressive strength and building mass are noted to be other relatively key parameters for evaluating the seismic response of the building frame.

It is observed that when considering roof displacement, inter-storey drift ratio, and concrete compressive strain as response variables, the ML algorithms provide better predictions as compared to other investigated EDPs (Table 4.2). It should be noted that the sensitivity of the aforementioned EDPs to variations in the considered input parameters varies within different limits as compared to other EDPs, specifically floor acceleration and storey curvature. On an average, the variations in viscous damping, concrete compressive strength, and building mass contribute significantly, accounting for 55%, 30%, and 10% of the total variation in the response variables (RD, ISD, and MCC), respectively. Consequently, these three factors, namely viscous damping, concrete compressive strength and building mass, comprise nearly 95% of the variability in the EDPs, while the impact of other considered structural parameters (yield strength of steel and stiffness parameters) on the response variables remains relatively insignificant.

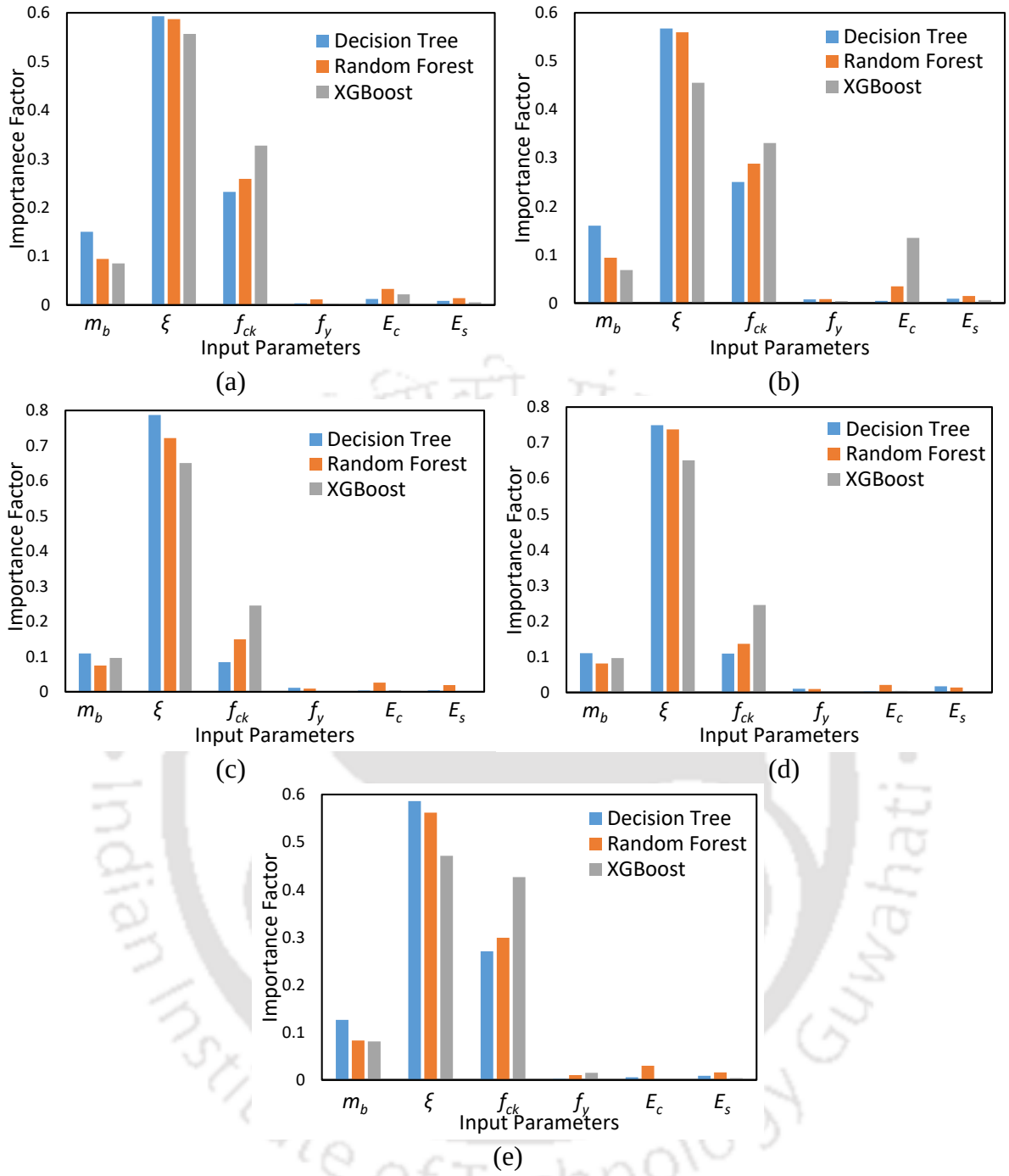

Figure 4.2 Sensitivity of (a) roof displacement, (b) drift ratio, (c) floor acceleration, (d) storey curvature and (e) concrete compressive strain for the considered structural properties.

4.5.2 Sobol Indices-based Sensitivity Analysis

In this section, the findings from the sensitivity of response variables to uncertain structural parameters by employing conventional approach of variance-based Sobol's indices are presented. It is a common understanding that in statistical analyses, especially when dealing with uncertain structural variables in complex structural systems, a larger sample size provides a more comprehensive representation of the inherent distribution. An increased

sample size reduces the impact of outliers and random variations, resulting in statistical analyses that are both more accurate and efficient. In this context, a total set of 14,000 structural models is considered to estimate the sensitivity of response parameters to uncertain structural parameters using the Sobol's indices approach. While it was possible to perform the Sobol's indices investigation using the seismic responses obtained earlier from the set of 200 structural models, a larger dataset of 14,000 structural models is chosen, recognizing the importance of a larger dataset for reliable statistical analysis results. These 14,000 structural models are also generated using the LHS technique with various realizations of the considered uncertain structural parameters. To conduct sensitivity analysis of the response parameters, it is necessary to estimate the seismic response of this extensive set of structural models. However, performing seismic response analysis for a total of 14,000 structural models would be computationally expensive. Therefore, the responses for this set of structural models are estimated using the ML-based prediction models established in the previous section. Among the ML algorithms considered, the XGBoost algorithm, which demonstrated the best predictive model (Table 4.2), is employed to determine the structural response for the set of 14,000 models.

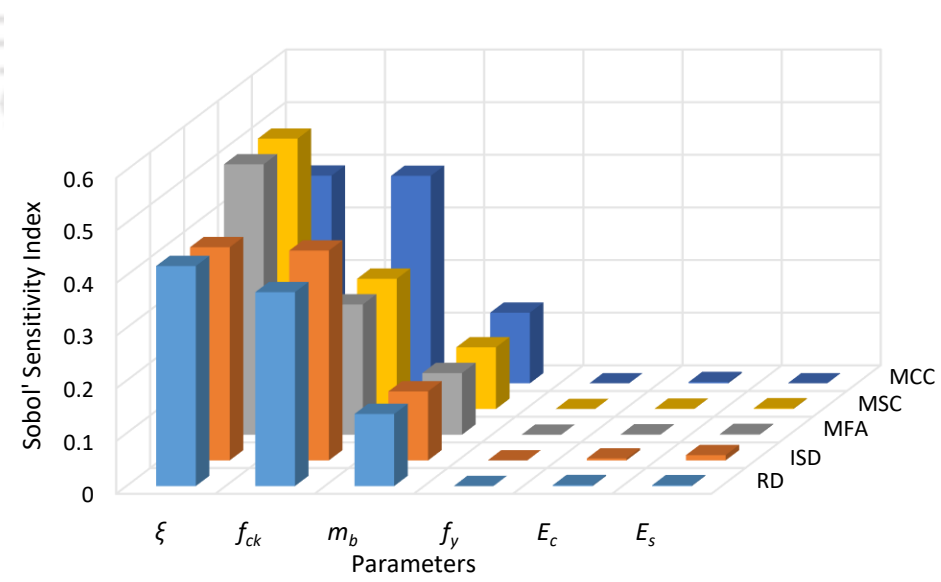

Figure 4.3 Sobol's 1st order indices for uncertain structural parameters.

The first-order Sobol's indices are computed for the response parameters of the RC wall-frame structure, taking into account the uncertain structural parameters. By decomposing the total response variance into contributions from individual parameters and their interactions, Sobol's indices reveal which input variables exert the greatest influence on the structural response. The variations in Sobol's indices for all the response variables, as shown in Figure

4.3, highlight viscous damping ratio, concrete compressive strength, and building mass as the critical parameters for predicting the response variables, which is consistent with the previous findings from complex ML algorithms. Additionally, it is observed that the seismic response variables of the considered building type exhibit minimal sensitivity to the uncertainty in yield strength of steel and stiffness parameters (E_c and E_s).

The findings of the current sensitivity analysis using ML algorithms and Sobol's indices on the response parameters of the RC wall-frame structure, reveal that viscous damping ratio, concrete compressive strength, and building mass have a significant influence on response variability. Whereas, yield strength of steel and stiffness parameters have a negligible impact on response variability. Thus, the parameters like viscous damping ratio, concrete compressive strength, and building mass, should be the primary focus for reducing variability and improving the efficiency of subsequent uncertainty analyses. In contrast, less influential parameters such as yield strength of steel and stiffness parameters can be treated as deterministic variables with fixed estimates, simplifying the computational process for efficient fragility estimation of the considered structural system.

4.6 Comparison of Uncertainty due to Earthquake Records and Structural Parameters

The variation in seismic response parameters within structural systems can mainly be ascribed to two key factors: the uncertainty stemming from differences among various ground motion records and the variability in structural capacity parameters. Following the evaluation of how uncertain structural parameters affect response parameters in the preceding section through comprehensive sensitivity analysis, the subsequent goal is to examine how the variability in ground motion impacts response parameters at varying levels of seismic intensity. To achieve this, incremental dynamic analysis (Vamvatsikos and Cornell, 2002) of the RC wall-frame structure is performed, considering median values for structural parameters, using a set of 11 ground motion records (Table 3.3). The impact of variation between different ground motion records on the considered response parameters is studied by examining the scatter of different EDPs at specific intensity levels. The variance of the response parameters caused by uncertainties in ground motion is graphically illustrated in Figure 4.4 through box-plot charts, where the solid lines represent the mean values of the considered EDPs. It is important to emphasize that the variability in response parameters depicted in Figure 4.4 is exclusively associated with the variability in ground motion records

and does not consider the impact of uncertain structural parameters, which are held constant at their median estimates during the development of the analyzed structural model. The plot illustrates that with the rise in seismic intensity levels, both the EDP values and the variance of seismic response notably increase, irrespective of the particular response parameters being examined. This underscores that the variability in seismic response parameters due to uncertainty in ground motion records is strongly influenced by the level of seismic intensity. Furthermore, it emphasizes that the variability in response parameters resulting from the uncertainty in ground motion record should not be presumed to remain consistent across varying seismic intensity levels.

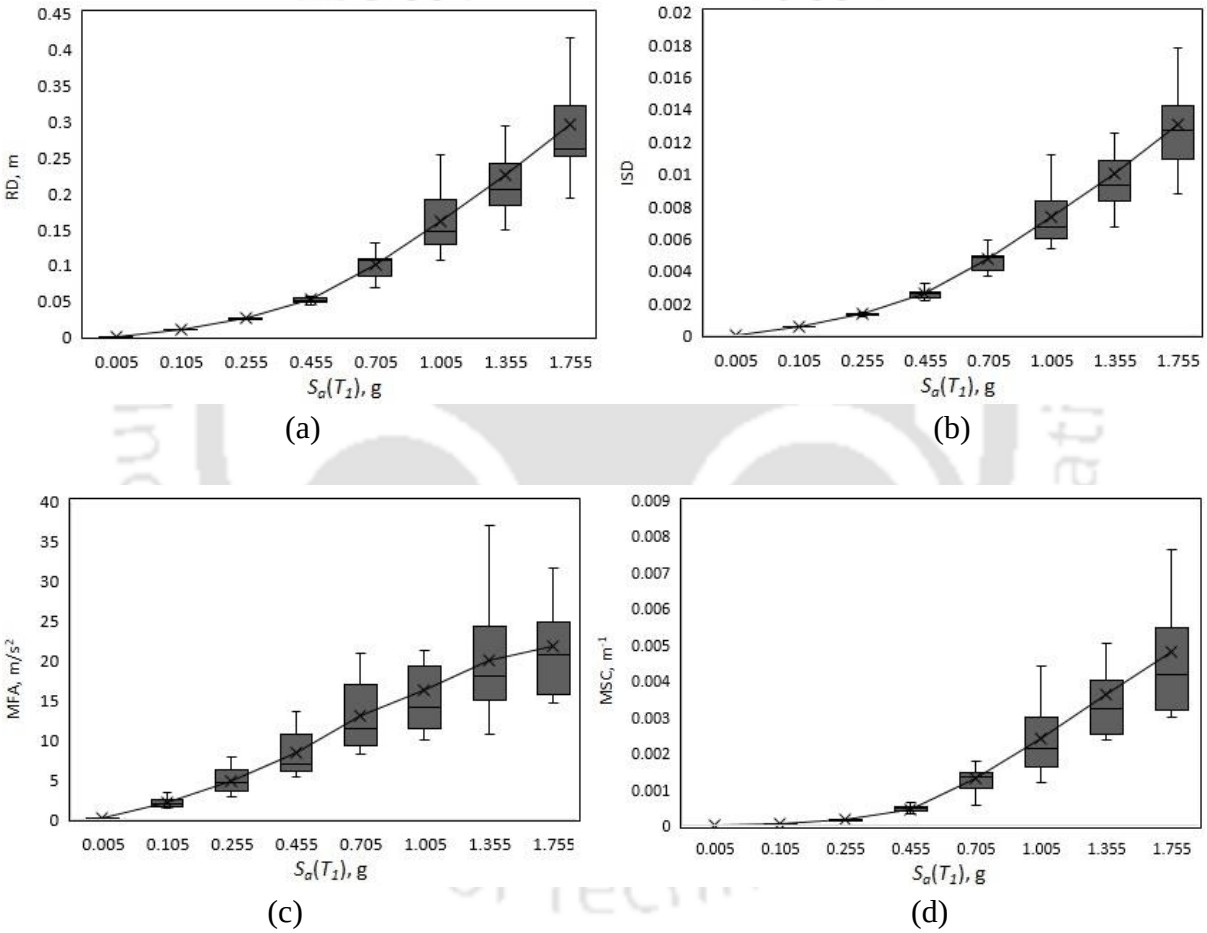

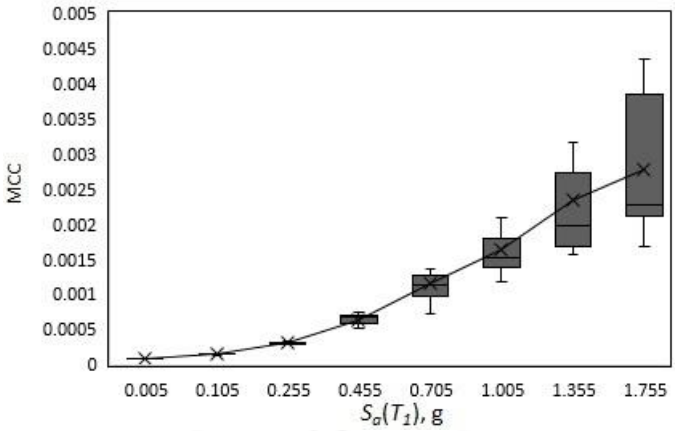

(e)

Figure 4.4 Influence of uncertainty in ground motion on the variance of (a) roof displacement (RD), (b) inter-storey drift (ISD), (c) floor acceleration (MFA), (d) storey curvature (MSC) and (e) concrete compressive strain (MCC).

A comparison of response parameter variability, as indicated by the coefficient of variation (c_v), resulting from uncertain structural parameters and record-to-record variability at specific intensity levels, is presented in Figure 4.5. In the figure, continuous lines represent the variation in response parameters due to uncertain ground motion records, while dotted lines represent variability due to structural parameters. Notably, at lower intensity levels, seismic responses are more affected by uncertainty in structural parameters than by ground motion variability. As seismic intensity levels increase, the influence of ground motion variability becomes more pronounced on structural response parameters as compared to the uncertain structural variables. However, variability of the floor acceleration values is observed to follow a different pattern, with the uncertain structural parameters exhibiting a lesser impact on its variability than those due to the ground motion randomness, irrespective of the seismic intensity levels. Moreover, seismic response variability due to uncertain structural parameters at lower intensity levels equals or exceeds that due to uncertainty in ground motion records at higher intensity levels. This underscores the importance of appropriately accounting for uncertainties related to structural capacity and modelling. Existing literature suggests that uncertainty in seismic demand governs seismic response variability more than uncertainty in structural parameters. Therefore, for computational simplicity, considering the former source of uncertainty alone may yield inaccurate stochastic seismic performance assessment results. As revealed by the results of the present study, addressing the uncertainty in both seismic demand and structural capacity is equally crucial for reliable seismic performance assessment, albeit at the cost of computational complexity.

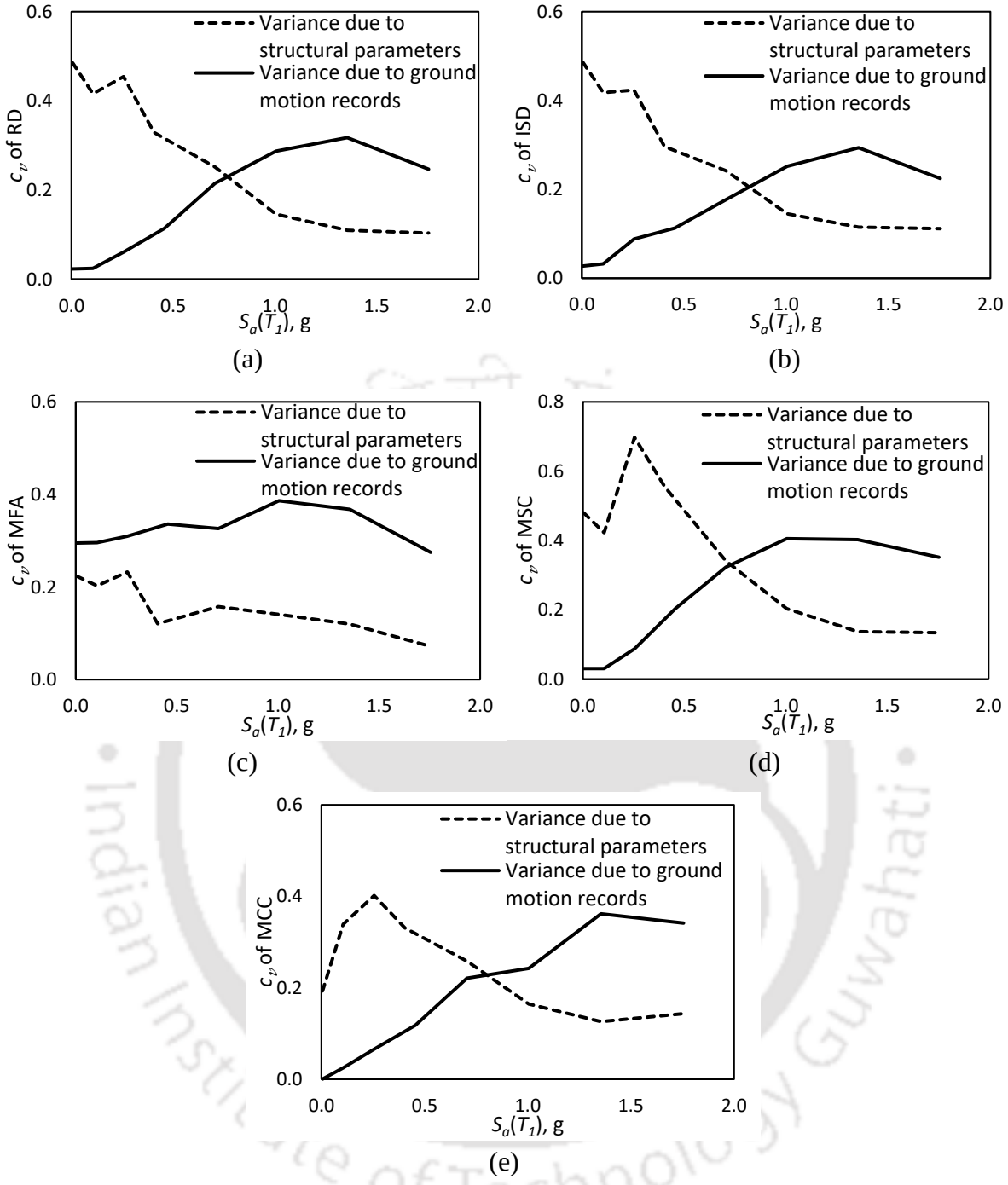

Figure 4.5 Comparison of variance in (a) roof displacement (RD), (b) inter-storey drift (ISD), (c) floor acceleration (MFA), (d) storey curvature (MSC) and (e) concrete compressive strain (MCC); due to uncertain structural parameters and ground motion records.

4.7 Summary

The present study aims to evaluate and quantify the sensitivity of seismic responses to uncertain structural parameters. Various random variables reflecting uncertainty in structural characteristics from previous research are identified and included in the present study. Latin Hypercube Sampling is used to create multiple structural models of the considered RC wall-

frame structure, each with unique realizations of the input random variables, and these models are analysed to explore the impact of uncertain structural parameter variability. The relative significance of these uncertain structural parameters on different response parameters is determined using modern ML algorithms, specifically regression tree models. Among the employed ML techniques, XGBoost stands out for its superior performance in predicting structural seismic responses. The sensitivity analysis of the response parameters to these uncertain structural parameters is estimated using model coefficients or feature importance values derived from the ML-based prediction models. Additionally, conventional Sobol's index methodology is employed to perform sensitivity analysis of different response parameters to these uncertain structural parameters.

The findings of the present study reveals that the viscous damping ratio, concrete compressive strength, and building mass significantly influence the response variability of the RC wall-frame structure; thus, emphasizing the importance of focusing on these parameters to reduce variability and enhance efficiency in subsequent uncertainty analyses. Conversely, the yield strength of steel and stiffness parameters have minimal impact on response variability, allowing these less influential factors to be treated as deterministic variables with fixed estimates, simplifying the computational process for efficient fragility estimation of the considered structural system.

Besides the assessment of uncertain structural parameters' impact on various seismic response factors, the present study explores the influence of uncertainty in ground motion records on seismic response variability. The relationship between record-to-record variability and seismic response variability is established through IDA performed on the RC wall-frame structure. An examination of the scatter of different EDPs at specific intensity levels indicates that both the EDP values and the response variance increase as the seismic intensity level increases. A comparison of seismic response variability stemming from uncertain structural properties and record-to-record variability denote that except for floor acceleration response variables, seismic response variability due to structural parameter variations is more prominent at lower seismic intensity levels. Conversely, seismic response variability is primarily driven by uncertainty in ground motion records at higher seismic intensity levels. These findings stress the importance of considering both main sources of uncertainty—structural capacity and ground motion records—for reliable seismic performance assessment.

CHAPTER 5

UNCERTAINTY MODELLING FOR SEISMIC PERFORMANCE ASSESSMENT

5.1 Overview and Motivation

Assessing seismic fragility holds significant importance as it encompasses inherently unpredictable elements, enabling a quantitative evaluation of the susceptibility of structures to earthquake-related vulnerabilities. To ensure the development of a genuinely reliable seismic fragility relationship, it becomes essential to meticulously address and incorporate the multitude of uncertain factors that impact the seismic behaviour of buildings and infrastructure. The randomness in ground motions (aleatory) and uncertainties related to structural capacity (epistemic) are the two main sources of output response variability, and exhaustive knowledge of these uncertainties is indispensable in order to enhance the efficacy of seismic vulnerability assessment. Lack of proper consensus on appropriate consideration of aleatory as well as epistemic uncertainties into the seismic fragility estimates is often the stumbling block for reliable and coherent risk assessment procedures. Furthermore, the dispersion measure values specified in seismic design reference documents lack categorization for different building archetypes or intermediate structural performance levels.

In Chapter 4, the outcome of sensitivity analysis was discussed in detail in order to gauge the influence of independent random variables on the overall system output variability and identify the most influential parameters. However, although sensitivity analysis helps identify the relative importance of random parameters, it serves as an intermediate step in uncertainty analysis and falls short in quantifying the effect of uncertain variables on seismic performance assessments. Therefore, it is crucial to accurately characterize and propagate the various sources of uncertainty throughout the analysis to ensure dependable estimates of seismic damage.

While recognizing the importance of uncertainty analysis in assessing seismic performance for structures, it is worth noting that there are only a limited number of studies in the literature that comprehensively address various sources of uncertainty in vulnerability analysis, particularly for RC wall-frame buildings. For instance, the work by Karaton et al. (2020) focused solely on damping characteristic variability and did not account for aleatory

uncertainties. The present study aims to provide a comprehensive treatment of the uncertainty in structural capacity and the randomness of strong motion throughout the assessment of potential damage scenarios for the RC wall-frame structure during seismic events. To achieve this, extended incremental dynamic analysis (Dolsek, 2009) is employed within a probabilistic framework, striking a balance between simplifying FOSM approximations and the computational demands of Monte Carlo techniques. The insights gained from the sensitivity analysis conducted in the previous chapter are applied here to explore the differences in seismic responses when considering only essential epistemic variables as compared to all considered epistemic variables, as highlighted earlier. The results from this chapter are subsequently utilized for the formulation of damage exceedance probabilities in the following chapters, incorporating both epistemic and aleatory uncertainties into fragility functions derived from summarized IDA curves.

5.2 Framework for Uncertainty Analysis

The impetus of IDA is to perform nonlinear response history analyses of the deterministic mathematical model of a structure put through a suite of ground motion records, which are proportioned to different seismic intensity levels in such a way that it necessitates the structure to encompass complete range of response from linear elasticity to final global collapse state. In conventional IDA, only the influence of aleatory uncertainty is considered, affecting the structural response parameters through a set of ground motions. Essentially, this means accounting for the variability from one record to another and incorporating it into the seismic performance assessment in the form of IDA curves. However, in this approach, the aim is to capture not only aleatory uncertainty but also epistemic uncertainty. To achieve this, conventional IDA is conducted on a set of structural models for the RC wall-frame structure, aiding in the assessment of uncertainty in structural capacity. By doing so, the intention is to integrate epistemic uncertainty, related to variations in structural models, with aleatory uncertainty arising from different ground motion records within the fragility assessment framework.

The extended IDA procedure introduced by Dolsek (2009), in contrast to the conventional IDA presented by Vamvatsikos and Cornell (2002), involves conducting nonlinear dynamic analyses for a range of structural models. This procedure includes the additional step of specifying this set of structural models, which distinguishes it from the conventional IDA process. Subsequently, IDA curves are generated for each of these individual structural

models when subjected to specific earthquake records. The creation of single-record IDA curves employs the hunt and fill algorithm (Vamvatsikos and Cornell, 2004). Finally, the summarized IDA curves are derived from the analysis results obtained for the predefined set of structural models across the complete suite of ground motion records.

The summarized IDA curves, incorporating the influence of both epistemic and aleatory uncertainties, are then used to derive comprehensive seismic fragility estimations for the RC wall-frame structure. The formulation of fragility functions from the summarized IDA curves is elaborated upon in the subsequent chapters. However, to emphasize the importance of uncertainty analysis and dispersion quantification related to various sources of uncertainty, this chapter includes an introductory section on IDA-based fragility formulation and the subsequent assessment of dispersion measures.

In the past, numerous researchers (e.g., Ellingwood et al., 2007; Zareian et al., 2010) have investigated the development of IDA-based fragility curves. Essentially, IDA curves visually illustrate the relationship between structural seismic response and seismic hazard for specific structural systems. The representation of the structural seismic response involves an appropriate Engineering Demand Parameter (EDP), while the seismic hazard is characterized by an Intensity Measure (IM). At a particular IM level, determination of the median value of EDP (μ_d) can be made from the extended IDA results. This median EDP, μ_d, can be expressed as a function of the IM level:

$$\mu_d = a(IM)^b \varepsilon \tag{5.1}$$

where ε represents a lognormal random variable with a median value of 1, and the uncertainty in the relationship is indicated by the logarithmic standard deviation, $\sigma_{\ln \varepsilon}$, as defined in Eq. 5.2. This dispersion measure, referred to as β_{EDP}, quantifies the variability in seismic response resulting from various sources of uncertainty. Thus, at a specific seismic intensity level, β_{EDP} signifies the impact of different sources of uncertainty on the structural response parameters. The parameters " a " and " b " in Eq. 5.1 are determined through linear regression in the logarithmic scale (Cornell et al., 2002), as illustrated in Eq. 5.3.

$$\beta_{EDP} = \sigma_{\ln \varepsilon} \tag{5.2}$$

$$\ln \mu_d = \ln a + b \ln IM \tag{5.3}$$

As extensively discussed in Section 3.6, a set of 11 ground motion records (presented in Table 3.3) is utilized to examine aleatory uncertainty modeling in formulating fragility

functions for the RC wall-frame structure. To efficiently represent seismic performance in terms of an EDP-IM relationship, the chosen EDP is inter-storey drift, and the seismic Intensity Measure (IM) is the spectral acceleration at the fundamental period ($S_a(T_1)$). Section 3.7 provides a comprehensive discussion regarding the selection of EDP and IM. To characterize epistemic uncertainty in the performance analysis for fragility formulation, which relates to variability in structural parameters, several key variables are considered, as highlighted in Section 4.4. In this investigation, the epistemic source of uncertainty is manifested through variations in several key structural capacity parameters, incorporated into the analysis via the use of different structural models for the considered building system. These diverse structural models are developed using the Latin Hypercube Sampling (LHS) technique, each representing different realizations of the uncertain input structural parameters. The optimal number of structural models, effectively capturing and propagating epistemic uncertainty into seismic performance analysis, is determined by investigating the influence of variation in the number of structural models on seismic response variability.

The results of the sensitivity analysis conducted in the preceding chapter revealed that the seismic response variability is primarily influenced by key structural parameters, including viscous damping ratio, concrete compressive strength, and building mass. Conversely, parameters such as yield strength of steel and stiffness parameters, such as the elastic moduli of concrete and steel, have a lesser impact on seismic response variability. Therefore, in this chapter, uncertainty modelling for seismic performance assessment is carried out by considering both aleatory and epistemic uncertainties with a focus on two distinct scenarios for characterizing epistemic uncertainty, namely (a) one that includes only influential uncertain structural parameters and (b) that encompasses all uncertain structural parameters. This approach aims to assess any discernible difference in dispersion quantities, which measure seismic response variability, while considering different combinations of variables for epistemic and aleatory uncertainties.

5.3 Uncertainty Analysis

5.3.1 Number of Structural Models

As previously discussed, aleatory uncertainty is inherently accounted for in seismic response through IDA, utilizing different ground motion records. In contrast, the impact of epistemic uncertainty is considered by exploring various combinations of structural models. Employing the LHS technique, diverse structural models are developed for the RC wall-frame structure.

This ensures the effective inclusion of uncertain structural parameters, which constitute the epistemic uncertainties, in the seismic response analysis. To investigate the two distinct combinations of uncertain variables for characterizing epistemic uncertainties, two separate sets of structural models are developed and analysed.

Prior to conducting uncertainty analysis to appropriately treat the various uncertainties in seismic response analysis, it is imperative to select an optimal number of structural models. This is as important as selecting the number of ground motion records to effectively characterize the wide spectrum of seismic demand, accounting for record-to-record variability (details available in Section 3.6.1). Using too few structural models may not adequately capture the diverse variations in uncertain structural parameters that influence seismic response variability. Conversely, an excessive number of structural models can lead to redundancy. Thus, considering the appropriate number of numerical models is essential for effectively characterizing epistemic uncertainties. Additionally, optimal model selection maximizes the efficient use of computational resources to ensure that the chosen structural models adequately represent variability in structural capacity parameters.

In this context, the optimal number of structural models is determined by randomly sampling input variables to generate various sample sizes (S_s = 5, 10, 15, 20, 30, 50). While the uncertainty modelling in the performance assessment and subsequent fragility formulation for the RC wall-frame structure focuses on using ISD as the EDP, this investigation considers multiple response parameters to select the optimal number of structural models. The impact of varying sample sizes of structural models on various seismic response parameters, including roof displacement (RD), maximum inter-storey drift (ISD), maximum floor acceleration (MFA), maximum storey curvature (MSC), and maximum concrete compressive strain (MCC), is assessed. Through statistical analyses of these response variables, the appropriate number of samples in a set is determined. All the considered uncertain input structural parameters (Table 4.1) are utilized in this process for developing the structural models. The seismic response variability due to the variation in the number of structural models is evaluated by performing IDA for the structural models using only the median ground motion record, specifically the Northridge 1991 earthquake record (Carson – Water Station), from the set of 11 ground motion records (Table 3.3). Collapse points, indicating global dynamic instability, are identified from the IDA of the structural models based on various response parameters. The dispersion values of the collapse points for each set of models, considering different numbers of structural models, are determined using Eq. 5.2 and

presented in Table 5.1. Additionally, the absolute difference (Δ) between the dispersion measure (β) for a given number of S_s and those obtained when S_s = 50, which has the highest S_s number in this case, is calculated. These absolute differences (Δ) between the β values for different response parameters are shown in Figure 5.1 as a function of the number of samples.

Table 5.1 Comparison of the dispersion measure of collapse points for different number of structural models

S_s	β_{RD}	Δ_{RD}[1]	β_{ISD}	Δ_{ISD}[1]	β_{MFA}	Δ_{MFA}[1]	β_{MSC}	Δ_{MSC}[1]	β_{MCC}	Δ_{MCC}[1]
5	0.047	0.0052	0.044	0.0077	0.052	0.008	0.065	0.0054	0.050	0.018
10	0.031	0.0210	0.035	0.017	0.031	0.003	0.038	0.0210	0.067	0.001
15	0.043	0.0087	0.040	0.011	0.052	0.009	0.064	0.0042	0.052	0.016
20	0.047	0.0051	0.042	0.010	0.063	0.0024	0.064	0.0045	0.063	0.005
30	0.052	0.0001	0.053	0.002	0.071	0.011	0.059	0.0003	0.055	0.013
50	0.052	0	0.051	0	0.061	0	0.059	0	0.068	0

[1] $\Delta = |\beta_{Ss,50} - \beta_{Ss,i}|$

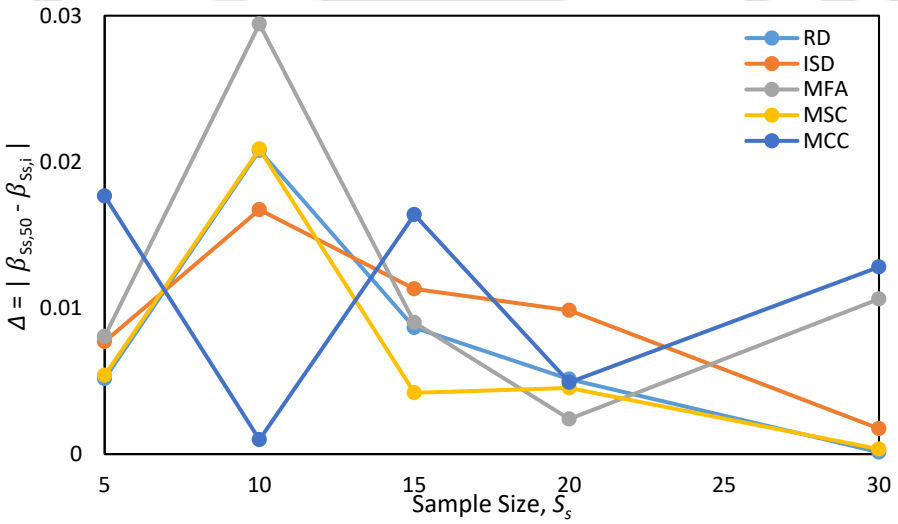

Figure 5.1 The absolute difference Δ between the dispersion measures of S_s = 50 and other considered S_s.

Table 5.1 demonstrates that dispersion values (β) generally exhibit an increasing trend as the S_s number increases, except for MSC. Notably, when S_s = 10 is considered, the β values appear distinct from those obtained for other cases, regardless of the response parameter. Furthermore, the Δ values reveal that the difference between the β values of S_s = 50 and the

other considered S_s is smallest for S_s = 30, but for response parameters such as MFA and MCC, these differences are relatively larger. Figure 5.1 further illustrates that, calculated Δ values for S_s = 20 lie in a reasonable range for all response parameters and as compared to other sample sizes, the Δ values for S_s = 20 are relatively small. Although S_s values other than 20 also exhibit Δ values smaller than those obtained for S_s = 20, these smaller Δ values are not consistently observed for all response parameters as they are for S_s = 20. This suggests that S_s = 20 is a suitable choice for the optimal number of structural models, as it consistently shows lower Δ values across various response parameters. Therefore, a sample size of 20 structural models is considered to strike the right balance between computational efficiency and the statistical significance of results in terms of the dispersion of various response parameters. As a result, a set of structural models with S_s = 20 is employed to accurately characterize and propagate epistemic uncertainty in the seismic response analysis and subsequent fragility formulation of the RC wall-frame structure.

5.3.2 Extended Incremental Dynamic Analysis

In this section, the results obtained from IDA conducted on the deterministic structural model for the suite of considered ground motions are discussed, which helps acknowledge aleatory uncertainties. Additionally, the summarized IDA curves are presented, derived from the extended IDA performed on the sets of structural models (to incorporate epistemic uncertainties), with each set comprising 20 models, for all the considered ground motions.

Nonlinear dynamic analyses are conducted on the deterministic structural model for each of the considered records. Suitable EDP and IM estimates (in the present study, ISD and $S_a(T_1)$) are determined from these analyses, resulting in a unique set of values within the EDP-IM space. These discrete points form individual record IDA curves. Subsequently, multiple IDA curves are generated for all the considered records and displayed in Figure 5.2(a), alongside the IDA points. The randomness observed in the IDA curves in Figure 5.2(a) primarily stems from record-to-record variability, reflecting aleatory uncertainties. Figure 5.2(b) presents summarized IDA curves for the deterministic model, representing the 16th, 50th, and 84th percentile values.

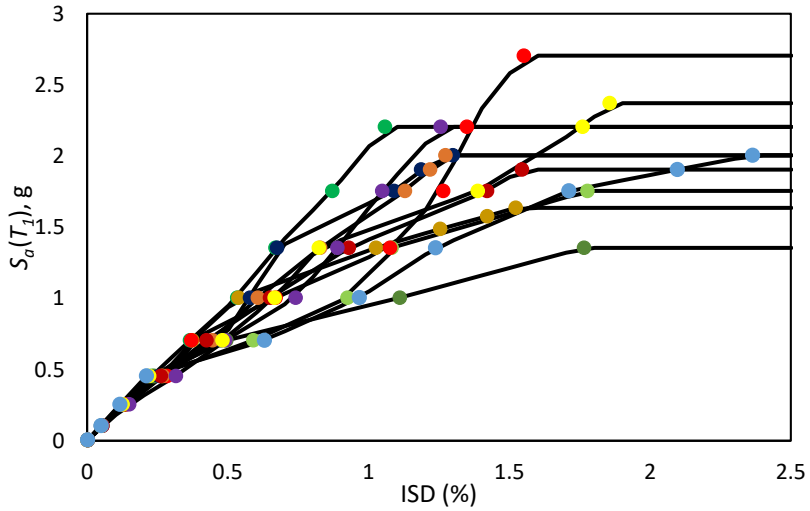

(a)

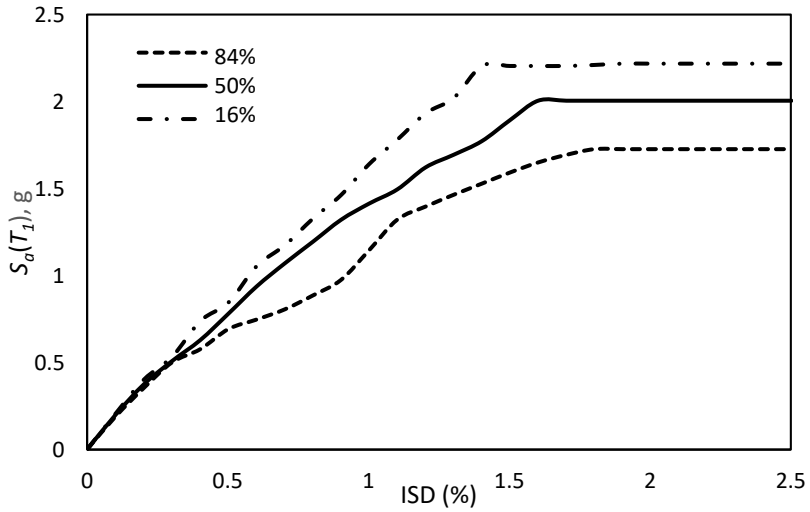

(b)

Figure 5.2 (a) IDA curves and IDA points and (b) Summarized IDA curves for the deterministic structural model.

The findings from the extended IDA, which accounts for both epistemic and aleatory uncertainties within the IDA framework using different sets of structural models, are presented in Figure 5.3 and 5.4. Two distinct sets of structural models are employed wherein, the first set includes only the important structural capacity parameters identified through sensitivity analysis (Section 4.5), and the second set incorporates all the epistemic uncertainty sources (listed in Table 4.1). The extraction of IDA points and summarizing the IDA curves for extended IDA are performed on similar lines as for conventional IDA.

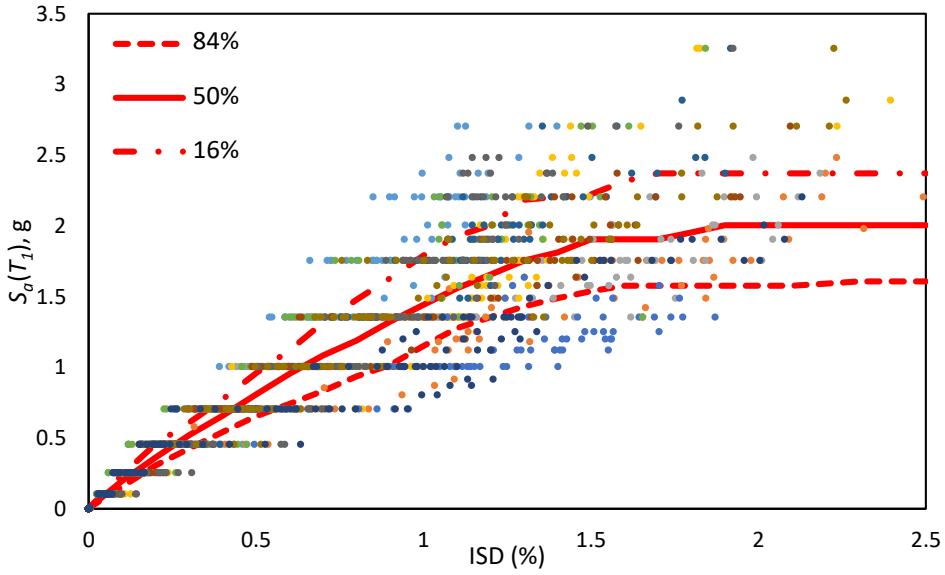

(a)

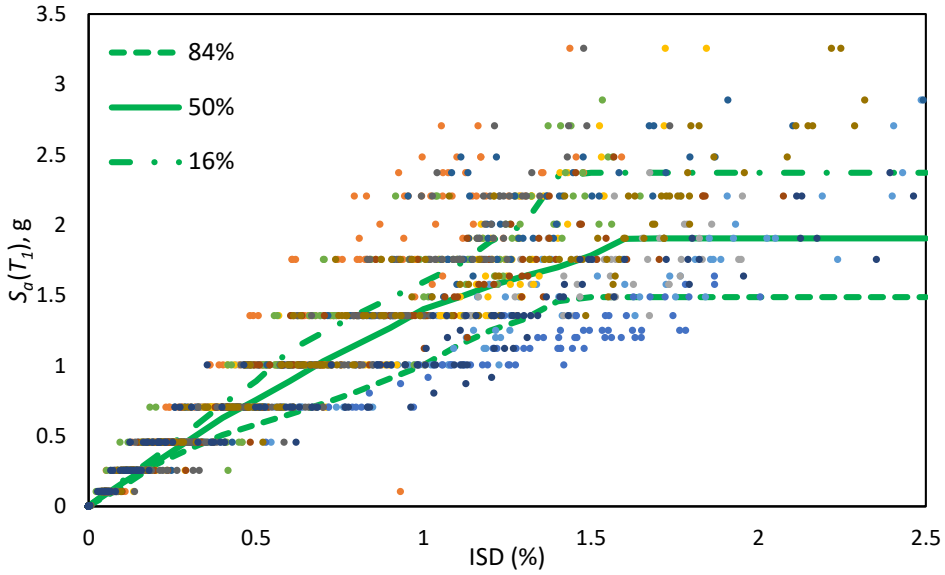

(b)

Figure 5.3 Summarized IDA curves and IDA points for the set of models realized using (a) important epistemic uncertainties; (b) all epistemic uncertainties.

Figures 5.3(a) and 5.3(b) display the summarized IDA curves along with the IDA points derived from extended IDA performed on the first and second sets of structural models, respectively. It is observed from Figure 5.3 that the IDA points for structural models using all input epistemic variables (Figure 5.3(b)) are slightly more scattered than those for the structural models using only the important epistemic variables (Figure 5.3(a)), although the difference is marginal. This observation is further confirmed by comparing the summarized IDA curves from extended IDA for two separate classes of structural models in Figure 5.4(a).

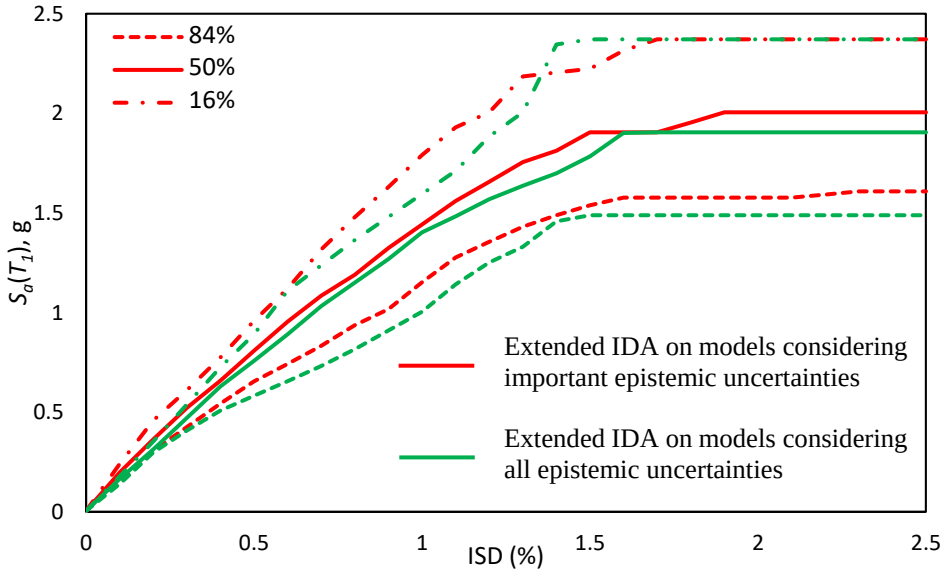

(a)

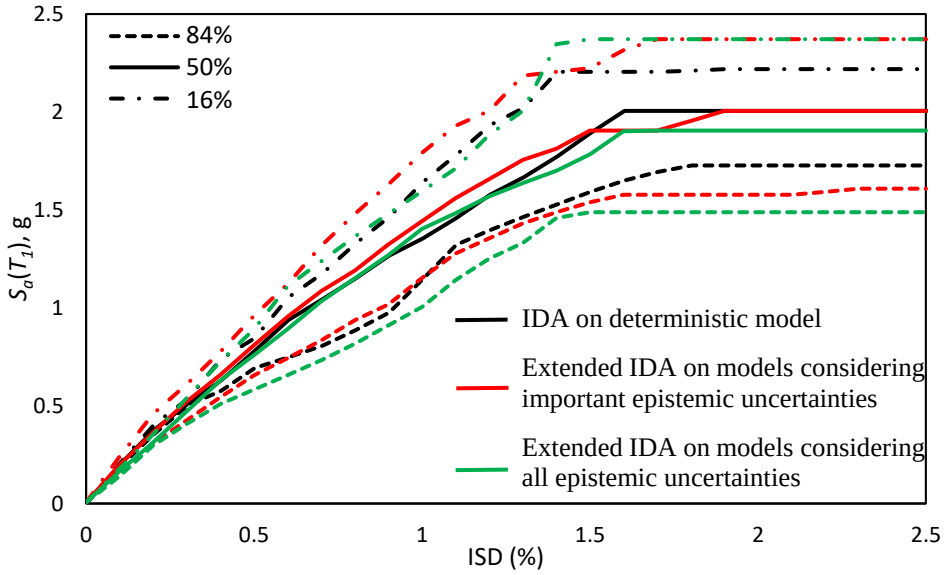

(b)

Figure 5.4 Comparison of the summarized IDA curves for (a) the two structural model categories; (b) the deterministic model and the two sets of models.

From Figure 5.4(a), it is evident that the two sets of summarized IDA curves are identical, especially the median curves (50th percentile), regardless of the seismic intensity level. However, the summarized curves derived from the second set of models, considering all input structural parameters, exhibit slightly more deviation, primarily in the 84th percentile curves. This increased deviation can be attributed to the larger number of uncertain epistemic variables considered as compared to the first set of models. Nevertheless, given that both sets of models incorporate important epistemic variables and differ mainly in terms of insignificant variables, the variance between the two categories of summarized IDA curves

remains minimal. This reinforces the notion that aside from the significant epistemic uncertainties, other variables have a negligible impact on structural seismic response variability.

Finally, a comparison between the summarized curves obtained from IDA on the deterministic model (Figure 5.2(b)) and on both sets of structural models (Figure 5.4(a)) is depicted in Figure 5.4(b). Figure 5.4(b) illustrates that the deviation between the sets of summarized curves is minimal, with the median curves are found to overlap. However, a notable observation is that considering epistemic uncertainties alongside aleatory uncertainties in the analysis, at least for the given scenario, increases the variability of the output seismic response variables. The 16^{th} and 84^{th} percentile curves for extended IDA on the sets of structural models, accounting for epistemic uncertainties, exhibit greater dispersion from the median curves as compared to those for IDA curves on the deterministic model, which considers only aleatory uncertainties. This observation underscores the significant influence of epistemic uncertainties on the overall variability of seismic response, emphasizing the need for their proper consideration in addition to aleatory uncertainties.

5.3.3 Quantification of Dispersion Measure due to Various Uncertainty Sources

Another contribution of the current study is to establish a framework for quantification of the uncertainty in seismic response considering both epistemic and aleatory uncertainties through dispersion measures. Identifying the appropriate dispersion measure value is a pivotal step in the development of seismic fragility functions, as it is central to representing the uncertainty associated with structural responses and, consequently, for assessing the seismic vulnerability of structures. To ensure the reliability of fragility functions, it becomes imperative to ascertain a dispersion measure value that effectively encompasses the variability in structural responses resulting from both aleatory and epistemic uncertainties. This selected value should provide a comprehensive representation of the spread or scatter in response values corresponding to specific seismic intensity levels. The choice of an appropriate dispersion measure value is influenced by various factors, including the structural performance parameters under consideration and the specific objectives of the fragility analysis. Achieving the desired level of confidence and precision in fragility assessments requires an exhaustive evaluation to determine the most suitable dispersion measure value.

A seismic fragility function serves as a statistical tool to quantify the likelihood of surpassing specific damage levels under varying seismic intensities. Its formulation entails mathematical

integration of damage state thresholds, dispersion measures linked to these thresholds, and median values of response parameters tied to distinct seismic intensity levels. Consequently, establishing the dispersion measure corresponding to a particular damage state level is a prerequisite before estimating fragility relationships. In the subsequent chapter, different damage state thresholds are defined for the analysis of the current RC wall-frame structure. Subsequently, after these thresholds are established, the framework presented here can be employed to evaluate the dispersion measures associated with each threshold. These measures are then utilized to construct the fragility function for the RC wall-frame structure. To underscore the significance of the dispersion measure stemming from various sources of uncertainty, the present study aims to compare the dispersion measures across different seismic intensity levels, ranging from low (0.5g) to high (2g), without focusing on a specific damage state threshold.

Dispersion measures can be represented either through vertical statistics (IM-based dispersion) or horizontal statistics (EDP-based dispersion). In the former case, it involves quantifying the dispersion of $S_a(T_1)$ values, which represent IM, at a particular seismic response parameter value. In the latter case, it entails quantifying the dispersion of ISD values, representing EDP, at a specific seismic intensity level. In the current study, the dispersion measure characterizing the influence of sources of uncertainty is determined using EDP-based dispersion values. This measure is calculated as the standard deviation of the natural logarithm of ISD values at designated levels of seismic intensity.

The dispersion value derived from the IDA curves of the deterministic model, denoted as β_A, quantifies the variation in response parameters solely attributable to aleatory uncertainties (Figure 5.2(b)). By utilizing summarized curves from the extended IDA across sets of structural models, it becomes possible to assess the dispersion of EDP values (β_E) attributable solely to epistemic uncertainties. β_E values are computed based on EDP values for different structural models but under the same ground motion. Consequently, β_E estimates exhibit record-to-record variation. However, this investigation focuses on the average β_E values obtained across different ground motion records. Subsequently, the deviation of EDP values (β_{AE}) can be quantified for both aleatory and epistemic uncertainties, considering the extended IDA results performed on sets of structural models for various ground motion records (Figure 5.4(a)). The dispersion measures accounting for different sources of uncertainty are detailed in Table 5.2. Additionally, the overall variation in EDP values is influenced by modelling uncertainties (β_M), distinct from aleatory and epistemic

uncertainties. A commonly adopted value for β_M is 0.2, which assumes that the considered modelling framework of the structural system characterizes the true building response within ±30% of the actual value, with 90% confidence (Celik and Ellingwood, 2010). To obtain the total dispersion measure ($\beta_{AE,t}$), which considers various sources of uncertainty, these dispersion values can be integrated using the square root of the sum of the squares (SRSS) combination technique (Aslani et al., 2012), expressed as follows:

$$\beta_{AE,t} = \sqrt{{\beta_A}^2 + {\beta_E}^2 + {\beta_M}^2} \tag{5.4}$$

Table 5.2 Dispersion measure of ISD values due to various sources of uncertainties

$S_a(T_1)$, g	β_A	β_E		β_{AE} (extended IDA)			β_{AE} (SRSS rule)	
		Important Variables	All Variables		Important Variables	All Variables	Important Variables	All Variables
0.1	0.060	0.214	0.220	β_{AE}	0.228	0.232	0.222	0.228
				$\beta_{AE,t}$	0.303	0.306	0.299	0.303
0.5	0.130	0.176	0.184	β_{AE}	0.216	0.224	0.219	0.225
				$\beta_{AE,t}$	0.294	0.300	0.296	0.301
1.0	0.163	0.162	0.173	β_{AE}	0.223	0.234	0.230	0.238
				$\beta_{AE,t}$	0.300	0.308	0.305	0.311
1.5	0.183	0.156	0.167	β_{AE}	0.231	0.244	0.240	0.248
				$\beta_{AE,t}$	0.306	0.315	0.313	0.318
2.0	0.196	0.152	0.164	β_{AE}	0.238	0.251	0.248	0.256
				$\beta_{AE,t}$	0.311	0.321	0.319	0.325

The dispersion measures, which only account for aleatory uncertainties, consistently increase with the seismic intensity levels. Notably, these dispersion values (β_A) are relatively smaller for lower damage state thresholds as compared to those employed in the previous study by Surana et al. (2016). This relative difference in the values of dispersion measure can be attributed to the fact that these values are typical to the current set of earthquake records used and the considered building frame, which yields a lesser dispersed seismic response across different seismic intensity levels, and can be different when a different suite of ground motion records is used.

The findings from estimating β_E values, representing dispersion in the response parameter solely due to epistemic uncertainties, for both sets of structural models – one involving only the important uncertain parameters and the other including all the adopted uncertain parameters – reaffirm that seismic response variability is primarily driven by important epistemic variables among all the considered structural parameters. The estimated β_E values corresponding to the two different sets of structural models, one including only the important uncertain parameters and the other including all uncertain parameters, yield similar dispersion quantities across various levels of seismic intensity. Regardless of seismic intensity levels, incorporating all uncertain epistemic variables results in β_E values that are only slightly higher, with an increment ranging from 2.8% at a $S_a(T_1)$ value of 0.1g to 7.8% at a $S_a(T_1)$ value of 2g, as compared to considering only the important uncertain parameters. This suggests that efficient characterization of epistemic uncertainty in the analysis framework can be achieved by using only the important variables, thereby reducing computational time and effort. The estimated β_E values for the RC wall-frame structure range between 0.15 and 0.22, similar to those observed in the work of Ellingwood et al. (2007).

An interesting observation regarding the variation of response parameters solely due to epistemic uncertainties is that β_E values decrease at higher levels of seismic intensity. In other words, β_E values counter the general trend of increasing dispersion measures with higher seismic intensity levels. This indicates that the influence of epistemic uncertainties on seismic response parameters relatively diminishes as seismic intensity levels increase, while the effect of aleatory uncertainties, in terms of dispersion measures, intensifies with higher damage state threshold levels. This observation aligns with similar findings from an earlier study (Lee and Mosalam, 2005), suggesting that epistemic uncertainties have a more pronounced effect at lower intensity levels, while aleatory uncertainties dominate at higher intensity levels.

To quantify the significance of the epistemic variables (characterized using only the important variables) in the variability of response parameters, Table 5.3 provides a comparison of β_A and β_{AE} (estimated from the extended IDA results) values, signifying the contribution of β_E values to the total dispersion values of β_{AE}. Since any assessment involving a numerical structural model inherently includes modelling uncertainty, the comparison of β_A and β_{AE} values in Table 5.3 incorporates these values along with β_M values using the SRSS rule. It is evident that the incorporation of epistemic uncertainties into the analysis significantly increases seismic response variability, especially at lower levels of

seismic intensity, where the increase is as high as 45% for a $S_a(T_1)$ value of 0.1g. The differences between β_A and β_{AE} values also highlight the greater significance of epistemic uncertainty at lower intensity levels (a 45% difference at 0.1g $S_a(T_1)$) as compared to higher intensity levels, where the difference is only 10% at a $S_a(T_1)$ value of 2g. This comparison underscores the importance of effectively characterizing and propagating epistemic uncertainties through the analysis framework for reliable structural seismic assessment.

Table 5.3 Comparison of β_A and β_{AE} values

$S_a(T_1)$, g	β_A	β_{AE}	% increase = $(\beta_{AE} - \beta_A)/\beta_A$
0.1	0.209	0.303	45.33
0.5	0.239	0.294	23.20
1.0	0.258	0.300	16.16
1.5	0.271	0.306	12.90
2.0	0.280	0.311	10.95

The dispersion measure (β_{AE}) value, considering both aleatory and epistemic uncertainties, as quantified by statistical analysis of summarized curves from extended IDA on both sets of structural models, ranges between 0.20 and 0.25. Integrating the β_{AE} values obtained from the extended IDA curves with the β_M values using the SRSS method results in the estimation of $\beta_{AE,t}$ values, with a maximum value of 0.32 and a minimum value of 0.30 corresponding to $S_a(T_1)$ values of 2g and 0.1g, respectively. The β_{AE} values determined using the SRSS method to combine the individual components, namely β_A, β_E, and β_M values, are slightly higher than those obtained from the extended IDA, with only marginal differences across seismic intensity levels. Another noteworthy observation is that the β_{AE} values do not exhibit a consistently increasing or decreasing trend with increasing seismic intensity levels. This is primarily due to its constituents—β_A and β_E values—exhibiting contrasting trends, with the former increasing and the latter decreasing as seismic intensity levels rise. Additionally, the influence of considering only the important epistemic variables, as opposed to all variables, is observed to be negligible in the β_{AE} values. The $\beta_{AE,t}$ values evaluated in the current study using both methods lie in the range of 0.30 to 0.35, which is similar to the observations from past studies (Dolsek, 2009; Choudhury and Kaushik, 2019). However, it is noted that the dispersion measures here are smaller than those suggested in HAZUS, which range from 0.70

to 0.80. This suggests that the dispersion measures recommended in HAZUS are on the higher end of the spectrum, at least for the considered building typology.

5.4 Summary

In the present chapter, the uncertainty values corresponding to a wide range of seismic intensity levels are quantified through statistical analysis of results from nonlinear response history analyses of the RC wall-frame structures. These uncertainties are quantified using extended Incremental Dynamic Analysis, which strikes a reasonable balance between the simplification of FOSM approximations and the computational demands of Monte Carlo techniques. Conventional IDA propagates aleatory uncertainty into seismic response parameters through various ground motion records. In contrast, epistemic uncertainties are characterized and propagated into the analysis through IDA on a set of structural models created using the LHS technique with different realizations of considered uncertain variables.

To ensure a comprehensive characterization of epistemic uncertainties, a set of 20 structural models is employed for analysis, effectively balancing computational costs and the statistical implications in terms of the dispersion of various response parameters. It is important to note, however, that this specific number of structural models in the set is tailored to this case study and may not be suitable for other structural systems. The insights gained from the sensitivity analysis conducted in the previous chapter are utilised here to explore the difference in the influence of considering only the important epistemic variables as compared to all the epistemic variables. This analysis suggests that focusing on the important variables alone may suffice for propagating epistemic uncertainties into the analysis, as they account for a significant portion of the seismic response variability contributed by the entire set of considered epistemic variables.

The findings from the present study underscore the substantial potential for seismic response variability attributable to epistemic uncertainties, particularly at lower seismic intensity levels. It is worth noting that epistemic uncertainties exert a significant influence on total dispersion measure values at performance levels far from collapse, while aleatory uncertainties predominantly contribute to response variability at higher seismic intensity levels. Specifically, the contribution of epistemic uncertainties to the total response variability ranges from approximately 10% at higher seismic intensity levels to a substantial 45% at lower seismic intensity levels. This highlights the indispensability of considering epistemic

uncertainties alongside aleatory uncertainties to ensure a reliable assessment of structural performance.

The importance of selecting the appropriate dispersion value becomes evident when analysing the fragility function plots developed in the subsequent chapters, highlighting significant differences between functions based on dispersion measures tied to diverse damage state thresholds and considering multiple sources of uncertainty. Recognizing the substantial impact of epistemic uncertainties on response variability alongside aleatory uncertainties and the feasibility of effectively characterizing them by considering only key variables, the formulation of fragility functions will be discussed in the subsequent chapters. These functions will be based on results from extended IDA performed on the set of structural models that consider only the essential epistemic variables and incorporate the appropriate dispersion measure value as outlined in this chapter.

CHAPTER 6

DAMAGE STATE THRESHOLDS FOR RC WALL

6.1 Overview and Motivation

The damage state of seismic force-resisting components, such as structural walls in a wall-frame building, serves as an indicator of the overall performance level of the entire structural system, which is important for efficient structural vulnerability assessment at varying levels of seismic intensity. A damage state threshold signifies the expected extent of damage that a building or structural element may endure when exposed to significant seismic forces. Thus, it is important to establish quantitative thresholds for specific damage states, especially for the critical structural components within a building system. Although seismic damage to different components can have implications on structural safety and economy, evaluating the likelihood of reaching each damage state in the structural walls is extremely important as the structural wall primarily provides the lateral load resistance in a wall-frame structure.

The current damage state definitions for RC structural walls (Ghobarah, 2004; Rossetto and Elnashai, 2003), rely on empirical fitting of several experimental results of walls that differ for each definition. However, RC structural walls can exhibit a broad spectrum of potential interconnected design attributes that significantly influence the damage characteristics of these elements. Consequently, traditional attempts at defining damage states have proposed empirical limits that demonstrate obvious inefficiencies and insufficient reliability when applied to estimate experimental outcomes beyond those used to initially formulate these definitions (Kazaz, 2012; Xiong, 2019). To the best of the authors' knowledge, the available damage state definitions for RC structural walls are empirical limits that do not predict damage thresholds based on key wall geometrical and structural characteristics, including the work of Kazaz (2012), which proposed damage limit prediction equations but did not cover the entire range of structural wall seismic damage. The limited capability of available empirical damage state definitions calls for more state-of-the-art damage state prediction equations articulated upon key wall parameters.

To address this challenge, Genetic Programming (GP), a form of artificial intelligence, is used to prescribe expressions for lateral drift prediction at various damage states, using a dataset of 8,125 numerically studied specimens of RC structural walls. These expressions

take into account the effects of various structural parameters, such as wall aspect ratio, axial load ratio, boundary element longitudinal reinforcement ratio, web longitudinal reinforcement ratio, and the ratio of boundary element length to wall length, in determining deformation limits. The developed prediction expressions have been evaluated for accuracy and validity using various statistical measures. In addition, the proposed drift prediction expressions have been compared with other available deformation limits in relevant design standards and literature to predict the experimental results of RC wall components. The findings of these analyses indicate that the developed expressions provide significantly higher accuracy and improved predictions as compared to existing empirical damage state definitions.

6.2 Available Deformation Limit Criteria

As inter-storey drift (ISD) is used as the response parameter in the present study involving evaluation of seismic fragility functions for an RC wall-frame building, the same parameter ISD is used to establish damage state thresholds. This choice of ISD as the response parameter is supported by its ease of correlation with experimental results and its effectiveness in representing both structural and non-structural damage. Notably, it has been widely employed as a response parameter in previous research and various building codes to quantify damage across different structural performance levels. Consequently, lateral drift ratios of cantilever specimens are employed to evaluate the damage in RC structural walls.

Although several design guidelines have defined structural performance levels using qualitative descriptions, quantitatively defined damage state thresholds are more suitable for seismic design of structures (Wen et al., 2003), as those thresholds are closely related to either forces or deformations in structural or non-structural components. Corresponding to different component damage conditions, the NEHRP provisions (FEMA 2009) include four performance levels for RC structures, namely Operational (OP), Immediate Occupancy (IO), Life Safety (LS), and Collapse Prevention (CP) levels. ASCE/SEI 41-06 (2007) classifies limit state thresholds for structural walls in terms of ISD at 0.5%, 1%, and 2% for IO, LS, and CP, respectively. In the SEAOC blue book (1999), four damage states are recommended, each associated with ISDs of 0.4%, 0.9%, 1.4%, and 2.1%, representing performance levels SP1 (negligible damage), SP2 (minor to moderate reparable damage), SP3 (moderate to major irreparable damage), and SP4 (collapse).

These lateral drift limits proposed in design guidelines are often deemed as conservative, as compared to those suggested by researchers based on experimental and analytical investigations. Researchers such as Rossetto and Elnashai (2003), Brown (2008), Gulec and Whittaker (2010), and Birely (2012) have proposed empirical damage state thresholds for structural walls through statistical analysis of experimental results. Others, including Mwafy (2012), Alwaeli et al. (2016), and Xiong et al. (2019), have conducted analytical studies on concrete wall structures to investigate damage state thresholds. For example, Ghobarah (2004) suggested damage states for ductile structural wall members in terms of ISDs: 0.4 (light reparable damage), 0.8 (irreparable damage or yield point), 1.5 (severe damage or life safety), and 2.5 (collapse). Mwafy (2012) performed a numerical investigation on RC wall-frame buildings with varying storey numbers (10-60 storeys) and proposed ISDs corresponding to the different limit states, namely (a) IO with the range of ISD as 0.32% - 0.83%, (b) LS with the range of ISD as 0.81% - 1.35%, and (c) CP with ISD > 2.50%. In another study, Ji et al. (2009) suggested conservative damage states for a 54-storey RC wall-frame building based on pushover and time-history analyses, with ISDs proposed at 0.20% (serviceability), 0.52% (damage control), and 1.1% (CP). Further discussion on the definition of damage state thresholds is presented in Section 2.4.3.

6.3 Genetic Programming

Over the past few years, Machine Learning (ML) techniques have demonstrated their efficiency as an alternative to classical methods for empirical modelling in various fields, including engineering (e.g., Jasmine and Arun, 2021; Kabir et al., 2021). Despite their higher accuracy as compared to classical techniques, ML models have certain limitations, such as their inability to generate explicit functions for evaluating the target variable based on input parameters (Perez, 2012). Within this context, Genetic Programming (GP), a variant of artificial intelligence conceptualized by Koza (1992), is gaining prominence as a superior evolutionary computing technique. Grounded in the principles of Darwinian natural selection for evolving models, GP is well-suited for capturing complex mathematical relationships from suitable learning datasets and producing easy-to-use predictive equations (Gandomi et al., 2014; Kara, 2011).

GP belongs to the category of soft computing algorithms that provide adaptive solutions in the form of computer programs for solving complex phenomena. Inspired by Darwin's theory of evolution, GP employs techniques reminiscent of natural selection. In nature, species

better adapted to their environment have a higher likelihood of survival and evolution. Similarly, GP conducts a series of operations to explore the entire space of provided learning data, ultimately yielding a near-optimal solution of significantly enhanced efficiency (Kara, 2011, Yosri et al., 2019).

GP begins by randomly generating a preconfigured number of tree-shaped mathematical solutions, each representing an unbiased search across the entire solution space. Each solution is treated as an individual, embodying a potential predictive expression. These individuals comprise a combination of terminal elements, including input parameters and constants, and nonterminal elements, which consist of functional operators. Subsequently, the fitness value of each individual is evaluated utilising a designated fitness function. Various genetic operations, such as elitism, crossover, and mutation, are implemented to evolve updated generations. A preconfigured fraction of individuals displaying superior fitness values advances explicitly to the ensuing generation (elitism). The residual fraction of individuals undergoes a process of random combination and permutation through crossover and mutation to generate new offspring individuals. Crossover involves adopting two individuals, either at random or based on their fitness value (excluding inferior ones), and integrating them to produce new individuals. Mutation randomly alters specific individuals by recombining or substituting one or more of their constituents. This operation continues until a predetermined termination condition is satisfied, which can be specified based on computational time, fitness function value, or a stipulated maximum number of generations. A flowchart illustrating the GP procedure is presented in Figure 6.1.

The final expression produced by the GP algorithm is a distinct near-optimal solution, typically represented as a tree with a specific depth. Several GP parameters influence the resulting solution, such as the termination criterion, population size, generation size, functional operator set, percentage of elitism, crossover, mutation, and more. Consequently, when different GP parameter settings are applied to the same underlying dataset, the final solution obtained can vary.

In several previous studies (Yosri et al., 2019; Gondia et al., 2021), the classic GP, combined with a multigenetic approach, has been adopted. This approach combines multiple standard GP models using linear regression. It strives to create a linear combination of smaller trees with reduced complexity, as opposed to a solitary complex numerical relationship, which is a common output of traditional GP (Searson et al., 2010). The coefficients for each tree,

determined through the multigenetic technique, are established via linear regression, with the goal of reducing the least squared error with respect to the dependent variable. In the current investigation, aimed at establishing damage state thresholds for RC structural wall components, a multigenetic GP approach is employed utilizing the MATLAB toolbox GPTIPS proposed by Searson et al. (2010).

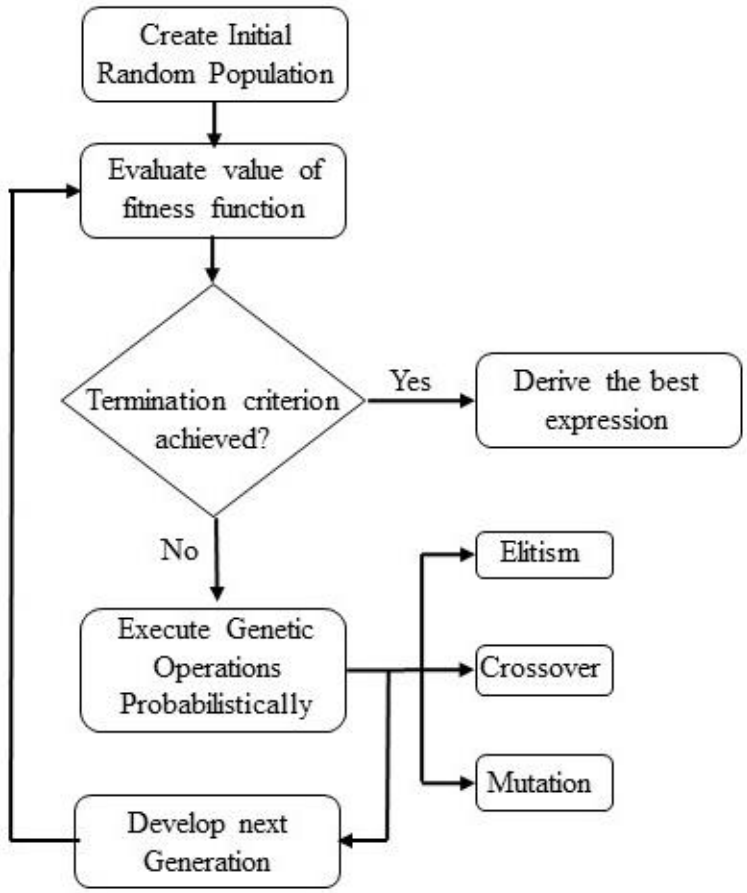

Figure 6.1 Flowchart of Genetic Programming (Koza, 1992).

6.4 Analytical Framework for the Investigation of Performance Limits

To create the dataset required for input into any mathematical programming algorithm for model formulation, it is essential to conduct a parametric study based on either experimental or analytical findings. From the existing literature, a selection of experimental studies (e.g., El-Azizy et al., 2015; Lu et al., 2017) focused on the seismic response characteristic of structural walls has been reviewed, yielding a total of 60 data points. Statistical analysis of these experimental results reveals significant variation in deformation limits for a given damage state across different wall specimens. To address this variability and uncertainty within the dataset derived from experimental results, a series of numerical studies are

conducted using Finite Element Method (FEM). Additionally, it is important to note that laboratory tests typically involve geometrical and material parameters that are constrained within specific limits. Furthermore, those experimental test results may not cover a wide range of effective variables needed to develop a relevant constitutive model. Therefore, in this context, a parametric study based on numerical results is favoured over an extensive experimental test dataset. Subsequently, the resulting mathematical expressions are verified using a subset of experimental results.

6.4.1 Wall Parameters

A parametric study is conducted to assess the deformation response associated with various damage states of rectangular cantilever RC structural wall specimens subjected to cyclic lateral loads applied at the top of the specimen. The parameters, expected to significantly influence the seismic damage characteristics of structural wall, are selected based on a comprehensive review of contemporary design guidelines and relevant literature (ACI 318-19, 2019; ASCE 41-13, 2013; Kazaz, 2012; Abdullah and Wallace, 2019; Birely, 2012).

Taking into account earlier analytical parametric studies on RC wall members, the key variables being considered for this investigation include wall Aspect Ratio (*AR*), Axial Load Ratio (*ALR*), boundary element longitudinal reinforcement ratio (ρ_{be}), web longitudinal reinforcement ratio (ρ_{web}), and the ratio of boundary element length to wall length ($^{L_{be}}/_{L_w}$). *AR* represents the ratio of wall height (H_w) to wall length (L_w), while *ALR* is defined as the ratio $^{P}/_{A_g f_{ck}}$, where P denotes the axial force acting at the top of the specimen, and A_g and f_{ck} represent the wall cross-sectional area and characteristic cube compressive strength of concrete, respectively. The regression techniques used for predictive model formulation are typically dimensionally insensitive to the physical units of measurement related to the input parameters. Therefore, the dimensionless parameter $^{L_{be}}/_{L_w}$ is chosen instead of considering the individual variables L_{be} and L_w separately.

In this investigation, the impact of each parameter, except $^{L_{be}}/_{L_w}$, is examined using the same sample size to avoid bias due to variations in sample size. The parametric study includes a total of 8125 specimens, with parameters being varied accordingly. A frequency histogram depicting the considered parameters is presented in Figure 6.2. The histogram for

the parameter L_{be}/L_w indicates different frequencies for the variable, while all other parameters exhibit uniform frequencies. The majority (35.4%) of specimens have an L_{be}/L_w value between 0.15 and 0.20, while the fewest (1.5%) lie in the range of 0.35 to 0.40. The study evaluates walls with lengths of 3 m, 4 m, 5 m, and 6 m (L_w), resulting in varying L_{be}/L_w values ranging from 0.1 to 0.4 and differences in sample sizes.

The wall models analysed here are considered to be slender walls according to IS 13920 (BIS, 2016a), which defines slender walls as those with *AR* > 2.0. RC structural walls with aspect ratios as high as 10 are often incorporated into the design of high-rise buildings. Therefore, in the present study, wall specimens with aspect ratios of 3, 4, 6, 8, and 10, are analysed.

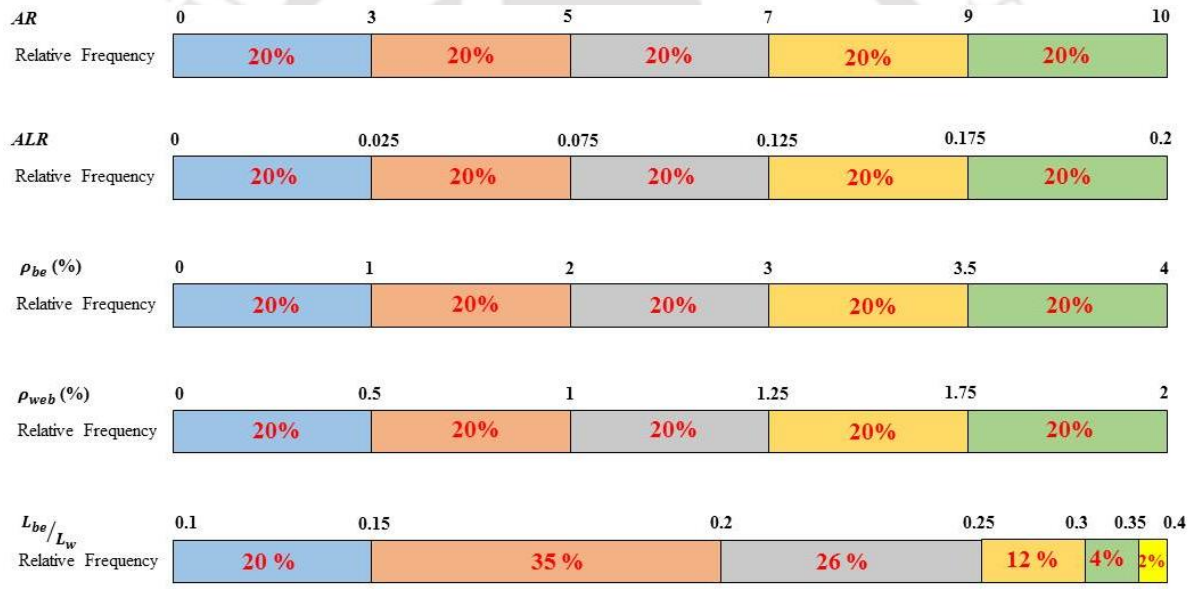

* *AR*: Aspect Ratio, *ALR*: Axial Load Ratio, ρ_{be}: Boundary element longitudinal reinforcement, ρ_{web}: Web longitudinal reinforcement, L_{be}/L_w: Ratio of boundary element length to wall length

Figure 6.2 Frequency histogram for different structural parameters considered in the analyses of wall specimens.

In practice, axial load ratios for tall buildings with structural walls typically range from 0 to 0.15 (Priestly et al., 2007). Accordingly, five different axial load ratio values are used for each wall specimen: 0.01, 0.05, 0.10, 0.15, and 0.20. Indian seismic design principles suggest that the longitudinal reinforcement ratio in the boundary elements of structural walls lies in the range of 0.8% - 4%. The ρ_{be} values employed in this parametric study are 0.80%, 1.65%, 2.50%, 3.25%, and 4.00%. In typical RC structural wall sections, the longitudinal reinforcement ratio in the web, ρ_{web}, typically lies in the range of 0.005 - 0.04. In the present

study, ρ_{web} values of 0.25%, 0.70%, 1.13%, 1.50%, and 2.00%, are used for the design and analysis of wall models.

6.4.2 Specimen Design

The parametric study involves idealized rectangular wall models that include special confining reinforcement bars at the end portions to simulate the effect of boundary elements in a wall model. These wall specimens are designed in accordance with the latest Indian seismic design standards (BIS, 2000; BIS, 2016a). The RC structural walls analysed here maintain a constant f_{ck} value of 30 MPa, as this parameter has minimal impact on the seismic behavior of RC structural walls (Lefas et al., 1990). The wall models are designed to have a thickness greater than 150 mm but smaller than $L_w/4$, following IS 13920 (BIS, 2016a) guidelines. Various thickness values (ranging from 200 mm to 500 mm) are selected based on L_w. For example, when $L_w = 3$m, the wall thickness ranges from 200 mm to 300 mm, while for $L_w = 6$m, it varies from 200 mm to 500 mm. However, wall thickness is not considered as an isolated variable in this parametric study, as it interacts with other parameters such as $P/A_g f_{ck}$, ρ_{be} and ρ_{web}. In compliance with IS 13920 (BIS, 2016a) recommendations, the boundary elements of the walls are designed with a L_{be} value smaller than twice the wall thickness. For a specific ρ_{be} and ρ_{web}, the required reinforcement bar area in the boundary element and web portion is determined, followed by the calculation of the number of longitudinal bars of a certain diameter. The maximum spacing for both boundary element and web longitudinal bars considered in this investigation is 300 mm. Confining ties are provided in the boundary element throughout its height with a spacing of 100 mm, and their diameter meets the special confining tie requirement outlined in IS 13920 (BIS, 2016a). All the wall models can be considered adequately confined at the boundary elements, so the boundary element confinement ratio is not considered a variable in the present study. The steel reinforcement bars used in wall design is assumed to be of grade Fe 500 so that the corresponding yield strength of the bars is considered at 500 MPa. A cross-sectional view of a representative wall specimen is depicted in Figure 6.3.

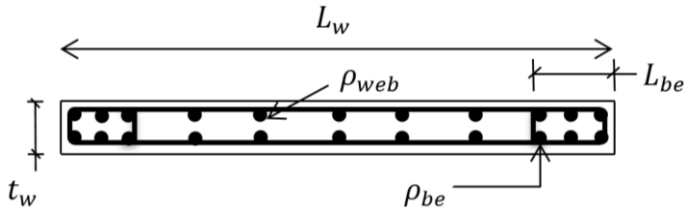

Figure 6.3 Cross-sectional view of a representative wall specimen.

6.4.3 Finite Element Models

OpenSEES, an object-oriented software framework (McKenna et al., 2000), is utilized to develop and analyse the nonlinear model of the RC wall specimens. Taking advantage of the symmetrical wall geometry and aiming to simplify computational time and effort, the wall specimens are modelled and analysed using two-dimensional models. The cross-sections of the specimens are represented as fibre elements. To capture the nonlinear behaviour of the specimens, the "*NonLinear Beam-Column Element*" in OpenSEES is employed. This element allows plasticity to propagate throughout the member length using a fibre cross-sectional model. For this purpose, five integration points are utilized along the length of the element. In the fibre cross-sectional modelling approach, cross-sections are divided into layers, which represent the concrete portion of the section and the steel bars. For modelling the structural wall specimens, an equivalent frame element modelling approach is implemented, offering advantages such as simplicity and computational efficiency (Beyer et al., 2008; Lowes et al., 2019). In this method, one-dimensional frame elements are used to model the RC walls, with cross-sectional properties similar to the actual wall properties. Concrete modelling is achieved using the *Concrete02* model (Mazzoni et al., 2009) in OpenSEES, based on the Kent-Scott-Park concrete model (Kent and Park 1971; Scott et al. 1982) and incorporating concrete tensile strength. The steel bars are modelled using the *Steel02* model (Mazzoni et al., 2009) in OpenSEES, which employs the Giuffre-Menegotto-Pinto steel model (Menegotto and Pinto 1973) with isotropic strain hardening. The response parameters corresponding to various local damage indicators are obtained from the *StressStrain* recorders defined at both ends of the wall specimen, located at the element's lowermost integration point. Nonlinear cyclic analysis of the modelled wall specimens is conducted for the displacement histories depicted in Figure 6.4.

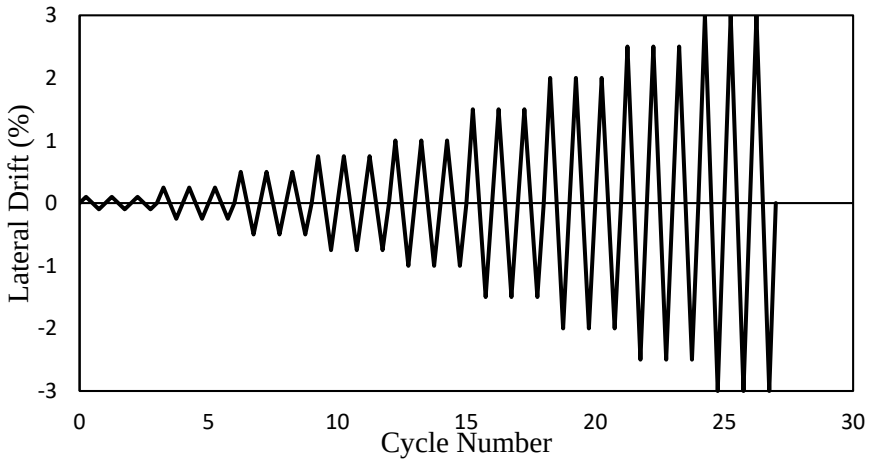

Figure 6.4 Displacement history utilized for cyclic analyses of the developed wall models.

6.4.4 Specification of Damage States

Several previous studies (Rossetto and Elnashai, 2003; Birely, 2012; Alwaeli, 2016) have explored the evaluation of damage state thresholds for RC structural wall members by establishing correlations between seismic damage characteristics and different performance levels (Table 6.1). Specifically, for the 'Complete' performance level, two distinct damage indicators have been identified, namely core concrete crushing and buckling of the boundary element reinforcement bars. The threshold for the 'Complete' level is determined based on the smallest lateral drift value corresponding to a specific damage indicator.

Table 6.1 Damage states and local damage descriptions for RC structural walls

Level	Damage State	Damage description
Damage State 1 (DS1)	Minor	Initial flexural crack.
Damage State 2 (DS2)	Moderate	Tensile yield of extreme longitudinal steel.
Damage State 3 (DS3)	Extensive	Spalling of boundary region cover concrete.
Damage State 4 (DS4)	Complete	Core concrete crushing. Bar buckling.

Presently, the threshold for flexural cracking damage is established by identifying the lateral drift level at which the tensile strength of concrete reaches its ultimate capacity. The initiation of yielding in the steel reinforcement bars is considered to occur when the stress in the critical bar reaches its yield strength. In the unconfined cover regions of a wall section, concrete spalling may occur, and the corresponding spalling strain is defined as the strain at which the stress in the post-peak, linear descending branch reaches zero. For well-confined walls with boundary elements, concrete crushing is mobilized when the residual concrete stress (defined as 20% of the peak confined concrete stress) is reached on the post-peak linear descending branch of the concrete stress-strain curve. The onset of longitudinal bar buckling in boundary elements is determined by monitoring the attainment of the limiting strain in concrete, based on the recommendations of Papia and Russo (1989) for RC elements subjected to compression.

6.5 Damage State Definitions

In this section, the findings from the parametric study conducted on the developed RC structural wall models are presented and discussed. The predictive expressions for defining the damage state thresholds based on the GP framework are derived using the parametric

study results as the input dataset. The validity and accuracy of the resulting predictive equations are assessed using different statistical measures and by evaluating their effectiveness in estimating the lateral drift levels at various performance levels for wall specimens previously tested by other researchers.

6.5.1 Influence of Structural Parameters

As discussed in the preceding section, lateral drift levels at which various damage indicators initiate are identified through nonlinear cyclic analyses of wall specimens, establishing corresponding damage state thresholds. Figure 6.5 illustrates the lateral drift limits at different damage states as a function of various wall parameters. Although wall aspect ratio and axial load ratio significantly influence the lateral drift limits of the walls (Figures 6.5(a) and 6.5(b)), the correlation between other parameters and the lateral drift limits appears relatively weak. Figure 6.5(a) reveals that, in general, lateral drift limits corresponding to different damage indicators for structural walls increase with a higher wall aspect ratio. Notably, the impact of aspect ratio on lateral drift limits is more pronounced at higher damage states than at lower ones, as indicated by the steeper slope in Figure 6.5(a). Figure 6.5(b) suggests that higher axial load ratios lead to the onset of extensive and complete damage states at earlier stages. This is expected because higher axial load ratios result in greater compressive forces on the wall section, causing damage indicators such as bar buckling, concrete spalling, and crushing to occur at lower lateral drift ratios. On the other hand, increasing the axial load ratio does not appear to affect the occurrence of minor and moderate damage states, which are primarily caused by tensile forces in the section. Furthermore, an increase in both the longitudinal reinforcement ratio in the boundary element and the ratio of boundary element length to wall length moderately delays the occurrence of extensive and complete damage states (Figures 6.5(c) and 6.5(e)). Figure 6.5(d) shows that an increase in the web longitudinal reinforcement ratio leads to a relatively delayed onset of the moderate damage state. It is important to note that, in assessing the influence of a specific parameter on the lateral drift limit, all other parameters are held constant in the wall specimen, and only the chosen parameter is varied.

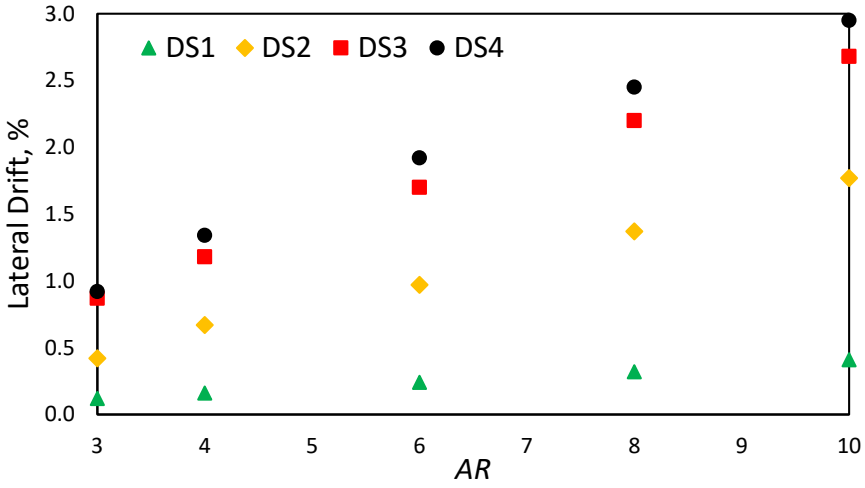

(a)

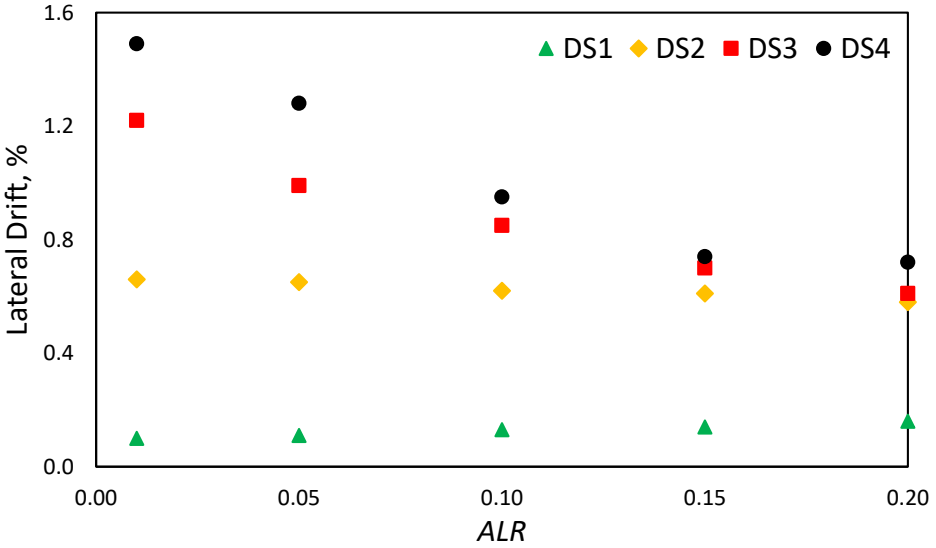

(b)

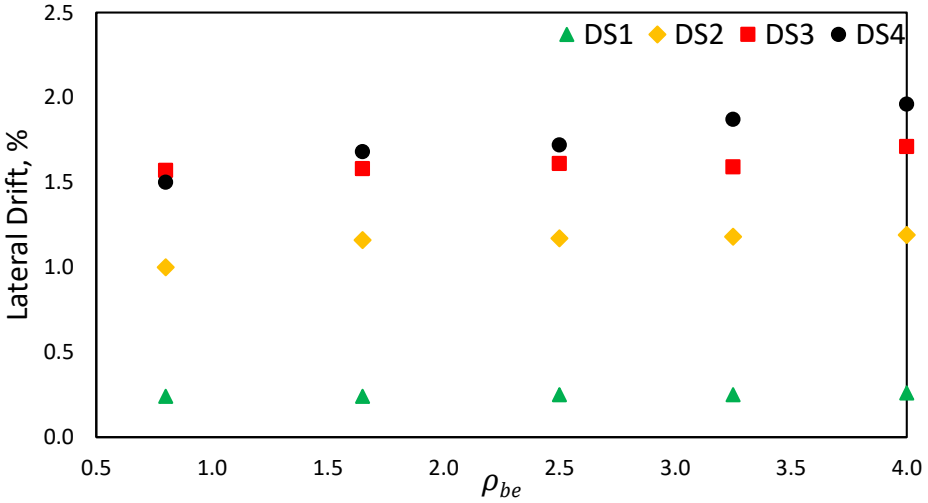

(c)

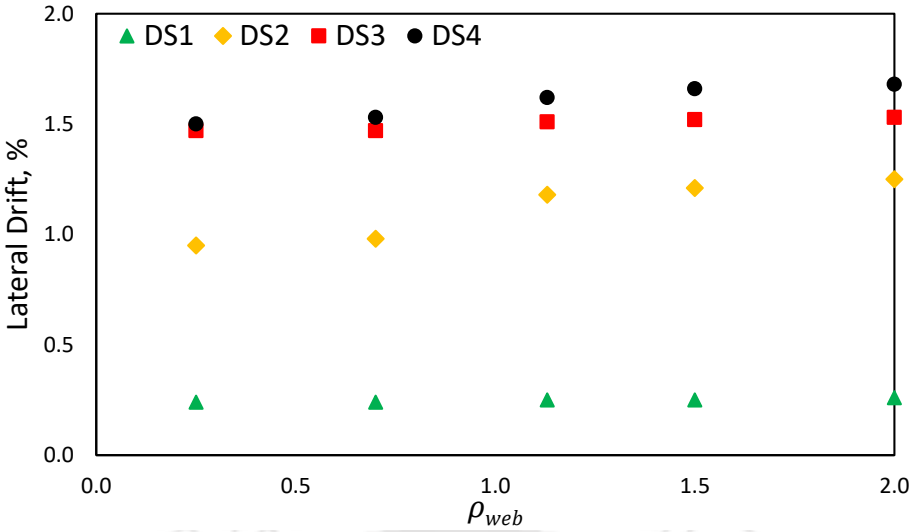

(d)

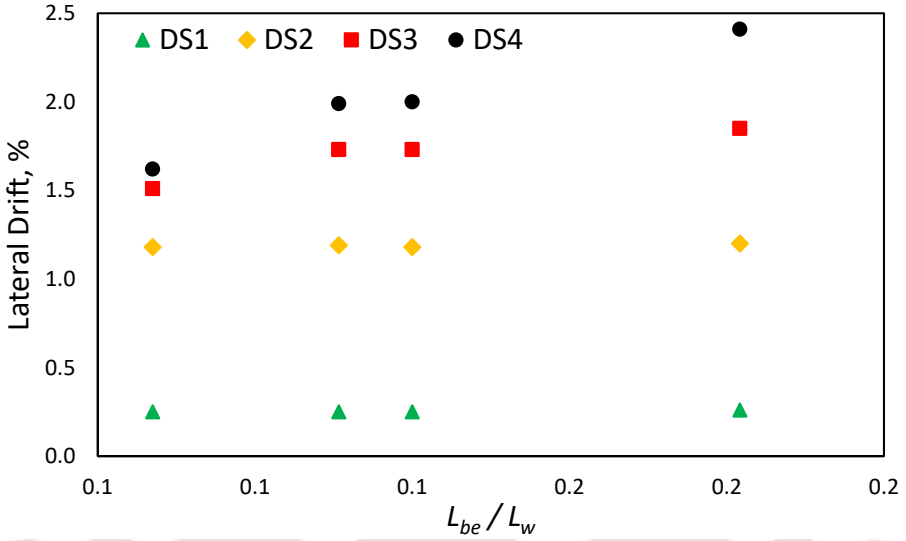

(e)

Figure 6.5 Variation of damage state thresholds in rectangular structural walls with (a) *AR*, (b) *ALR*, (c) ρ_{be}, (d) ρ_{web}, and (e) $^{L_{be}}/_{L_w}$.

6.5.2 GP based Predictive Relationship Development

This section offers a comprehensive description of the GP algorithm's implementation in the present chapter, which is used to evolve the proposed prediction expressions for lateral drift limits associated with various damage states of RC structural walls. The results obtained from the parametric study on the wall specimens serve as the learning dataset for executing the GP technique.

The formulation of the lateral drift limit ($\Delta_{DS,i}$) for a specific damage state is as follows:

$$\Delta_{DS,i} = f(AR, ALR, \rho_{be}, \rho_{web}, {}^{L_{be}}/_{L_w}) \quad (6.1)$$

Various combinations of GP parameter configurations were explored through multiple GP runs. The final expressions for different damage states were generated using the GP parameters presented in Table 6.2. The choice of these parameters had an appreciable impact on the generalization capability of the GP algorithm. The population size determines the number of programs evolved by GP, with larger population sizes resulting in longer run times. The optimal population size can vary in accordance with the intricacy of the problem and the size of the solution space. To discover models with minimal error, numerous populations were evaluated. The program continued execution until the model's performance showed no appreciable improvement. The structure of the models developed by GP depends on two key factors: tree depth and the number of genes. Tree depth gauges the intricacy of every term in the model, while the number of genes per population influences the number of terms in the model. The GP algorithm-based model considered here utilized only elementary functional relationships, including addition, subtraction, multiplication, squares, and cubic functions. Efforts were made to explore a broader range of mathematical functions, such as division, square root, trigonometric, logarithmic, and exponential functions. However, the ensuing relationships were observed to be excessively lengthy, overly complex, and did not substantially enhance prediction accuracy.

Preventing overfitting is a crucial concern in machine learning, and one effective approach is to evaluate the developed solutions for a validation dataset to enhance their generalization capability. To achieve this, datasets were randomly partitioned into three categories: learning, validation, and testing. The learning dataset was used for model development (genetic evolution), while the validation dataset assessed the models' ability to generalize to unseen data that was not part of the training set (model selection). Both the learning and validation datasets played a role in the modelling process and collectively constituted the training data, accounting for 70% of the total dataset (Ahangar-Asr et al., 2011; Fiore et al., 2014). The testing dataset was reserved for evaluating the performance of the optimized GP model on data that was not used during model development. The objective function employed in this framework to select the best GP model is the root mean square error ($RMSE$) function:

$$RMSE = \sqrt{\frac{1}{n}\sum_{i=1}^{n}\left(\Delta_{DSi,pred} - \Delta_{DSi,sim}\right)^2} \tag{6.2}$$

where n = number of specimens; $\Delta_{DSi,sim}$ = simulated lateral drift level for i^{th} sample; and $\Delta_{DSi,pred}$ = predicted lateral drift level value for i^{th} sample.

Table 6.2 Parameter settings for GP based damage state lateral drift level prediction expressions

Parameters	Settings
Population Size	500
No. of Generations	500
No. of Genes	3
Max Tree Depth	3
Elitism Fraction	0.05
Crossover Rate	0.84
Mutation Rate	0.14
Termination Criteria	Number of Generations
Function Set	+, -, ×, ^2, ^3

The final prediction expressions for lateral drift thresholds corresponding to different damage states, derived from the GP algorithm, are as follows:

$$\Delta_{DS1}= \left[12.1\left(\rho_{web}+{}^{L_{be}}/_{L_w}\right)+0.5(AR^2+{\rho_{be}}^2)+24.3AR(1+0.04\rho_{be}+4.53ALR)-15.4\right]\times 10^{-3} \quad (6.3)$$

$$\Delta_{DS2}= 0.24(AR+\rho_{web}-ALR^2)+0.098\rho_{be}(1-0.5\rho_{web})+0.005AR(\rho_{web}-AR)-0.56 \quad (6.4)$$

$$\Delta_{DS3}= 13.9ALR^3(\rho_{be}+\rho_{web})+0.302AR\left(1+{}^{L_{be}}/_{L_w}\right)-4.5ALR(1+0.2AR)+0.589 \quad (6.5)$$

$$\Delta_{DS4}= 5.77\left({}^{L_{be}}/_{L_w}-\left({}^{L_{be}}/_{L_w}\right)^2-ALR\right)+0.61ALR.AR(0.18\rho_{web}-1)+0.3AR+0.1\rho_{be}+0.04 \quad (6.6)$$

Figure 6.6 compares the predicted lateral drift levels for different damage states with the analytical results, using only the testing datasets. These testing datasets were not utilized during model development, providing an accurate assessment of the prediction models' performance. Table 6.3 displays the statistical results of the GP-based prediction models across the learning, validation, and testing datasets. Both Figure 6.6 and Table 6.3 illustrate that the GP models, with high R-squared values and low MAE and RMSE values, effectively estimate lateral drift levels with an adequate level of precision. It is important to note that the error quantities not only have small magnitudes but also exhibit consistency between the

training and testing datasets, indicating that the developed models demonstrate both strong predictive capability (low error values) and generalizability (analogous error values).

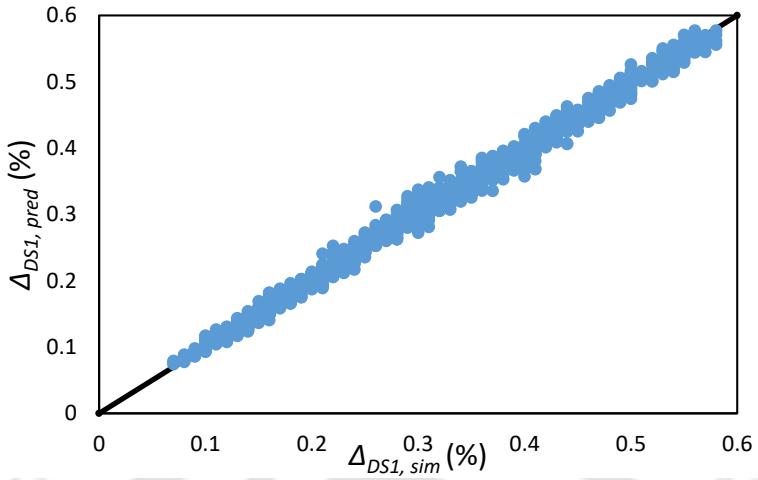

(a)

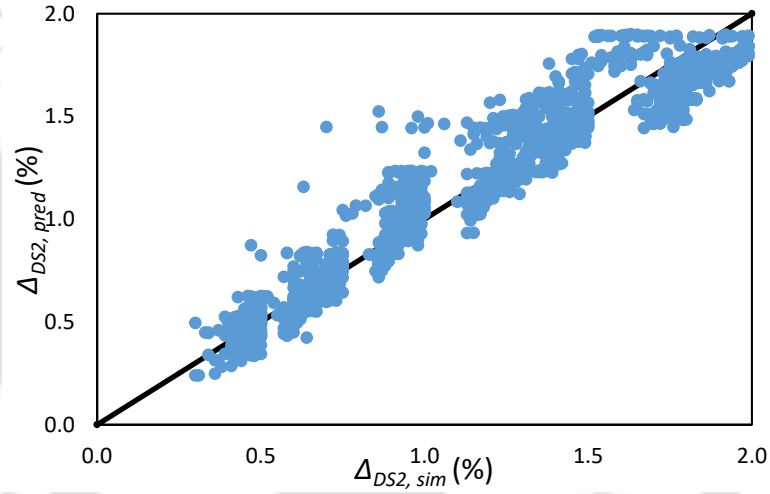

(b)

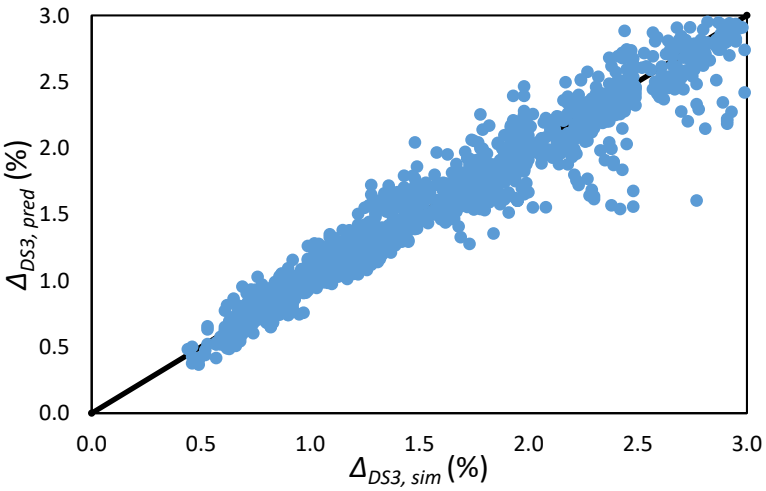

(c)

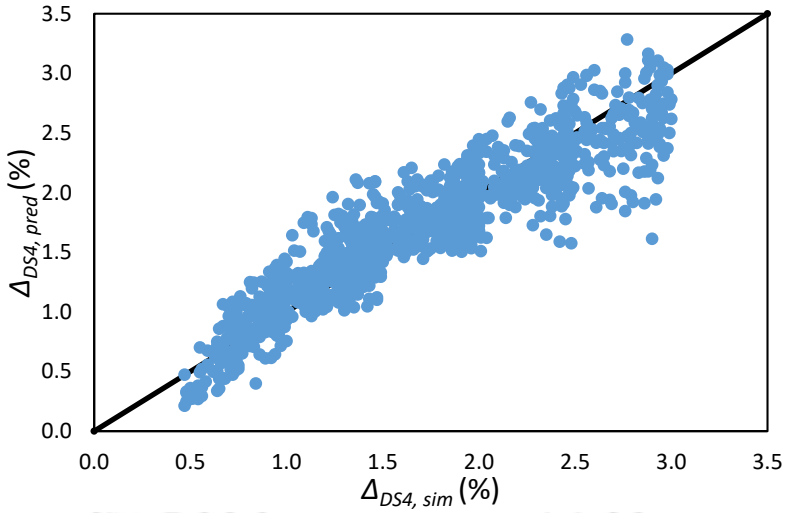

(d)

Figure 6.6 Comparison of predicted and simulated lateral drift values at (a) Minor, (b) Moderate, (c) Extensive and (d) Complete damage level for the testing dataset using proposed expressions.

Table 6.3 Performance results of the proposed expressions for different damage states

	$\Delta_{DSi,pred}$ vs $\Delta_{DSi,sim}$											
	DS1			**DS2**			**DS3**			**DS4**		
	R^2	**RMSE (%)**	**MAE (%)**	**R^2**	**RMSE (%)**	**MAE (%)**	**R^2**	**RMSE (%)**	**MAE (%)**	**R^2**	**RMSE (%)**	**MAE (%)**
Training	0.99	0.96	0.71	0.92	13.3	9.9	0.94	15.4	10.8	0.85	25.5	19.2
Validation	0.99	0.99	0.74	0.92	12.7	9.4	0.93	15.8	11.0	0.85	24.9	19.3
Testing	0.99	0.94	0.70	0.92	12.8	9.6	0.94	15.6	10.9	0.85	24.6	18.6

6.5.3 Validation of Proposed Expressions

According to Smith's (1986) rational postulation, an *R* value greater than 0.8 and minimal error values (e.g., RMSE and MAE) in a model indicate a high degree of correspondence between the estimated and the observed values, hence confirming the acceptability of the model. All the proposed expressions in this chapter indicate *R* values well above 0.8, demonstrating their acceptability. The sufficiency of data used to model any physical phenomenon significantly impacts the adequacy of proposed relationships. Frank and Todeschini (1994) suggest a minimum ratio of 3 objects to selected variables, with a ratio of 5 often being more justifiable. In the present study, the ratio is notably higher, approximately 8125/5 ≈ 1625, indicating a high level of data sufficiency.

Furthermore, the GP-based prediction expressions underwent external verification using advanced measures recommended by Golbraikh and Tropsha (2002) on the testing dataset. These criteria stipulate that at least one of the regression lines should exhibit a slope (k or k') that is in proximity to unity. Roy and Roy (2008) proposed a confirmation index (R_m^2) for assessing the external predictability of models, where a suitable model should yield an R_m^2 value greater than 0.5. Additionally, the coefficient of determination (R_o^2 or $R_o'^2$) between predicted and actual values should be approximately 1. Table 6.4 presents the validation metrics and the associated outcomes achieved by the proposed expressions. Compliance with the stipulated criteria determines the legitimacy of these expressions. The validation stage signifies that the established lateral drift prediction expressions are robust and capable of reasonably accurate prediction of lateral drift levels for the damage state thresholds.

Table 6.4 Statistical metrics for external validation of proposed expressions for different damage states

Validation Criteria	**Acceptable Limit**	**Proposed Expressions**			
		Δ_{DS1}	Δ_{DS2}	Δ_{DS3}	Δ_{DS4}
$R = \frac{\sum(y_i - \bar{y})(y_i^* - \overline{y^*})}{\sqrt{\sum(y_i - \bar{y})^2 (y_i^* - \overline{y^*})^2}}$	R >0.8	0.99	0.96	0.96	0.92
$k = \frac{\sum y_i y_i^*}{\sum {y_i^*}^2}$	0.85< k<1.15	1	0.99	1	0.99
$k' = \frac{\sum y_i y_i^*}{\sum {y_i}^2}$	0.85< k'<1.15	0.99	0.98	0.99	0.98
$R_o^2 = 1 - \frac{\sum(y_i^* - y_i^{r0})^2}{\sum(y_i^* - \overline{y^*})^2}$ where, $y_i^{r0} = k y_i^*$	$R_o^2 \approx 1$	0.99	0.99	0.99	0.99
$R_o'^2 = 1 - \frac{\sum(y_i - y_i^{*r0})^2}{\sum(y_i - \bar{y})^2}$ where, $y_i^{*r0} = k' y_i$	$R_o'^2 \approx 1$	0.99	0.99	0.99	0.99
$R_m^2 = R^2 \times \left(1 - \sqrt{\lvert R^2 - R_o^2 \rvert}\right)$	R_m^2>0.5	0.92	0.67	0.71	0.52

y_i = simulated output for i^{th} sample; $\bar{y}$ = average of simulated outputs; y_i^* = predicted output for i^{th} sample; and $\overline{y^*}$ = average of predicted outputs.

The adequacy of the proposed lateral drift limit equations for different damage states is assessed by comparing them with available experimental results from relevant structural wall

tests. Additionally, the applicability of the proposed prediction expressions is examined by comparing them to existing damage state definitions. The dataset used for this analysis comprises 60 RC structural wall cantilever specimens from fourteen distinct research studies. Among these specimens, 44 specimens have rectangular-end configurations, while 16 specimens have barbell-end configurations. Of these specimens, 20 specimens were subjected to static monotonic loading, while the remaining ones were subjected to static cyclic loading. Table 6.5 provides the essential characteristics and a summary of outcomes for the experiments included in the dataset.

To ensure a fair comparison between the proposed prediction equations and existing damage state definitions, different damage state thresholds corresponding to various damage indicators are categorized. The cohort of different damage state definitions considered for comparison on the experimental database is shown in Table 6.6.

Figure 6.7 provides a comparison of prediction accuracy for various proposed expressions on the experimental dataset by showing the frequency distribution of the ratio between experimental (Δ_{exp}) and predicted (Δ_{pred}) lateral drift limits. When the ratio of experimental to predicted lateral drift limit ($\Delta_{exp}/\Delta_{pred}$) equals one, it signifies excellent predictive accuracy. As per Figure 6.7, it becomes evident that GP-based damage thresholds exhibit a frequency distribution with a mode close to one for all damage state levels, indicating strong prediction accuracy. Conversely, the mode of the distribution frequency for the other considered damage state thresholds significantly deviates from one, suggesting poorer performance as compared to the GP-based damage thresholds. It is noteworthy that while the majority of experimental wall properties exist beyond the span of the GP-based expressions training dataset, the suggested models for various damage states still yield a ratio of experimental and predicted lateral drift limits close to 1 for most wall specimens. Therefore, the GP-based damage state definitions outperforms the existing damage thresholds considered in case of slender RC structural walls.

Table 6.5 Experimental test specimen utilized for comparing proposed damage thresholds with existing damage thresholds

No.	Specimen	Shape	Loading	$\frac{H_w}{L_w}$	$\frac{P}{A_g f_c'}$(%)	ρ_{be} (%)	ρ_{web} (%)	$\frac{L_{be}}{L_w}$	DS1	DS2	DS3	DS4
1	PilaSW4[1]	R	C	*2*	*0*	*6.85*	0.75	0.4	0.08	0.46	-	-
2	PilaSW5[1]	R	C	*2*	*0*	*11.41*	0.79	0.4	0.08	0.69	-	-
3	PilaSW6[1]	R	C	*2*	*0*	*6.85*	0.75	0.4	0.08	0.47	1.33	-
4	PilaSW7[1]	R	C	*2*	*0*	*11.08*	0.79	0.4	0.08	0.62	-	1.83
5	PilaSW8[1]	R	C	*2*	*0*	*7.14*	0.75	0.4	0.08	0.44	1.5	-
6	PilaSW9[1]	R	C	*2*	*0*	*7.14*	0.75	0.4	0.08	0.41	1.5	-
7	DaziWSH1[2]	R	C	*2.28*	0.05	1.57	0.3	0.15	0.17	0.21	-	0.69
8	DaziWSH2[2]	R	C	*2.28*	0.06	1.57	0.3	0.15	0.16	0.23	1.15	1.15
9	DaziWSH3[2]	R	C	*2.28*	0.06	1.74	0.54	0.2	0.26	0.34	1.02	1.7
10	DaziWSH4[2]	R	C	*2.28*	0.06	1.74	0.54	0.2	0.25	0.31	1.01	1.01
11	DaziWSH5[2]	R	C	*2.28*	0.13	*0.77*	0.27	0.2	0.1	0.13	0.55	1.08
12	DaziWSH6[2]	R	C	*2.26*	0.11	1.74	0.54	0.2	0.22	0.28	0.57	1.42
13	LefaSW21[3]	R	*M*	*2*	*0*	2.99	*2.49*	*0.43*	0.02	0.38	-	-
14	LefaSW22[3]	R	*M*	*2*	0.12	2.99	*2.49*	*0.43*	0.03	0.31	-	-
15	LefaSW23[3]	R	*M*	*2*	*0.21*	2.99	*2.49*	*0.43*	0.04	0.4	-	-
16	LefaSW24[3]	R	*M*	*2*	*0*	2.99	*2.49*	*0.43*	0.02	0.41	-	-
17	LefaSW25[3]	R	*M*	*2*	*0.21*	2.99	*2.49*	*0.43*	0.05	0.38	-	-
18	LefaSW26[3]	R	*M*	*2*	*0*	2.99	*2.49*	*0.43*	0.03	0.42	-	-
19	LefaSW30[3]	R	*M*	*2*	*0*	2.99	1.55	*0.43*	0.06	0.38	-	-
20	LefaSW31[3]	R	*M*	*2*	*0*	2.99	1.55	*0.43*	0.05	0.3	-	-
21	LefaSW32[3]	R	*M*	*2*	*0*	2.99	1.55	*0.43*	0.05	0.32	-	-
22	LefaSW33[3]	R	*M*	*2*	*0*	2.99	1.55	*0.43*	0.05	0.44	-	-
23	OestR1[4]	R	C	*2.4*	*0*	1.47	0.25	0.15	0.04	0.15	1.09	2.2
24	OestR2[4]	R	C	*2.4*	*0*	4	0.25	0.15	0.06	0.3	-	3.33
25	OestB1[4]	*B*	C	*2.4*	*0*	1.11	0.29	0.32	0.05	0.17	-	1.67
26	OestB2[4]	*B*	C	*2.4*	*0*	3.67	0.29	0.32	0.04	0.38	0.54	2.23
27	OestB3[4]	*B*	C	*2.4*	*0*	1.11	0.29	0.32	0.04	0.23	-	3.89
28	OestB4[4]	*B*	*M*	*2.4*	*0*	1.11	0.29	0.32	0.05	0.23	1.11	4.97
29	OestB5[4]	*B*	C	*2.4*	*0*	3.67	0.29	0.32	0.03	0.42	0.53	2.62
30	OestB6[4]	*B*	C	*2.4*	0.13	3.67	0.29	0.32	0.11	0.54	1.11	1.11
31	OestB7[4]	*B*	C	*2.4*	0.08	3.67	0.29	0.32	0.15	0.54	0.28	2.19
32	OestB8[4]	*B*	C	*2.4*	0.09	3.67	0.29	0.32	0.23	0.49	0.53	2.17
33	OestB9[4]	*B*	C	*2.4*	0.09	3.67	0.29	0.32	0.16	0.26	1.24	2.99
34	OestB1[4]	*B*	C	*2.4*	0.08	1.97	0.29	0.32	0.14	0.22	0.63	3.37

35	MorgW1[5]	*B*	C	*2.86*	0.05	1.11	0.42	0.18	0.11	0.1	1.1	-
36	LiuW1[6]	R	C	3.08	0.08	3	0.33	0.33	0.09	0.54	1.5	2.64
37	LiuW2[6]	R	C	3.08	0.04	3	0.33	0.33	0.09	0.66	1.3	2.92
38	TuppW3[7]	R	C	3.9	0.1	*5.36*	0.44	0.36	0.15	0.72	1.6	-
39	MobeW1[8]	*B*	C	*2.98*	0.15	1.6	0.67	*0.67*	0.08	0.35	1.17	-
40	ShiuC1[9]	R	C	*2.88*	*0*	*5.58*	0.24	0.23	0.14	0.52	-	2.86
41	KhalC1[10]	R	C	*1.1*	0.07	*10*	0.83	0.4	0.1	-	-	-
42	AzizW1[11]	R	C	*2.2*	0.04	3.17	1.10	0.1	-	0.21	0.57	0.84
43	AzizW3[11]	*B*	C	*2.2*	0.03	1.32	0.37	0.21	-	0.21	0.63	0.84
44	AzizW4[11]	R	C	*2.2*	0.03	*6.56*	*2.74*	0.1	-	0.23	0.84	-
45	AzizW6[11]	*B*	C	*2.2*	0.02	2.07	1.41	0.21	-	0.26	1.05	-
46	LuC5[12]	R	C	*2*	0.07	0.84	0.35	0.32	-	-	1.5	1.5
47	LuC6[12]	R	C	*2*	0.03	0.84	0.35	0.32	-	-	1	2
48	LefaSW11[3]	R	*M*	*1*	*0*	3.1	*2.4*	0.37	0.04	0.48	-	1.1
49	LefaSW12[3]	R	*M*	*1*	0.12	3.1	*2.4*	0.37	0.03	0.39	-	1.18
50	LefaSW13[3]	R	*M*	*1*	*0.21*	3.1	*2.4*	0.37	0.05	0.51	-	1.18
51	LefaSW14[3]	R	*M*	*1*	*0*	3.1	*2.4*	0.37	0.04	0.52	-	1.5
52	LefaSW15[3]	R	*M*	*1*	0.12	3.1	*2.4*	0.37	0.04	0.38	-	1.07
53	LefaSW16[3]	R	*M*	*1*	*0.21*	3.1	*2.4*	0.37	0.05	0.33	-	0.77
54	LefaSW17[3]	R	*M*	*1*	*0*	3.1	*2.4*	0.37	0.05	0.52	-	1.43
55	VallSW3[13]	*B*	*M*	*1.3*	0.08	3.53	0.82	0.21	0.05	0.41	-	3.85
56	VallSW4[13]	*B*	C	*1.3*	0.08	3.53	0.82	0.21	0.06	0.41	-	2.07
57	VallSW5[13]	R	*M*	6.6	0.06	*5.58*	0.54	0.23	0.03	0.49	0.82	0.86
58	VallSW6[13]	R	C	6.6	0.06	*5.58*	0.54	0.23	0.03	-	0.63	1.35
59	GhorA2C[14]	R	C	*2.08*	0.01	*5*	0.61	*0.61*	-	0.52	-	3.02
60	GhorB2C[14]	R	C	*2.08*	0.01	*5.63*	0.59	*0.61*	-	0.63	-	2.22

***Note*:** The values highlighted in italics indicate the values that lie beyond the parametric values range used to build the GP-based prediction models.

Reference: [1]Pilakoutas and Elnashai (1995), [2]Dazio et al. (2009), [3]Lefas and Kotsovos (1990), [4]Oesterle et al. (1976), [5]Morgan et al. (1986), [6]Liu (2004), [7]Tupper (1999), [8]Mobeen (2002), [9]Shiu et al. (1981), [10]Khalil and Ghobarah (2005), [11]El-Azizy et al. (2015), [12]Lu et al. (2017), [13]Vallenas (1979), [14]Ghorbanirenani et al. (2009).

Shape: R = Rectangular, B = Barbell; ***Loading:*** C = Cyclic, M = Monotonic

Table 6.6 Damage state definitions categorized as per damage indicators in RC wall specimens

Current Study	SEAOC Blue Book (1999)	Ghobarah (2004)	Ji et al. (2009)	Rossetto and Elnashai (2003)
DS1	-	No Damage	Serviceability	Slight
DS2	SP1	Light Reparable Damage	Damage Control	Light
DS3	SP3	Severe Damage	Collapse Prevention	Moderate
DS4	SP4	Collapse	-	Extensive

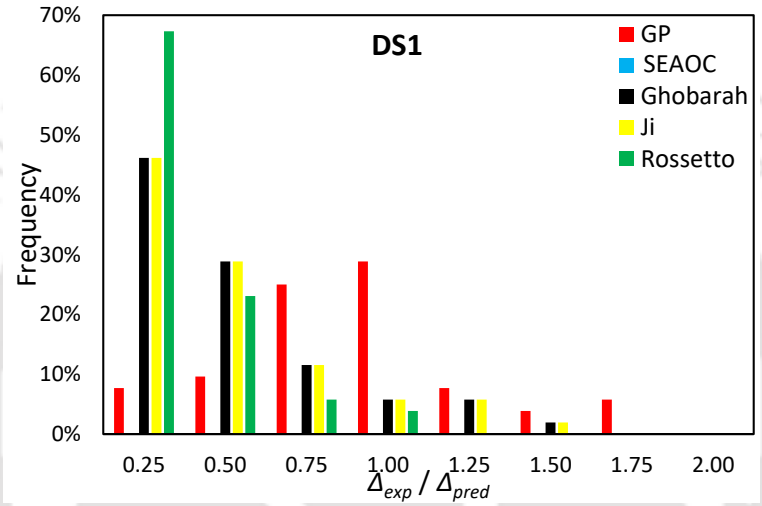

(a)

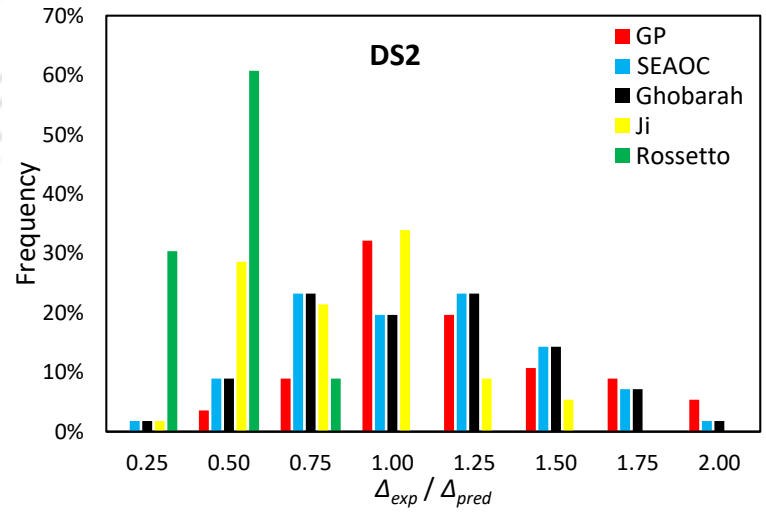

(b)

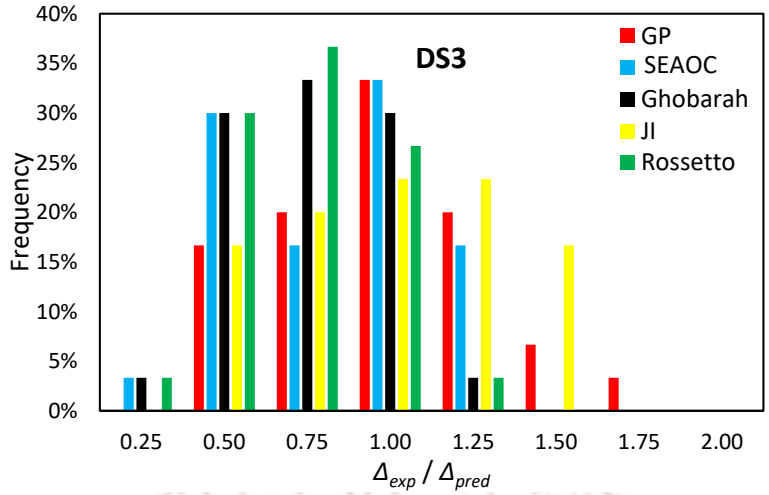

(c)

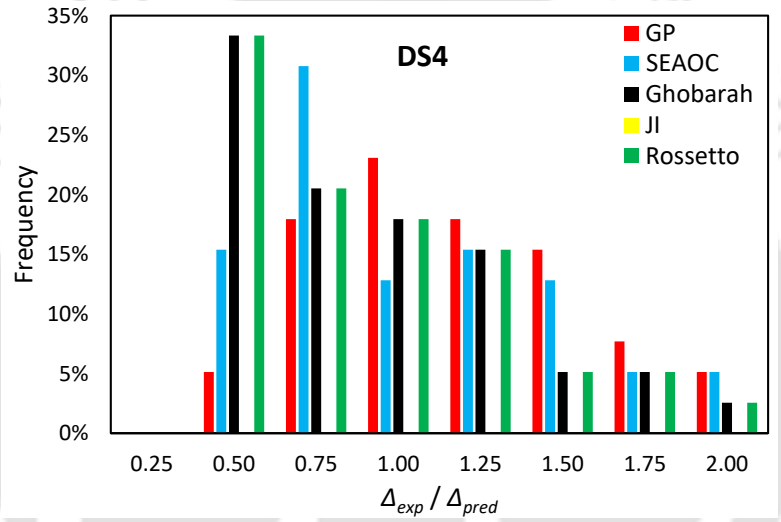

(d)

Figure 6.7 A comparison between experimental and predicted lateral drift limits for (a) Minor, (b) Moderate, (c) Extensive and (d) Complete damage states for slender RC structural wall.

6.6 Summary

Despite the existence of various empirical damage state definitions and codified lateral drift limits for RC structural walls, there remains a need for more robust prediction expressions that consider key wall parameters and encompass a wide range of performance levels. To bridge this gap, the present study is based on GP, a type of artificial intelligence, to establish reliable expressions for predicting lateral drift limits at different damage levels in adequately confined RC structural wall elements.

The present study utilizes a comprehensive dataset comprising numerical responses of 8125 RC structural wall specimens. These responses are used to train, validate, and assess the GP-

based expressions, taking into account various wall design parameters, including wall aspect ratio, axial load ratio, boundary element longitudinal reinforcement ratio, web longitudinal reinforcement ratio, and the ratio of boundary element length to wall length. Multiple performance assessment metrics, such as RMSE, R, R^2, and others, are employed to gauge the accuracy of the GP-based expressions. The results indicate that the GP-based lateral drifts as damage state threhsolds establish the deformation limits of slender RC structural walls in an improved manner as compared to the earlier studies. The validity of the GP-based prediction expressions is also examined for testing data outside the training data domain, and the models are found to meet the criteria used for external validation. Furthermore, a comparative investigation is undertaken between the potential of the existing damage state thresholds and the developed damage state defintions, involving a few existing experimental observations on RC structural wall specimens. The findings reveal that the proposed GP-based expressions offer improved predictions of experimental results as compared to other damage thresholds presented in relevant design standards or past studies. Subsequently, in the following chapters, these thresholds are utilized to estimate fragility functions for the RC wall-frame building across various damage states.

It is important to note that the expressions produced through the data-driven approach employed in this chapter, much like other similar models, have certain limitations regarding their practical use. While these derived expressions have been shown to be effective for other experimentally tested RC wall specimens that possess design parameters not explicitly considered during their modeling, it is advisable to exercise caution. These expressions should only be applied to structural walls whose design characteristics fall within the specified limits used in the training process. This investigation underscores the potential of accurate numerical studies in predicting the deformation limits of structural members, considering the impact of various structural parameters, and overcoming the limitations of test setups.

CHAPTER 7

FRAGILITY FUNCTIONS FOR RC WALL-FRAME STRUCTURES

7.1 Overview

In the domain of seismic vulnerability assessment, fragility functions are commonly employed to quantify the probability of structural damage across varying levels of earthquakes. These functions serve as a means to express the likelihood of damage occurrence and provide valuable insights for assessing structural vulnerabilities in seismic risk assessments. To develop fragility curves, the necessary damage data can be acquired through various means, such as field observations, experimental results, numerical simulations, empirical expert judgement, or a combination of these approaches. In the present context, the emphasis is placed on analytical fragility functions that can be derived using results of dynamic analyses. In this chapter, the fragility relations are developed and assessed for a specific RC wall-frame structure and an entire RC wall-frame building. Fragility, as a concept, is typically associated with inherent uncertainty, stemming from various sources of both aleatory (random) and epistemic (knowledge-based) uncertainties (Ellingwood and Kinali, 2009; Der Kiureghian and Ditlevsen, 2009). Consequently, the present study attempts to evaluate and analyse the combined influence of these uncertainty sources on fragility. Additionally, the characteristics of the established fragility relationships considering scalar intensity measures and vector-valued intensity measures, are also compared. In conclusion, a simplified methodology is showcased, which allows for the derivation of fragility estimates using a reduced number of ground motion records. These fragility relations developed using selected records maintain similar exceedance probabilities as compared to those derived from the entire record dataset, resulting in a computationally less intensive process.

7.2 Seismic Fragility Formulation

The fragility relations developed here are derived from the statistical analysis of the results of Incremental Dynamic Analyses (IDA), discussed in the preceding chapters. Also, in line with earlier discussions, the response parameters are characterised by the maximum inter-storey drift ratio (ISD), while the seismic intensity measure (IM) is represented by the spectral

acceleration at the fundamental period ($S_a(T_1)$). The limit state conditional probability in seismic vulnerability assessment is defined as

$$F_r = P[EDP \geq DS|IM] \tag{7.1}$$

where F_r indicates the likelihood of engineering demand parameter (EDP) attaining or exceeding a specific performance damage state (DS), given the seismic intensity measure is IM. Several studies (Shinozuka et al., 2000; Singhal and Kiremidjian, 1996) available on the fragility assessment of buildings and bridges, have consistently demonstrated that the fragility term in Eq. 7.1 can be effectively represented by a lognormal distribution, as depicted in Eq. 7.2.

$$F_r = \Phi\left[\frac{ln(\mu_d/\theta_{ds})}{\beta}\right] \tag{7.2}$$

$$\mu_d = a(IM)^b\varepsilon \tag{7.3}$$

where, Φ is the standard normal cumulative distribution function; μ_d represents the estimated median demand parameter (calculated using Eq.7.3) based on the regression analysis using the best-fit power-law line, given the value of IM; θ_{ds} is the considered threshold value for each damage state; β is the standard deviation value of the natural logarithm of response parameter and ε is a lognormal random variable with median value of 1. The parameters a and b are evaluated using linear regression in the logarithmic scale (Cornell et al., 2002) as follows

$$\ln \mu_d = \ln a + b \ln IM \tag{7.4}$$

The dispersion values (β) represent the overall variability and uncertainty integrated with the fragility functions for a specific damage state. In the current study, the aleatoric uncertainties in seismic demand, the epistemic uncertainties in structural capacity and modelling uncertainties are considered to determine their impact on the fragility estimates of the considered building typology.

7.3 Damage State Thresholds

Given that the structural wall functions as the primary component for resisting lateral loads in the RC wall-frame system, it can be anticipated that the damage state thresholds obtained for isolated cantilever wall members can serve as the initiation point of damage states for the entire wall-frame structure. The same has been considered in a few past studies (Ji et al.,

2009; Kazaz et al., 2012; Xiong et al., 2019). In the present study, different damage state thresholds for the considered building frame are evaluated using Eqs. (6.3) to (6.6).

To implement the equations defining the damage state, it is necessary to determine the critical parameters of the structural wall. In this context, the key parameters of the RC structural wall illustrated in Figures 3.1 and 3.2 are identified. To calculate the effective wall aspect ratio, the effective height of the wall is estimated in terms of the effective shear span ratio, which is determined by calculating the ratio of moment to shear at the base of the wall section. For this purpose, nonlinear cyclic static analysis of the RC wall-frame is conducted, enabling the determination of the base moment and base shear, which are subsequently used to estimate the effective height. Finally, the effective wall aspect ratio is obtained by dividing the effective height by the wall length. In this particular instance, the effective wall height is determined to be 12.93m, and with a wall length of 3.40m, the resulting effective wall aspect ratio is 3.8. Moreover, the axial load ratio is determined by considering the total gravity load that is effective at the base of the structural wall section. The critical structural wall parameters and various damage state thresholds, calculated using the proposed equations, are presented in Table 7.1.

Table 7.1 Critical parameters and damage states for the structural wall component

Parameters	ρ_{be}	ρ_{web}	AR	ALR	L_{be}/L_w
Values	1.30	0.44	3.80	0.14	0.24
Damage State	Minor	Moderate	Extensive	Complete	
ISD (%)	0.16	0.50	0.90	1.20	

7.4 Fragility Function for RC wall-frame

The fragility functions are developed utilizing the results of dynamic analyses conducted on the RC wall-frame structural system discussed in Chapter 5. The Incremental Dynamic Analyses (IDA) take into account the response variability due to the variation in seismic records, representing the aleatory uncertainty. In the fragility relationships derived from the IDA results, the β value represents the variation in the response parameter due to the influence of aleatory uncertainty (referred to as β_A). On the other hand, the Extended IDA (ExIDA) results consider the combined effect of the variation in structural capacity and

uncertainty in seismic demand on the response parameters. In this case, the β value in the fragility relationship reflects the variation in the response parameter due to both aleatory and epistemic uncertainties (represented as β_{AE}). To account for modelling uncertainty, the individual β values are integrated with the dispersion value (β_m = 0.2) using the square root of the summation of squares technique, as elaborated in detail in Chapter 5.

In the case of IDA, the dynamic analyses are performed on the RC wall-frame structure using 11 selected ground motion records. However, for the ExIDA, to factor in the variability of the structural parameters, a total of 20 different structural specimens are analyzed. Each of these 20 models is subjected to the same set of 11 ground motion records, resulting in a total of 220 IDAs performed for the ExIDA case.

The results of the IDAs and ExIDAs, in terms of EDP-IM points, are shown in Figures 7.1 and 7.2, respectively. The depicted best-fit lines represent the mean value (median or 50th percentile) of the random variable (ISD) corresponding to different $S_a(T_1)$ values, which indicates the value at which there is a 50% probability that the random variable will be less than or equal to that value. In these figures, the high values of the coefficient of determination (R^2 = 0.85 for the IDAs and R^2 = 0.87 for the ExIDAs) demonstrate a strong statistical interrelationship between the selected EDPs and IMs.

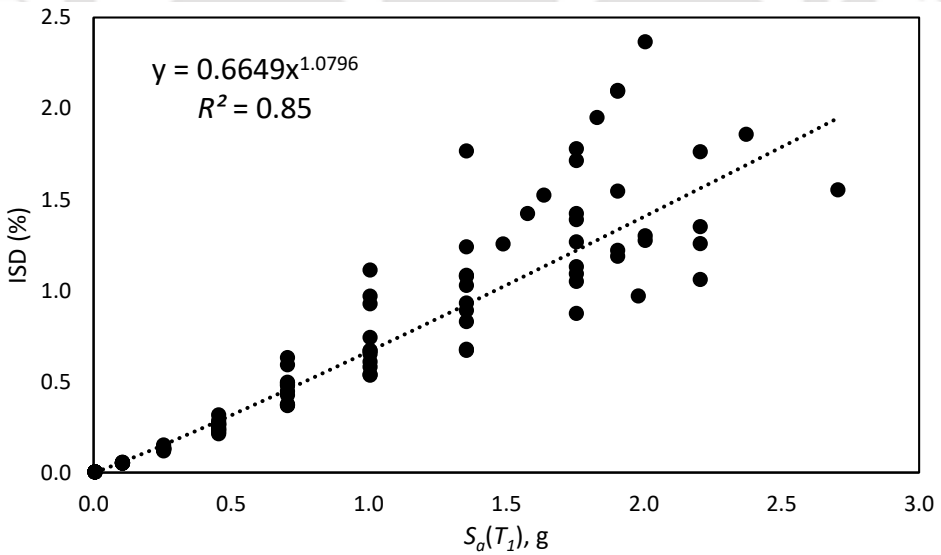

Figure 7.1 ISD- $S_a(T_1)$ relationship for analyses of RC wall-frame considering only aleatory uncertainty.

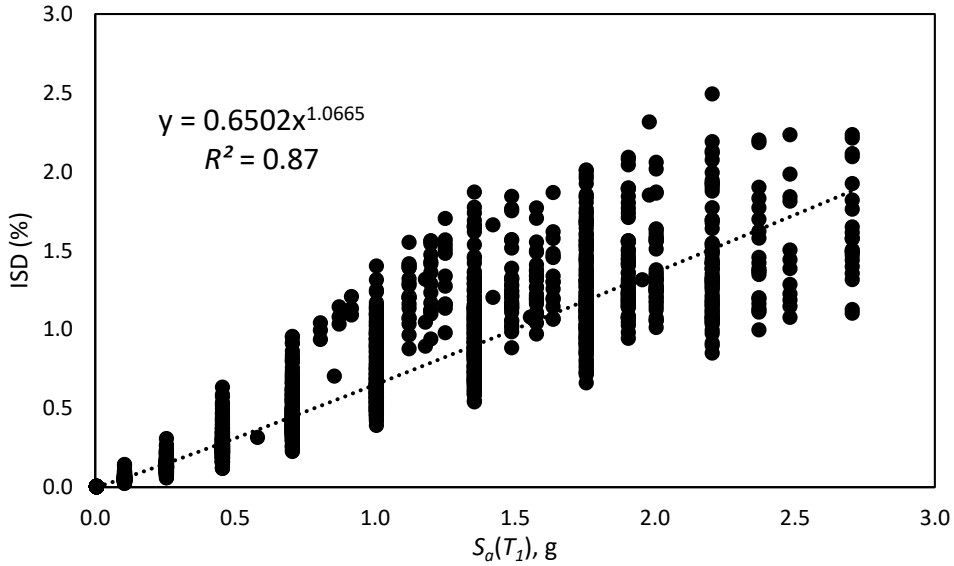

Figure 7.2 ISD- $S_a(T_1)$ relationship for analyses of RC wall-frame considering both aleatory and epistemic uncertainties.

For each specific ground motion record, similar power-law relationships between ISD and $S_a(T_1)$ are established. These relationships allow for the determination of the 16th, 50th (mean), and 84th percentile values of ISD and $S_a(T_1)$ at each damage state threshold considered. The 16th, 50th (mean), and 84th percentile values of ISD and $S_a(T_1)$ at each damage state, are provided in Table 7.2 for the RC wall-frame structure considering only aleatory uncertainty (IDAs), and in Table 7.3 for the case of both aleatory and epistemic uncertainties (ExIDAs). The scatter of the IDA points, expressed as the Δ value, at specific damage state thresholds, is presented in Tables 7.2 and 7.3. The scatter value (Δ) is evaluated as the average value of the $\Delta_{16} = \log(y_{50}) - \log(y_{16})$ and $\Delta_{84} = \log(y_{84}) - \log(y_{50})$, where y_{16}, y_{50} and y_{84} indicate the estimated 16th, 50th and 84th percentile values of ISD and $S_a(T_1)$, corresponding to different damage state thresholds. The calculated Δ values indicate that, at a particular damage state threshold, the dispersion of the response parameters (Δ_{ISD}) is greater as compared to that of the intensity measures ($\Delta_{Sa(T1)}$). Furthermore, it is observed that the scatter values are relatively higher for the ExIDA results as compared to the IDA results. This is attributed to the consideration of both the uncertainty in structural capacity and the variability in seismic records in the ExIDA analysis.

By utilizing the data depicted in Figures 7.1 and 7.2, the parameters for the fragility functions are estimated (Table 7.4) for both the simple IDAs and ExIDAs performed on the analyzed wall-frame structure. The dispersion values, β_A and β_{AE}, are calculated as the standard deviation of the natural logarithmic values of the response parameters at each individual damage state threshold for the IDAs and ExIDAs, respectively. Also, the total deviation of

the EDP values is influenced by the modelling uncertainties (β_M), apart from the aleatoric and epistemic uncertainties, and a value of 0.2 is frequently adopted considering that the structure is modelled in a way to characterise the true response of the building which is within ±30% of the actual value, with 90% confidence (Celik and Ellingwood, 2010). Substantially, the dispersion values considering the various sources of uncertainties can be integrated to obtain the total dispersion measure (β) using the SRSS rule of combination (Aslani et al., 2012).

Table 7.2 Estimated ISD, $S_a(T_1)$ and the dispersion values at damage state thresholds for the considered wall-frame structure considering aleatory uncertainty

Damage States	ISD (%) at damage state thresholds			Δ_{ISD}	$S_a(T_1)$, g at damage state thresholds			$\Delta_{Sa(T1)}$
	16th Percentile	50th Percentile	84th Percentile		16th Percentile	50th Percentile	84th Percentile	
Minor	0.15	0.16	0.18	0.10	0.24	0.27	0.29	0.09
Moderate	0.45	0.50	0.61	0.15	0.64	0.77	0.85	0.14
Extensive	0.85	0.97	1.22	0.18	1.14	1.40	1.57	0.16
Complete	1.06	1.21	1.55	0.19	1.38	1.72	1.94	0.17

Table 7.3 Estimated ISD, $S_a(T_1)$ and the dispersion values at damage state thresholds for the considered wall-frame structure considering both aleatory and epistemic uncertainties

Damage States	ISD (%) at damage state thresholds			Δ_{ISD}	$S_a(T_1)$, g at damage state thresholds			$\Delta_{Sa(T1)}$
	16th Percentile	50th Percentile	84th Percentile		16th Percentile	50th Percentile	84th Percentile	
Minor	0.13	0.16	0.20	0.19	0.22	0.27	0.32	0.18
Moderate	0.41	0.51	0.64	0.22	0.63	0.77	0.95	0.20
Extensive	0.78	0.97	1.24	0.23	1.14	1.42	1.75	0.21
Complete	0.97	1.22	1.57	0.24	1.40	1.74	2.15	0.22

The dispersion values (β) of the response parameters at individual damage state thresholds, obtained from the ExIDA results considering both aleatory and epistemic uncertainties, are comparatively higher than those obtained from the IDA results considering only aleatory uncertainty. It is evident that the incorporating epistemic uncertainty, along with aleatory uncertainty, leads to an increase of the β value by approximately 31.1%, 18.7%, 13.5%, and 12.1% for the minor, moderate, extensive, and complete damage states, respectively. These increased β values highlight the importance of considering both epistemic and aleatory uncertainties in the analysis. Furthermore, it is noteworthy that the significance of the

epistemic uncertainty is relatively more pronounced for the lower damage states as compared to the higher damage states. In other words, as the damage states shift from complete to minor, the increment in the β value due to the inclusion of epistemic uncertainty increases. This can be primarily attributed to the fact that at higher damage states, the dispersion of the response parameters is primarily governed by aleatory uncertainty. Conversely, the influence of aleatory uncertainty is relatively less significant for the lower damage states, leading to a more pronounced influence of epistemic uncertainty at these damage states.

Table 7.4 Estimated log-normal distribution fragility function parameters for the simple IDAs and ExIDAs on the wall-frame structure

Damage State	θ_{ds}	IDA results			ExIDA results		
		μ_d	β_A	β	μ_d	β_{AE}	β
Minor	0.16	$\mu_d = 0.66S_a^{1.08}$	0.10	0.22	$\mu_d = 0.65S_a^{1.07}$	0.21	0.29
Moderate	0.50		0.15	0.25		0.22	0.30
Extensive	0.90		0.18	0.27		0.23	0.30
Complete	1.20		0.19	0.27		0.24	0.31

Figures 7.3 and 7.4 present the fragility estimates for the adopted wall-frame structure, considering only aleatory uncertainty and both aleatory and epistemic uncertainties, respectively. These estimates are derived considering the intensity measure $S_a(T_1)$ and the mean values (median or 50th percentile) of the response parameter (ISD) used to define the damage state thresholds. The developed fragility relationships, which take into account different sources of uncertainty, are evaluated and compared to gain a deeper understanding of the variations in the vulnerability of the RC wall-frame structure.

It is observed from Table 7.2 and Figure 7.3 that the mean value of the intensity measure, $S_a(T_1)$, for the extensive damage state is determined to be 1.396g. This value corresponds to the median intensity measure at which the wall-frame structure attains the threshold for extensive damage state, considering that the variability in the response is solely influenced by aleatory uncertainty. In other words, there is a 50% probability that the extensive damage state, characterized by the initiation of spalling of the cover concrete at critical sections of the structural wall, will be reached when the $S_a(T_1)$ value reaches 1.396g. Similarly, in the analyses (ExIDAs) that consider both aleatory and epistemic uncertainties, as shown in Table 7.3 and Figure 7.4, the wall-frame structure attains the threshold for the extensive damage

state at a median $S_a(T_1)$ value of 1.418g. This indicates a slight variation in the median value of the intensity measure corresponding to different damage state thresholds under the impact of various sources of uncertainties. It is important to note that the consideration of different sources of uncertainties not only affects the dispersion values but also alters the relationship between the median response parameter and intensity measure ($\mu_d - S_a(T_1)$). Consequently, differences can be observed in the percentile values of the intensity measure (Tables 7.2 and 7.3) corresponding to the damage state thresholds when comparing the results of the analyses that consider only aleatory uncertainty and those that consider both aleatory and epistemic uncertainties.

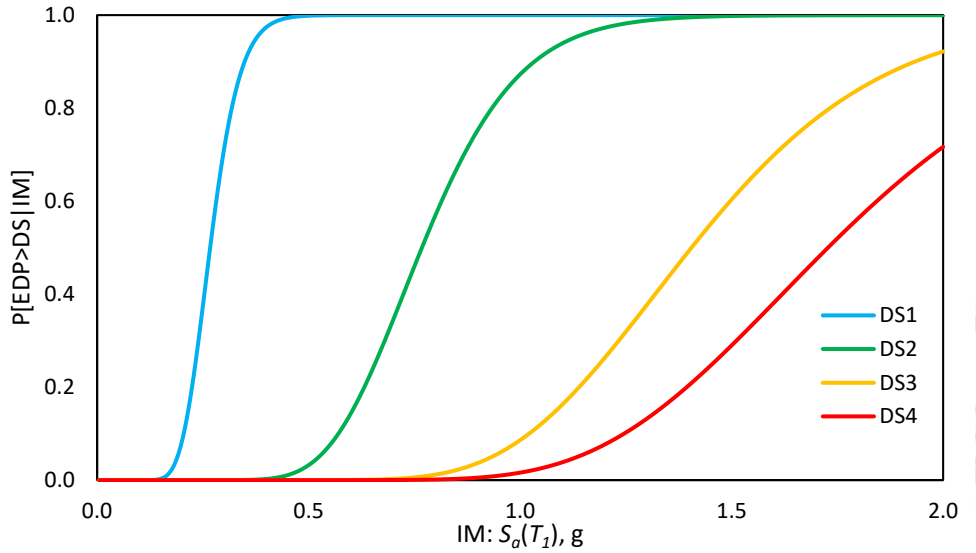

Figure 7.3 Fragility curves for RC wall-frame considering aleatory uncertainty.

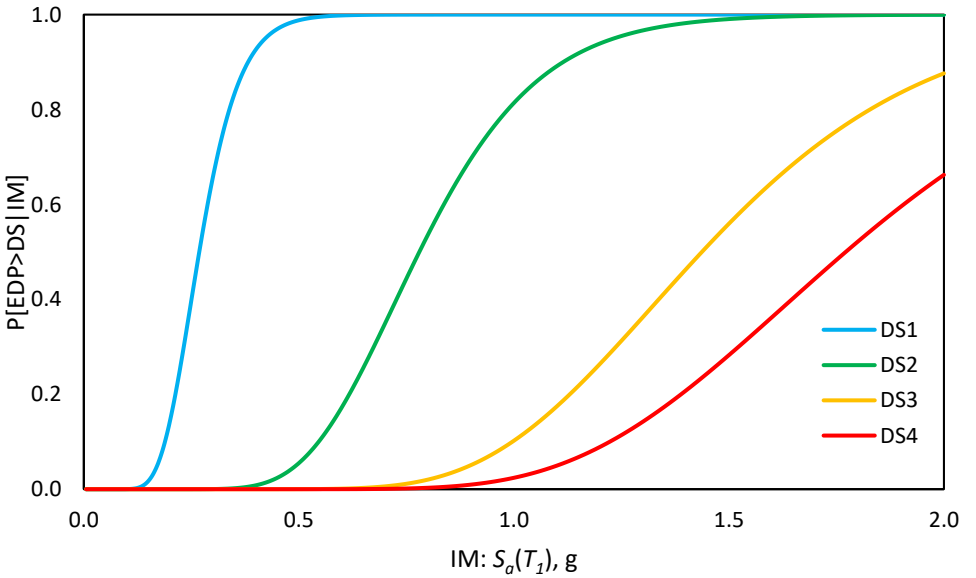

Figure 7.4 Fragility curves for RC wall-frame considering both aleatory and epistemic uncertainties.

Figure 7.5 presents the compiled fragility curves for the RC wall-frame structure, considering only aleatory uncertainty and both aleatory and epistemic uncertainties, in order to facilitate the evaluation and comparison of these developed fragility curves. It is apparent that the steepness of the curves is determined by the dispersion of the response parameter values at specific damage state thresholds. The inclusion of both sources of uncertainty results in an increased β value (dispersion value, as shown in Table 7.3), which consequently reduces the slope of the fragility curves as compared to when considering only aleatory uncertainty. Analysing the data presented in Figure 7.5, it is noticeable that the maximum differences in the probability of exceedance between the fragility relations developed for the RC wall-frame considering only aleatory uncertainty and both aleatory and epistemic uncertainties are 7.13%, 6.00%, 5.65%, and 5.41% for the minor, moderate, extensive, and complete damage states, respectively.

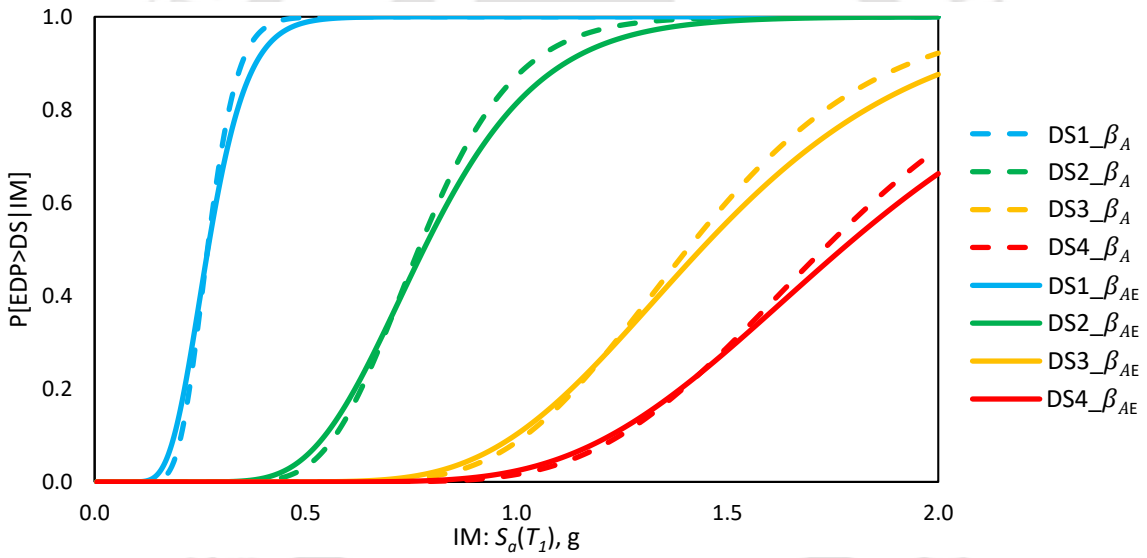

Figure 7.5 Comparison of fragility curves derived considering different uncertainty sources.

Table 7.5 provides the "± 1 × standard deviation" confidence interval for the mean values of the response parameter ISD and intensity measure $S_a(T_1)$, as well as their relative widths for each damage state, in the analyses considering both aleatory and epistemic uncertainties (ExIDAs) of the adopted RC wall frame. A confidence interval is a statistical range that offers an estimation of the apprehension linked with a sample statistic, such as a mean. It is used to assess the level of accuracy of the derived estimates. The "± 1 × standard deviation" confidence interval for a log-normally distributed random variable, indicating an 84% probability, is assessed along with its relative width in the following manner:

$$x_{l,u} = \tilde{x}.\, e^{\pm\frac{\sigma}{\sqrt{n}}} \tag{7.5}$$

$$x_i = 100.\frac{x_u - x_l}{\tilde{x}}\% \quad (7.6)$$

where, x_l and x_u represent two limits defining the 84% confidence interval for the mean of a log-normal random variable, $\tilde{x}$ represents the sample mean value of random variable (from Table 7.3), $\sigma/\sqrt{n}$ represents the standard error of the mean, σ represents the standard deviation of the sample mean (from Table 7.4), and n represent the sample size (220 in this case). The lower and upper bounds of the 84% confidence interval for the mean values of the response parameter ISD and intensity measure $S_a(T_1)$ are indicated as $({x_l}^{ISD}, {x_u}^{ISD})$ and $({x_l}^{S_a(T_1)}, {x_u}^{S_a(T_1)})$, respectively. ${x_i}^{ISD}$ and ${x_i}^{S_a(T_1)}$ represent the relative width of confidence interval for the mean values of ISD and $S_a(T_1)$, respectively.

Table 7.5 Relative width of 84% confidence interval for the mean values of ISD and $S_a(T_1)$

Damage State	ISD (%)		Relative width of confidence interval, ${x_i}^{ISD}$ (%)	$S_a(T_1)$, g		Relative width of confidence interval, ${x_i}^{S_a(T_1)}$ (%)
	Lower and upper bounds of the 84% confidence interval			Lower and upper bounds of the 84% confidence interval		
	${x_l}^{ISD}$	${x_u}^{ISD}$		${x_l}^{S_a(T_1)}$	${x_u}^{S_a(T_1)}$	
Minor	0.157	0.164	3.964	0.262	0.272	3.825
Moderate	0.495	0.516	4.008	0.758	0.787	3.839
Extensive	0.954	0.994	4.114	1.391	1.446	3.923
Complete	1.197	1.248	4.163	1.705	1.774	3.963

In numerical applications, it is generally considered acceptable if the relative width of the confidence interval lies in the 10% range (e.g., Pejovic and Jankovic, 2016). However, for the estimated mean values of ISD and $S_a(T_1)$ at the thresholds of the selected damage states, the relative width of the confidence interval evaluated is even narrower than 5%. These values are well below the acceptable limit, indicating a narrow interval width that contains the mean value with a relatively high probability of 84%. The small relative widths of these confidence intervals demonstrate acceptable accuracy in the ensuing fragility relationships.

7.5 Fragility Function for RC Wall-Frame using Vector Valued IMs

Seismic force imposes complex loading on a structure, and characterizing it with a single parameter, such as $S_a(T_1)$, is insufficient. Despite this complexity, fragility curves are typically derived utilizing only one parameter to correlate the seismic intensity level to the anticipated structural damage. However, employing a single ground-motion parameter

overlooks the variations in the estimated damage, leading to an oversight in properly propagating uncertainty in subsequent risk analyses and assessing the significance of this variability. To address this limitation, in recent times, there have been endeavours to consider the influence of multiple seismic IMs on structural damage. For instance, investigations by Rajeev et al. (2008), Seyedi et al. (2010), and Radu and Grigoriu (2018) have introduced the impact of various ground-motion parameters. Kafali and Grigoriu (2007) proposed an alternate IM involving earthquake magnitude and distance to the source, and subsequently, fragility functions have been developed for single-degree-of-freedom systems utilising ordinary artificial earthquake records. Also, investigations into a vector-valued seismic IM that includes pseudo-spectral acceleration and supplementary factors associated with the shape of the response spectrum have also been explored, as seen in the work of Baker and Cornell (2005). Despite the recognition of the importance of considering multiple IMs for assessing the seismic performance of structures, it is observed that there is a scarcity of existing literature which have attempted to investigate the development of fragility functions using vector-valued IMs, in particular for RC wall-frame building typologies. The present study aims to enhance the characterisation of strong ground motion by establishing the concept of fragility surfaces in risk analysis for the considered RC wall-frame structure through IDA of the nonlinear models. In this approach, the seismic loading on the structure is represented by two IMs. The chosen IMs should have a low correlation for an effective representation of the earthquake shaking. On the other hand, the seismic response must show a strong correlation with the selected parameters. By using this approach, it is intended to better understand the correlation between seismic characteristics and structural response to enhance the efficiency and reliability of fragility assessments for RC wall-frame buildings.

7.5.1 Formulation of Fragility Surface

The fragility relationship between a structural response parameter and seismic demand measure, represented by a single IM (or scalar IM), can be expressed by Eq. 7.1. Alternatively, to assess the fragility function, one can utilize the value of the IM that corresponds to a specific damage state threshold, denoted by IM^{DSi}. This can be expressed as follows:

$$P(EDP > DS|IM = x) = P\left(IM^{DSi} \leq x\right) \tag{7.7}$$

Eq. 7.7 can be expanded to include the vector-valued IM scenario, leading to:

$$P(EDP > DS|IM_1 = x, IM_2 = y) = P\left(IM_1^{DSi} \leq x \cap IM_2^{DSi} \leq y\right) = F_{IM_1^{DSi}, IM_2^{DSi}}(x, y) \quad (7.8)$$

which formulates the fragility surface as the joint distribution function of the intensity measure vector $\left\{IM_1^{DSi}, IM_2^{DSi}\right\}$.

Assuming that $\left\{IM_1^{DSi}, IM_2^{DSi}\right\}$ follows a joint Lognormal distribution characterized by logarithmic mean $\{\eta_1^*, \eta_2^*\}$, logarithmic standard deviation $\{\sigma_1^*, \sigma_2^*\}$, and correlation coefficient ρ^*, its joint probability density function can be defined as follows:

$$f_{IM_1^{DSi}, IM_2^{DSi}}(x, y) = \frac{1}{2\pi\sigma_1^*\sigma_2^*\sqrt{1-\rho^{*2}}xy} \times exp\left\{\frac{-1}{2(1-\rho^{*2})}\left[\left(\frac{\ln x - \eta_1^*}{\sigma_1^*}\right)^2 - 2\rho^* \frac{(\ln x - \eta_1^*)(\ln y - \eta_2^*)}{\sigma_1^*\sigma_2^*} + \left(\frac{\ln y - \eta_2^*}{\sigma_2^*}\right)^2\right]\right\} \quad (7.9)$$

The fragility surface is obtained through the double integration of the joint probability density function.

7.5.2 Choice of Intensity Measures

Before arriving at the fragility surface, it is necessary to identify a limited set of seismic IM variables that, when used together to characterize seismic loading, result in the least variation in the estimated damage as quantified through the considered RC wall-frame structural model. It is attempted to identify mutually uncorrelated parameters that encompass different aspects of a seismic event, namely the amplitude, frequency content, and duration, with the aim of using the least number of parameters. However, it requires a trade-off between introduction of more parameters, which could reduce the dispersion in the fragility estimates, and the variability in evaluating these parameters for specific seismic event scenarios. The selected parameter to characterize ground motion in constructing fragility functions have to be both indicative of the earthquake's damage potential and readily measurable with information about the earthquake's attributes. A comprehensive list of ground motion parameters investigated is provided in Table 7.6.

Figure 7.6 displays the correlation (ρ) between various considered ground motion parameters and the structural response, specifically ISD. The different IM values are calculated from the unscaled ground motion data of the eleven selected records. The structural response is evaluated using the RC wall-frame structural model subjected to the original strong motion data. The selection of periods for examining the spectral accelerations has been based on the outcomes from eigenvalue analysis of the modelled RC wall-frame. The two key eigen

periods in the Y-axis (the direction of seismic input) have been identified as 0.51 seconds and 0.1 seconds.

Table 7.6 List of ground motion parameters investigated

Parameter	Description
$S_a(T_1)$	Spectral acceleration at the period of the first mode
$S_a(T_2)$	Spectral acceleration at the period of the second mode
PGA	Peak ground acceleration
AI	Arias Intensity
A95	The level of acceleration which contains up to 95% of the Arias intensity.
S75	Slope75: the slope of the Husid plot (e.g. cumulative Arias intensity over time) between 5% and 75% of the total Arias intensity.
S95	Slope95: the slope of the Husid plot between 5% and 95% of the total Arias intensity.
SD	Significant Duration: based on the interval between 5% and 95% Arias intensity

Choosing appropriate IMs, having low correlation, is crucial to effectively characterize ground motion while ensuring that the structural damage (represented by response parameters) correlates well with the chosen parameters. After analysing the data in Figure 7.6, it is observed that among the considered IMs, the one with the best correlation (ρ=0.99) with the structural response (ISD) is the spectral acceleration at the fundamental time period ($S_a(T_1)$). Therefore, $S_a(T_1)$ is considered as the first IM to characterize the ground motion. For the second IM, it should have a relatively low correlation with $S_a(T_1)$ but a strong correlation with ISD. From Figure 7.6, it is found that the Peak Ground Acceleration (PGA) exhibits a good correlation (ρ=0.96) with ISD but also has a high correlation (ρ=0.95) with $S_a(T_1)$. Thus, PGA cannot be adopted as the second IM. After exploring various permutations and combinations, it is identified that $S_a(T_2)$, with correlation values of 0.90 and 0.88 with ISD and $S_a(T_1)$ respectively, is a relatively better choice to represent the ground motion along with $S_a(T_1)$. This combination fulfils the criteria of high correlation with ISD and low correlation between the adopted IMs. As a result, the present study considers the spectral accelerations at the first two natural periods of the considered structural system as the IMs to effectively capture ground motion characteristics and their influence on the structural response.

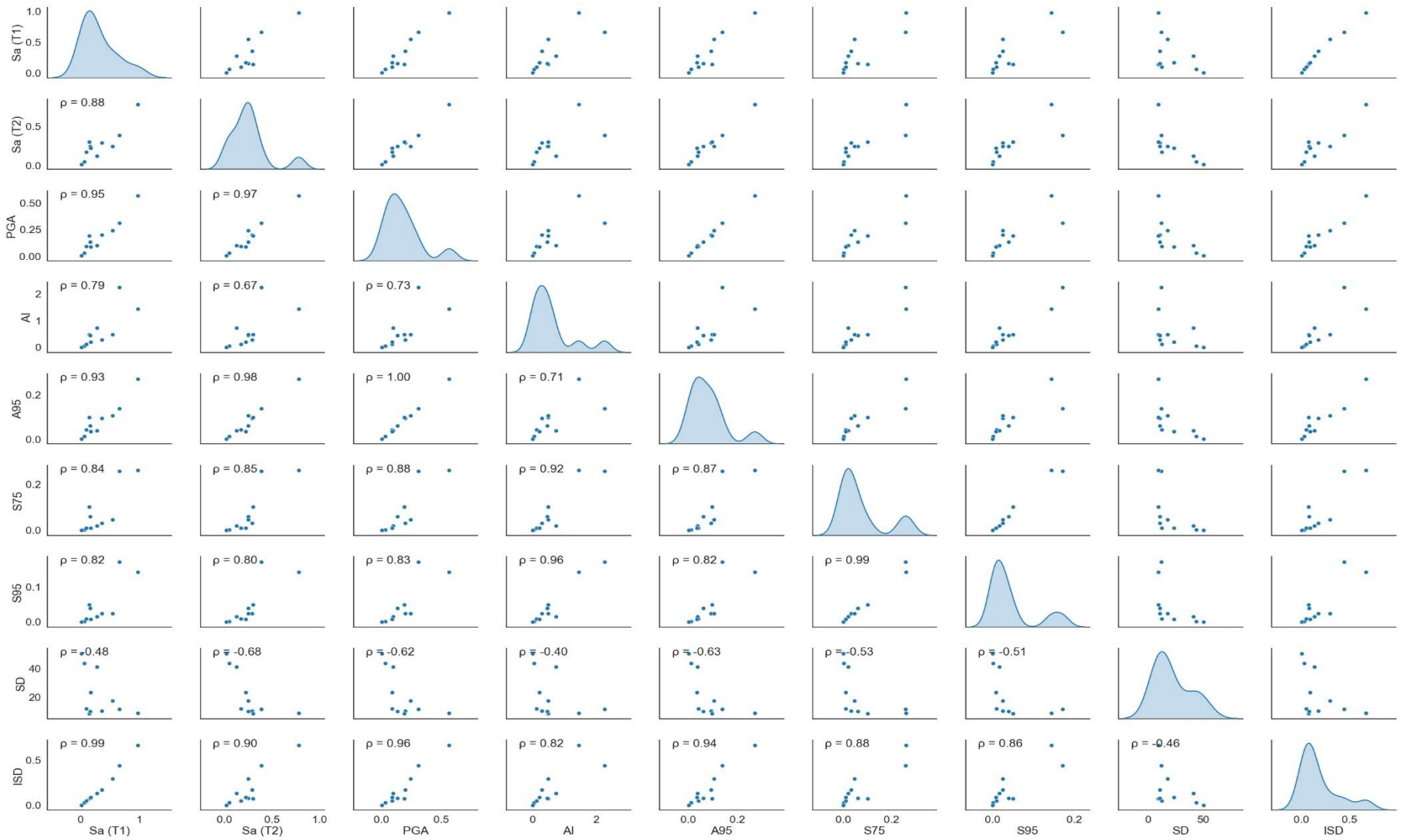

Figure 7.6 Correlation of different considered IMs with ISD.

7.5.3 Assessment of Fragility Surfaces

Fragility surfaces are developed for different values of $S_a(T_1)$ and $S_a(T_2)$ using bi-variate lognormal distribution function (Eq. 7.9). The parameters used to construct the fragility surfaces are presented in Table 7.7, guided by the outcomes obtained through the investigation of the adopted RC wall-frame structure considering only aleatory uncertainty (IDA) and both aleatory and epistemic uncertainties (ExIDA). For the fragility surfaces, the σ^* values are calculated as the standard deviation of the logarithmic IM values corresponding to specific damage state thresholds. These values are integrated with the modelling uncertainty value of 0.2 using the SRSS technique. The EDP-IM relationships, for both the considered IMs, tabulated in Table 7.7 are utilized for identifying the IM values corresponding to different damage state thresholds.

Table 7.7 Estimated log-normal distribution fragility surface parameters for the simple IDAs and ExIDAs on the RC wall-frame structure

	Damage State	μ_d		η_1^*	η_2^*	σ_1^*	σ_2^*	ρ^*
		$S_a(T_1)$	$S_a(T_2)$					
IDA Results	**Minor**	$\mu_d = 0.66S_a(T_1)^{1.08}$	$\mu_d = 0.63S_a(T_2)^{0.99}$	-1.32	-1.38	0.22	0.61	-0.05
	Moderate			-0.26	-0.23	0.24	0.63	0.11
	Extensive			0.34	0.43	0.26	0.63	0.18
	Complete			0.55	0.65	0.27	0.64	0.20
ExIDA Results	**Minor**	$\mu_d = 0.65S_a(T_1)^{1.07}$	$\mu_d = 0.61S_a(T_2)^{0.98}$	-1.32	-1.35	0.28	0.61	0.19
	Moderate			-0.25	-0.20	0.28	0.61	0.21
	Extensive			0.36	0.46	0.29	0.62	0.24
	Complete			0.57	0.68	0.29	0.62	0.25

Figures 7.7 and 7.8 illustrate the fragility surfaces for four different damage state thresholds of the RC wall-frame structure, analysed considering only aleatory uncertainty and both aleatory and epistemic uncertainties, respectively. Each fragility surface estimates the conditional probability of attaining or surpassing an individual damage state threshold for a particular combination of $S_a(T_1)$ and $S_a(T_2)$ values. For both analysis scenarios (IDA and ExIDA), it is evident that the probability of the structural response exceeding the damage state thresholds decreases as the level of damage increases from 'Minor' to 'Complete.' Comparing the fragility surfaces derived from the two different analysis scenarios (IDA and

ExIDA), it is notable that the consideration of epistemic uncertainty along with aleatory uncertainty leads to a relatively lower probability of reaching or exceeding a damage state threshold for a specific combination of $S_a(T_1)$ and $S_a(T_2)$ values when compared to the probabilities obtained by considering only aleatory uncertainty. In light of the outcomes presented in Figures 7.7 and 7.8, it can be observed that, for instance, at a value of 1g for both $S_a(T_1)$ and $S_a(T_2)$, the mean probability of exceeding the moderate damage state threshold is 56.43% for the RC wall-frame when analysed considering only aleatory uncertainty, and 53.09% when considering both aleatory and epistemic uncertainties.

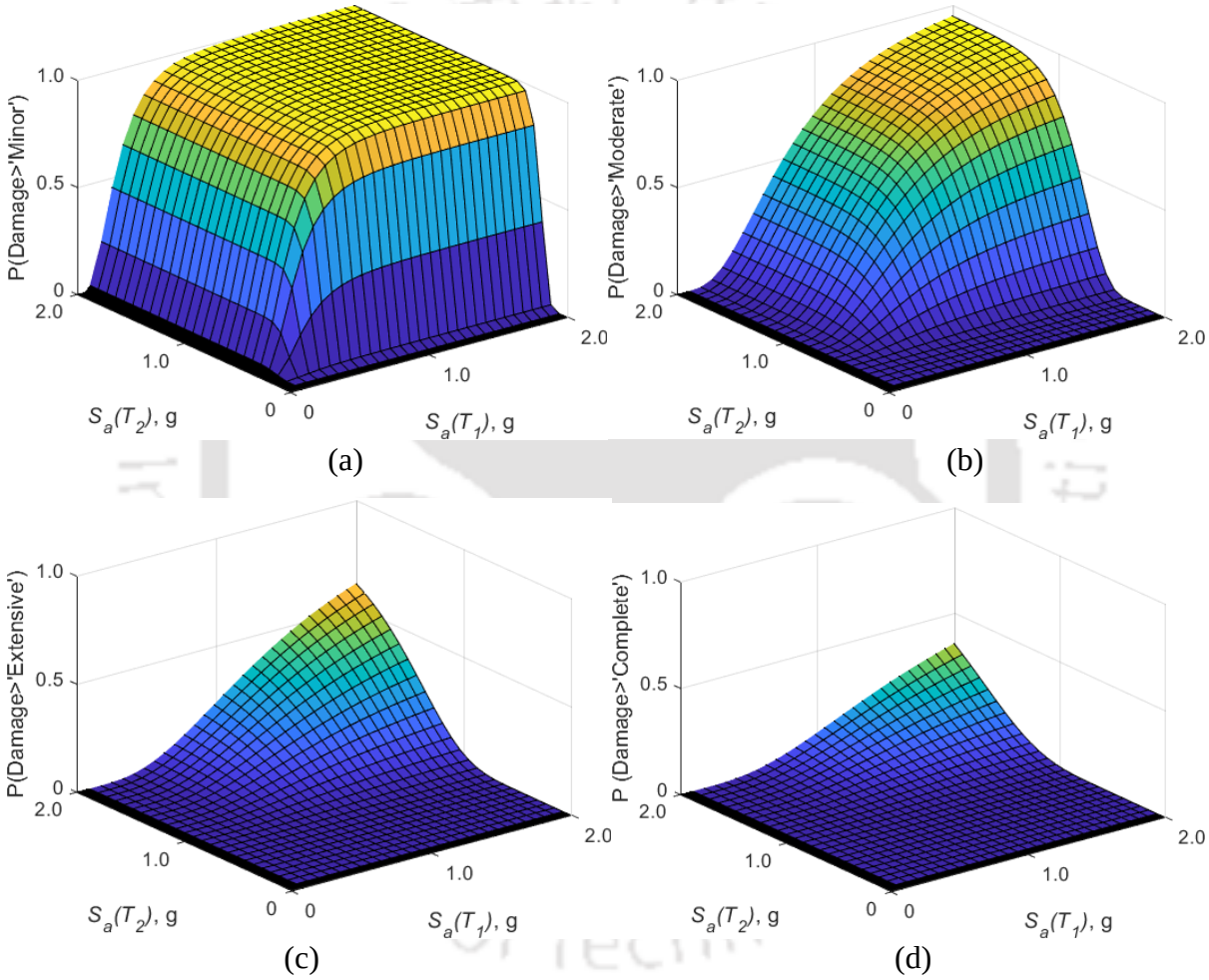

Figure 7.7 Fragility surface of RC wall-frame, considering aleatory uncertainty, for damage state levels of (a) Minor, (b) Moderate, (c) Extensive and (d) Complete.

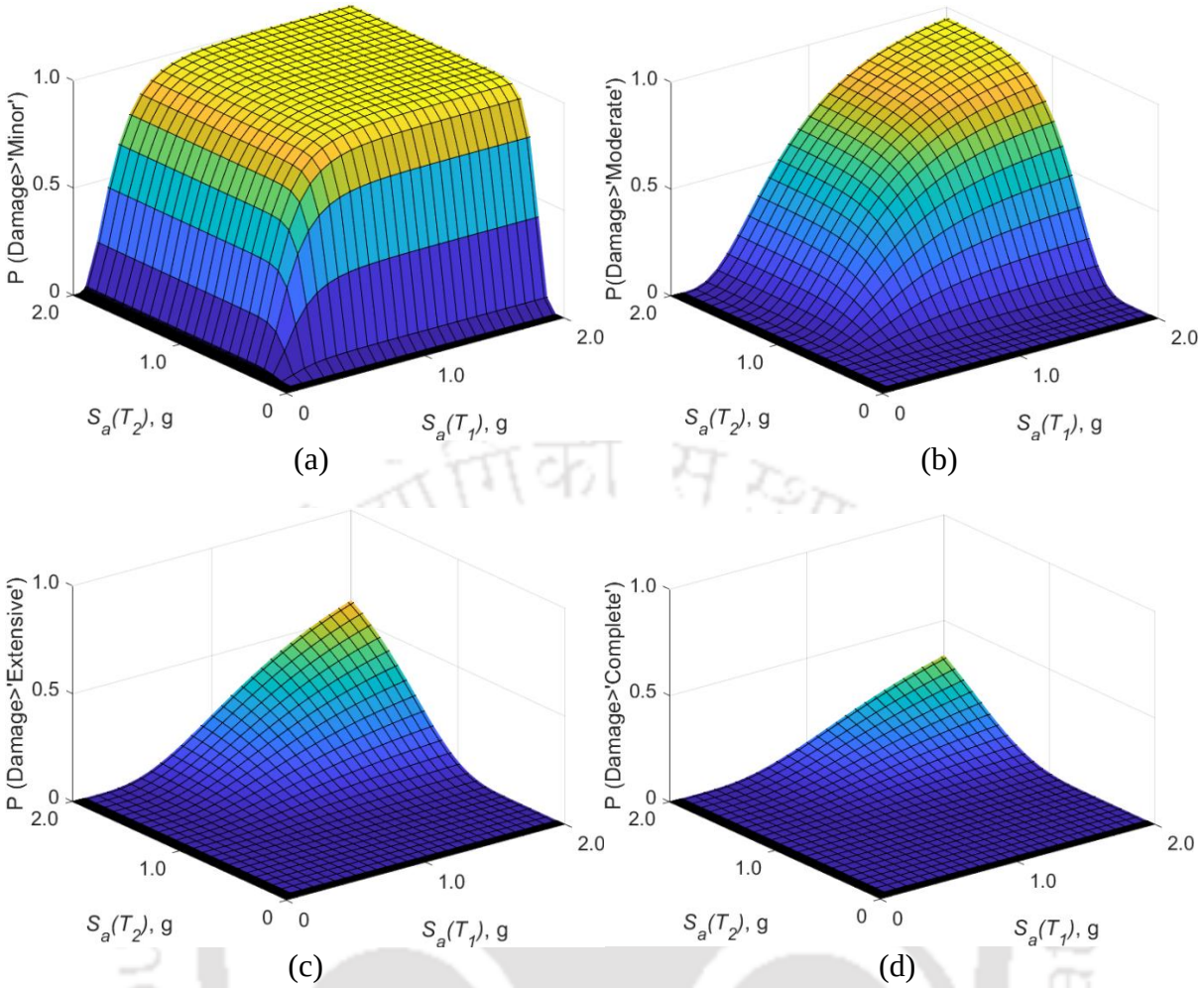

Figure 7.8 Fragility surface of the RC wall-frame, considering both aleatory and epistemic uncertainties, for damage state levels of (a) Minor, (b) Moderate, (c) Extensive and (d) Complete.

The primary motivation behind developing fragility surfaces is to achieve a more accurate fragility estimate using relatively precise definition of the seismic hazard level, potentially leading to a reduction in the uncertainty associated with the representation of the hazard (often represented by a single parameter). To corroborate both approaches, the estimated fragility surface is transformed into 2D curves by distinguishing "slices" that characterise the failure conditional probability as a function of one IM ($S_a(T_1)$) while maintaining the second one ($S_a(T_2)$) as constant. An illustrative example of this is presented in Figures 7.9 and 7.10, for different damage state levels of the RC wall-frame structure, analysed considering only aleatory uncertainty and both aleatory and epistemic uncertainties, respectively.

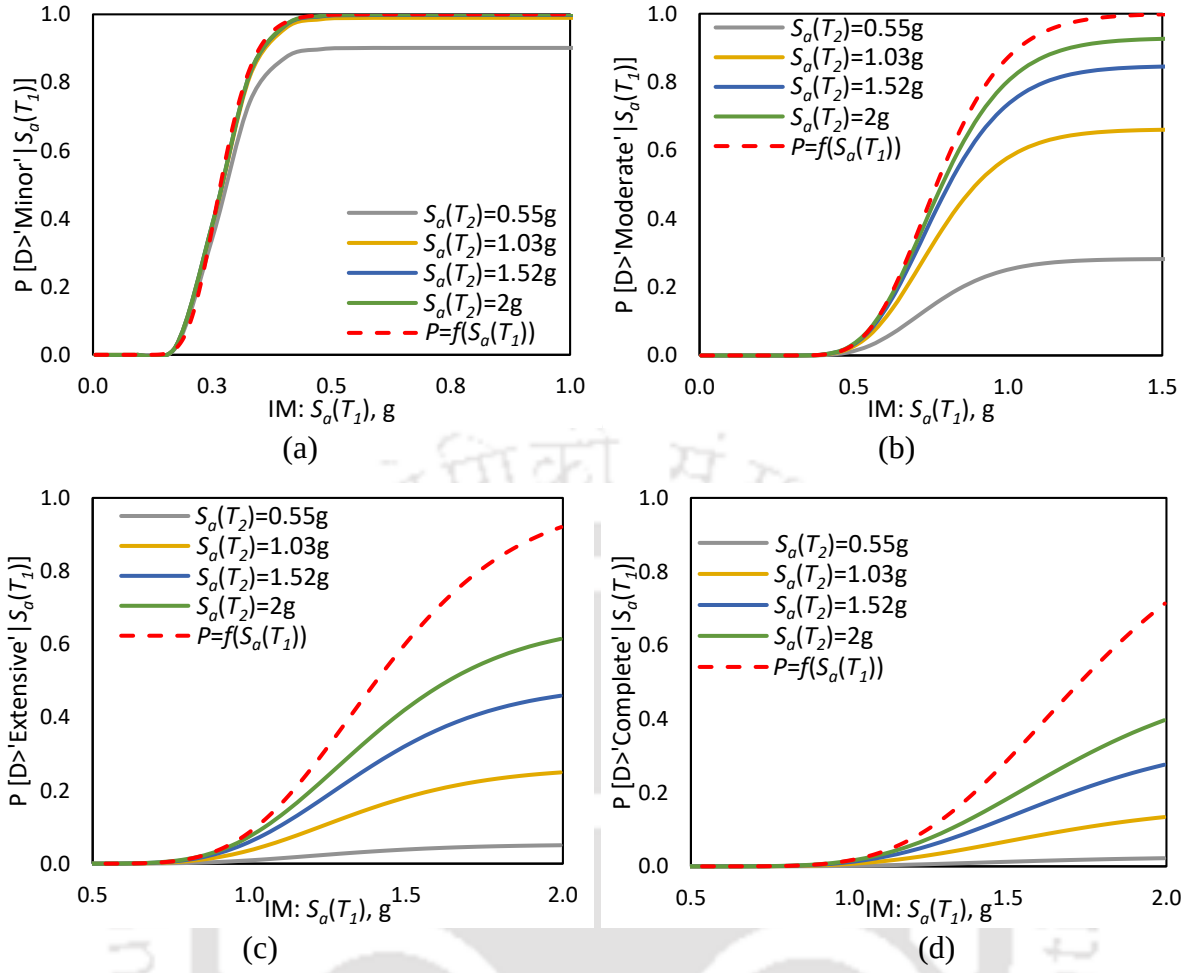

Figure 7.9 Single-parameter fragility curve (dotted line) as compared to slices of the fragility surface for damage levels of (a) Minor, (b) Moderate, (d) Extensive and (d) Complete for IDA case.

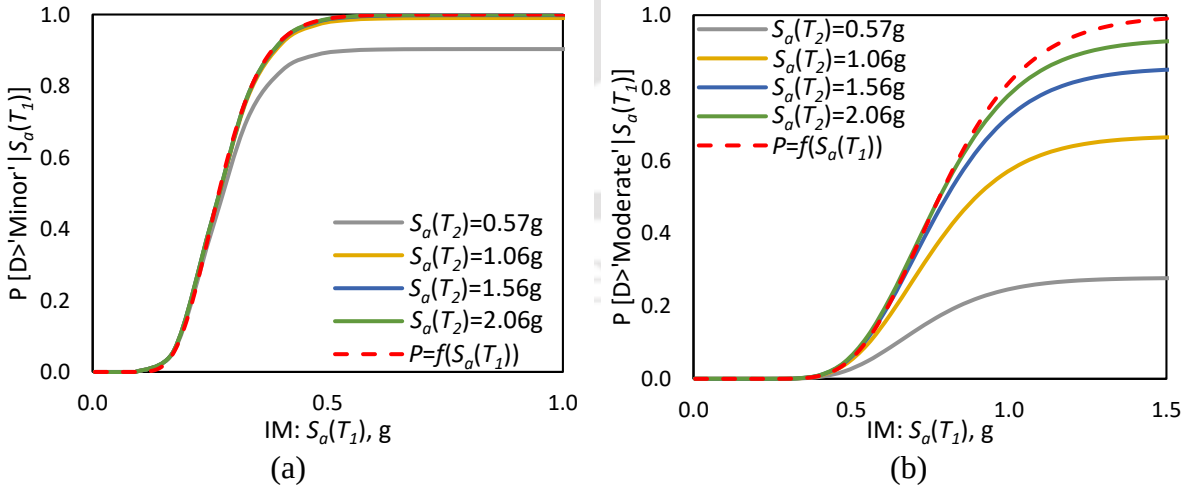

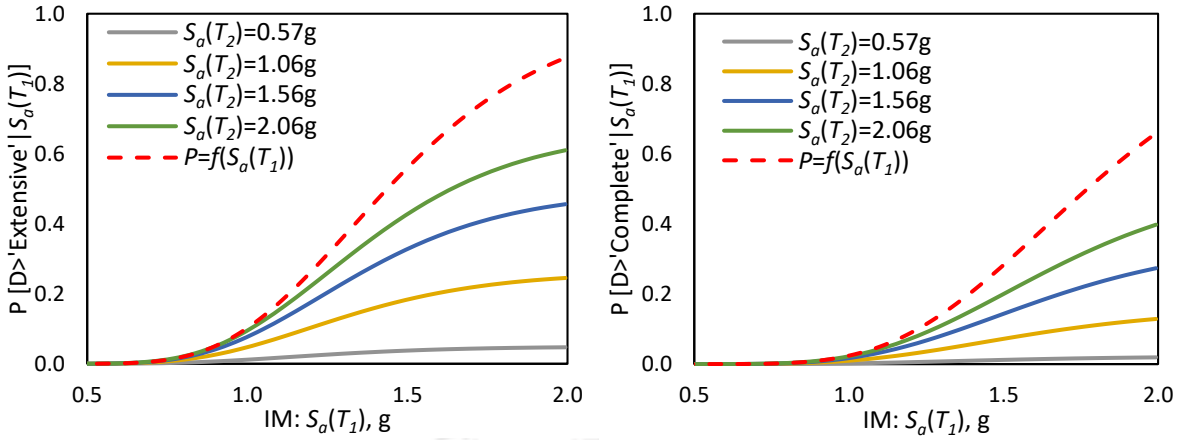

(c) (d)

Figure 7.10 Single-parameter fragility curve (dotted line) as compared to slices of the fragility surface for damage levels of (a) Minor, (b) Moderate, (d) Extensive and (d) Complete for ExIDA case.

Firstly, it is evident that the disparity between the fragility curves and fragility surfaces becomes more prominent as the structural damage state levels progress from 'Minor' to 'Complete'. While the variation in the fragility relationships for different values of $S_a(T_2)$ is minimal at the 'Minor' damage level, this difference becomes significantly more pronounced for higher damage state thresholds. These figures showcase the substantial differences that may emerge among fragility curves when relying on a single IM parameter, thus emphasizing the important role of fragility surfaces in seismic risk assessment. When focussing solely on a single IM parameter, like $S_a(T_1)$, it is possible to derive a mean curve that fails to encompass the fluctuations in ground motions observed in relation to another parameter, such as $S_a(T_2)$.

Table 7.8 Average difference between exceedance probabilities from fragility curves and fragility surfaces corresponding to average IM difference for IDA and ExIDA analyses

Damage State	Δ_{IM}	Δ_{FF}	
		Results from IDA	Results from ExIDA
Minor	> 100%	2.42%	2.03%
Moderate	> 60%	21.04%	18.52%
Extensive	> 40%	30.50%	29.80%
Complete	> 40%	46.40%	44.92%

Δ_{IM}: Average difference between $S_a(T_1)$ and $S_a(T_2)$ values.
Δ_{FF}: Average difference between fragility estimates using single IM and two IMs.

To quantify the disparity between failure probabilities determined from fragility curves and those derived from the 'slices' of fragility surfaces, an attempt is made to estimate the expected average failure probability difference, for the RC wall-frame, corresponding to the

average difference between the two considered IMs, namely $S_a(T_1)$ and $S_a(T_2)$. The average difference in the probability of exceeding different damage state thresholds between the fragility functions developed using a single IM and two IMs, corresponding to the IM difference, is presented in Table 7.8 for the RC wall-frame structure analyzed considering only aleatory uncertainty (IDA) and both aleatory and epistemic uncertainties (ExIDA).

As seen in Figures 7.9 and 7.10, Table 7.8 also demonstrates that the disparity between the fragility estimates derived from single IM and two IMs increases with higher damage state levels. For the lowest damage state level, *i.e.*, the 'minor' damage state, the disparity between the exceedance probabilities obtained from the fragility curves and from the 2D extracts of fragility surfaces is approximately 2% when the average difference between the IMs exceeds 100%. This suggests that when the two considered IMs, $S_a(T_1)$ and $S_a(T_2)$, differ by more than 100%, which is highly unlikely for regular structures, the disparity between the exceedance probabilities obtained from fragility curves and fragility surfaces is only around 2%. Hence, for the 'minor' damage state of the RC wall-frame structure, estimating the fragility function using a single IM is expected to yield similar exceedance probabilities as those obtained using two IMs, as the difference is merely 2% when the IM difference exceeds 100%, a scenario highly improbable in practice. Significant differences of 100% in the spectral acceleration at the first two natural periods of a structure would require substantial disparities in the respective natural periods, which is unlikely for typical structures. Therefore, the computational effort involved in obtaining fragility surfaces for the 'minor' damage state of an RC wall-frame structure can be minimized by estimating fragility curves, as they are expected to yield similar exceedance probabilities to those of the fragility surfaces for regular structures.

The significance of employing fragility surfaces in the risk analysis of RC wall-frame structures becomes more apparent for higher damage states. When transitioning from 'moderate' to 'extensive' and 'complete' damage states, it can be noted that the difference in exceedance probabilities between the fragility functions considering a single IM and two IMs increases, even though the difference between the considered IMs ($S_a(T_1)$ and $S_a(T_2)$) decreases towards the higher damage states. For instance, in the case of the 'extensive' damage state of the RC wall-frame structure, the difference between the exceedance probabilities estimated from fragility curves and fragility surfaces can be as substantial as 30% when the considered IMs differ by 40%, a difference that is more likely for regular structures. This observation suggests that for higher damage states of RC wall-frame

structures, when the difference between $S_a(T_1)$ and $S_a(T_2)$ values is around 40%-60%, the use of single IM as compared to two IMs can lead to a significant difference in fragility estimates, up to 45%. Consequently, when dealing with higher damage state levels in RC wall-frame structures, employing simple fragility curves over complex fragility surfaces may not be the most prudent approach for efficient risk analysis.

Table 7.8 provides valuable insights for deciding whether to utilize complex fragility surfaces in the efficient risk assessment of RC wall-frame structures, depending on the disparity between the spectral accelerations at the first two natural periods and the acceptable difference between fragility curves and fragility surfaces. For a specific RC wall-frame structure and damage level of interest, the difference between the spectral acceleration at the first two natural periods can be determined and conditioned on the level of accuracy sought for fragility estimates, the fragility functions can be determined using single IM (simplistic) or two IMs (computationally expensive). Furthermore, it is noteworthy that no substantial difference is observed in the fragility estimate disparity (considering single IM and two IMs) when the analyses are conducted for only aleatory uncertainty and both aleatory and epistemic uncertainties. Nevertheless, regardless of the damage state levels, a slightly lower difference in fragility estimates is observed for the analyses considering both aleatory and epistemic uncertainties as compared to those obtained with only aleatory uncertainty.

7.6 Fragility Function for RC Wall-Frame Building

The fragility functions developed thus far are specifically for a 2D RC wall-frame structure, which is a part of the entire building structure presented in Figure 7.11. This 2D frame is an exterior frame located in the global y-direction of the building. In this section, it is attempted to develop fragility estimates for the global RC wall-frame building system (Figure 7.11) utilising the outcomes from Incremental Dynamic Analysis (IDA) carried out for the considered suite of earthquake records (Table 3.3). The IDA of the wall-frame building system is performed for unidirectional ground motion applied in the global y-direction, considering only the impact of aleatory uncertainty, specifically the record-to-record variability. Due to the significant time and computational resources required for transitioning from dynamic analysis of a 2D structure to a 3D structure, the investigation of epistemic uncertainty's influence on the IDA results for the 3D structure is not further pursued in the present study.

In a manner similar to the 2D wall-frame, the analysis of the wall-frame building is conducted, representing the seismic intensity levels using spectral acceleration at the first two natural periods of the structure. The first two natural periods of the building are determined as 0.93 seconds and 0.88 seconds, obtained from eigenvalue analysis results of the building system.

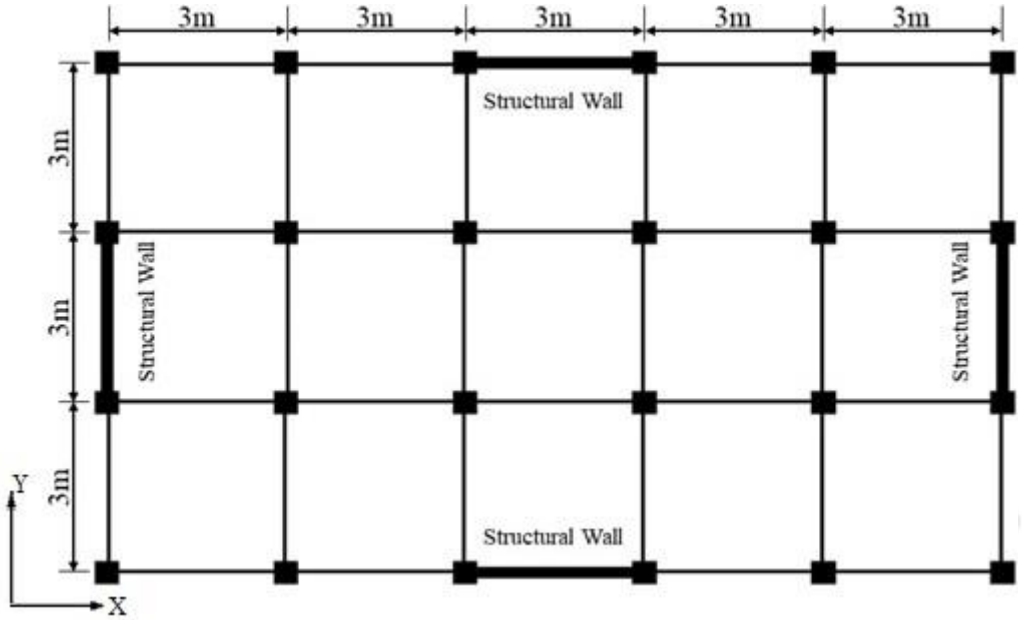

Figure 7.11 Typical plan for the considered RC wall-frame building.

7.6.1 Fragility Function using Single IM

The outcomes of the IDA performed on the RC wall-frame building are depicted in Figure 7.12, illustrating a scatter plot of ISD-$S_a(T_1)$ parameters. Additionally, the figure includes the best fit power law line, representing the relationship between the median value of ISD (μ_d) and $S_a(T_1)$. The IDA results are utilized to derive the fragility functions for the considered RC wall-frame building. The fragility functions, using a single IM, for various damage state thresholds of the RC wall-frame building, are developed using Eq. 7.2. The damage state thresholds (θ_{ds}) used for developing the fragility functions of the overall building are the same as those used for the 2D wall-frame structure. The parameters for the fragility curves are evaluated (Table 7.9) by utilizing the data depicted in Figure 7.12, which corresponds to the outcomes of IDA conducted on the studied building system. The dispersion values (β_A) are calculated as the standard deviation of the natural logarithmic values of the response parameters (ISD) at each individual damage state threshold. Finally, the overall β values are

evaluated by combining the β_A values with the dispersion value (β_M = 0.2) due to modelling uncertainties, using the SRSS technique.

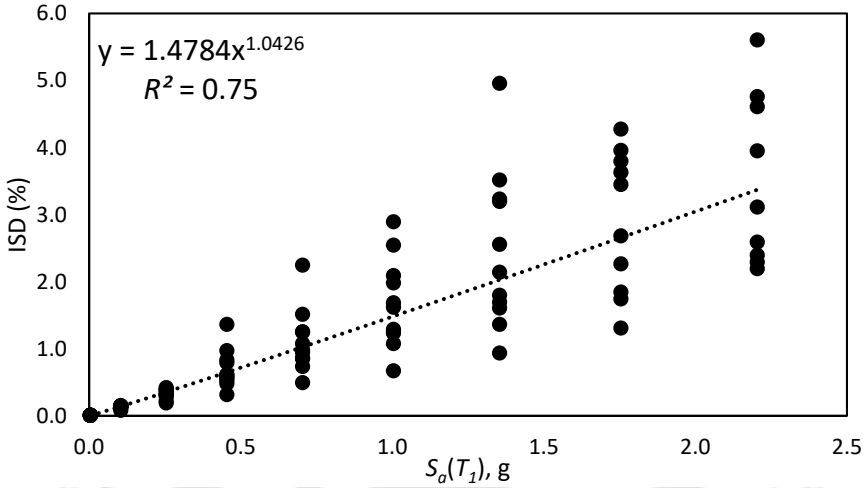

Figure 7.12 ISD- $S_a(T_1)$ relationship for IDA of RC wall-frame building.

Table 7.9 Estimated log-normal distribution fragility curve parameters for the wall-frame building

Damage State	θ_{ds}	μ_d	β_A	β
Minor	0.16	$\mu_d = 1.48S_a^{1.04}$	0.22	0.30
Moderate	0.50		0.28	0.34
Extensive	0.90		0.32	0.37
Complete	1.20		0.33	0.39

The fragility functions for various damage state thresholds of the considered RC wall-frame building, developed using a single IM ($S_a(T_1)$), are presented in Figure 7.13. It is noted that the probability of exceeding different damage state thresholds for the RC wall-frame building reaches 100% for all damage levels. To enhance understanding of these fragility functions, the ensuing section elaborates on comparing fragility estimates between the RC wall-frame building and the RC wall-frame structure.

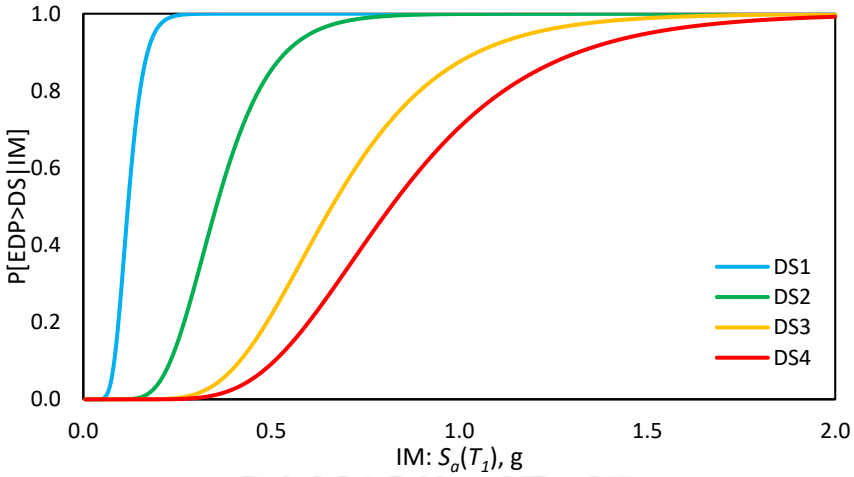

Figure 7.13 Fragility curves for RC wall-frame building.

7.6.2 Fragility Function Using Vector-Valued IM

In this section, fragility relations for the RC wall-frame building are established by utilizing vector-valued intensity measures to achieve better characterization of the seismic loading. Fragility surfaces are developed for the 3D structural model of the considered building, considering various combinations of $S_a(T_1)$ and $S_a(T_2)$ using the bi-variate lognormal distribution function (Eq. 7.9). The parameters used for constructing the fragility surfaces are outlined in Table 7.10, derived from the analysis of the RC wall-frame building considering only aleatory uncertainty. The σ^* values in this context are computed as the standard deviation of the logarithmic IM values corresponding to specific damage state thresholds of the 3D building model. The obtained values are combined with the modelling uncertainty value of 0.2 using the SRSS technique. The EDP-IM relationships for the RC wall-frame building, pertaining to both the considered IMs, as presented in Table 7.10, are employed to determine the IM values corresponding to various damage state thresholds.

Table 7.10 Estimated bivariate log-normal distribution fragility surface parameters for the RC wall-frame building structure

Damage State	μ_d		η_1^*	η_2^*	σ_1^*	σ_2^*	ρ^*
	$S_a(T_1)$	$S_a(T_2)$					
Minor	$\mu_d = 1.48S_a(T_1)^{1.04}$	$\mu_d = 1.44S_a(T_2)^{1.03}$	-2.13	-2.12	0.29	0.35	0.94
Moderate			-1.04	-1.02	0.34	0.39	0.96
Extensive			-0.41	-0.39	0.37	0.43	0.97
Complete			-0.20	-0.17	0.38	0.44	0.97

Figure 7.14 displays the fragility surfaces representing four distinct damage state thresholds of the considered RC wall-frame building, analysed solely under the influence of aleatory uncertainty. Each fragility surface showcases the conditional probability of attaining or exceeding a specific damage state threshold for the particular combination of $S_a(T_1)$ and $S_a(T_2)$ values. The fragility surfaces derived for the RC wall-frame building depict that the exceedance probabilities reach nearly 100% for all damage state levels. In contrast, the fragility surfaces obtained for the 2D wall-frame (as shown in Figure 7.7) did not achieve 100% conditional probability of exceeding specific damage state levels, particularly for the 'extensive' and 'complete' damage states.

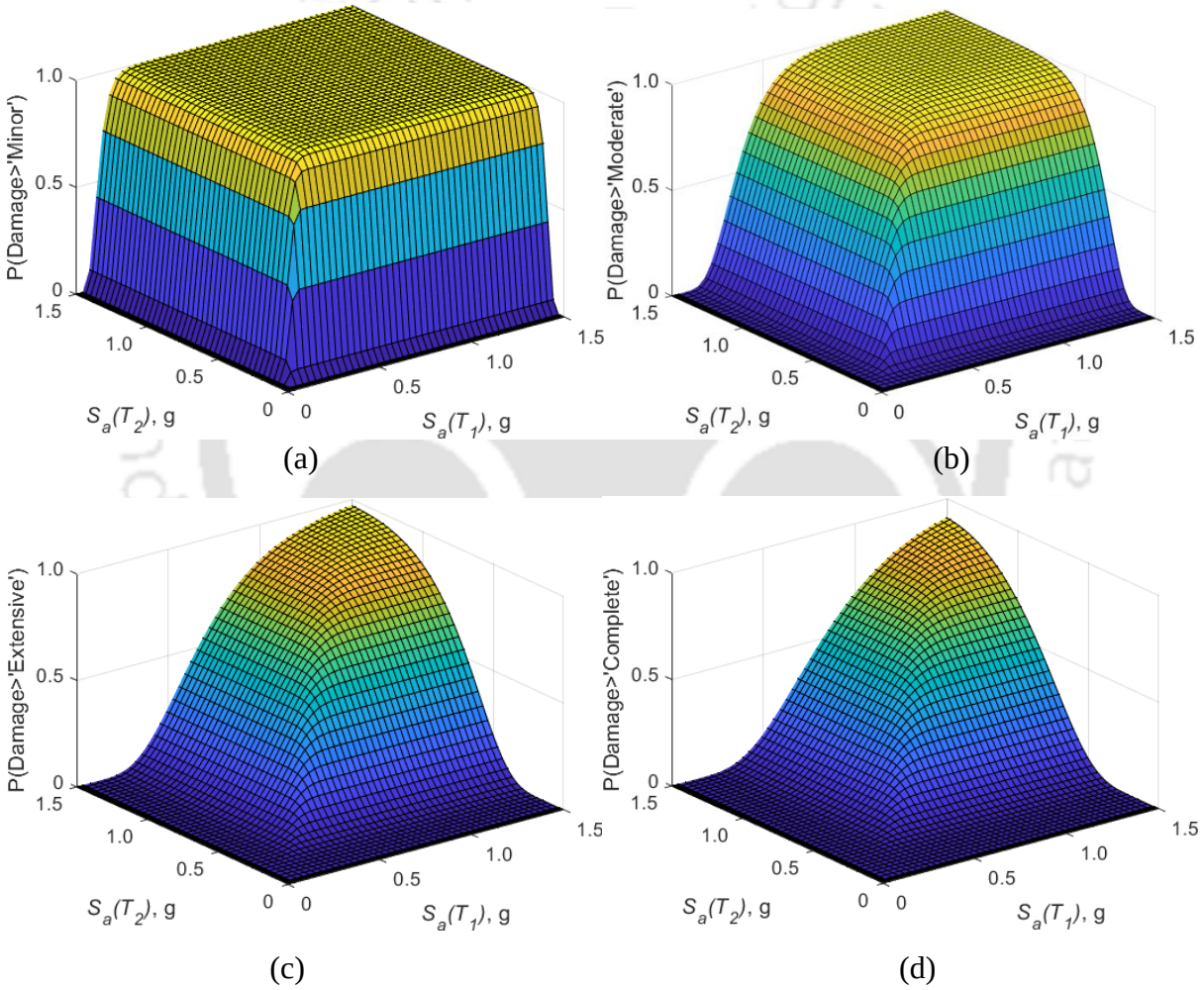

Figure 7.14 Fragility surface of the RC wall-frame building for damage state levels of (a) Minor, (b) Moderate, (c) Extensive and (d) Complete.

7.6.3 Comparison of Fragility Functions

For the appropriate comparison between the fragility functions of the RC wall-frame structure and the RC wall-frame building, it is important to accurately account for the 2D structure's dynamic characteristics to mirror those of the entire building. Given that the contribution of

the RC structural wall components to the overall lateral load resistance of the building system is significantly higher as compared to other structural elements, the major part of the total lateral force on the building is carried by the exterior wall-frames (as indicated in the building plan in Figure 7.11). Furthermore, in comparison to the lateral stiffness of the exterior wall-frames, the lateral stiffness of the interior bare frames is considered to be negligibly small. Consequently, each of the exterior wall-frames is assumed to bear an equal share of the total lateral force on the building. As a result, the considered 2D wall-frame structure requires to be analysed with a seismic mass measuring up to half the building's seismic mass (Dabaghi et al., 2019).

Hence, this analysis focuses on the 2D wall-frame structure coupled with half of the building's mass, employing IDA for the considered set of eleven ground motion records (Table 3.3). The first two natural periods of this structure—0.88 seconds and 0.17 seconds—are obtained from the eigenvalue analysis of the structural system. The fragility functions are established by considering both single and multiple IMs, relying on the findings obtained from the IDA results using Eqns. 7.2 and 7.10, respectively. Figure 7.15 depicts the results of the IDA conducted on the specified 2D wall-frame structure, presenting a scatter plot of ISD-$S_a(T_1)$ parameters. The parameters utilized in formulating the fragility curves and fragility surfaces, based on the IDA outcomes, are detailed in Tables 7.11 and 7.12, respectively. Specifically, the estimation of dispersion value only takes into account the effects of record-to-record variability (β_A) and modelling uncertainties ($\beta_M = 0.2$). Figures 7.16 and 7.17 showcase the derived fragility curves and fragility surfaces, respectively, for the specified RC wall-frame structure, assigned with half the building mass.

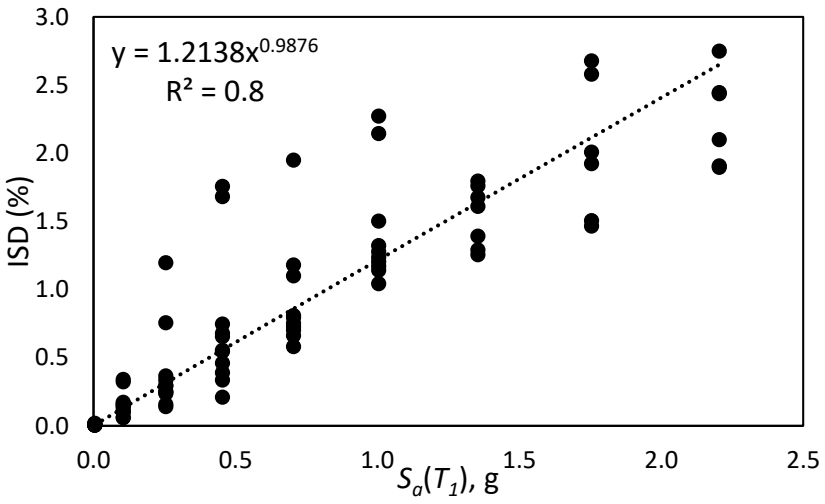

Figure 7.15 ISD- $S_a(T_1)$ relationship for IDA of 2D RC wall-frame structure.

Table 7.11 Estimated log-normal distribution fragility curve parameters for the 2D wall-frame structure

Damage State	θ_{ds}	μ_d	β_A	β
Minor	0.16	$\mu_d = 1.2138S_a^{0.99}$	0.39	0.44
Moderate	0.50		0.41	0.46
Extensive	0.90		0.42	0.46
Complete	1.20		0.42	0.46

Table 7.12 Estimated bivariate log-normal distribution fragility surface parameters for the 2D wall-frame structure

Damage State	μ_d		η_1^*	η_2^*	σ_1^*	σ_2^*	ρ^*
	$S_a(T_1)$	$S_a(T_2)$					
Minor	$\mu_d = 1.21S_a(T_1)^{0.99}$	$\mu_d = 1.02S_a(T_2)^{0.95}$	-2.05	-1.94	0.43	0.50	-0.06
Moderate			-0.90	-0.75	0.46	0.50	-0.20
Extensive			-0.24	-0.06	0.46	0.51	-0.28
Complete			-0.01	0.17	0.46	0.51	-0.19

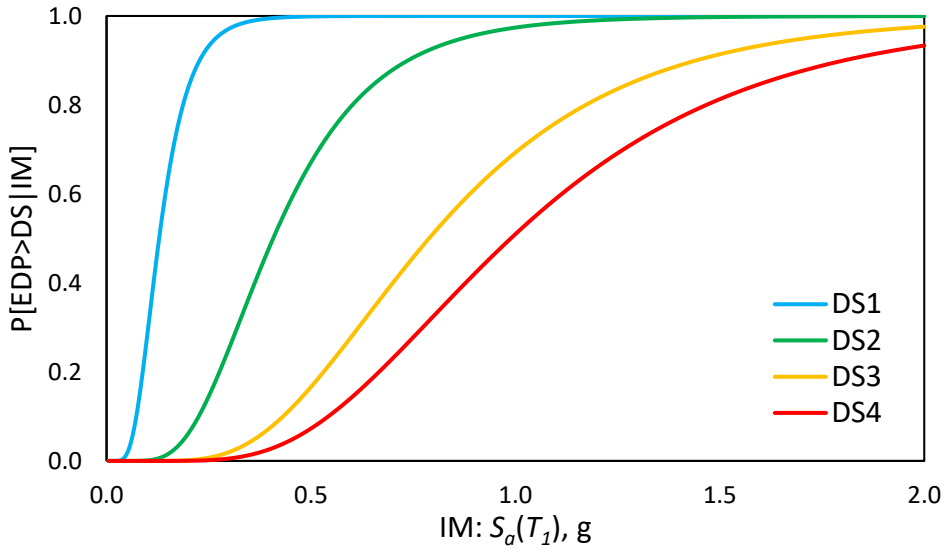

Figure 7.16 Fragility curves for 2D wall-frame structure.

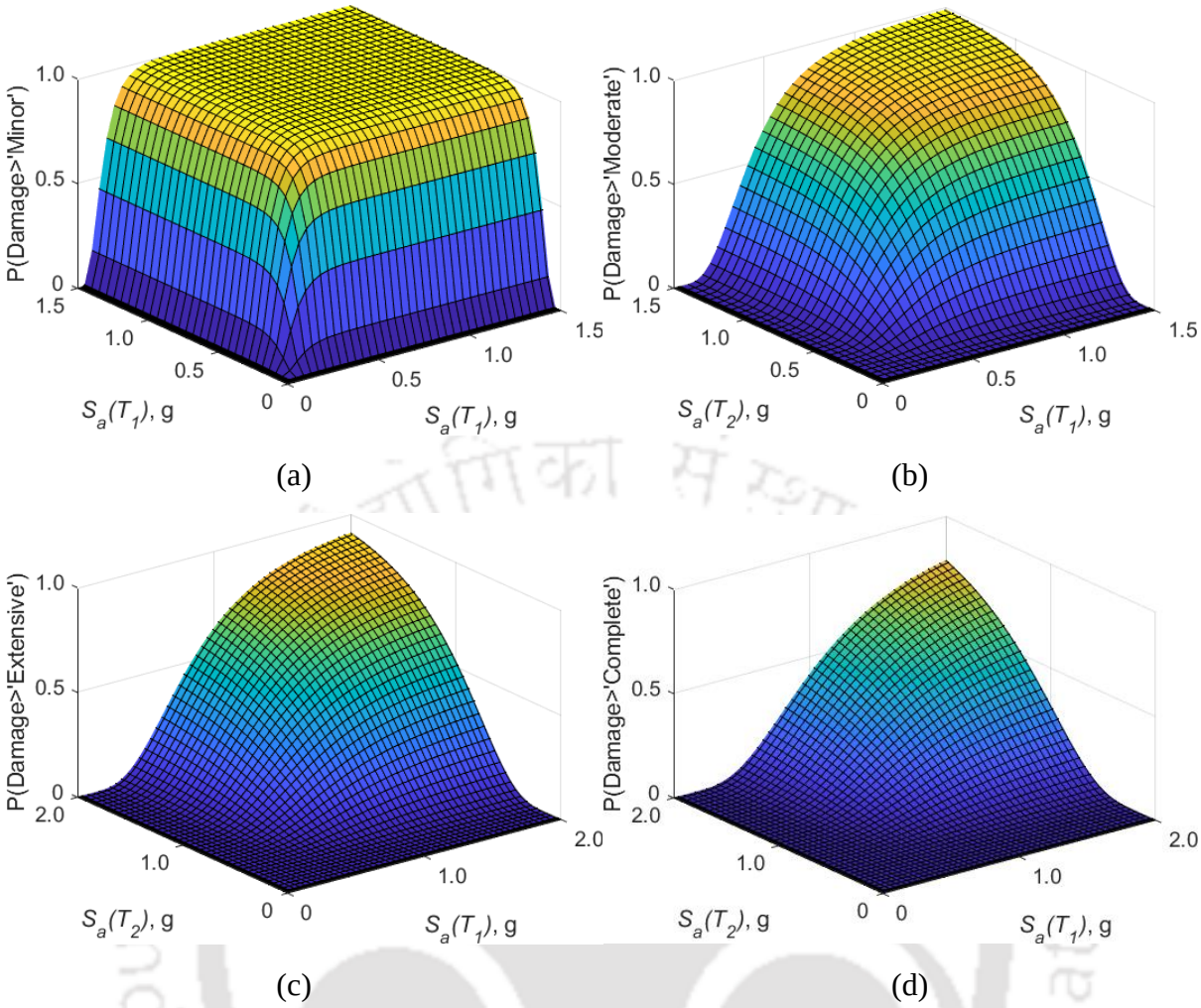

Figure 7.17 Fragility surface of the 2D wall-frame structure for damage state levels of (a) Minor, (b) Moderate, (c) Extensive and (d) Complete.

Figure 7.18 presents a convenient way to assess and compare the fragility functions developed using a single IM for both 2D wall-frame structure and the wall-frame building. The compiled fragility curves are derived from the IDA results of these structural systems, considering only the influence of aleatory uncertainty. This allows for a comprehensive analysis of the structural response to seismic loading and aids in understanding the differences between the fragility estimates for the two types of structural model for the considered building system.

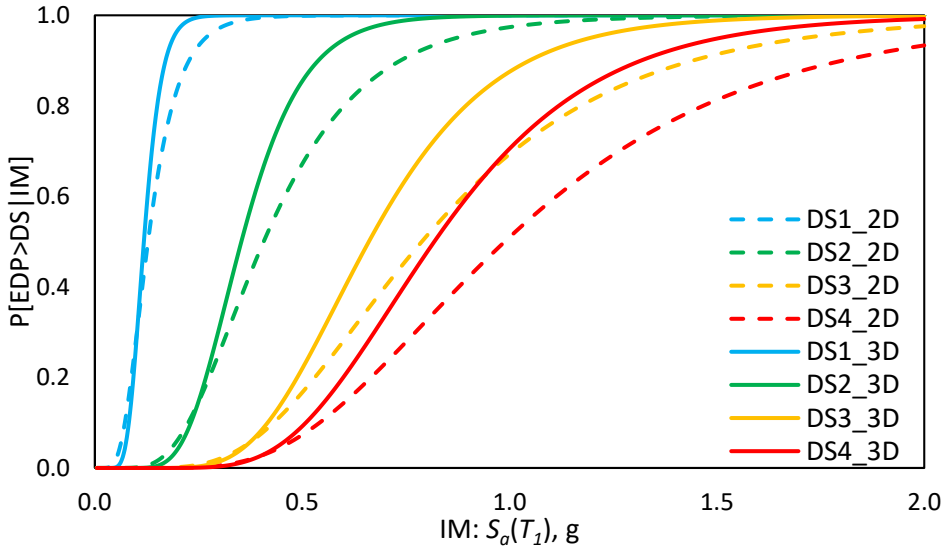

Figure 7.18 Comparison of fragility curves for the 2D wall-frame structure and the RC wall-frame building.

The comparison between the fragility curves of the wall-frame building and the 2D wall-frame structure reveals a notable difference in the probability of exceeding the damage state thresholds. The vulnerability of the entire building system, analysed at a specific intensity level, appears to be higher than that of the simpler 2D frame representation of the structure. As an illustration, the mean value of the IM, $S_a(T_1)$, for the extensive damage state is found to be 0.66g and 0.79g for the considered building analysed as a realistic RC wall-frame building and as a simplistic 2D wall-frame structure, respectively. This value signifies the median IM at which the structure reaches the threshold for extensive damage state, signifying a 50% probability that the extensive damage state, marked by the initiation of spalling of the cover concrete at critical sections of the structural wall, will be attained. Hence, it is apparent that the damage state thresholds are exceeded at a lower median IM, $S_a(T_1)$, for the analysis results derived from the RC wall-frame building as compared to those obtained from the 2D wall-frame structure, irrespective of the damage state levels. The difference in median $S_a(T_1)$ values, obtained from the analysis of the wall-frame building and the 2D wall-frame, increases with higher damage state levels. Specifically, the differences in median $S_a(T_1)$ values for the 'minor', 'moderate', 'extensive', and 'complete' damage states are found to be 0.01g, 0.05g, 0.13g, and 0.17g, respectively. Thus, the fragility estimates for the RC wall-frame building demonstrate exceedance probabilities of 'minor', 'moderate', 'extensive', and 'complete' damage states that are 7.8%, 13.2%, 16.2%, and 17.2% higher, respectively, as compared to those obtained for the RC wall-frame structure concerning the median IM. As evident from Tables 7.9 and 7.11, the β values, which represent the dispersion of the response

parameters at individual damage state thresholds, are relatively higher for the 2D RC wall-frame structure as compared to the RC wall-frame building. This higher β value is reflected in the reduced steepness of the fragility curves (Figure 7.18) for the 2D wall-frame structure when compared to those obtained for the wall-frame building.

Furthermore, for a better evaluation and comparison of the estimated fragility relationships using vector-valued IMs, both for 2D wall-frame and wall-frame building, Table 7.13 presents a compilation of the median IM values corresponding to different damage state thresholds. These median IM values represent the combination of $S_a(T_1)$ and $S_a(T_2)$ at which there is a 50% probability of exceeding a particular damage state threshold. The median IM values for exceeding the damage state thresholds of the RC wall-frame building are notably lower than those obtained for the 2D wall-frame structure. This implies that for any given combination of $S_a(T_1)$ and $S_a(T_2)$ values, the probability of exceeding a particular median damage state threshold is anticipated to be comparatively higher for the considered building analysed as a computationally expensive RC wall-frame building rather than a simpler 2D wall-frame structure. Thus, consistent with the comparison of fragility curves, the fragility estimates developed using vector-valued IMs for the RC wall-frame building show higher vulnerability to exceed specific damage state thresholds as compared to those obtained for the 2D wall-frame structure.

Table 7.13 Median IM values corresponding to median values of damage state thresholds for wall-frame building and 2D wall-frame structure

Damage State	Wall-frame building		2D wall-frame structure	
	$S_a(T_1)$, g	$S_a(T_2)$, g	$S_a(T_1)$, g	$S_a(T_2)$, g
Minor	0.12	0.13	0.17	0.19
Moderate	0.37	0.38	0.54	0.63
Extensive	0.69	0.71	1.05	1.27
Complete	0.85	0.88	1.31	1.59

In summary, the study of fragility relations, developed using scalar and vector-valued IMs for the RC wall-frame building, indicates that the vulnerability of the response parameters to seismic demand is higher as compared to the analysis of the 2D model of the building. While 2D analysis is often chosen for its simplicity and computational efficiency, the results show that 2D frame model analysis yields conservative fragility estimates for this specific building typology. Hence, depending on the available resources and the importance of accurate structural performance assessment, it is recommended to analyse a 3D model of the structural

system for reliable vulnerability estimates, especially for the specific building typology, such as the wall-frame building considered in the present study. Although the 3D analysis may be time-consuming and computationally intense, it provides more precise and realistic results for understanding the seismic vulnerability of the building.

7.7 Simplified approach

In this section, it is attempted to demonstrate a simplified procedure to identify a subset of earthquake records that can yield fragility surfaces comparable to those obtained from the entire set of available earthquake records. The resulting fragility surfaces for the RC wall-frame building, derived using this approach are referred to as Efficient Fragility Surfaces (EFS). The term "Efficient" underscores the significant reduction in time and effort attainable by using this simplified approach.

Development of analytical fragility curves for risk analysis in Performance-Based Earthquake Engineering (PBEE) involves a considerable amount of computational effort, particularly in performing IDA, which are pivotal in deriving these estimates. Additionally, aiming to achieve a more accurate characterization of the seismic hazard in PBEE, fragility relations using vector-valued IMs can be developed, but this, in turn, significantly increases the numerical effort as compared to the fragility curves. Obtaining reliable and accurate fragility functions for RC wall-frame buildings demands a substantial investment of time and effort in performing background analyses. In an attempt to simplify this analysis procedure, researchers in the past have advocated various techniques. Some methods involve replacing dynamic nonlinear analysis results with outcomes obtained from a fusion of IDA of a single degree of freedom system and nonlinear static analyses of a multi-degree of freedom system (Vamvatsikos and Cornell, 2005; Han and Chopra, 2006).

Efficient selection of a suite of ground motion records that properly represent an earthquake scenario, constitutes the elementary course of action in performing the analyses for estimating optimal fragility functions. For this purpose, several earthquake record selection criteria are available in the literature (Kiani and Khanmohammadi, 2015; Cimellaro et al., 2011). The key seismic characteristics governing the selection procedure of actual earthquake records are magnitude, site-to-source distance and duration. The structural attributes of the considered structural system are not categorically considered in this selection procedure. In addition to the key seismic characteristics, it would be important to incorporate an additional

criterion into the selection procedure, ensuring that the chosen input records are the most suitable representations for the seismic response of the analysed structures. Researchers in the past (Alwaeli et al., 2020; Kim et al., 2021) have utilised this selection technique, requiring the evaluation of structural seismic response for the earthquake records characterizing a seismic hazard. By utilizing this approach, it is possible to obtain efficient and accurate fragility estimates with a significantly reduced number of selected earthquake records.

In light of the preceding discussion, a distinctive earthquake record selection procedure is employed to facilitate the simplified approach of developing fragility surfaces, considering the record-to-record variability of ground motion data. Using this approach, EFSs are derived for the RC wall-frame building, requiring remarkably low input motion data.

The following steps outline the simplified approach for estimating EFSs for RC structural systems.

a) First the considered structure needs to be designed as per the relevant seismic design guidelines with reference to the seismic zone and the associated design response spectrum.
b) Next, numerical modelling of the considered structure needs to be carried out considering realistic material properties. The appropriate response parameters, *i.e.*, the EDPs and IMs are to be identified for executing IDA of the model(s), along with the selection of an appropriate damage state definition.
c) Then, the true seismic accelerograms need to be selected from the relevant strong motion databases. In the current simplified approach, the process begins with the selection of a minimum of two ground motion records.
d) Each of the chosen input records from step (c) needs to be verified to ensure that it satisfies the predefined record tolerance value (GMR_{Tol}). If any of the records does not meet the GMR_{Tol} criterion, that record is discarded and steps (c) and (d) need to be revisited by selecting new ground motion records.
e) IDAs are to be carried out for the developed numerical model, considering the records associated with a specific trial. For instance, the number of records associated with the first trial (t_i = 1) is 2. The subsequent IDA results are to be used for identifying the median EDP-IM relationships.
f) Based on the outcomes of step (e), the derived EFSs are to be verified for ensuring that they satisfy the predefined fragility surface tolerance value (FS_{Tol}). Once the FS_{Tol} values

of the derived EFSs from two consecutive trials (namely t_i^{th} trial and t_i-1^{th} trial) do not exceed the predefined acceptance value, then those are to be considered for further step. If the predefined acceptance value is exceeded, one more ground motion record needs to be considered in addition to the current suite of records and steps (e) and (f) need to be followed again.

g) The EFSs obtained at trial (t_i-1^{th}) is defined as the final considered fragility surface for the considered structural system.

In the following sections, the proposed approach is used for developing EFSs for the RC wall-frame building by utilising a smaller number of input earthquake records. The building is considered to be located in the North-Eastern (NE) region of India, and ground motion data recorded on a rock stratum in this region is used to derive the EFSs. The derived EFSs for the considered structure are compared with the fragility surfaces estimated using the entire suite of ground motion records to verify its efficacy.

7.7.1 Ground Motion Records Considered for EFSs

The fragility functions estimated so far were derived from IDA results using a suite of 11 ground motion records, characterizing significant earthquake events from different locations worldwide. However, for demonstrating the current approach of developing EFSs for the RC wall-frame building situated in the NE India, specifically the ground motions recorded on a rock stratum in this region are utilised. Table 7.14 provides the details of the entire considered NE India earthquake data recorded on a rock stratum. The ground motion records are acquired from the COSMOS VIRTUAL DATACENTRE. All the ground motion records utilized can be characterized as ordinary, originating from measurements recorded using free-field instrumentation and on sites classified as to soil type A, as per the Indian Standard IS 1893 Part I (BIS, 2016b). Additionally, near-field records, which have the nearest distance to fault rupture smaller than 10 km, were excluded to mitigate pulse-type effects.

Table 7.14 NE India ground motion data recorded on rocky stratum

Record Name	Earthqauke Name	Date	Station	Hypocentral Distance (km)	Magnitude	PGA (m/s^2)	Duration (sec)
GMR1	North East India	10-Sep-86	Pynursla	48.2	4.5	0.91	18.58
GMR2	North East India	10-Sep-86	Khliehriat	52.5	4.5	0.45	13.4
GMR3	North East India	10-Sep-86	Ummulong	44.9	4.5	1.11	16.94

GMR4	North East India	10-Sep-86	Nongkhlaw	68.1	4.5	0.91	29.64
GMR5	North East India	10-Sep-86	Nongpoh	71.4	4.5	0.545	14.06
GMR6	North East India	10-Sep-86	Umsning	58.3	4.5	0.995	20.06
GMR7	India-Burma Border	18-May-87	Nongpoh	248.5	5.9	0.171	20.48
GMR8	India-Bangladesh Border	06-Feb-88	Ummulong	117.2	5.8	0.553	24.52
GMR9	India-Bangladesh Border	06-Feb-88	Nongpoh	145.5	5.8	0.846	17.58
GMR10	India-Bangladesh Border	06-Feb-88	Pynursla	84.6	5.8	0.487	34.6
GMR11	India-Bangladesh Border	06-Feb-88	Mawphlang	94.7	5.8	0.796	28.16
GMR12	India-Bangladesh Border	06-Feb-88	Nongkhlaw	117.3	5.8	1.12	45.28
GMR13	India-Bangladesh Border	06-Feb-88	Shillong	110.2	5.8	0.467	11.74
GMR14	India-Burma Border	06-Aug-88	Nongkhlaw	366.8	7.2	1.42	70.96
GMR15	India-Burma Border	06-Aug-88	Umsning	343.8	7.2	1.32	70.62
GMR16	India-Burma Border	06-Aug-88	Khliehriat	292.7	7.2	0.701	61.46
GMR17	India-Burma Border	06-Aug-88	Ummulong	314.5	7.2	1.6	66.14
GMR18	India-Burma Border	06-Aug-88	Loharghat	388.1	7.2	0.568	38.36
GMR19	India-Burma Border	06-Aug-88	Mawkrywat	379.6	7.2	0.453	22.68
GMR20	India-Burma Border	06-Aug-88	Nongstoin	400.2	7.2	0.512	52.96
GMR21	India-Burma Border	06-Aug-88	Shillong	340	7.2	0.735	34.78
GMR22	India-Burma Border	06-Aug-88	Mawphlang	351.2	7.2	1.17	52.14
GMR23	India-Burma Border	09-Jan-90	Ummulong	342.9	6.1	0.503	11.84
GMR24	India-Burma Border	08-May-97	Nongpoh	124.1	6	0.703	47.66

7.7.2 Fragility Surfaces Using All the Ground Motions

The intention of using the current methodology to derive the EFSs is to minimize the time and effort required for deriving computationally intensive fragility surfaces for a structure by

considering a reduced number of earthquake records for the IDAs. To substantiate the accuracy of the derived EFSs for the RC wall-frame building, the derived EFSs need to be validated against the fragility surfaces developed considering the entire set of the earthquake records. In this context, the fragility surfaces for the RC wall-frame building are developed by considering the entire suite of earthquake records. The IDAs for the adopted building are conducted utilising the complete suite of earthquake records, with ISD as the response parameter. The damage state definitions used for estimating the fragility relations are consistent with the ones defined in Chapter 6. The fragility surfaces for the RC wall-frame building are estimated using the spectral acceleration values at the first two natural periods of the considered structure as the IMs. Figure 7.19 presents the fragility surfaces representing four distinct damage state thresholds of the RC wall-frame building, developed using the IDA results for the entire set of records. These derived fragility surfaces will serve as indicators to validate the accuracy of the estimated EFSs.

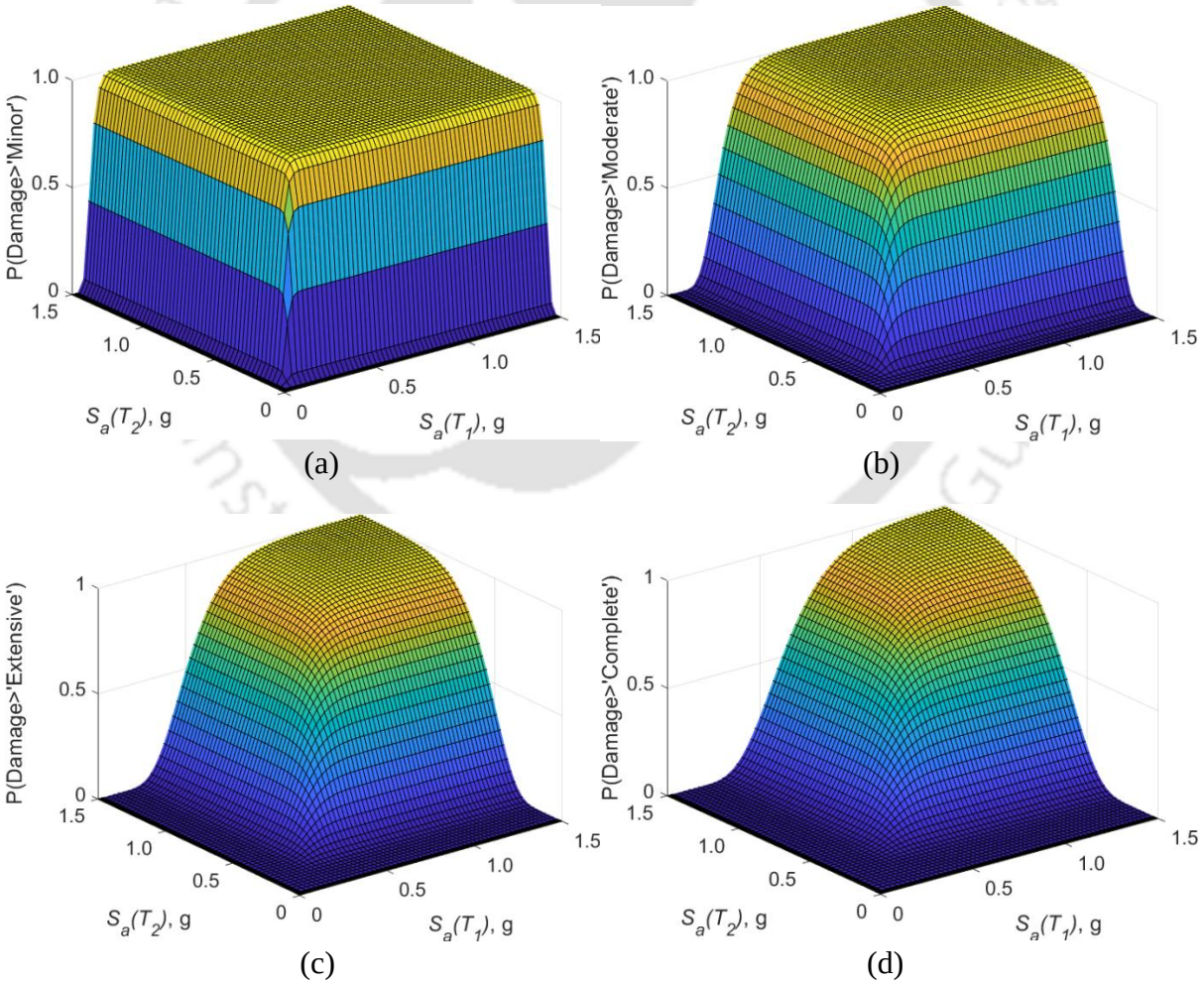

Figure 7.19 Fragility surface considering entire set of NE India earthquake records for damage state levels of (a) Minor, (b) Moderate, (c) Extensive and (d) Complete.

7.7.3 Selection of Ground Motion Records for Simplified Methodology

In order to implement the current simplified methodology for developing EFSs with a reduced number of earthquake records, a well-defined standard criterion needs to be used for selection of the records. In the past, various researchers have proposed several ground motion selection techniques. One of the popular approaches involves selecting earthquake records based on how closely the individual response spectrum match the target mean response spectrum. Nonetheless, relying solely on the matching of the target mean response spectrum may be inadequate in certain scenarios, as it disregards the inherent variability that might prevail in the response spectrum (Jayaram et al., 2011). For example, the conditional mean spectrum primarily considers the spectral acceleration value at the fundamental natural period, $S_a(T_1)$, overlooking the response spectra variance present at other periods. Hence, in this approach, the ground motion records are selected comparing the individual record spectrum with the target response spectrum, conditioned on the spectral acceleration values at various periods, which can be defined as follows:

- $S_a(T_1)$: Spectral acceleration at the natural period for the first natural mode of vibration of the structure.
- $S_a(T_2)$: Spectral acceleration at the natural period for the second natural mode of vibration of the structure.
- $S_{a,geo}(T)$: Geometric average of spectral acceleration from the period range of 0.1 second to 2.5 seconds (Kim et al., 2021).
- $S_{a,geo}(T_1,2\times T_1)$: Geometric average of $S_a(T_1)$ and $S_a(2\times T_1)$ (Cordova et al., 2000).

Essentially, the selection process involves prioritizing and adopting those ground motion records from the entire set that exhibit a response spectrum shape similar to the target response spectrum. The design response spectrum for soil type A, as recommended in IS 1893 Part I (BIS, 2016b), is employed as the target response spectrum for this purpose. The ground motion record tolerance value (GMR_{Tol}) is used to assess the similarity between the shape of individual response spectrum and the target response spectrum, in accordance with the considered spectral acceleration values at different time periods. The GMR_{Tol} is obtained as follows:

$$GMR_{Tol} = c_v \left[\left\{ \frac{S_a^{GMR}(T_1)}{S_a^{TRS}(T_1)} \right\} , \left\{ \frac{S_a^{GMR}(T_2)}{S_a^{TRS}(T_2)} \right\} , \left\{ \frac{S_{a,geo}^{GMR}(T)}{S_{a,geo}^{TRS}(T)} \right\} , \left\{ \frac{S_{a,geo}^{GMR}(T_1,2.T_1)}{S_{a,geo}^{TRS}(T_1,2.T_1)} \right\} \right] \quad (7.10)$$

where GMR_{Tol} is the ground motion record tolerance value, c_v is the coefficient of variation, S_a^{GMR} is the spectral acceleration value of the ground motion record at the considered time period, S_a^{TRS} is the spectral acceleration value of the target response spectrum at the considered time period.

To ensure the similarity of the considered record spectrum to the target response spectrum shape, the aim is to maintain consistency among the chosen records and reduce the impact of record-to-record variability on the estimated fragility functions. A smaller GMR_{Tol} value indicates a closer match between the shapes of the earthquake record spectrum and the target response spectrum. For categorizing and selecting the input earthquake records to develop the EFSs, a GMR_{Tol} value of 15% is adopted. This specific value is determined through trial and error, ensuring satisfactory EFSs are obtained. The upper bound value of GMR_{Tol} can be variable given that the selected ground motions lead to suitable EFSs.

Figure 7.20 shows the acceleration response spectra of the selected ground motion records used in the development of the EFSs, along with the target response spectrum. The figure also emphasizes the spectral acceleration values at various time periods that have been considered. As the choice of earthquake records for developing EFSs relies on the similarity of the individual record spectrum to the target response spectrum shape, rather than on the magnitude of the spectra, the target response spectrum is scaled by a factor of 5. This scaling guarantees the comparability of the target response spectrum values with the values of the individual record spectrum. In Table 7.15, the spectral acceleration values of the selected ground motion records and the target response spectrum are presented. Based on this data, the GMR_{Tol} value is estimated, leading to the choice of 7 ground motion records for deriving the EFSs from the 24 considered ground motion records recorded in NE India.

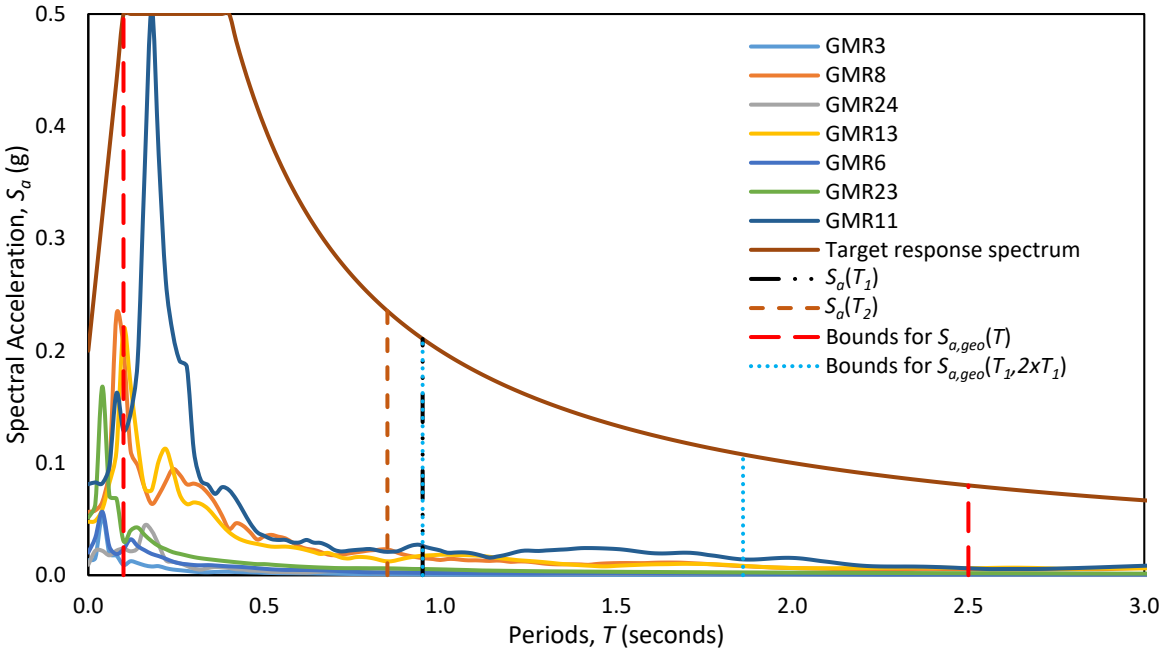

Figure 7.20 Response spectra for selected earthquake records and target response spectrum.

Table 7.15 R_{Tol} values to be used for selecting ground motion records for EFSs

Record Name	$\frac{S_a^{GMR}(T_1)}{S_a^{TRS}(T_1)}$	$\frac{S_a^{GMR}(T_2)}{S_a^{TRS}(T_2)}$	$\frac{S_{a,geo}^{GMR}(T)}{S_{a,geo}^{TRS}(T)}$	$\frac{S_{a,geo}^{GMR}(T_1,2.T_1)}{S_{a,geo}^{TRS}(T_1,2.T_1)}$	GMR_{Tol} (%)
GMR3	0.053	0.059	0.054	0.052	5.19
GMR8	0.074	0.088	0.081	0.075	8.25
GMR24	0.053	0.054	0.063	0.051	9.27
GMR13	0.084	0.067	0.081	0.082	9.63
GMR6	0.050	0.052	0.062	0.051	10.72
GMR23	0.040	0.037	0.050	0.043	13.21
GMR11	0.130	0.094	0.132	0.129	14.77

7.7.4 Estimated EFSs Using the Simplified Procedure

The current simplified procedure for developing EFSs, as discussed in the preceding section, involves performing the IDAs after selecting the earthquake records (Table 7.15). Subsequently, the fragility surfaces are estimated, varying the number of earthquake records considered in each run. The initial attempt to develop EFSs begins by considering only the first two records, namely GMR3 and GMR8, as observed from Table 7.15. Eventually, in the next trial, the EFSs are developed by including one more earthquake record in the input dataset, *i.e.*, GMR24 in addition to GMR3 and GMR8. NGMR represents the number of ground motion records considered in a set for developing EFSs in a particular trial. The EFSs estimated in consecutive trials are then compared and assessed for similarity and accuracy

using a fragility surface tolerance value (FS_{Tol}) as defined in Eq. 7.11, and other parameters in the Eqs. 7.12 to 7.17 as,

$$FS_{Tol} = 0.25\left(c_{v_{NGMR}}^{NGMR+1}\right) + 0.75\left(S_{a_{NGMR}}^{NGMR+1}\right) \tag{7.11}$$

$$c_{v_{NGMR}}^{NGMR+1} = \frac{\sum_{i=1,2}\left(c_{v_{NGMR}}^{NGMR+1}\right)_{@S_a(T_i)}}{2} \tag{7.12}$$

$$S_{a_{NGMR}}^{NGMR+1} = \frac{\sum_{i=1,2}\left(S_{a_{NGMR}}^{NGMR+1}\right)_{@S_a(T_i)}}{2} \tag{7.13}$$

$$c_{v_{S_a(T_i)}}^{NGMR+1} = c_v\left[\left\{S_{a(T_i)}^{NGMR+1}\right\}_{@16\%\,EP} ; \left\{S_{a(T_i)}^{NGMR+1}\right\}_{@50\%\,EP} ; \left\{S_{a(T_i)}^{NGMR+1}\right\}_{@84\%\,EP}\right] \tag{7.14}$$

$$c_{v_{S_a(T_i)}}^{NGMR} = c_v\left[\left\{S_{a(T_i)}^{NGMR}\right\}_{@16\%\,EP} ; \left\{S_{a(T_i)}^{NGMR}\right\}_{@50\%\,EP} ; \left\{S_{a(T_i)}^{NGMR}\right\}_{@84\%\,EP}\right] \tag{7.15}$$

$$\left(c_{v_{NGMR}}^{NGMR+1}\right)_{@S_a(T_i)} = abs\left(\frac{c_{v_{S_a(T_i)}}^{NGMR+1} - c_{v_{S_a(T_i)}}^{NGMR}}{c_{v_{S_a(T_i)}}^{NGMR}}\right) \tag{7.16}$$

$$\left(S_{a_{NGMR}}^{NGMR+1}\right)_{@S_a(T_i)} = abs\left[\frac{\left\{S_{a(T_i)}^{NGMR+1}\right\}_{@50\%\,EP} - \left\{S_{a(T_i)}^{NGMR}\right\}_{@50\%\,EP}}{\left\{S_{a(T_i)}^{NGMR}\right\}_{@50\%\,EP}}\right] \tag{7.17}$$

where FS_{Tol} is the fragility surface tolerance value; $S_a(T_i)$ is the spectral acceleration values either at the first or second natural period of the structure; $c_{v_{S_a(T)}}^{NGMR}$ is the coefficient of variation of the $S_a(T)$ values for the fragility surfaces developed for $NGMR$ set run, associated with exceedance probability (EP) of 16%, 50% and 84%; $c_{v_{S_a(T)}}^{NGMR+1}$ is the coefficient of variation of the $S_a(T)$ values for the fragility surfaces developed for $NGMR + 1$ set run, associated with exceedance probability (EP) of 16%, 50% and 84%; $\left(c_{v_{NGMR}}^{NGMR+1}\right)_{@S_a(T_i)}$ is the absolute value of the ratio of the difference between $c_{v_{S_a(T_i)}}^{NGMR+1}$ and $c_{v_{S_a(T_i)}}^{NGMR}$ corresponding to the different $S_a(T_i)$ values, and the average of $\left(c_{v_{NGMR}}^{NGMR+1}\right)_{@S_a(T_i)}$ is $c_{v_{NGMR}}^{NGMR+1}$; $\left(S_{a_{NGMR}}^{NGMR+1}\right)_{@S_a(T_i)}$ is the absolute value of the ratio of the difference between $\left\{S_{a(T_i)}^{NGMR+1}\right\}_{@50\%\,EP}$ and $\left\{S_{a(T_i)}^{NGMR}\right\}_{@50\%\,EP}$ corresponding to the different $S_a(T_i)$ values, and the average of $\left(S_{a_{NGMR}}^{NGMR+1}\right)_{@S_a(T_i)}$ is $S_{a_{NGMR}}^{NGMR+1}$. The process of developing EFSs involves performing similar trials with an updated set of earthquake records, following the sequence of records determined as per Table 7.15. These trials are continued until the FS_{Tol} value of the estimated EFSs becomes smaller than a predefined threshold value or similar FS_{Tol} values are obtained in consecutive trials.

The parameters $c_{v_{S_a(T_i)}}^{NGMR}$ and $c_{v_{S_a(T_i)}}^{NGMR+1}$, used in estimating FS_{Tol}, represent the slope of the fragility surfaces corresponding to $S_a(T_i)$ values derived considering $NGMR$ and $NGMR + 1$, respectively. A lower value of $c_{v_{S_a(T_i)}}^{NGMR}$ or $c_{v_{S_a(T_i)}}^{NGMR+1}$ indicates a more gradual fragility surface, while a higher value suggests a steeper surface. The estimated $c_{v_{NGMR}}^{NGMR+1}$ parameter represents the difference in slope between the two considered fragility surfaces. The parameter $S_{a_{NGMR}}^{NGMR+1}$ serves as a metric to assess the proximity between two considered fragility surfaces, specifically focusing on the $S_a(T_i)$ values associated with the 50% EP of a particular damage state threshold. In the comparison of two fragility estimates, the difference between the $S_a(T_i)$ values at a specific exceedance probability holds greater significance than the disparity in the slope of the surfaces. As a result, the final tolerance factor FS_{Tol} takes into account a higher contribution (75%) from the $S_{a_{NGMR}}^{NGMR+1}$ parameter, which measures the proximity of $S_a(T_i)$ values, and a lesser contribution (25%) from the slope comparison $c_{v_{NGMR}}^{NGMR+1}$ parameter. A tolerance factor FS_{Tol} value of 10% is used to assess the accuracy of the ensuing EFSs. To evaluate the adequacy of the assumed FS_{Tol} value of 10%, the derived EFSs are compared with the fragility surfaces developed using complete set of ground motion records.

The EFSs are derived for different damage state levels of the considered RC wall-frame building, using a varying set of ground motion records as listed in Table 7.15. The final adopted EFSs are the ones that satisfy the predefined value of FS_{Tol} or the ones that do not reflect a significant reduction in FS_{Tol} value with an increase in the number of earthquake records used. Table 7.16 presents the computed FS_{Tol} values for each successive increase in the number of considered earthquake records. The data in this table indicate that the FS_{Tol} values are below the predefined limit of 10% for the derived EFSs in two consecutive runs, considering 6 and 7 ground motion records. Using the values from the previous run as a benchmark, the computed FS_{Tol} values for the 'minor,' 'moderate,' 'extensive,' and 'complete' damage states are (2.19%, 3.16%, 3.64%, 3.83%) and (2.41%, 2.27%, 2.51%, 2.60%) for the EFSs generated considering 6 ground motion records and 7 ground motion records, respectively. This suggests that when 7 ground motion records are used to estimate EFSs, there is no significant improvement observed in the resulting FS_{Tol} values as compared to those obtained considering 6 records. Thus, among the 7 chosen ground motion records tabulated in Table 7.15, it is found that 6 input records are sufficient to generate EFSs with satisfactory FS_{Tol} values.

The estimated EFSs are compared with the All-Inclusive Fragility Surfaces (AIFSs), derived using the complete set of ground motion records. This comparison verifies the adequacy and appropriateness of the estimated EFSs and confirms the sufficiency of the assumed values of GMR_{Tol} and FS_{Tol} used in generating the EFSs. Figures 7.21 to 7.24 illustrate the comparison between the EFSs and the AIFSs developed for different damage state levels of the considered RC wall-frame building. Additionally, these figures present the 2D planar view of the fragility estimates corresponding to the two considered IMs, plotted along both axes. The data presented in these figures demonstrate a strong qualitative agreement between the EFSs and AIFSs derived for the RC wall-frame building. Also, the 2D view of the fragility estimates corresponding to the EFSs and the AIFSs shows a close proximity. Table 7.17 provides a quantitative assessment and comparison of the derived EFSs and AIFSs by presenting the conditional exceedance probability of the different damage state levels estimated from both sets at specific intensity levels. The largest variation between the fragility estimates from the EFSs and the AIFSs, in terms of exceedance probability for 'minor', 'moderate', 'extensive', and 'complete' damage states at the different considered intensity levels, is found to be 4.75%, 5.70%, 4.80%, and 5.28%, respectively. The discrepancies in exceedance probabilities between the EFSs and the AIFSs are minimal and inconsequential when considering the reduction in time and effort required for generating EFSs using fewer input records. By utilizing only 6 ground motion records out of the 24 records used for deriving the AIFSs, the resulting EFSs are deemed acceptable, leading to a noteworthy reduction in both time and computational effort. This approach makes the entire process of estimating fragility surfaces for the considered RC wall-frame building computationally less demanding while achieving relatively dependable results.

Table 7.16 FS_{Tol} values resulting from the EFSs generated using different number of considered ground motion records

NGMR	Damage State	$\{S_{a(T_i)}^{NGMR}\}_{@}$, (g)						$c_{v_{S_a(T_i)}}^{NGMR}$		$(c_{v_{NGMR}}^{NGMR+1})_{@S_a(T_i)}$		$c_{v_{NGMR}}^{NGMR+1}$	$(S_{a_{NGMR}}^{NGMR+1})_{@S_a(T_i)}$		$S_{a_{NGMR}}^{NGMR+1}$	FS_{Tol} (%)
		@16% EP		@50% EP		@84% EP		$S_a(T_1)$	$S_a(T_2)$	$S_a(T_1)$	$S_a(T_2)$		$S_a(T_1)$	$S_a(T_2)$		
		$S_a(T_1)$	$S_a(T_2)$	$S_a(T_1)$	$S_a(T_2)$	$S_a(T_1)$	$S_a(T_2)$									
2	Minor	0.083	0.101	0.104	0.125	0.129	0.156	0.217	0.218	-	-	-	-	-	-	-
	Moderate	0.250	0.303	0.306	0.371	0.374	0.453	0.200	0.200	-	-	-	-	-	-	-
	Extensive	0.466	0.565	0.571	0.692	0.698	0.845	0.201	0.201	-	-	-	-	-	-	-
	Complete	0.576	0.697	0.706	0.856	0.866	1.049	0.203	0.203	-	-	-	-	-	-	-
3	Minor	0.077	0.090	0.097	0.113	0.135	0.157	0.283	0.283	0.299	0.300	0.300	0.060	0.098	0.079	13.4
	Moderate	0.229	0.266	0.290	0.338	0.371	0.431	0.240	0.241	0.203	0.204	0.204	0.053	0.090	0.072	10.5
	Extensive	0.424	0.493	0.542	0.630	0.694	0.807	0.245	0.245	0.220	0.221	0.221	0.052	0.089	0.070	10.8
	Complete	0.522	0.608	0.670	0.779	0.859	1.001	0.247	0.247	0.218	0.219	0.218	0.052	0.089	0.071	10.8
4	Minor	0.089	0.095	0.110	0.117	0.137	0.147	0.218	0.218	0.230	0.229	0.229	0.129	0.038	0.083	12.0
	Moderate	0.260	0.279	0.323	0.346	0.402	0.431	0.217	0.217	0.098	0.097	0.097	0.112	0.024	0.068	7.56
	Extensive	0.478	0.513	0.597	0.641	0.748	0.802	0.222	0.223	0.092	0.091	0.092	0.103	0.016	0.059	6.75
	Complete	0.588	0.631	0.737	0.790	0.925	0.993	0.225	0.225	0.091	0.089	0.090	0.100	0.014	0.057	6.54
5	Minor	0.081	0.087	0.103	0.111	0.131	0.141	0.238	0.238	0.093	0.092	0.093	0.062	0.055	0.058	6.68
	Moderate	0.231	0.249	0.299	0.322	0.386	0.416	0.255	0.255	0.175	0.173	0.174	0.074	0.068	0.071	9.69
	Extensive	0.419	0.452	0.550	0.593	0.720	0.776	0.268	0.268	0.206	0.204	0.205	0.079	0.075	0.077	10.9
	Complete	0.514	0.554	0.677	0.730	0.891	0.961	0.273	0.273	0.214	0.212	0.213	0.080	0.076	0.078	11.2
6	Minor	0.082	0.087	0.103	0.109	0.129	0.137	0.223	0.224	0.062	0.061	0.061	0.002	0.015	0.009	2.20
	Moderate	0.232	0.246	0.295	0.313	0.375	0.398	0.238	0.239	0.065	0.064	0.064	0.012	0.029	0.021	3.17
	Extensive	0.418	0.443	0.539	0.572	0.694	0.736	0.251	0.251	0.065	0.064	0.064	0.019	0.035	0.027	3.64
	Complete	0.512	0.543	0.663	0.703	0.856	0.909	0.255	0.255	0.065	0.064	0.065	0.022	0.037	0.030	3.83
7	Minor	0.086	0.086	0.107	0.107	0.133	0.134	0.219	0.220	0.019	0.017	0.018	0.034	0.019	0.026	2.41
	Moderate	0.237	0.238	0.302	0.304	0.385	0.388	0.242	0.243	0.015	0.017	0.016	0.021	0.028	0.025	2.27
	Extensive	0.422	0.426	0.547	0.552	0.709	0.717	0.257	0.258	0.027	0.029	0.028	0.014	0.035	0.024	2.51
	Complete	0.515	0.520	0.670	0.677	0.875	0.885	0.263	0.264	0.031	0.033	0.032	0.012	0.036	0.024	2.60

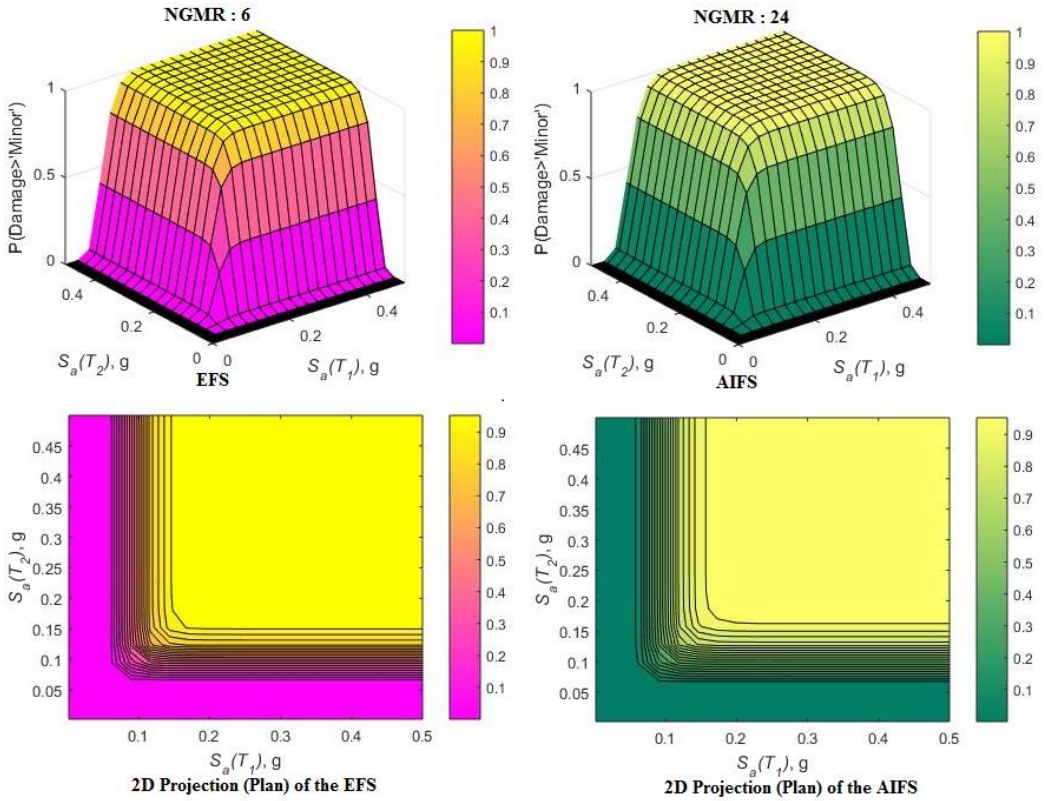

Figure 7.21 Comparison of EFS, derived using 6 ground motion records, with AIFS for the minor damage state.

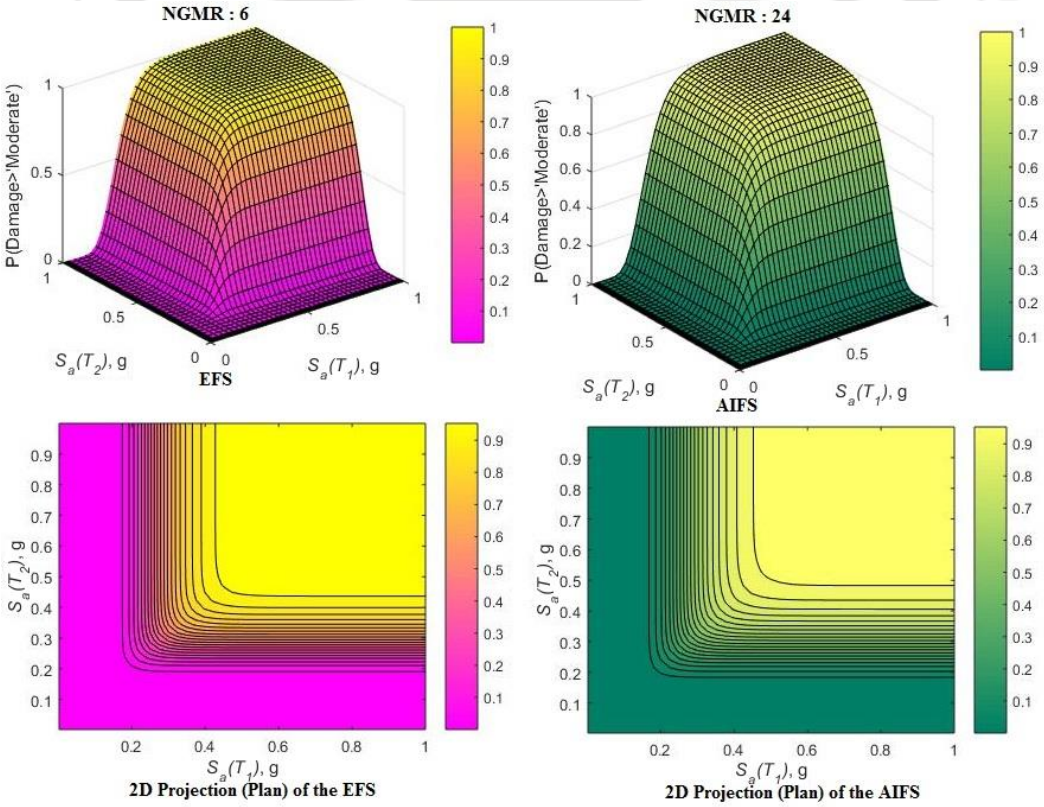

Figure 7.22 Comparison of EFS, derived using 6 ground motion records, with AIFS for the moderate damage state.

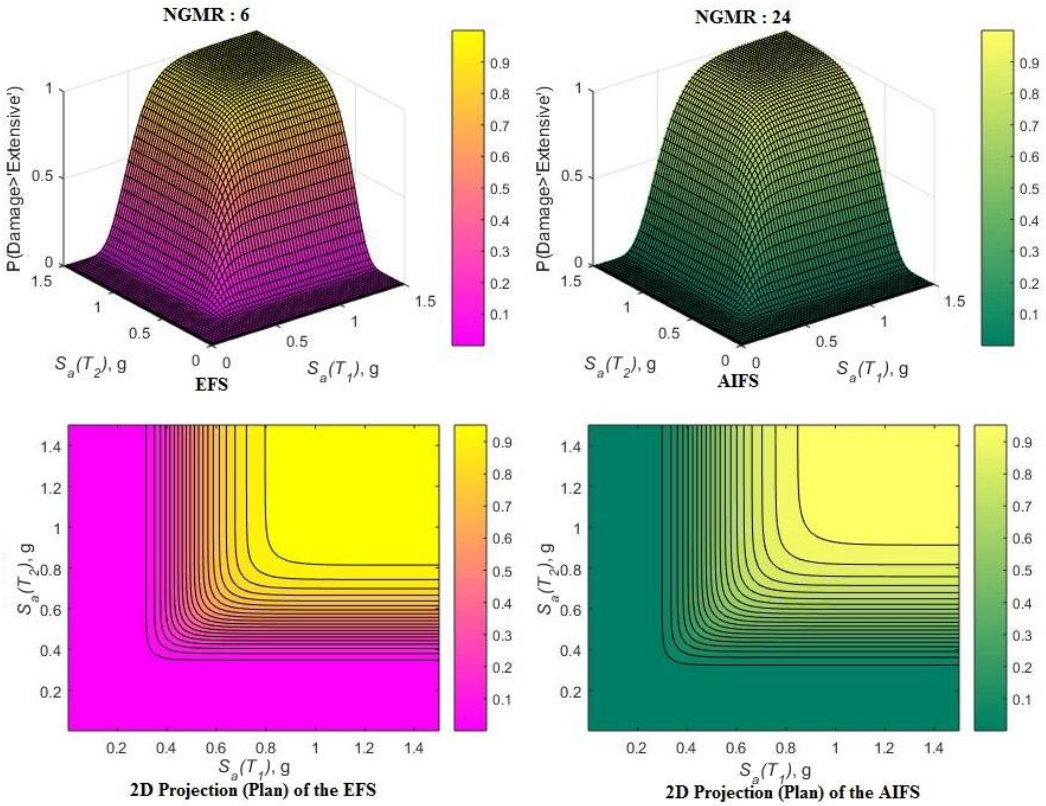

Figure 7.23 Comparison of EFS, derived using 6 ground motion records, with AIFS for the extensive damage state.

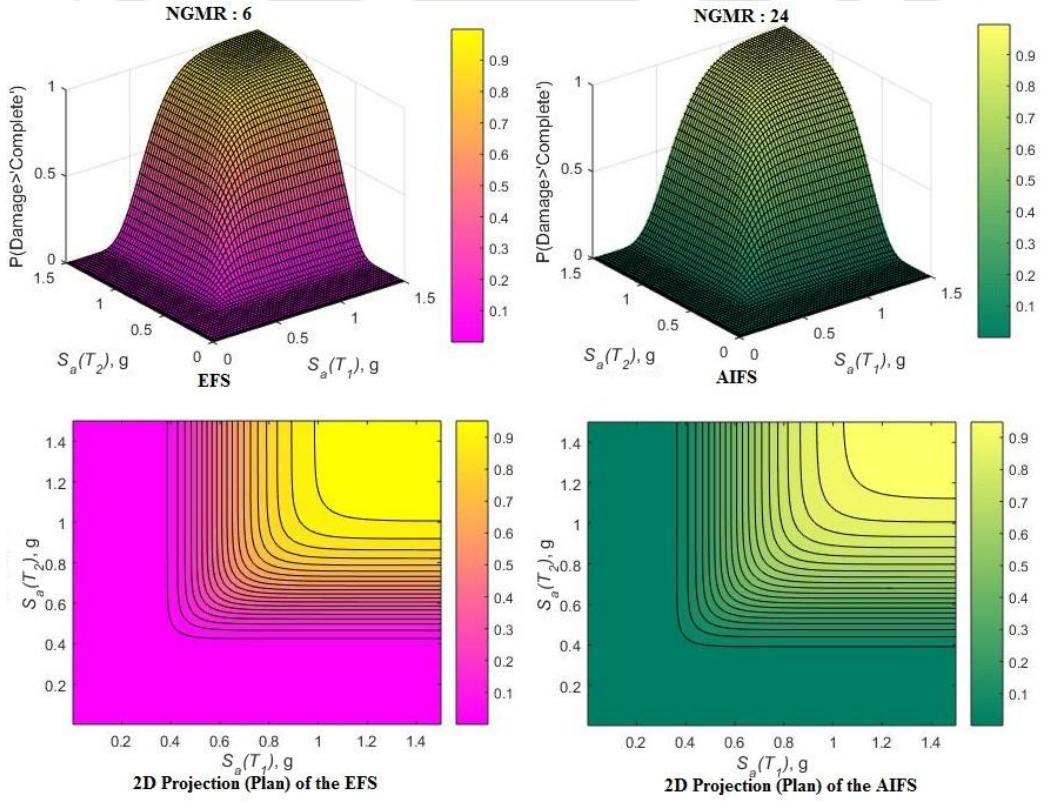

Figure 7.24 Comparison of EFS, derived using 6 ground motion records, with AIFS for the complete damage state.

Table 7.17 Exceedance probability of different damage states, estimated from the EFSs and the AIFSs at specific intensity levels

Seismic Intensity Level	$S_a(T_1)$, g $S_a(T_2)$, g	**0.1**		**0.2**		**0.4**		**0.6**		**0.8**		**1.0**	
Fragility Surface		**AIFS**	**EFS**	**AIFS**	**EFS**	**AIFS**	**EFS**	**AIFS**	**EFS**	**AIFS**	**EFS**	**AIFS**	**EFS**
Exceedance probability of Damage State	**Minor**	0.39	0.34	0.99	1.00	1.00	1.00	1.00	1.00	1.00	1.00	1.00	1.00
	δ_{minor} **(%)**	4.75		0.68		-		-		-		-	
	Moderate	0.00	0.00	0.05	0.04	0.80	0.86	0.99	1.00	1.00	1.00	1.00	1.00
	$\delta_{moderate}$ **(%)**	-		1.24		5.70		0.74		0.04		-	
	Extensive	0.00	0.00	0.00	0.00	0.12	0.10	0.56	0.61	0.87	0.92	0.97	0.99
	$\delta_{extensive}$ **(%)**	-		0.02		2.17		4.40		4.80		1.86	
	Complete	0.00	0.00	0.00	0.00	0.03	0.02	0.31	0.30	0.67	0.72	0.88	0.92
	$\delta_{complete}$ **(%)**	-		-		1.53		0.42		5.28		4.68	

δ_{DS} = Difference in exceedance probability of specific damage states

7.8 Summary and Conclusions

In this chapter, the findings from the preceding chapters are used for estimation of seismic fragility for the considered building typology, namely RC wall-frame building. The influence of epistemic uncertainty along with the commonly considered aleatory uncertainty on the fragility relations is assessed. Additionally, the variability of the fragility functions derived for both the RC wall-frame building and a typical exterior RC wall-frame taken from the reference building, is also studied. Moreover, the fragility functions for the considered building typology have been developed while considering scalar IM as well as vector-valued IMs. Finally, a simplified procedure for deriving reliable fragility estimates, achieved through a reduced number of ground motion records, is developed while maintaining comparability with the fragility estimates developed using the complete set of records.

The salient conclusions drawn from this chapter are summarized as follows:

- The incorporation of both aleatory and epistemic uncertainties in the analysis leads to higher dispersion values (β) of response parameters at different damage state thresholds, the dispersion tends to reduce from the minor damage state to the complete damage state. Epistemic uncertainty's significance is more pronounced for lower damage states, and its influence increases as damage states shift from complete to minor. Consequently, the fragility relations developed for the RC wall-frame exhibit discrepancies of 7.13%, 6.00%, 5.65%, and 5.41% for the exceedance probability of minor, moderate, extensive, and complete damage states, respectively, when comparing analysis results with only aleatory uncertainty to those with both aleatory and epistemic uncertainties. These results underscore the importance of considering both types of uncertainties to accurately assess the seismic vulnerability of structures.
- The fragility relations derived for the RC wall-frame using vector-valued IMs, particularly spectral acceleration at the first two natural periods, exhibit significant variations in damage exceedance probability as compared to those obtained from the fragility curves conditioned on specific damage state levels. Based on the desired level of accuracy for fragility estimates, the spectral acceleration difference at the first two natural periods for a specific RC wall-frame structure can determine whether to opt for single IM (simplistic) or two IMs (computationally expensive) when deriving fragility functions.

- The assessment of fragility relations for a RC wall-frame building, developed using scalar and vector-valued IMs, indicates a higher vulnerability of response parameters to seismic demand as compared to the analysis of a 2D model of the building. While 2D analysis is favoured for its simplicity and computational efficiency, it yields conservative fragility estimates for this specific building typology. Therefore, for accurate structural performance and subsequently vulnerability assessment, it is recommended to analyse a 3D model of the structural system, especially for wall-frame buildings.
- The simplified procedure for estimating Efficient Fragility Surfaces (EFSs) for the specific RC wall-frame building demonstrates significant improvements in reducing the required time and effort as compared to development of All-Inclusive Fragility Surfaces (AIFS) with a complete set of records. The differences in exceedance probabilities between the EFSs and AIFSs are negligible and not of consequence, in light of the reduced time and effort needed to generate EFSs with fewer input records. By utilizing only six ground motion records out of the twenty-four used for deriving AIFSs, the resulting EFSs are deemed acceptable, leading to a noteworthy reduction in both time and computational effort. This approach makes the entire process of estimating fragility surfaces for the considered RC wall-frame building computationally less demanding while achieving relatively reliable results.

CHAPTER 8

SUMMARY, CONCLUSION AND FUTURE SCOPE

8.1 Overview

In earthquake-prone regions, the lateral load-resisting system of multi-storied RC frame buildings is enhanced with the presence of RC structural walls. Understanding the seismic behaviour of RC structural wall framing system is important for carrying out seismic vulnerability assessment of such buildings. As part of seismic vulnerability assessment, developing fragility relationships is required to estimate the extent of damage under different levels of shaking, and it is quantified though the computation of exceedance probability for a particular damage state. The intention of the present study is to assess seismic fragility functions for RC wall-frame buildings. This chapter offers a summary of the entire study, highlights the primary findings, and enumerates the study's limitations and potential scope of work for future research.

8.2 Summary

The current study endeavours to perform a thorough seismic fragility assessment of RC wall-frame buildings. To accomplish this, it involves exhaustive nonlinear dynamic analyses to establish accurate fragility functions for the considered building typology. A detailed examination of various aspects related to the fragility assessment of RC wall-frame buildings is conducted. The following outlines the key components and steps taken in the present study:

Preliminary Analysis: The response analysis for the considered RC wall-frame building as well as the extracted exterior RC wall-frame structure is based on finite element modelling, along with consideration of appropriate material and geometric properties. To ensure the reliability of modelling methodology, the same has been validated by comparing the numerical results with experimentally obtained results from past studies. Also, the appropriate EDP is selected for accurately characterising structural response-seismic demand relationship, along with the suite of ground motion records among two different sets, for reliable fragility assessment through nonlinear dynamic analysis.

Sensitivity Analysis: Various random variables representing uncertainty in structural characteristics have been identified, encompassing factors such as the viscous damping ratio,

concrete compressive strength, building mass, yield strength of steel, and the elastic modulus of concrete and steel rebar. Through the application of Latin Hypercube Sampling, 200 different structural models of the RC wall-frame structure have been generated, each incorporating unique realization of the input random variables. These models have been subsequently analysed to investigate the influence of the considered variability in uncertain structural parameters. Modern Machine Learning (ML) algorithms and conventional Sobol's Indices have been utilized to determine the relative significance of these uncertain structural parameters on various response parameters.

Uncertainty Treatment: In order to achieve a reliable seismic fragility assessment, randomness in structural capacity and variability across different seismic records are investigated. This has been achieved by employing extended Incremental Dynamic Analysis (IDA) for the RC wall-frame building, encompassing 20 different structural models and 11 ground motion records for characterizing the epistemic and aleatory uncertainties, respectively. Furthermore, the influence of uncertainties on the seismic response assessment of the considered RC wall-frame structure is quantified, based on statistical analysis of outcomes derived from the nonlinear response history analysis of the RC wall-frame structure.

Damage State Threshold: For the RC wall-frame structure, Genetic Programming (GP) is employed to propose closed-form expressions for lateral drift to identify the various damage state thresholds. A dataset of 8,125 numerically studied specimens of RC structural walls has been utilized, taking into account design characteristics such as wall aspect ratio, axial load ratio, boundary element reinforcement ratios, and boundary element length to wall length ratio. The accuracy of the developed lateral drift expressions is checked using statistical measures and through comparison with other available deformation limits in relevant design standards and literature.

Fragility Function Formulation: Fragility relationships have been developed and assessed for a specific RC wall-frame structure and an entire RC wall-frame building, considering the influence of both epistemic uncertainty and the commonly considered aleatory uncertainty, as well as scalar IMs as well as vector-valued IMs. Finally, a simplified procedure is developed for deriving reliable fragility estimates, using a reduced number of ground motion records while still ensuring comparability with fragility estimates derived using the complete set of records.

8.3 Conclusions

The salient conclusions from the present study are mentioned as follows:

Preliminary Analysis

- For two sets of ground motion record, selected either based on strong ground motion factors (peak ground acceleration, peak ground velocity) or geophysical factors (magnitude, source-to-site distance), the median outcomes for inter-storey drift (ISD) as the response parameter for RC wall-frame buildings exhibit virtual equivalence when one set of records is adjusted to align with the median spectral acceleration of the other set. Thus, the choice of ground motion between the two sets is expected to exert negligible influence on the seismic response of the examined RC wall-frame building with the appropriate response parameter as ISD.
- Inter-storey drift as the EDP provides a more accurate estimate of seismic response for RC wall-frame buildings as compared to other response parameters, as it exhibits the least variability from the regression line in IDA outcomes, signifying its robustness against randomness in input ground motion. The minimal variation is also indicated by the estimated coefficient of variation in ISD values across various seismic intensity levels. ISD has a significantly strong correlation coefficient with the seismic IM as the spectral acceleration at the fundamental period ($S_a(T_1)$).

Sensitivity Analysis

- Within the set of investigated uncertain structural parameters, the viscous damping ratio, concrete compressive strength, and building mass substantially impact response variability for RC wall-frame structure, underscoring the importance of prioritizing these factors to diminish variability and improve the effectiveness of subsequent uncertainty analyses.
- The yield strength of steel reinforcement and the modulus of elasticity of concrete and steel reinforcement minimally impact response variability of RC wall-frame structure, accounting for less than 5% of the total variation in response variables and can be treated as deterministic variables with fixed values within the analysis framework. This is expected to hold good for other configurations of RC wall as well, and this leads to further simplification of the computational effort for fragility estimation.

- Variability in ground motion tends to have a significant influence on the seismic response parameters. With higher EDPs, response variation also increases with the ascending seismic intensity level.
- Comparing the effects of uncertain structural parameters and record-to-record variability on response variation reveals that the former dominate at lower intensity levels, while the latter takes precedence at higher intensity levels.

Uncertainty Treatment

- For realistic estimate of fragility function of RC wall-frame structure, the effects of both epistemic uncertainty and the aleatory uncertainty should be considered in the analysis.
- The contribution of epistemic uncertainties to the total response variability ranges from approximately 10% at higher seismic intensity levels ($S_a(T_1)$ = 2g) to a substantial 45% at lower seismic intensity levels ($S_a(T_1)$ = 0.1g), highlighting the indispensability of considering epistemic uncertainties.
- Integrating both aleatory and epistemic uncertainties in the analysis leads to higher dispersion values (β) of response parameters as compared to considering only aleatory uncertainty at different damage state thresholds.
- Incorporating all uncertain epistemic variables, regardless of seismic intensity levels, leads to β_E values that are only slightly higher, with an increment ranging from 2.8% at $S_a(T_1)$ = 0.1g to 7.8% at $S_a(T_1)$ = 2g, as compared to considering only the important uncertain parameters. Thus, efficient characterization of epistemic uncertainty in the analysis framework can be achieved by using only the important variables, thereby reducing the computational time and effort.

Damage State Threshold

- For the different damage state thresholds in the RC wall-frame structure, the GP-based prediction models demonstrate excellent efficacy in predicting lateral drift levels for testing data outside the training data domain, as evidenced by multiple performance assessment metrics and other external validation measures.
- The proposed prediction expressions show strong potential in estimating lateral drift levels pertaining to different damage characteristics observed in several existing experimental studies involving RC structural wall specimens.
- A comparison between the effectiveness of several existing damage state definitions and the developed damage prediction models reveals that the proposed expressions provide

more accurate predictions of experimental results than the other damage state thresholds considered earlier in the past studies.

Fragility Function Formulation

- Despite substantial response variability stemming from various sources of uncertainty, the fragility relations established for the RC wall-frame structure demonstrate maximum disparity of less than 8% in terms of exceedance probability for all the four damage states. This outcome was noted during comparison of the analyses that account solely for aleatory uncertainty to those that consider both aleatory and epistemic uncertainties.
- The fragility relations derived for the RC wall-frame using vector-valued IMs, particularly spectral acceleration at the first two natural periods, show significant variations in damage exceedance probability as compared to those obtained from fragility curves (using a single IM of $S_a(T_1)$), conditioned on specific damage state levels.
- The average deviation between the comprehensive fragility surface (considering two IMs) and the simplified fragility curves (based on a single IM) for the RC wall-frame structure is 2%, 20%, 30%, and 45%, depending on spectral acceleration differences at the first two natural periods exceeding specific thresholds of 100%, 60%, 40%, and 40%, corresponding to ‘minor’, ‘moderate’, ‘extensive’, and ‘complete’ damage state levels, respectively.
- The choice between transitioning from a single IM to two IMs when developing fragility functions for a particular RC wall-frame structure is contingent upon the desired level of accuracy in the fragility estimates, influenced by the spectral acceleration difference at the structure's first two natural periods, with the consideration of two IMs leading to greater precision inspite of higher computational demand.
- The evaluation of fragility relations for the overall RC wall-frame building, utilizing both scalar and vector-valued IMs, reveals greater vulnerability of response parameters to seismic demand when compared to those derived from the analyses of a 2D RC wall-frame representation of the structure.
- As indicated by the median IM value corresponding to the exceedance of the damage state thresholds, the increase in the vulnerability for the overall RC wall-frame building is observed to be in the range of 8% to 17% as compared to those obtained for the 2D RC wall-frame structure.

- The simplified approach for estimating Efficient Fragility Surfaces (EFSs) for the specific RC wall-frame building significantly reduces the time and effort required as compared to developing All-Inclusive Fragility Surfaces (AIFS) using the complete set of ground motion records from the North-Eastern region of India.
- The maximum difference between the fragility estimates derived from the EFSs and the AIFSs for the considered structure is less than 6%, concerning exceedance probabilities for all the four damage states.
- Utilizing only 6 of the original 24 ground motion records for deriving EFSs leads to very less differences in the exceedance probabilities between the EFSs and AIFSs, along with a notable reduction in both time and computational effort.

8.4 Recommendations from the Present Study

In accordance with the conclusions drawn from the study, the following recommendations can be provided regarding the incorporation of specific factors into seismic response analysis for an efficient fragility assessment, particularly for the RC wall-frame building typology.

- **Addressing Uncertainty Sources:** The prevailing approach of solely considering aleatory uncertainty to account for seismic response variability in RC wall-frame buildings, as adopted by numerous researchers, represents an oversimplification that may lead to unfavourable outcomes. Recognizing the insights gleaned from the present study, it is underscored that accounting for both epistemic and aleatory sources of uncertainties is indispensable for ensuring a dependable vulnerability assessment for the mentioned building typology, even with a requirement of greater computational time and effort.
- **Comprehensive Building Analysis:** In light of the outcomes yielded by the assessment, it is reasonable to assert that the conventional practice of analysing a representative frame instead of the entire RC wall-frame building, with the aim of simplification and assuming equivalent behaviour, can lead to notably conservative fragility estimates. Regardless of the performance level under consideration and whether single or multiple IMs are employed, evaluating the entire building yields fragility estimates that are relatively more vulnerable as compared to those derived from an individual frame. This underscores the importance of assessing the entire building system, despite the potential increase in computational time and effort.
- **Utilizing Vector-Valued IMs:** When the difference between spectral accelerations for the first two natural periods of an RC wall-frame building exceeds 50%, it is advisable to

derive fragility surfaces using vector-valued IMs, except for the 'minor' damage state level where fragility curves and fragility surfaces exhibit similar damage threshold exceedance probabilities.

- **Simplified Fragility Assessment Framework:** The proposed framework for developing fragility surfaces for RC wall-frame buildings, using a smaller set of ground motion records, can significantly reduce the computational time and effort required. Even when reducing the number of considered ground motion records by 75%, the resulting difference in fragility estimates remains minimal, typically around 6%, thus emphasizing its practical significance.

8.5 Limitations of the Present Study

The findings presented in the dissertation are subject to the following limitations:

- The conclusions from the study are typical to the mid-rise 8-storey RC wall-frame building.
- The fragility assessment framework employed in the present study does not account for the influence of plan and vertical irregularities in the building on its seismic structural behaviour.
- The presence of infill walls in the building is not considered in the seismic fragility assessment of the RC wall-frame building.
- No soil-structure interaction is considered in the present study on the fragility assessment of RC wall-frame building.
- The present study does not take into account the impact of near-field ground motion records, including the pulse-type effect on seismic response.

8.6 Future Scope of Work

The study can be expanded by addressing some of the aforementioned limitations and exploring the following aspects:

- The analytical fragility relationships derived using the framework employed in the present study can be extended for integration with seismic hazard assessments and structural repair cost considerations. This integration can facilitate the evaluation of seismic vulnerability and, consequently, support risk assessment.

- Expanding the present study could involve investigating the impact of strategically placed structural walls within the building plan on resulting fragility estimates.
- The analytical framework utilized in the present study has the potential to serve as a valuable tool for generating fragility estimates for diverse structural components and systems subjected to various types of hazards in future research.

REFERENCES

Abdullah, S.A., and Wallace, J.W. (2019). "Drift capacity of reinforced concrete structural walls with special boundary elements." *ACI Structural Journal*, 116(1): 183-194.

ACI. (2019). "Building code requirements for structural concrete." ACI 318-19, *American Concrete Institute*, Farmington Hills, MI.

Ahangar-Asr, A., Faramarzi, A., Mottaghifard, N., and Javadi, A. (2011). "Modelling of permeability and compaction characteristics of soils using evolutionary polynomial regression." *Computers and Geosciences*, 37 (11): 1860–1869.

Ahmed, B.F., and Dasgupta, K. (2022). "Seismic limit states of the components in reinforced concrete integral abutment bridges." *Bulletin of Earthquake Engineering*, 20: 477-516.

Alwaeli, W., Mwafy, A., Pilakoutas, K., and Guadagini, M. (2016). "A methodology for defining seismic scenario-structure-based limit state criteria for RC high-rise wall buildings using net drift." *Earthquake Engineering and Structural Dynamics*, 46:1325-1344.

Alwaeli, W., Mwafy, A., Pilakoutas, K., and Guadagini, M. (2020). "Rigorous versus less-demanding fragility relations for RC high-rise buildings." *Bulletin of Earthquake Engineering*, 18: 5885-5918.

ASCE. (2007). "Seismic rehabilitation of existing buildings." ASCE/SEI 41-06, *American Society of Civil Engineers* (ASCE), Reston, VA.

ASCE. (2010). "Minimum design loads for buildings and other structures." ASCE/SEI 7-10, *American Society of Civil Engineers* (ASCE), Reston, VA.

ASCE. (2013). "Seismic evaluation and retrofit of existing buildings." ASCE/SEI 41-13, *American Society of Civil Engineers*, Reston, VA.

Aslani, H., Cabrera, C., and Rahnama, M. (2012). "Analysis of the sources of uncertainty for portfolio- level earthquake loss estimation." *Earthquake Engineering and Structural Dynamics*, 41(11): 1549–68.

ATC. (1985). "Earthquake damage evaluation data for California." ATC-13, *Applied Technology Council*, Redwood City, CA.

ATC. (2009). "Guidelines for seismic performance assessment of buildings." ATC-58 50% Draft, *Applied Technology Council*, Redwood City, CA.

ATC. (1996). "Seismic Evaluation and Retrofit of Concrete Buildings." ATC-40, *Applied Technology Council*, Volumes 1 and 2, Redwood City, CA.

Baker, J.W., and Cornell, C.A. (2005). "A vector-valued ground motion intensity measures consisting of spectral acceleration and epsilon." *Earthquake Engineering and Structural Dynamics*, 34: 1193-1217.

Baker, J.W., and Cornell, C.A. (2008). “Uncertainty propagation in probabilistic seismic loss estimation.” *Structural Safety*, 30(3): 236–252.

Barbat, A.S., Pujades, L.G., and Lantada, N. (2007). “Seismic damage evaluation in urban areas using the capacity spectrum method: Application to Barcelona.” *Soil Dynamics and Earthquake Engineering*, 28: 851-865.

Basoz, N., and Kiremidjian, A.S. (1997). “Evaluation of bridge damage data from the Loma Prieta and Northridge CA earthquakes (Report No. MCEER-98-0004).” Buffalo, NY: MCEER, University at Buffalo, The State University of New York.

Benjamin, J.R. and Cornell, C.A. (1970). “Probability, Statistics and Decision for Civil Engineers.” McGraw Hill, Inc., New York.

Beyer, K., Dazio, A., and Priestley, M.J.N. (2008). “Quasi-static cyclic tests of two u-shaped reinforced concrete walls.” *ASCE Journal of Structural Engineering*, 12(7): 1023-1053.

Billah, A., and M, Alam. (2014). “Seismic fragility assessment of highway bridges: A state-of-the-art review.” *Structure and Infrastructure Engineering*, 1–29.

Birely, A.C. (2012). “Seismic performance of slender reinforced concrete structural walls.” PhD Dissertation, University of Washington.

BIS. (2000). “Plain and reinforced concrete–code of practice.” IS:456, *Bureau of Indian Standards*, New Delhi, India.

BIS. (2016a). “Ductile design and detailing of reinforced concrete structures subjected to seismic forces–code of practice.” IS:13920, *Bureau of Indian Standards*, New Delhi, India.

BIS. (2016b). “Criteria for earthquake resistant design of structures – Part 1: General provision and buildings.” IS:1893 (Part 1), *Bureau of Indian Standards*, New Delhi, India.

Breiman, L. (1996). “Bagging predictors.” *Machine Learning*, 24(2): 123-140.

Calvi, G.M., Pinho, R., Magenes, G., Boomer, J.J., Restrepo-Velez, L.F. and Crowley, H. (2006). “Development of seismic vulnerability assessment methodologies over the past 30 years.” *ISET Journal of Earthquake Technology*, 43(3): 75-104.

Celik, O.C., and Ellingwood, B.R. (2010). “Seismic fragilities for non-ductile reinforced concrete frames–Role of aleatoric and epistemic uncertainties.” *Structural Safety*, 32(1): 1–12.

CEN. (2003). “Eurocode 8: design of structures for earthquake resistance—part 1: general rules, seismic actions and rules for buildings.” *European Committee for Standardisation* (CEN), Brussels.

Chaallal, O., and Ghlamallah, N. (1996). “Seismic response of flexibly supported coupled shear walls.” *Journal of Structural Engineering*, 122(10): 1187–1197.

Chen, T., and Guestrin, C. (2016). "XGBoost: A Scalable Tree Boosting System." In: *Proceedings of 22nd ACM SIGKDD International Conference on Knowledge Discovery and Data Mining*, 785–794.

Chopra, A.K., and Goel, R.K. (2000). "Evaluation of NSP to estimate seismic deformation: SDF systems." *ASCE Journal of Structural Engineering*, 126(4): 482–490.

Choudhury, T., and Kaushik, H.B. (2018). "Seismic response sensitivity to uncertain variables in RC frames with infill walls." *ASCE Journal of Structural Engineering*, 144 (10): 04018184.

Choudhury, T., and Kaushik, H.B. (2019). "Treatment of uncertainties in seismic fragility assessment of RC frames with masonry infill walls." *Soil Dynamics and Earthquake Engineering*; 126: 105771.

Cimellaro, G.P., Reinhorn, A.M., D'Ambrisi, A., and De Stefano, M. (2011). "Fragility analysis and seismic record selection." *ASCE Journal of Structural Engineering*, 137(3): 379-390.

Clemen, R.T., and Winkler, R.L. (1999). "Combining probability distributions from experts in risk analysis." *Risk Analysis*, 19: 187-203.

Cooke, R.M. (1991). "Experts in uncertainty - opinion and subjective probability in science." Environmental Ethics and Science Policy Series. Oxford University Press, New York 10016.

Cooke, R.M., and Goossens, L.H.J. (2000). "Expert Judgment Elicitation in Risk Assessment." In: *Assessment and Management of Environmental Risks*. NATO Science Series, 4, Springer, Dordrecht.

Cordova, P.P., Deierlein, G.G., Mehanny, S.S.F., and Cornell, C.A. (2000). "Development of a two-parameter seismic intensity measure and probabilistic assessment procedure." In: *Proceedings of 2nd U.S.-Japan Workshop on PBEE Methodology for Reinforced Concrete Building Structures*, Sapporo, Japan.

Cornell, C.A., Jalayer, F., Hamburger, R.O., and Foutch, D.A. (2002). "Probabilistic basis for 2000 SAC federal emergency management agency steel moment frame guidelines. *Journal of Structural Engineering*, 128 (4): 526–533.

Crozet, V., Politopoulos, I., Yang, M., Martinez, J.M., and Erlicher. S. (2018). "Sensitivity analysis of pounding between adjacent structures." *Earthquake Engineering and Structural Dynamics*, 47 (1): 219–235.

CSI (2015). "Structural Analysis Program (SAP2000) – Advanced, static and dynamic finite element analysis of structures," Computers and Structures Inc., Berkeley, USA.

Dabaghi, M., Saad, G., and Allhassania, N. (2019). "Seismic collapse fragility analysis of reinforced concrete shear wall buildings." *Earthquake Spectra*, 35(1): 383-404.

Dalkey, N. (1969). “The Delphi method: An experimental study of group opinion.” *Futures*, 1(5): 408-426.

D’Ayala, D., Meslem, A., Vamvatsikos, D., Porter, K., Rossetto, T., Crowley, H. and Silva, V. (2014). “Guidelines for analytical vulnerability assessment of low/mid-rise buildings – methodology.” Vulnerability Global Component Project. GEM Technical Report. GEM Foundation. Pavia, Italy.

D'Ayala, D., and Yeomans, D. (2004). “Assessing The Seismic Vulnerability of Late Ottoman Buildings in Istanbul.” In: *Proceedings of the IV International Seminar on Structural Analysis of Historical Constructions* - SAHC04, Padua, Italy.

Dazio, A., Beyer, K., and Bachmann, H., (2009). “Quasi-static cyclic tests and plastic hinge analysis of RC structural walls.” *Engineering Structures*, 31: 1556-1571.

Deger, Z.T., and Wallace, J.W. (2016). “Seismic performance of reinforced concrete dual-system buildings designed using two different design methods.” *The Structural Design of Tall and Special Buildings*, 25: 45-59.

Deger, Z.T., Yang, T.Y., Wallace, J.W., and Moehle, J. (2016). “Seismic performance of reinforced concrete core wall buildings with and without moment resisting frames.” *The Structural Design of Tall and Special Buildings*, 24: 477-490.

Del Gaudio, C., Ricci, P., Verderame, G.M. and Manfredi, G. (2015). “Development and urban-scale application of a simplified method for seismic fragility assessment of RC buildings.” *Engineering Structures*, 91: 40-57.

Der Kiureghian, A., and Ditlevsen, O. (2009). “Aleatory or epistemic? Does it matter?” *Structural Safety*, 31(2): 105–112.

Der Kiureghian, A. (2002). “Bayesian methods for seismic fragility assessment of lifeline components.” In A.D. Kiureghian (Ed.), *Acceptable risk processes: Lifelines and natural hazards*, Monograph No. 21. Reston, VA: Technical Council for Lifeline Earthquake Engineering, ASCE.

Deierlein, G.G., Krawinkler, H., and Cornell, C.A. (2003). “A framework for performance-based earthquake engineering. In: *Proceedings of the 7th Pacific conference on earthquake engineering*, University of Canterbury, Christchurch, New Zealand, Paper Number 140.

Dolsek, M. (2009). “Incremental dynamic analysis with consideration of modeling uncertainties.” *Earthquake Engineering and Structural Dynamics*, 38: 805–825.

Dumova-Jovanoska, E. (2004) “Fragility Curves for RC Structures in Skopje Region.” In: *Proceedings of the 13th World Conference on Earthquake Engineering*, Vancouver, Canada, Paper No. 3.

Ebrahimian, H., and Jalayer, F. (2020). “Selection of seismic intensity measures for prescribed limit states using alternative nonlinear dynamic analysis methods.” *Earthquake Engineering and Structural Dynamics*, 50: 1235-1250.

Echeverria, M.J., Junemann, R., and Liel, A.B. (2022). "Seismic fragility assessment of medium-rise fishbone-type reinforced concrete wall buildings." *Journal of Building Engineering*, 59: 105044.

El-Azizy, O.A., Shedid, M.T., El-Dakhakhni, W.W., and Drysdale, R.G. (2015). "Experimental evaluation of the seismic performance of reinforced concrete structural walls with different end configurations." *Engineering Structures*, 101:246-263.

Elenas, A., and Meskouris, K. (2001). "Correlation study between seismic acceleration parameters and damage indices of structure," *Engineering Structures*, 23: 698–704.

Ellingwood, B.R., Celik, O.C., and Kinali, K. (2007). "Fragility assessment of building structural systems in Mid-America." *Earthquake Engineering and Structural Dynamics*, 36: 1935-1952.

Ellingwood, B., Galambos, T.V., and MacGregor, J.G. (1980). "Development of a probability-based load criterion for American national standard a58." National Bureau of Standards: Washington, DC.

Ellingwood, B.R., and Kinali, K. (2009). "Quantifying and communicating uncertainty in seismic risk assessment." *Structural Safety*, 31(2): 179–187.

Esteghamati, M.Z., Banazadeh, Z., and Huang, Q. (2018). "The effect of design drift limit on the seismic performance of RC dual high-rise buildings." *The Structural Design of Tall and Special Buildings*, 27: 1464.

Fajfar, P. (1999) "Capacity spectrum method based on inelastic demand spectra." *Earthquake Engineering and Structural Dynamics*, 28(9): 979–993.

FEMA. (2005). "Improvement of Nonlinear Static Seismic Analysis Procedures." FEMA-440, *Federal Emergency Management Agency*, Washington, DC, USA.

FEMA. (2003). "Multi-hazard loss estimation methodology earthquake model." HAZUS-MH MR 1, *Federal Emergency Management Agency*, Washington, DC, USA.

FEMA. (2000). "Prestandard and commentary for the seismic rehabilitation of buildings." FEMA-356, *American Society of Civil Engineers* (ASCE), Washington DC.

FEMA. (2008). "Quantification of building seismic performance factors." FEMA-P695, *American Society of Civil Engineers* (ASCE), Washington DC.

FEMA. (2009). "NEHRP recommended seismic provisions for new buildings and other structures. FEMA P-750, Part 1: Provisions and Part 2: Commentary to ASCE/SEI 7-05." *Federal Emergency Management Agency*, Washington, DC.

Filippou, F.C., Popov, E.P., and Bertero, V.V. (1983). "Effects of bond deterioration on hysteretic behavior of reinforced concrete joints." Report EERC 83-19, Earthquake Engineering Research Center, University of California, Berkeley.

Fiore, A., Quaranta, G., Marano, G.C., and Monti, G. (2014). "Evolutionary polynomial regression–based statistical determination of the shear capacity equation for reinforced

concrete beams without stirrups." *Journal of Computing in Civil Engineering*, 30(1): 04014111.

Fox, M.J., Sullivan, T.J., and Beyer, K. (2015). "Evaluation of seismic assessment procedures for determining deformation demands in RC wall buildings." *Earthquakes and Structures*, 9(4): 911-936.

Frank, I.E., and Todeschini, R. (1994). "The Data Analysis Handbook." Elsevier, Amsterdam, Netherland.

Freeman, S. (2004). "Review of the development of the capacity spectrum method." *ISET Journal of Earthquake Technology*, 41(1): 1–13.

Freeman, S., Nicoletti, J., and Tyrell, J. (1975). "Evaluations of existing buildings for seismic risk--A case study of Puget Sound Naval Shipyard, Bremerton, Washington." In: *Proceedings of the 1st US National Conference on Earthquake Engineering*, 113-122.

Gandomi, A.H., Alavi, A.H., Kazemi, S., and Gandomi, M. (2014). "Formulation of shear strength of slender RC beams using gene expression programming. Part I: Without shear reinforcement." *Automation in Construction*, 42: 112–121.

Gaudio, C.D., Rosti, A., Penna, A., Ricci, P., Rota, M., and Verderame, M. (2023). "Empirically based approaches for the derivation of fragility curves of Italian RC building typologies." *Procedia Structural Integrity*, 44: 259-266.

Gehl, P., Seyedi, D.M. and Douglas, J. (2012). "Vector-Valued Fragility Functions for Seismic Risk Evaluation." *Bulletin of Earthquake Engineering*, 11(2): 365–384.

Ghobarah, A. (2004). "On Drift Limits Associated with Different Damage Levels." In: *Proceedings of an International Workshop on performance–based seismic design concepts and implementation*, Bled Slovenia, 321–332.

Ghorbanirenani, I., Tremblay, R., Leger, P., and Leclerc, M. (2012). "Shake Table Testing of Slender RC Shear Walls Subjected to Eastern North America Seismic Ground Motions." *ASCE Journal of Structural Engineering*, 138(12): 1515-1529.

Gidaris, I., Padgett, J.E., Barbosa, A.R., Chen, S., Cox, D., Webb, B., and Cerato, A. (2017). "Multiple-hazard fragility and restoration models of highway bridges for regional risk and resilience assessment in the united states: state-of-the-art review." *ASCE Journal of Structural Engineering*, 143(3): 04016188.

Gogus, A., and Wallace, J.W. (2015). "Seismic safety evaluation of reinforced concrete walls through FEMA P695 methodology." *ASCE Journal of Structural Engineering*, 141: 04015002-1– 04015002-17.

Gokkaya, B.U., Baker, J.W., and Deierlein, G.G. (2016). "Quantifying the impacts of modeling uncertainties on the seismic drift demands and collapse risk of buildings with implications on seismic design checks." *Earthquake Engineering and Structural Dynamics*, 45(10): 1661–1683.

Golbraikh, A., and Tropsha, A. (2002). “Beware of q2.” *Journal of Molecular Graphics and Modelling*, 20(4): 269–276.

Gondia, A., Ezzeldin, M., and El-Dakhakhni, W., (2021). “Mechanics-Guided Genetic Programming Expression for Shear-Strength Prediction of Squat Reinforced Concrete Walls with Boundary Elements.” *ASCE Journal of Structural Engineering*, 146(11): 04020223.

Grùnthal. (1998). “European Macrosiesmic Scale 1998.” *European Seismological Commission*, Luxembourg, Joseph Beffort, Helfent-Bertrange.

Gulec, C.K., Whittaker, A.S., and Hooper, J.D. (2010). “Fragility functions for low aspect ratio reinforced concrete walls.” *Engineering Structures*, 32: 2894-2901.

Han, S.W., and Chopra, A.K., (2006). “Approximate incremental dynamic analysis using the modal pushover analysis procedure.” *Earthquake Engineering and Structural Dynamics*, 35(15): 1853-1873.

Hancock, J., Boommer, J.J. (2007). “Using spectral matched records to explore the influence of strong-motion duration on inelastic structural response.” *Soil Dynamics and Earthquake Engineering*, 27: 291–299.

Hariri-Ardebili, M.A., Segura Jr., C.L., and Sattar, S. (2024). “Modeling and material uncertainty quantification of RC structural components.” *Structural Safety*, 106: 102401.

Haselton, C.B. (2006). “Assessing seismic collapse safety of modern reinforced concrete moment frame buildings.” PhD. Dissertation, Stanford University.

Huang, H., and Burton, H.V. (2019). “Classification of in-plane failure modes for reinforced concrete frames with infills using machine learning.” *Journal of Building Engineering*, 25: 100767.

Hwang, S.H., Mangalathu, S., Shin, J. and Jeon, J.S. (2021). “Machine learning-based approaches for seismic demand and collapse of ductile reinforced concrete building frames.” *Journal of Building Engineering*, 34: 101905.

Iman, R.L., and Conover, W.J. (1980) “Small sample sensitivity analysis techniques for computer models: With an application to risk assessment.” *Communications in Statistics*, 9(17): 1749–1842.

International Code Council. (2006). *International Building Code*, Falls Church: VA.

Jaiswal, K.S., Aspinal, W.P., Perkins, D., Wald, D., and Porter, K.A. (2012). “Use of expert judgment elicitation to estimate seismic vulnerability of selected building types.” In *Proceedings of the 15th World Conference on Earthquake Engineering* (WCEE). Lisbon, Portugal.

Jasmine, P.H., and Arun, S. (2021). “Machine learning applications in structural engineering - a review.” *IOP Conference Series: Materials Science and Engineering*, 1114.

Jayaram, N., Lin, T., and Baker, J.W. (2011). "A computationally efficient ground-motion selection algorithm for matching a target response spectrum mean and variance." *Civil and Environmental Engineering Faculty Research and Publications*, 115.

Jalayer, F., and Cornell, C.A. (2009). "Alternative non-linear demand estimation methods for probability-based seismic assessments." *Earthquake Engineering and Structural Dynamics*, 38: 951-972.

Jalayer, F. (2003). "Alternative non-linear demand estimation methods for probability-based seismic assessments." PhD. dissertation. Stanford (CA): Department of Civil and Environmental Engineering and the committee on graduate studies of Stanford University.

Ji, J., Elnashai, A.S., and Kuchma, D.A. (2009). "Seismic fragility relationships of reinforced concrete high-rise buildings." *The Structural Design of Tall and Special Buildings*, 259-277.

Jia, K., Xu, C., Du, X., Cui, C., Dou, P., and Song, J. (2023). "Seismic response comparison and sensitivity analysis of pile foundation in liquefiable and non-liquefiable soils." *Earthquake Engineering and Engineering Vibration*, 22: 87-104.

Jiang, H., Liu, X., and Hu, L. (2015). "Seismic Fragility Assessment of RC Frame-Shear Wall Structures Designed According to the Current Chinese Seismic Design Code." *Journal of Asian Architecture and Building Engineering*, 14(2): 459-466.

Kabir, M.A.B., Hasan, A.S., and Billah, A.H.M.M. (2021). "Failure mode identification of column base plate connection using data-driven machine learning techniques." *Engineering Structures*, 112389.

Kafali, C., and Grigoriu, M. (2007). "Seismic fragility analysis: Application to simple linear and nonlinear systems." *Earthquake Engineering and Structural Dynamics*, 36: 1885-1900.

Kappos, A.J. (1997). "Discussion of paper: Damage scenarios simulation for seismic risk assessment in urban zones." *Earthquake Spectra*, 13: 549–551.

Kappos, A.J., Panagopoulos, G., Panagiotopoulos, C., and Penelis, G. (2006). "A hybrid method for the vulnerability assessment of R/C and URM buildings." *Bulletin of Earthquake Engineering*, 4: 391–413.

Kappos, A.J., Stylianidis, K.C. and Pitilakis, K. (1998) "Development of seismic risk scenarios based on a hybrid method of vulnerability assessment." *Natural Hazards*, 17(2): 177- 192.

Kara, I.F. (2011). "Prediction of shear strength of FRP-reinforced concrete beams without stirrups based on genetic programming." *Advances in Engineering Software*, 42(6): 295–304.

Karaton M, Osmanli OF, Gülşan ME. (2020). "Investigation of uncertainties in nonlinear seismic analysis of the reinforced concrete shear walls." *International Journal of Civil Engineering*.

Kazantzi, A.K., and Vamvatsikos, D. (2015). "Intensity measure selection for vulnerability studies of building classes." *Earthquake Engineering and Structural Dynamics*, 44: 2677-2694.

Kazantzi, A.K., Vamvatsikos, D., and Lignos, D.G. (2013). "Seismic performance of a steel moment-resisting frame subject to strength and ductility uncertainty." In: *Proceedings of 11th International Conference on Structural Safety and Reliability* (ICOSSAR'05), New York.

Kazaz, I. (2010). "Dynamic characteristics and performance assessment of reinforced concrete structural walls." PhD. dissertation. Ankara, Turkey: The Graduate School of Natural and Applied Sciences, Middle East Technical University.

Kazaz, I., Gulkan, P., and Yakut, A. (2012). "Deformation limits for structural walls with confined boundaries." *Earthquake Spectra*, 28(3): 1019-1046.

Kennedy, R.P., Cornell, C.A., Campbell, R.D., Kaplan, S., and Perla, H.F. (1980). "Probabilistic seismic safety study of an existing nuclear power plant", *Nuclear Engineering and Design*, 59(2): 315–338.

Kent, D.C., and Park, R. (1971). "Flexural members with confined concrete." *Proceedings ASCE*, 97(7): 1969-1990.

Khalil, A., and Ghobarah, A. (2005). "Behaviour of rehabilitated structural walls." *Journal of Earthquake Engineering*, 9(3): 371-391.

Kiani, J., and Khanmohammadi, M. (2015). "New approach for selection of real input ground motion records for incremental dynamic analysis (IDA)." *Journal of Earthquake Engineering*, 19: 592–623.

Kim, T., Kwon, O.S., and Song, J. (2021). "Clustering-based adaptive ground motion selection algorithm for efficient estimation of structural fragilities." *Earthquake Engineering and Structural Dynamics*, 50:1755-1776.

Kim, J., Park, J.H. and Lee, T.H. (2011). "Sensitivity analysis of steel buildings subjected to column loss." *Engineering Structures*, 33: 421-432.

Kinali, K., and Ellingwood, B.R. (2007). "Seismic fragility assessment of steel frames for consequence-based engineering: A case study for Memphis, TN." *Engineering Structures*, 29: 1115-1127.

Kircher, C.A., Nassar, A.A., Kustu, O., and Holmes, W.T. (1997). "Development of Building Damage Functions for Earthquake Loss Estimation." *Earthquake Spectra*, 13(4).

Ko. Y.F., and Phung, C. (2014). "Nonlinear static cyclic pushover analysis for flexural failure of reinforced concrete bridge columns with combined damage mechanisms." Acta Mechanica, Springer, 225: 477–492.

Koutsourelakis, P. (2010). "Assessing structural vulnerability against earthquakes using multi-dimensional fragility surfaces: a bayesian framework." *Probabilistic Engineering Mechanics*, 25: 49–60.

Koza, J.R. (1992). "Vol. 1 of Genetic programming: On the programming of computers by means of natural selection." Cambridge, MA: MIT Press.

Kwon, O.S., and Elnashai, A. (2006). "The effect of material and ground motion uncertainty on the seismic vulnerability curves of RC structure." *Engineering Structures*, 28: 289-303.

Lagomarsino, S., and Giovinazzi, S. (2006) "Macroseismic and Mechanical Models for the Vulnerability and Damage Assessment of Current Buildings." *Bulletin of Earthquake Engineering*, 4: 415-443.

LATBSDC. (2008). "An alternative procedure for seismic analysis and design of tall buildings located in the Los Angeles Region." *Los Angeles Tall Buildings Structural Design Council*.

Lee, T.H., and Mosalam, K.M. (2005). "Seismic demand sensitivity of reinforced concrete shear wall building using FOSM method." *Earthquake Engineering and Structural Dynamics*, 34: 1719–1736.

Lefas, I.D., and Kotsovos, M.D. (1990). "Strength and deformation characteristics of reinforced concrete walls under load reversals." *ACI Structural Journal*, 87(6): 716-726.

Liao, W., Loh, C., and Wan, S. (2001). "Earthquake responses of RC moment frames subjected to near-fault ground motions." *The Structural Design of Tall and Special Buildings*, 10(3): 219–229.

Liel, A.B., Haselton, C.B., Deierlein, G.G., and Baker, J.W. (2009). "Incorporating modeling uncertainties in the assessment of seismic collapse risk of buildings." *Structural Safety*, 31(2): 197–211.

Liu, H. (2004). "Effect of concrete strength on the response of ductile shear walls." Master's Dissertation, McGill University.

Lowes, L.N., Lehman, D.E., and Whitman, Z. (2019). "Investigation of failure mechanisms and development of design recommendations for flexural reinforced concrete walls." *Engineering Structures*, 186: 323-335.

Lu, Y., Henry, R.S., Gultom, R., and Ma, Q.T. (2017). "Cyclic Testing of reinforced concrete walls with distributed minimum vertical reinforcement." *ASCE Journal of Structural Engineering*, 143(5): 04016225.

Luco, N., &and Cornell, A.C. (2007). “Structure-specific scalar intensity measures for near source and ordinary earthquake ground motions.” *Earthquake Spectra*, 23: 357–392.

Mackie, K., and Stojadinovic, B. (2005). “Fragility basis for California highway overpass bridge seismic decision making.” Pacific Earthquake Engineering Research Center, College of Engineering, University of California, Berkeley.

Manfredi, V., Masi, A., Nicodemo, G., and Digrisolo, A. (2023). “Seismic fragility curves for the Italian RC residential buildings based on non-linear dynamic analyses.” *Bulletin of Earthquake Engineering*, 21: 2173-2214.

Mangalathu, S., and Jeon, J.S. (2018). “Classification of failure mode and prediction of shear strength for reinforced concrete beam-column joints using machine learning techniques.” *Engineering Structures*, 160: 85-94.

Mazzoni, S., McKenna, F., Scott, M.H., and Fenves, G.L. (2009). “Open system for earthquake engineering simulation user command language manual-OpenSees Version 2.0.” Pacific Earthquake Engineering Research Center, University of California, Berkeley, USA.

McKenna, F., Fenves, G.L., and Scott, M.H. (2000). “Open system for earthquake engineering simulation.” University of California, Berkeley, USA.

Menegotto, M., and Pinto, P.E. (1973). “Method of analysis of cyclically loaded RC plane frames including changes in geometry and non-elastic behavior of elements under normal force and bending.” IASBE Proceedings, Lisbon, Portugal, 15–22.

Metwally, Z., Zeng, B., and Li, A. (2022). “Probabilistic behavior and variance-based sensitivity analysis of reinforced concrete masonry walls considering slenderness effect.” *ASCE-ASME Journal of Risk and Uncertainty in Engineering Systems, Part A: Civil Engineering*, 04022051.

Mirza, S.A., MacGregor, J.G., and Hatzinikolas, M. (1979). “Statistical descriptions of strength of concrete.” *Journal of the Structural Division*, 105(6): 1021–37.

Mirza, S.A., MacGregor, J.G. (1979). “Variability of mechanical properties of reinforcing bars.” *Journal of the Structural Division*, 105(5): 921–37.

Mobeen, S. (2002). “Cyclic tests of shear walls confined with double head studs.” Master's Dissertation, University of Alberta.

Mohamed, H., Skoulidou, D., and Romao, X. (2023). “Quantification of the effects of different uncertainty sources on the seismic fragility functions of masonry-infilled RC frames.” *Structures*, 50: 1069-1088.

Morgan, B.J., Hiraishi, H., and Corley, W.G. (1986). “U.S.-Japan quasi-static test of isolated wall planar reinforced concrete structure, Volume I.” Technical Report, National Science Foundation.

Morris, P.A. (1997). "Combining expert judgments. A Bayesian approach." *Management Science*, 23(7): 679-693.

Mostafaei, H., Behnamfar, F., and Alembagheri, M. (2022). "Reliability and sensitivity analysis of wedge stability in the abutments of an arch dam using artificial neural network." *Earthquake Engineering and Engineering Vibration*, 21: 1019-1033.

Mwafy, A. (2012). "Analytically derived fragility relationships for the modern high-rise buildings in the UAE." *The Structural Design of Tall and Special Buildings*, 21: 824-843.

Mwafy, A., Hussain, N., and El-Sawy, K. (2015). "Seismic performance and cost-effectiveness of high-rise buildings with increasing concrete strength." *The Structural Design of Tall and Special Buildings*, 24: 257-279.

Nazari, Y.R., and Saatcioglu, M. (2017). "Seismic Vulnerability Assessment of Concrete Shear Wall Buildings through Fragility Analysis." *Journal of Building Engineering*, 12: 202-209.

Oesterle, R.G., Fiorato, A.E., Johal, L.S., Carpenter, J.E., Russell, H.G., and Corley, W.G. (1976). "Earthquake resistant structural walls-tests of isolated walls." Technical report, National Science Foundation.

Papia, M., and Russo, G. (1989). "Compressive concrete strain at buckling of longitudinal reinforcement." *ASCE Journal of Structural Engineering*, 115(2): 382-397.

Park, Y.J., and Ang, A.H.S. (1985). "Mechanistic Seismic Damage Model for Reinforced Concrete." *ASCE Journal of Structural Engineering*, 111(4): 722-739.

PEER strong motion database: http://peer.berkeley.edu/smcat/

Pejovic, J., and Jankovic, S. (2016) "Seismic fragility assessment for reinforced concrete high-rise buildings in Southern Euro-Mediterranean zone." *Bulletin of Earthquake Engineering*, 14: 185-212.

Penelis, G.G., Sarigiannis, D., Stavrakakis, E., and Stylianidis, K.C. (1989). "A statistical evaluation of damage to buildings in the Thessaloniki. Greece, earthquake of June, 20, 1978." In: *Proceedings of 9th World Conference on Earthquake Engineering*, Tokyo-Kyoto, Maruzen, Japan, VII, 187–192.

Perez, J.L., Cladera, A., Rabunal, J.R., and Martinez-Albella, F. (2012). "Optimization of existing equations using a new genetic programming algorithm: application to the shear strength of reinforced concrete beams." *Advances in Engineering Software*, 50: 82-96.

Pilakoutas, K., and Elnashai, A.S. (1995). "Cyclic behavior of reinforced concrete cantilever walls, Part I: Experimental results." *ACI Structural Journal*, 92(3): 271-281.

Porter, K.A., Beck, J.L., and Shaikhutdinov, R.V. (2002). "Sensitivity of building loss estimates to major uncertain variables." *Earthquake Spectra*, 18(4): 719–743.

Pozo, J.D., Hube, M.A., and Kurama, Y.C. (2023). "Quantification of variability in simulated seismic performance of RC wall buildings." *Engineering Structures*, 295: 116872.

Priestley, M. (1997). "Displacement-based seismic assessment of reinforced concrete buildings." *Journal of Earthquake Engineering*, 1(1): 157–192.

Priestley, M.J.N., Calvi, G.M., and Kowalsky, M.J. (2007). "Displacement-based seismic design of structures." IUSS Press, Pavia, Italy.

Radu, A., and Grigoriu, M. (2018). "An earthquake-source-based metric for seismic fragility analysis." *Bulletin of Earthquake Engineering*, 16: 3771-3789.

Rajeev, P., Franchin, P., and Pinto, P.E. (2008) "Increased Accuracy of Vector-IM-Based Seismic Risk Assessment?" *Journal of Earthquake Engineering*, 12(S1): 111-124.

Rivera, J.P., and Whittaker, A.S. (2019). "Updated fragility functions for shear-critical reinforced concrete walls." *ACI Structural Journal*, 116(2): 139-146.

Rossetto, T., and Elnashai, A. (2003). "Derivation of vulnerability functions for European-type RC structures based on observational data." *Engineering Structures*, 25: 1241–1263.

Rossetto, T., D'Ayala, D., Ioannou, I., and Meslem, A. (2014). "Evaluation of existing fragility curves." In *SYNER-G: Typology Definition and Fragility Functions for Physical Elements at Seismic Risk, Geotechnical, Geological and Earthquake Engineering*, Pitilakis, K., Ed.; Springer: Dordrecht, The Netherlands, 27: 47–93.

Rossetto, T., Ioannou, I. and Grant, D.N. (2013). "Existing empirical fragility and vulnerability relationships: compendium and guide for selection." GEM Technical Report 2013-X. GEM Foundation. Pavia, Italy.

Roy, P.P., and Roy, K. (2008). "On some aspects of variable selection for partial least squares regression models." *QSAR and Combinatorial Science*, 27: 302–313.

Sadraddin, H.L., Shao, X., and Hu, Y. (2016). "Fragility assessment of high-rise reinforced concrete buildings considering the effects of shear wall contributions." *The Structural Design of Tall and Special Buildings*, 25: 1089-1102.

Saltelli, A., Chan, K., and Scott, E.M. (2000). "Sensitivity analysis." Vol. 134, New York, Wiley.

Scott, B.D., Park, R., and Priestley, M.J.N. (1982). "Stress-strain behavior of concrete confined by overlapping hoops at low and high strain rates." *ACI Structural Journal*.

SEAOC. (1999). "Recommended lateral force requirements and commentary." SEAOC-Bluebook, Seismology Committee, Structural Engineers Association of California.

Searson, D.P., Leahy, D.E., and Willis, M.J. (2010). "GPTIPS: An open source genetic programming toolbox for multigene symbolic regression." In: *Proceedings of the International Conference of Engineers and Computer Scientists*, Vol I, IMECS, March 17 -19, Hong Kong.

Sengupta, P., and Li, B. (2016). "Seismic Fragility Assessment of Lightly Reinforced Concrete Structural Walls." *Journal of Earthquake Engineering*, 20(5): 809-840.

Seo, J., and Linzell, D.G. (2013) "Nonlinear seismic response and parametric examination of horizontally curved steel bridges using 3D computational models." *Journal of Bridge Engineering*, 18(3): 220–231.

Seyedi, D., Gehl, P., Douglas, J., Davenne, L., Mezher, N., and Ghavamian, S. (2010). "Development of seismic fragility surfaces for reinforced concrete buildings by means of nonlinear time-history analysis." *Earthquake Engineering and Structural Dynamics*, 39: 91-108.

Shinozuka, M., Feng, N.Q., Lee, J., and Naganuma, T. (2000). "Statistical analysis of fragility curves." *ASCE Journal of Structural Engineering*, 126(12): 1224–31.

Shiu, K.N., Daniel, J.I., Aristizabal-Ochoa, J.D., Fiorato, A.E., and Corley, W.G. (1981). "Earthquake resistant structural walls-tests of walls with and without openings." Technical report, National Science Foundation.

Shome, N., Cornell, C.A., Bazzurro, P., and Carballo, J.E. (1998). "Earthquakes, records, and nonlinear responses," *Earthquake Spectra*. 14(3): 469–500.

Siam, A., Ezzeldin, M., and El-Dakhakhni, W. (2019). "Machine learning algorithms for structural performance classifications and predictions: application to reinforced masonry shear walls." *Structures*, 22: 252–265.

Singhal, A., and Kiremidjian, A.S. (1996). "Method for probabilistic evaluation of seismic structural damage." *ASCE Journal of Structural Engineering*, 122(12): 1459–1467.

Smith, G.N. (1986). "Probability and statistics in civil engineering." Collins, London.

Sobol′, I.M. (1993). "Sensitivity estimates for nonlinear mathematical models." *Mathematical Modelling and Computational Experiments*, 1(4): 407–414.

Sousa, L., Silva, V., Marques, M., and Crowley, H. (2016). "On the treatment of uncertainties in the development of fragility functions for earthquake loss estimation of building portfolios." *Earthquake Engineering and Structural Dynamics*, 45: 1955-1976.

Spacone, E., Filippou, F.C., and Taucer, F.F. (1996). "Fibre beam-column model for non-linear analysis of R/C frames: part I. Formulation." *Earthquake Engineering and Structural Dynamics*, 25(7): 711–725.

Stocchi, A. and Richard, B. (2019). "Sensitivity of engineering demand parameters as a function of structural typology and assessment method." *Nuclear Engineering and Design*, 343: 151-165.

Surana, M., Singh, A., Lang, D.H. (2016). "Seismic performance of concrete-shear-wall buildings in India." In: *Proceedings of the Institution of Civil Engineers – Structures and Buildings*, 169(11): 809-824.

Teweldebrhan, B.T., Goda, K., Risi, R.D., and Tesfamariam, S. (2023). "Multi-variate seismic fragility assessment of CLT coupled wall systems." *Earthquake Spectra*, 39(4): 2100-2122.

Thomsen, J.H., and Wallace, J.W. (2004). "Displacement-based design of slender reinforced concrete structural walls—experimental verification." *Journal of Structural Engineering*, 30(4): 618-630.

Tian, Q., Ren, H., Shao, D., Wang, T., Zhang, W., and Ning, C. (2023). "A hybrid approach for seismic fragility analysis of reinforced concrete structural walls independent of failure pattern." *Structures*, 56: 104984.

Timchenko, I. (2002). "Seismic vulnerability assessment of buildings on the basis of numerical analyses." In: *Proceedings of 12th European Conference on Earthquake Engineering*, London.

Trifunac, M.D., and Brady, A.G. (1975). "A study on the duration of strong earthquake ground motion." *Bulletin of the Seismological Society of America*, 65(3): 581-626.

Tso, W.K., Zhu, T.J, and Heidebrecht, A.C. (1992). "Engineering implication of ground motion A/V ratio." *Soil Dynamics and Earthquake Engineering*, 11(3): 133-144.

Tupper, B. (1999). "Seismic response of reinforced concrete walls with steel boundary elements." Master's Dissertation, McGill University.

Vallenas, J.M., Bertero, V.V., and Popov, E.P. (1979). "Hysteretic behavior of reinforced concrete structural walls." PhD Dissertation. University of California, Berkeley.

Vamvatsikos, D., and Cornell, C.A. (2002). "Incremental dynamic analysis." *Earthquake Engineering and Structural Dynamics*, 31: 491–514.

Vamvatsikos, D., and Cornell, C.A. (2004). "Applied incremental dynamic analysis." *Earthquake Spectra*, 10(2): 523–553.

Vamvatsikos, D., and Cornell, C.A. (2005). "Direct estimation of seismic demand and capacity of multi degree-of-freedom systems through incremental dynamic analysis of single-degree-of-freedom approximation." *ASCE Journal of Structural Engineering*, 131(4): 589-599.

Verdugo, C.M., Hube, M.A., Favier, P., and Saitua, F. (2017). "Analytical fragility curves of high-rise reinforced concrete shear wall buildings." In *Proceedings of the 16th World Conference on Earthquake Engineering* (WCEE), Santiago, Chile.

Wang, Z., and Jia, G. (2022). "Sensitivity Analysis of Tsunami Evacuation Risk with Respect to Epistemic Uncertainty." *ASCE-ASME Journal of Risk and Uncertainty in Engineering Systems, Part A: Civil Engineering*, 04022037.

Wang, Z., Padgett, J.E., and Duenas-Osorio, L. (2013). "Influence of vertical ground motions on the seismic fragility modelling of a bridge-soil-foundation system." *Earthquake Spectra*, 29(3): 937-962.

Wen, Y.K., Ellingwood, B.R., Veneziano, D., and Bracci. J. (2003). “Uncertainty modelling in earthquake engineering.” MAE Center Project FD–2 Report.

Wen, Z.P., Hu, Y.X., and Chau, K.T. (2002). “Site effect on vulnerability of high-rise shear wall buildings under near and far field earthquakes.” *Soil Dynamics and Earthquake Engineering*, 22: 1175-1182.

Whittaker, A., Deierlein, G., Hooper, J., and Merovich, A. (2004). “Engineering demand parameters for structural framing systems.” Technical Report, Applied Technology Council, Redwood City, CA.

Xiong, C., Lu, X., and Lin, X. (2019). “Damage assessment of shear wall components for RC frame–shear wall buildings using story curvature as engineering demand parameter.” *Engineering Structures*, 189: 77-88.

Xu, C., Deng, J., Peng, S., and Li, C. (2018). “Seismic fragility analysis of steel reinforced concrete frame structures based on different engineering demand parameters.” *Journal of Building Engineering*, 20: 736-749.

Xu, W., Zhao, Y., Yang, W., Zhang, J., and Chen, D. (2023). “Seismic performance of RC frame-shear wall dual structural systems.” *Structures*, 58: 105610.

Yakut, A., and Yilmaz, H. (2008). “Correlation of deformation demands with ground motion intensity.” *ASCE Journal of Structural Engineering*, 134(12): 1818–1828.

Yamazaki, F., Hamada, T., Motoyama, H., and Yamauchi, H. (1999). “Earthquake damage assessment of expressway bridges in Japan.” *Technical Council on Lifeline Earthquake Engineering Monograph*, 16: 361–370.

Yazdani, A., Nicknam, A., Dadras, Y., and Eftekhari, S.N. (2017). “Entropy-based sensitivity analysis of global seismic demand of concrete structures.” *Engineering Structures*, 146: 118-126.

Yosri, A., Siam, A., El-Dakhakhni, W., and Dickson-Anderson, S. (2019). “A Genetic Programming–Based Model for Colloid Retention in Fractures.” *Groundwater*, 57(5): 693-703.

Yum, S.Y., Hamburger, R.O., Cornell, C.A., and Foutch, D.A. (2002). “Seismic performance evaluation for steel moment frames.” *ASCE Journal of Structural Engineering*, 128(4): 534-545.

Zareian, F., and Krawinkler, H. (2010). “Structural system parameter selection based on collapse potential of buildings in earthquakes.” *ASCE Journal of Structural Engineering*, 136(8): 933-943.

Zareian, F., Krawinkler, H., Ibarra, L., and Lingos, D. (2010). “Basic concepts and performance measures in prediction of collapse of buildings under earthquake ground motions.” *Earthquake Engineering and Structural Dynamics*, 19: 167–181.

Zembaty, Z., Kowalski, M. and Pospisil, S. (2006). “Dynamic identification of an RC frame in progressive states of damage.” *Engineering Structures*, 28(5): 668-681.

Zhang, D., Lin, X., Dong, Y., and Yu, X. (2023). “Machine-Learning-Based uncertainty and sensitivity analysis of Reinforced-Concrete slabs subjected to fire.” *Structures*, 53: 581-594.

PUBLICATIONS

Journal

Sarkar N., and Dasgupta K., "Uncertainty Assessment in the Seismic Vulnerability Estimates of Reinforced Concrete Wall-Frame Buildings." *The Structural Design of Tall and Special Buildings,* (Under Review).

Sarkar N., and Dasgupta K., "Machine Learning-Based Sensitivity Analysis of Engineering Demand Parameters for RC Frame-Wall Building." *Structures*, (Under Review).

Sarkar N., and Dasgupta K., "Genetic Programming-Driven Damage State Prediction of Reinforced Concrete Structural Walls." *Earthquake Engineering and Engineering Vibration,* (Under Review).

Sarkar N., and Dasgupta K., "Efficient Fragility Surfaces with Reduced Input Records for RC Shear Wall Frame Building." (Under preparation).

Conference

Sarkar N., and Dasgupta K., (2022). "Comparative Study of Concrete Models in OpenSEES for Performing Nonlinear Analysis." *Proceedings of the International Conference on Structural Engineering and Construction Management, SECON'21*, FISAT, Kerala, India.

Sarkar N., and Dasgupta K., (2022) "Influence of Structural Parameters on the Buckling of Longitudinal Steel Bar in RC Structural Wall." *Proceedings of 12th Structural Engineering Convention*, SEC-2022, MNIT Jaipur, India.

Sarkar N., and Dasgupta K., (2023) "Importance of Epistemic Uncertainty on Seismic Analysis of RC Wall-Frame Buildings." *Proceedings of the 17th Symposium on Earthquake Engineering*, IIT Roorkee, India.

Sarkar N., and Dasgupta K., "Influence of Ground Motion Variability on Seismic Response Parameters of an RC Wall-Frame Building." *In 18th World Conference in Earthquake Engineering*, Italy (Manuscript accepted).